Anisotropic Flow Measurements in ALICE at the Large Hadron Collider

A catalogue record is available from the Utrecht University Library.

ISBN:

Copyright © 2012 by A. Bilandzic

All rights reserved. No part of this book may be reproduced, stored in a database or retrieval system, or published, in any form or in any way, electronically, mechanically, by print, photoprint, microfilm or any other means without prior written permission of the author.

Typeset using LaTeX and printed by Ipskamp Drukkers, Enschede, The Netherlands.

Anisotropic Flow Measurements in ALICE at the Large Hadron Collider

Anisotrope stroming gemeten met de ALICE detector aan de grote hadronen-botser

(met een samenvatting in het Nederlands)

Proefschrift

ter verkrijging van de graad van doctor aan de Universiteit Utrecht op gezag van de rector magnificus, prof. dr. G.J. van der Zwaan, ingevolge het besluit van het college voor promoties in het openbaar te verdedigen op woensdag 7 maart 2012 des ochtends te 12.45 uur

DOOR

Ante Bilandžić

geboren te Split, Croatia

Promotor: Prof. dr. R.J.M. Snellings

Dit werk is een onderdeel van het onderzoeksprogramma van de "Stichting voor Fundamenteel Onderzoek der Materie" (FOM), financieel gesteund door de "Nederlandse Organisatie voor Wetenschappelijk Onderzoek" (NWO), Grant number 680-47-217.

It's all like an ocean, I tell you.
F.M.D.

Contents

1 Introduction **11**
- 1.1 Quantum Chromodynamics (QCD) . . . 11
- 1.2 Quark-gluon Plasma (QGP) . . . 12
- 1.3 Hydrodynamics and anisotropic flow . . . 14
  - 1.3.1 Introduction to hydrodynamics in the relativistic heavy-ion collisions 14
  - 1.3.2 Formalism of the relativistic ideal and viscous hydrodynamics . . . 16
  - 1.3.3 Anisotropic flow . . . 21
- 1.4 Historical snapshot . . . 30

2 Experimental setup **33**
- 2.1 Large Hadron Collider (LHC) . . . 33
- 2.2 A Large Ion Collider Experiment (ALICE) . . . 35
  - 2.2.1 Time Projection Chamber (TPC) . . . 36
  - 2.2.2 Inner Tracking System (ITS) . . . 38
  - 2.2.3 VZERO . . . 39
  - 2.2.4 Zero Degree Calorimeter (ZDC) . . . 40
- 2.3 Offline framework . . . 40
  - 2.3.1 Minimum bias event selection . . . 41
  - 2.3.2 Event reconstruction and tracking . . . 41

3 Q-cumulants **43**
- 3.1 A bit of history . . . 44
  - 3.1.1 Standard event plane method (EP) . . . 44
  - 3.1.2 Fitted q-distribution (FQD) . . . 44
  - 3.1.3 Lee-Yang Zeroes (LYZ) . . . 46
  - 3.1.4 Two- and multi-particle azimuthal correlations . . . 48
  - 3.1.5 Cumulants . . . 51
  - 3.1.6 Cumulants in flow analysis . . . 52
  - 3.1.7 Generating Function Cumulants (GFC) . . . 55
- 3.2 Q-cumulants (QC) . . . 57
  - 3.2.1 Main idea and calculating strategy . . . 57
  - 3.2.2 Reference flow results . . . 58
  - 3.2.3 Differential flow results . . . 59
  - 3.2.4 List of improvements . . . 62

3.2.5 Open questions . . . 64

4 Data selection **73**

5 Results **83**
5.1 Centrality determination . . . 83
5.2 Elliptic flow (v_2) . . . 84
5.2.1 Centrality dependence . . . 84
5.2.2 Transverse momentum dependence . . . 89
5.2.3 Energy dependence . . . 90
5.3 Higher harmonics . . . 99
5.3.1 Centrality dependence . . . 99
5.3.2 Transverse momentum dependence . . . 101
5.4 Outlook . . . 104

6 Epilogue **105**

Bibliography **107**

A Flow fluctuations **113**
A.1 Some general results . . . 113
A.2 $v\{2\}$ . . . 114
A.3 $v\{4\}$ . . . 115
A.4 $v\{6\}$ . . . 116
A.5 $v\{8\}$ . . . 116
A.6 Uniform flow fluctuations . . . 118

B Particle weights **121**
B.1 Weighted multiparticle azimuthal correlations . . . 122
B.1.1 Example for ϕ-weights: Correcting for the bias from non-uniform acceptance of the detector . . . 124

C Statistical errors **129**
C.1 Some general results . . . 129
C.2 Statistical errors for reference flow estimates . . . 132
C.2.1 2-particle estimate . . . 133
C.2.2 4-particle estimate . . . 134
C.2.3 6-particle estimate . . . 134
C.2.4 8-particle estimate . . . 136
C.3 Statistical errors for differential flow estimates . . . 137
C.3.1 2-particle estimate . . . 138
C.3.2 4-particle estimate . . . 139

D Non-uniform acceptance **143**
D.1 Example: Correcting with generalized cumulants for the bias coming from non-uniform acceptance . . . 149

E Toy model **153**
E.1 Brief summary . . . 153
E.2 Random walk . . . 154
E.3 Track splitting . . . 155
E.4 Monochromatic flow and track splitting . . . 158
E.5 Bichromatic flow and track splitting . . . 161

F Generating Function Cumulants **165**
F.1 Reference flow . . . 165
F.1.1 Estimating the reference flow harmonics v_n from the cumulants . . . 167
F.2 Numerical approach to calculating reference cumulants . . . 171
F.3 Differential flow . . . 173

G Multi-particle azimuthal correlations **179**
G.1 2-particle azimuthal correlations . . . 179
G.2 3-particle azimuthal correlations . . . 179
G.3 4-particle azimuthal correlations . . . 181
G.4 5-particle azimuthal correlations . . . 185
G.5 6-particle azimuthal correlations . . . 189
G.6 7-particle azimuthal correlations . . . 192
G.7 8-particle azimuthal correlations . . . 192

H $v_3\{5\}$ **193**

I Detailed derivations **199**
I.1 $\langle 2 \rangle$ . . . 199
I.2 $\langle 4 \rangle$ . . . 200
I.3 $\langle 6 \rangle$ . . . 202
I.4 $\langle 8 \rangle$ . . . 207
I.5 $\langle 2' \rangle$ and $\langle 4' \rangle$ . . . 208

J Isolating cumulants from correlations **213**

Samenvatting **218**

Acknowledgments **220**

Curriculum Vitae **222**

Chapter 1

Introduction

In this introductory chapter we present the basic terminology and the framework within which the phenomenon of *anisotropic flow* can be studied and understood, both from a theoretical and experimental point of view. We start by outlying the basics of Quantum Chromodynamics (QCD) in Section 1.1, the fundamental theory which comprises the part of the Standard Model (SM) that deals with elementary particles interacting via the strong force (quarks) and with the elementary particles which are the carriers of strong force (gluons). In Section 1.2 we introduce the quark-gluon plasma (QGP), the state of matter consisting of deconfined quarks and gluons, mutually interacting dominantly via the strong nuclear force. The QGP doesn't exist at ordinary temperatures and energy densities. However, in the ultrarelativistic high energy collisions of heavy ions, currently performed at BNL's Relativistic Heavy Ion Collider (RHIC) and CERN's Large Hadron Collider (LHC), sufficiently large temperatures and energy densities required for QGP formation can be achieved. One of the most important probes to assess the properties of QGP is anisotropic flow. Anisotropic flow will be introduced conceptually in Section 1.3, together with relativistic hydrodynamics, which is a suitable effective theory which is successful in describing the measured values of anisotropic flow observed in collisions of heavy ions prior to the LHC era. We will conclude this chapter by providing a historical snapshot of experimental anisotropic flow results in Section 1.4. Having introduced the required framework for the understanding of anisotropic flow phenomenon in this introductory chapter, the rest of the thesis will deal primarily with the novel experimental tools developed for anisotropic flow measurements (so-called Q-cumulants), as well as with the presentation of recent results for anisotropic flow measured in lead-lead collisions at LHC.

1.1 Quantum Chromodynamics (QCD)

According to the Standard Model, currently the most successful theory of elementary particles and their interactions, quarks interact via the strong nuclear force. The strong force is carried by other elementary particles called gluons. The physical quantity which is responsible for the strong interaction is *color*, which comes in three instances: red,

blue and green, and the corresponding negative units ("anti-red", "anti-blue" and "anti-green"). Both quarks and gluons are dressed in color, but in a different fashion. Quarks (antiquarks) carry only a single positive (negative) unit of color, while gluons are bi-colored, i.e. they carry one positive and one negative unit of color. Since the strong interaction between quarks is transmitted via gluons, which carry only a discrete number of colors (gluons, for instance, do not have mass, charge or flavor which are another set of fundamental physical properties distinguishing elementary particles), the strong interaction can only change the color of the interacting quarks by a discrete amount. For this reason the underlying fundamental theory of strong nuclear reaction is being dubbed *Quantum Chromodynamics (QCD)*.

There are two key fundamental phenomena associated with QCD. The first one is *confinement*, which refers to the experimental observation that quarks and antiquarks cannot be found isolated in nature. Namely, quarks and antiquarks are found only confined in hadrons, the composite objects they form[1]. Closely related with this phenomenon is so-called *asymptotic freedom*, which states that quarks interact weakly at large energies (or equivalently at short distances). As the distance between quarks in hadrons increases, their interaction energy increases as well, which prevents the quarks from hadrons to be separated. For instance, when the distance between a quark-antiquark pair in a meson is increased by inserting more and more energy in the system, at some point it becomes more energetically favorable to produce a new quark-antiquark pair from the vacuum, which will then with the original quark-antiquark pair combine and form two new mesons, preventing in turn the quarks and antiquarks from original meson to be deconfined and to be found isolated. The second fundamental phenomenon associated with QCD is *chiral symmetry restoration*. Chiral symmetry exists as an exact symmetry only in the limit of vanishing quark masses, and is approximately restored when quark masses are reduced from their large effective values in hadronic matter to their small bare ones at sufficiently high temperatures and energy densities [1].

These two fundamental phenomena will be tested in heavy-ion collisions at LHC energies, where deconfined quarks will be produced at unprecedented temperatures and energy densities and form a so-called quark-gluon plasma (QGP), the state of nuclear matter which we discuss in more detail in the next section.

1.2 Quark-gluon Plasma (QGP)

Based on the phenomenon of asymptotic freedom mentioned in previous section, it was expected by a vast majority of theorists that a new state of nuclear matter containing deconfined quarks and gluons, if ever managed to be produced in the laboratory at high temperatures and energy densities, should exhibit properties similar to a weakly interacting gas. It was first realized by Edward Shuryak in 1978 that the thermal fluctuations of gauge fields might actually produce a dominant effect over vacuum fluctuations, which would translate into dominant screening over anti-screening of color fields [2, 3]. For this reason he coined the term *quark-gluon plasma* for a state of matter consisting

[1] Hadrons are classified further with respect to their quark content: baryons are hadrons composed of three quarks, while mesons are hadrons composed of one quark and one antiquark.

of deconfined quarks and gluons.[2] The first prediction that the dramatic change in the effective mass of the fundamental constituents of nuclei might signal the various phase transitions which nuclear matter undergoes, goes back to T.D. Lee [4].

One of the first questions is what the transition temperature from hadronic to deconfined state is, and if this temperature can be achieved in the laboratory. Calculations on lattice predict the phase transition to occur at about $T_c \simeq 175$ MeV, and this temperature might be reached in heavy-ion collisions currently delivered both at RHIC and at the LHC, and even previously at CERN's Super Proton Synchrotron (SPS) accelerator. In particular, at RHIC gold ions were collided at a center of mass energy of 200 GeV per nucleon pair, while at LHC lead ions will be collided at a center of mass energy of 5.5 TeV per nucleon pair. Since such a deconfined state of matter is believed to have existed a few microseconds after the Big Bang, by producing and studying properties of QGP in heavy-ion collisions we are essentially at RHIC and LHC recreating the same conditions which existed in a distant past of our Universe. Because of this we improve on our current understanding of its origin and evolution. For completeness, other possible phases of nuclear matter, besides the QGP, are presented in Fig. 1.1, and the region explored with heavy-ion collisions at RHIC and at the LHC is indicated.

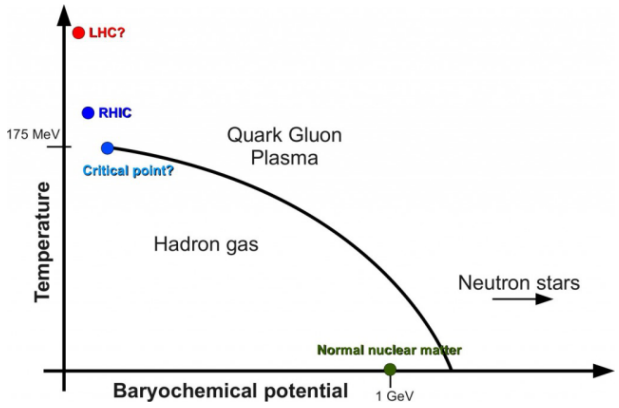

Figure 1.1: Phase diagram of nuclear matter.

Next, it was important to establish the physical observables which are sensitive to the QGP properties. Prior to experimental results obtained at RHIC it was expected that deconfined quarks and gluons behave as a weakly interacting gas. If this picture would be correct, then the response of produced interacting matter contained in an anisotropic volume (the anisotropy is resulting trivially from the geometry of non-central heavy-ion collisions) to initial anisotropy in coordinate space of this volume would not be significant, and a very tiny fraction of this initial anisotropy in the coordinate space would be transfered via mutual interactions into the final and observable anisotropy in momentum space, a phenomenon called *anisotropic flow*. This picture was found to be incorrect,

[2]Plasma is a general term used for physical system in which charges are screened due to the presence of other mobile charges (in the context of QGP the relevant charge is color).

given the sizable anisotropic flow measured at RHIC [5]. This will be elaborated in more details after, in the subsequent sections, we outline the detailed formal definition of anisotropic flow. First we highlight the main aspects of hydrodynamics, the effective theory which proved to be the most successful theory in describing experimental anisotropic flow data collected at collider energies so far.

1.3 Hydrodynamics and anisotropic flow

This section[3] is divided into three parts. In the first part we give a brief introduction to relativistic hydrodynamics in the context of heavy-ion collisions (H.I.C.). In the second part we present the formalism and some fundamental aspects of relativistic ideal and viscous hydrodynamics. Finally, in the third part we introduce formally the anisotropic flow phenomenon and our fundamental observables, namely the anisotropic flow coefficients v_n.

We use the natural units $c = \hbar = k_B = 1$ and the Minkowski metric $g^{\mu\nu} = \mathrm{diag}(1, -1, -1, -1)$ throughout this section.

1.3.1 Introduction to hydrodynamics in the relativistic heavy-ion collisions

The main goals of the physics of H.I.C. are to discover the deconfined nuclear matter under equilibrium, namely the Quark-gluon Plasma (QGP), and to understand its properties such as the equation of state (EoS), temperature and order of the phase transition, transport coefficients and so on. The system produced in H.I.C. dynamically evolves within a time duration of the order of 10-100 fm/c. Therefore one has to describe the space-time evolution of thermodynamic variables to fill the large gap between the static aspects of QGP properties and the dynamical aspects of H.I.C. It is hydrodynamics that plays an important role in connecting them. Various stages of H.I.C. are depicted in Fig. 1.2. Two energetic nuclei are coming in along the light-cone and collide with each other to create a multi-parton system. Through secondary collisions the system may reach thermal equilibrium and the QGP can be formed. This is a transient state and after further expansion and cooling the system hadronizes. Eventually, the expansion leads to a free-streaming stage and the particle spectra at this moment are seen by the detector. Hydrodynamics is applied to matter under local equilibrium in the intermediate stage.

There is also another good reason to apply hydrodynamics to H.I.C. A lot of experimental data have been published so far at various collision energies. Ideally, one may want to describe these data from the first principles, i.e. by using quantum chromodynamics (QCD). The QCD Lagrangean density reads

$$\mathcal{L} = \bar{\psi}_i \left(i\gamma_\mu D^\mu_{ij} - m\delta_{ij} \right) \psi_j - \frac{1}{4} F_{\mu\nu\alpha} F^{\mu\nu\alpha} \,, \tag{1.1}$$

where ψ_i is a quark field, γ^μ are Dirac matrices, D^μ is a covariant derivative, m is a quark mass, δ is Kronecker delta symbol and $F^{\mu\nu}_\alpha$ is the field strength of the gluons. However,

[3] For more details we refer the reader to [6].

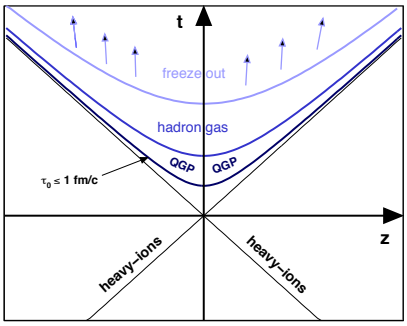

Figure 1.2: A schematic view of dynamics of a heavy ion collision along the collision axis.

in spite of its simple-looking Lagrangean, it is very difficult to make any predictions directly from QCD in H.I.C. This is due to its complexity which mainly arises from the non-linearity of the interactions of the gluons, the strong coupling, the dynamical many body system and confinement. One promising strategy to connect the first principles with observables is to introduce hydrodynamics as a phenomenological theory. An input to this phenomenological theory is the equation of state,

$$P = P(e, n), \tag{1.2}$$

which expresses the pressure P as a function of energy density e and baryon density n. Such an equation can be obtained by performing numerical simulations of QCD on the lattice. In the case of viscous hydrodynamics we need additionally the transport coefficients such as shear viscosity η, bulk viscosity ζ, heat conductivity λ, etc.

If hydrodynamics turns out to work quite well in describing the dynamics, one can utilize its output such as local temperature or energy density for other observables. For instance, in the current formalism of jet quenching, one needs information of parton density or energy density along a trajectory of an energetic parton. If one assumes J/ψ melts away above some temperature, one needs local temperature at the position of J/ψ. In the case of electromagnetic probes, one convolutes the emission rate (the number of produced particles per unit space-time volume at temperature T) of thermal photons and dileptons over the space-time volume under equilibrium. Hydrodynamics provides us with the information of the bulk matter. Therefore we can say that, in the context of H.I.C., hydrodynamics is the heart of the dynamical modeling: It not only describes expansion and collective flow of matter but also provides important informations in the intermediate stage for other phenomena.

1.3.2 Formalism of the relativistic ideal and viscous hydrodynamics

The second part of this section is more formal with many equations, but we try as much as possible to provide the intuitive picture behind the equations.

The basic equations

The basic hydrodynamical equations are energy-momentum conservation

$$\partial_\mu T^{\mu\nu} = 0\,, \tag{1.3}$$

where $T^{\mu\nu}$ is the energy-momentum tensor, whose physical meaning is outlined below, and the current conservation

$$\partial_\mu N_i^\mu = 0\,, \tag{1.4}$$

where N_i^μ is the i-th conserved current. In H.I.C., there are some conserved charges such as baryon number, strangeness, electric charges and so on. We mainly assume the net baryon current N_B^μ as an example of N_i^μ in the following. In the first step we decompose the energy-momentum tensor and the conserved current as follows:

$$T^{\mu\nu} = eu^\mu u^\nu - P\Delta^{\mu\nu} + W^\mu u^\nu + W^\nu u^\mu + \pi^{\mu\nu}\,, \tag{1.5}$$

$$N_i^\mu = n_i u^\mu + V_i^\mu\,. \tag{1.6}$$

All the terms in the above expansion will be discussed one by one later. Now we indicate that u^μ is the time-like, normalized four-vector

$$u_\mu u^\mu = 1\,, \tag{1.7}$$

while the tensor $\Delta^{\mu\nu}$ is defined in the following way,

$$\Delta^{\mu\nu} = g^{\mu\nu} - u^\mu u^\nu\,, \tag{1.8}$$

where $g^{\mu\nu}$ is the Minkowski metric. We refer to u^μ and $\Delta^{\mu\nu}$ as the "projection" vector and tensor operators, respectively. In particular, u^μ is the local flow four-velocity, but a more precise meaning will be given later. u^μ is perpendicular to $\Delta^{\mu\nu}$, as can easily be seen from the definition of $\Delta^{\mu\nu}$ given in Eq. (1.8) and from the fact that u^μ is normalized,

$$u_\mu \Delta^{\mu\nu} = u_\mu (g^{\mu\nu} - u^\mu u^\nu) = u^\nu - 1 \cdot u^\nu = 0\,. \tag{1.9}$$

Next we define the local rest frame (LRF) as the frame in which u^μ has only the time-like component non-vanishing and in which $\Delta^{\mu\nu}$ has only the space-like components non-vanishing, i.e.,

$$u^\mu_{\rm LRF} = (1,0,0,0)\,, \tag{1.10}$$

$$\Delta^{\mu\nu}_{\rm LRF} = {\rm diag}(0,-1,-1,-1)\,. \tag{1.11}$$

As is easily understood from the above equations, one can say that $u^\mu(\Delta^{\mu\nu})$ picks up the time-(space-)like component(s) when acting on some Lorentz vector/tensor.

We now discuss the physical meaning of each term in the expansion of the energy-momentum tensor (1.5) and the conserved current (1.6).

Decomposition of $T^{\mu\nu}$

The new quantities which appear on the RHS in the decomposition (1.5) of energy-momentum tensor are defined in the following way:

$$e = u_\mu T^{\mu\nu} u_\nu \qquad \text{(energy density)}\,, \tag{1.12}$$

$$P = P_s + \Pi = -\frac{1}{3}\Delta_{\mu\nu} T^{\mu\nu} \qquad \text{(hydrostatic + bulk pressure)}\,, \tag{1.13}$$

$$W^\mu = \Delta^\mu{}_\alpha T^{\alpha\beta} u_\beta \qquad \text{(energy (or heat) current)}\,, \tag{1.14}$$

$$\pi^{\mu\nu} = \langle T^{\mu\nu} \rangle \qquad \text{(shear stress tensor)}\,. \tag{1.15}$$

Each term corresponds to the projection of the energy-momentum tensor by one or two projection operator(s), u^μ and $\Delta^{\mu\nu}$. The first two equalities imply that the energy density e can be obtained from the time-like components of the energy-momentum tensor, while the pressure P is obtained from the space-like components. Contracting the energy-momentum tensor simultaneously with u^μ and $\Delta^{\mu\nu}$ gives the energy (heat) current W^μ. Finally, the angular brackets in the definition of the shear stress tensor $\pi^{\mu\nu}$ stand for the following operation:

$$\langle A^{\mu\nu} \rangle = \left[\frac{1}{2}(\Delta^\mu{}_\alpha \Delta^\nu{}_\beta + \Delta^\mu{}_\beta \Delta^\nu{}_\alpha) - \frac{1}{3}\Delta^{\mu\nu}\Delta_{\alpha\beta} \right] A^{\alpha\beta}\,. \tag{1.16}$$

This means that $\langle A^{\mu\nu} \rangle$ is a symmetric and traceless tensor which is transverse to u^μ and u^ν. More concretely, one can first decompose the energy-momentum tensor by two projection tensors symmetrically,

$$\tilde{\pi}^{\mu\nu} \;=\; \frac{1}{2}(\Delta^\mu{}_\alpha T^{\alpha\beta} \Delta_\beta{}^\nu + \Delta^\nu{}_\alpha T^{\alpha\beta} \Delta_\beta{}^\mu)\,, \tag{1.17}$$

and then decompose it once more into the shear stress tensor (traceless) and the pressure (non-traceless):

$$\tilde{\pi}^{\mu\nu} \;=\; \pi^{\mu\nu} - P\Delta^{\mu\nu}. \tag{1.18}$$

Decomposition of N^μ

In the decomposition (1.6) we have introduced the following quantities,

$$n_i = u_\mu N_i^\mu \qquad \text{(charge density)}\,, \tag{1.19}$$

$$V_i^\mu = \Delta^\mu{}_\nu N_i^\nu \qquad \text{(charge current)}\,. \tag{1.20}$$

The physical meaning of n_i and V_i^μ is clear from the properties of projection operators and definition (1.6), and is indicated in the brackets.

Ideal and dissipative parts of $T^{\mu\nu}$ and N^μ

The various terms appearing in the decompositions (1.5) and (1.6) can be grouped into two distinctive parts, which are the ideal and dissipative parts. In particular, for the

energy-momentum tensor we have,

$$\begin{aligned} T^{\mu\nu} &= T_0^{\mu\nu} + \delta T^{\mu\nu}\,, & (1.21)\\ T_0^{\mu\nu} &= e u^\mu u^\nu - P_s \Delta^{\mu\nu}\,, & (1.22)\\ \delta T^{\mu\nu} &= -\Pi \Delta^{\mu\nu} + W^\mu u^\nu + W^\nu u^\mu + \pi^{\mu\nu}\,, & (1.23) \end{aligned}$$

while for the charge current we have,

$$\begin{aligned} N^\mu &= N_0^\mu + \delta N^\mu\,, & (1.24)\\ N_0^\mu &= n u^\mu\,, & (1.25)\\ \delta N^\mu &= V^\mu\,. & (1.26) \end{aligned}$$

In the above relations $T_0^{\mu\nu}(N_0^\mu)$ denote the ideal part, while the $\delta T^{\mu\nu}(\delta N^\mu)$ denote the dissipative part of the $T^{\mu\nu}(N^\mu)$.

The meaning of u^μ

As we have already mentioned in Section 1.3.2, u^μ is the four-velocity of the "flow". Now we like to clarify what kind of flow we have in mind in this description. In literature two definitions of flow can be found:

1. flow of energy (Landau) [8]:

$$u_L^\mu = \frac{T^\mu{}_\nu u_L^\nu}{\sqrt{u_L^\alpha T_\alpha{}^\beta T_{\beta\gamma} u_L^\gamma}} = \frac{1}{e} T^\mu{}_\nu u_L^\nu\,, \qquad (1.27)$$

2. flow of conserved charge (Eckart) [9]:

$$u_E^\mu = \frac{N^\mu}{\sqrt{N_\nu N^\nu}}\,. \qquad (1.28)$$

In the first definition, u_L^μ also appears in the RHS of Eq. (1.27), so it should be understood as an equation with respect to u_L^μ. One may solve an eigenvalue problem for a given energy-momentum tensor $T^\mu{}_\nu$. u_L^μ is a normalized time-like eigenvector and the corresponding positive eigenvalue is the energy density e. If the dissipative currents are small enough, one can show the following relation between these two definitions of flow [10]:

$$u_L^\mu \approx u_E^\mu + \frac{W^\mu}{e + P_s},\;\; u_E^\mu \approx u_L^\mu + \frac{V^\mu}{n}. \qquad (1.29)$$

Obviously, $W^\mu = 0$ ($V^\mu = 0$) in the Landau (Eckart) frame. In the case of vanishing dissipative currents, both definitions represent a common flow. In other words, flow is uniquely determined in the case of ideal hydrodynamics.

Entropy

We start this subsection by briefly discussing the entropy conservation in ideal hydrodynamics. By ideal hydrodynamics we mean the case when entropy is not produced during the evolution. Neglecting the dissipative parts, the energy-momentum conservation (1.3) and the current conservation (1.4) reduce to

$$\partial_\mu T_0^{\mu\nu} = 0\,, \tag{1.30}$$
$$\partial_\mu N_0^{\mu} = 0\,, \tag{1.31}$$

where $T_0^{\mu\nu}$ and N_0^{μ} are the ideal parts introduced in Eqs. (1.22) and (1.25). Equations (1.30) and (1.31) are the basic equations of ideal hydrodynamics.

By contracting Eq. (1.30) with u_ν it follows,

$$\begin{aligned}
0 &= u_\nu \partial_\mu T_0^{\mu\nu} \\
&= u_\nu (u^\mu u^\nu)\partial_\mu e + e u_\nu \partial_\mu (u^\mu u^\nu) - P_s \cdot 0 \\
&= u^\mu T \partial_\mu s + u^\mu \mu \partial_\mu n + (Ts + \mu n) u_\nu (u^\nu \partial_\mu u^\mu + u^\mu \partial_\mu u^\nu) \\
&= T(u^\mu \partial_\mu s + s\partial_\mu u^\mu + s u_\nu u^\mu \partial_\mu u^\nu) \\
&\quad + \mu(u^\mu \partial_\mu n + n\partial_\mu u^\mu + n u_\nu u^\mu \partial_\mu u^\nu) \\
&= T(u^\mu \partial_\mu s + s\partial_\mu u^\mu) + \mu(u^\mu \partial_\mu n + n\partial_\mu u^\mu)\,.
\end{aligned} \tag{1.32}$$

In the second line above we have used the relation (1.9). We have introduced here the temperature T, entropy density s and chemical potential μ through the first law of thermodynamics $e = Ts + \mu n$. Also, we have used the fact that from $u_\mu u^\mu = 1$, and after contracting both sides with $u^\nu \partial_\nu$, it follows $u_\nu u^\mu \partial_\mu u^\nu = 0$. Here it is assumed that thermalization is maintained locally, i.e. thermodynamic equilibrium can be assumed in the neighborhood of each point in the system. The second term on the RHS in the last line of Eq. (1.32) vanishes due to Eq. (1.31). If we now introduce the entropy current as

$$S^\mu = s u^\mu\,, \tag{1.33}$$

it follows from Eq. (1.32) that

$$\partial_\mu S^\mu = \partial_\mu (s u^\mu) = u^\mu \partial_\mu s + s \partial_\mu u^\mu = 0\,, \tag{1.34}$$

hence the entropy is conserved in ideal hydrodynamics.

Now we go back to viscous hydrodynamics. Hereafter we consider only the Landau frame and omit the subscript L. For simplicity, we further assume that there is no charge in the system although in the realistic case a small amount of charge might exist. What we construct is the so-called first order theory of viscous hydrodynamics. The main assumption is that the non-equilibrium entropy current vector S^μ has linear dissipative term(s) constructed from V^μ, Π and $\pi^{\mu\nu}$ and can be written as

$$S^\mu = s u^\mu + \alpha V^\mu\,. \tag{1.35}$$

The first term on the RHS is the ideal part and the second term is the correction due to the dissipative part. It is impossible to construct a term which would form a Lorentz

Table 1.1: New variables and terminology.

Thermodynamic force	Transport coefficient	Current
$X^{\mu\nu} = \langle \nabla^\mu u^\nu \rangle$ tensor	η shear viscosity	$\pi_{\mu\nu}$
$X = -\partial_\mu u^\mu$ scalar	ζ bulk viscosity	Π

vector from $\pi^{\mu\nu}$ on the RHS in the above equation because $\pi^{\mu\nu}$ is perpendicular to u^μ by definition. Since we have also assumed that there is no charge in the system, i.e., $N^\mu = 0$, it follows that αV^μ vanishes.

We now calculate the product of the temperature T and the divergence of the entropy current (1.35). It follows,

$$\begin{aligned} T\partial_\mu S^\mu &= T(u^\mu \partial_\mu s + s\partial_\mu u^\mu) \\ &= u_\nu \partial_\mu T_0^{\mu\nu} \\ &= -u_\nu \partial_\mu \delta T^{\mu\nu} \\ &= \pi_{\mu\nu} \langle \nabla^\mu u^\nu \rangle - \Pi \partial_\mu u^\mu \,. \end{aligned} \tag{1.36}$$

where $\nabla^\mu = \Delta^{\mu\nu}\partial_\nu$. From the second to third line in the above calculation we have used the energy-momentum conservation, $\partial_\mu T^{\mu\nu} = 0$. It is important to note that due to the assumption that there is no charge in the system we could neglect the dissipative part of the entropy current (1.35), but the dissipative part of the energy-momentum tensor (1.23) does not vanish. The non-vanishing dissipative part of energy-momentum tensor gives a contribution which yields a difference between the equations characterizing the first order theory of viscous hydrodynamics and the equations of ideal hydrodynamics derived before.

To solve the hydrodynamic equations we must first define the dissipative current. We introduce the following two phenomenological definitions, so-called *constitutive equations*, for the shear stress tensor $\pi^{\mu\nu}$ and the bulk pressure Π,

$$\pi^{\mu\nu} = 2\eta \langle \nabla^\mu u^\nu \rangle \,, \tag{1.37}$$

$$\Pi = -\zeta \partial_\mu u^\mu = -\zeta \nabla_\mu u^\mu \,. \tag{1.38}$$

In Table 1.1 we outline the new variables and terminology used in these equations. Notice that, within our approximation $N^\mu = 0$, there is no vector component of the thermodynamic force.

After inserting the definitions (1.37) and (1.38) in the last line of (1.36), we arrive at (for positive transport coefficients)

$$\begin{aligned} T\partial_\mu S^\mu &= \frac{\pi_{\mu\nu}\pi^{\mu\nu}}{2\eta} + \frac{\Pi^2}{\zeta} \\ &= 2\eta \langle \nabla^\mu u^\nu \rangle^2 + \zeta \left(-\partial_\mu u^\mu\right)^2 \geq 0 \,. \end{aligned} \tag{1.39}$$

This ensures the second law of thermodynamics

$$\partial_\mu S^\mu \geq 0\,, \tag{1.40}$$

i.e. in the case of viscous hydrodynamics entropy is not decreasing.

Flow equation

After the basics of ideal and viscous hydrodynamics in the previous sections, we briefly indicate, in this section, the equation which, in the simplest case of no dissipative currents present in the system, relate the flow four-vector u^μ to the pressure gradients and energy density (for a detailed exposure we refer the reader to [11]).

We start by defining the speed of sound c_s as:

$$c_s^2 = \frac{\partial P_s}{\partial e}\,, \tag{1.41}$$

where P_s is pressure, and e is energy density (both quantities were defined in Eqs. (1.13) and (1.12)). Inserting the decomposition of the energy-momentum tensor and the decomposition of conserved current into the conservation laws (1.3) and (1.4), and keeping only non-dissipative terms, yields [11]:

$$\dot{u}^\mu = \frac{\nabla^\mu P_s}{e + P_s} = \frac{c_s^2}{1 + c_s^2}\frac{\nabla^\mu e}{e}\,. \tag{1.42}$$

In the equation the "dot" denotes the time derivative and $\nabla^\mu = \Delta^{\mu\nu}\partial_\nu$. We see clearly from this equation that pressure gradients, quantified via $\nabla^\mu P_s$, cause a fluid element to accelerate [11]. As an example, the equilibrated matter produced in an anisotropic volume when two heavy-ions collide in non-central collisions will give rise to, as a consequence of this anisotropy in coordinate space, the pressure gradients. These pressure gradients will cause, via above equation, the created fluid elements to move, i.e. to flow, anisotropically.

After this basic introduction of ideal and viscous hydrodynamics in this section, we now move on to the formal definition of anisotropic flow.

1.3.3 Anisotropic flow

Introduction

In non-central heavy-ion collisions the initial volume of the interacting system is anisotropic in coordinate space (see Fig. 1.3). Due to multiple interactions this anisotropy is transferred to momentum space, and is then quantified via so-called flow harmonics v_n [36]. In essence, anisotropic flow analysis is the measurement of flow harmonics v_n, which we formally define next.

Formal definitions

For historical reasons we first outline the traditional definition of anisotropic flow harmonics v_n. The azimuthal distribution $r(\varphi)$ of the physical quantity of interest (for

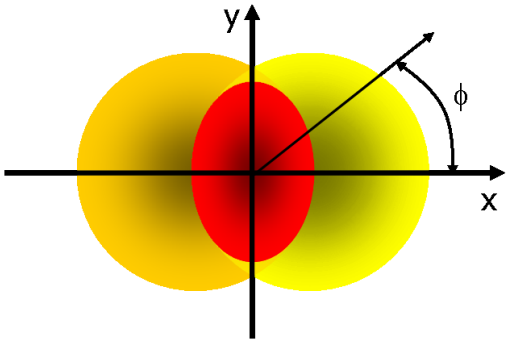

Figure 1.3: Coordinate space anisotropy of the initial volume of the interacting system (red) created in heavy-ion collisions.

instance the azimuthal distribution of total transverse momentum of particles produced in a heavy-ion collision) is a periodic quantity and it is natural to expand it in a Fourier series [36],

$$r(\varphi) = \frac{x_0}{2\pi} + \frac{1}{\pi}\sum_{n=1}^{\infty}\left[x_n \cos(n\varphi) + y_n \sin(n\varphi)\right] , \tag{1.43}$$

where

$$x_n = \int_0^{2\pi} r(\varphi)\cos(n\varphi)d\varphi \, , \tag{1.44}$$

$$y_n = \int_0^{2\pi} r(\varphi)\sin(n\varphi)d\varphi \, . \tag{1.45}$$

For each pair of Fourier coefficients, x_n and y_n, we define the corresponding flow harmonics v_n in the following way,

$$v_n \equiv \sqrt{x_n^2 + y_n^2} \, . \tag{1.46}$$

When the colliding nuclei are the same, the symmetry of the collision (Fig. 1.3) implies that all y_n are zero.[4] Moreover, when the colliding nuclei are the same the symmetry

[4]To see this explicitly, it suffices to observe that for a symmetric collision (as in Fig. 1.3) it is *equally probable* for a produced particle to be emitted in directions φ and $-\varphi$. As defined in Eq. (1.45), y_n is nothing but $\langle \sin(n\varphi) \rangle$, and when this average of sinus terms is being calculated for the measured particle's azimuthal angles, the contribution of particles emitted in direction φ and $-\varphi$ to the total average will always cancel each other for any angle φ and harmonic n:

$$\sin(n\varphi) + \sin[n(-\varphi)] = \sin(n\varphi) - \sin(n\varphi) = 0 \, . \tag{1.47}$$

We remark that for asymmetric collisions, like collisions between protons and heavy-ions, sinus terms are not averaged out to zero and their contribution to v_n defined in Eq. (1.46) has to be kept.

of the collision (Fig. 1.3) also implies that all x_n are zero for odd n.[5] Due to these symmetries the harmonics v_n defined in (1.46) are equal to x_n for symmetric colliding systems (like lead-lead beams), and are not trivially zero only for even n. Harmonics v_n can be related explicitly to the starting distribution $r(\phi)$ in the following way:

$$\begin{aligned} \langle \cos(n\varphi) \rangle &\equiv \frac{\int_0^{2\pi} \cos(n\varphi) r(\varphi) d\varphi}{\int_0^{2\pi} r(\varphi) d\varphi} \\ &= \frac{\frac{1}{\pi} v_n \int_0^{2\pi} \cos^2(n\varphi) d\varphi}{v_0} \\ &= \frac{v_n}{v_0} \,. \end{aligned} \tag{1.49}$$

From the first to second line in the equation above we have used the orthogonality relationship of the sine and cosine functions

$$\begin{aligned} \int_{-\pi}^{\pi} \sin(mx) \sin(nx) dx &= \pi \delta_{mn} \,, \\ \int_{-\pi}^{\pi} \cos(mx) \cos(nx) dx &= \pi \delta_{mn} \,, \\ \int_{-\pi}^{\pi} \sin(mx) \cos(nx) dx &= 0 \,, \end{aligned} \tag{1.50}$$

where δ_{mn} is the Kronecker delta symbol. By using a normalized distribution $r(\phi)$, for which $v_0 = \int_0^{2\pi} r(\varphi) d\varphi = 1$, it follows immediately from Eq. (1.49)

$$v_n = \langle \cos(n\varphi) \rangle \,. \tag{1.51}$$

The harmonic v_1 is called *directed* flow, the harmonic v_2 *elliptic* flow, the harmonic v_3 *triangular* flow, etc.[6] When flow harmonics are considered as a function of transverse momentum and rapidity, $v_n(p_t, y)$, we refer to them as *differential flow*.

[5] This can be understood as follows: For a symmetric collision (see Fig. 1.3) it is also *equally probable* for a particle to be emitted in φ and $\varphi + \pi$, for any angle φ, so when $\langle \cos(n\varphi) \rangle$ is being calculated these two contributions will cancel each other for odd harmonic n:

$$\begin{aligned} \cos(n\phi) + \cos[n(\phi + \pi)] &= \cos(n\phi) + \cos(n\phi)\cos(n\pi) - \sin(n\phi)\sin(n\pi) \\ &= \cos(n\phi) + \cos(n\phi)(-1)^n - \sin(n\phi) \cdot 0 \\ &= \cos(n\phi) \cdot (1 + (-1)^n) = 0 \text{ for odd } n \,. \end{aligned} \tag{1.48}$$

[6] As an elementary example, we consider the ellipse-like distribution $r(\varphi)$. When the polar coordinates (r, φ) used to parametrize the ellipse-like distribution are measured from the one of the foci of ellipse, then the distribution is determined by the following equation:

$$r(\varphi) = \frac{a(1 - \varepsilon^2)}{1 + \varepsilon \cos \varphi} \,, \tag{1.52}$$

where ε is the eccentricity defined as

$$\varepsilon^2 \equiv 1 - \frac{b^2}{a^2} \,, \tag{1.53}$$

The result (1.51), however, is of little use in the measurement of v_n. Namely, the orientation of impact parameter vector $\mathbf{b}$ (the vector connecting the centers of two colliding nuclei) changes event-by-event in heavy-ion collisions, which in turn yields a random reaction plane angle Ψ_{R} (the plane spanned by the impact parameter and the beam axis z, see Fig. 1.4). Due to these random fluctuations it is useless to measure

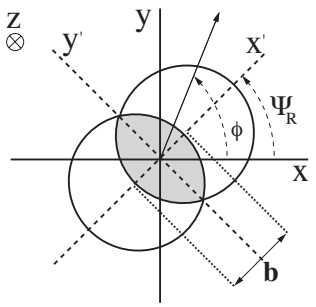

Figure 1.4: Schematic view of a non-central nucleus-nucleus collision in the transverse plane.

azimuthal angles φ needed in Eq. (1.51) in a fixed coordinate system in the laboratory. Namely, in such a coordinate system the initial non-trivial event-wise anisotropy will average out to zero when the averaging is extended to all events. As an example, in such a coordinate system one would get with equal probability the initial ellipsoidal anisotropy of the created volume elongated event-by-event along x or y axis, which would yield an event-by-event contribution to harmonic v_2 with positive or negative signature, respectively, which trivially cancel out in an average over all events. Measuring azimuthal angles of created particles with respect to the reaction plane angle Ψ_{R} would lead to the desired non-trivial result for v_n in Eq. (1.51). Therefore, if we would be able to measure for each event precisely the reaction plane angle Ψ_{R}, than it would be trivial to set up for each event the coordinate system for which the orientation of x-axis would coincide with Ψ_{R} measured in that event, so that Eq. (1.51) would become applicable. However, so far nobody has devised a precise experimental technique to measure the orientation Ψ_{R} of the reaction plane event-by-event. The way to circumvent this issue is to use observables which are sensitive only to flow harmonics v_n, but do not require the knowledge of reaction plane orientation event-by-event. Such observables can be constructed, but more on that later.

In addition to the created volume's spatial anisotropy originating solely from the idealized collision geometry, there are also the anisotropies stemming from the fluctuations in the initial positions of participating nucleons within the created volume [38].

and $a(b)$ is semimajor(semiminor) axis. With this parameterization all harmonics v_n can be calculated analytically in a closed form. In particular, we have obtained:

$$v_n = 2\pi b(-1)^n \left(\frac{a-b}{a+b}\right)^{\frac{n}{2}} . \tag{1.54}$$

Such fluctuations can in principle generate any type of anisotropy in coordinate space, which will be also via mutual interactions transferred to momentum space, where they can give rise to in principle any harmonic v_n. In order to accommodate effects of fluctuations in the anisotropic flow analysis, we refer now again to the original, most general Fourier decomposition presented in Eq. (1.43), but for convenience sake we rewrite it in a somewhat different way [39]. We start by using well known identities:

$$\begin{aligned} \cos(n\varphi) &= \frac{1}{2}(e^{in\varphi}+e^{-in\varphi})\,, \\ \sin(n\varphi) &= \frac{1}{2i}(e^{in\varphi}-e^{-in\varphi})\,, \end{aligned} \tag{1.55}$$

and defining

$$v_n = \begin{cases} x_n - iy_n, & n>0\,, \\ x_n + iy_n, & n<0\,, \\ x_0, & n=0\,. \end{cases} \tag{1.56}$$

After inserting relations (1.55) into (1.43), it follows

$$\begin{aligned} r(\varphi) &= \frac{x_0}{2\pi} + \frac{1}{\pi}\sum_{n=1}^{\infty}\frac{1}{2}(x_n - iy_n)e^{in\varphi} + \frac{1}{\pi}\sum_{n=1}^{\infty}\frac{1}{2}(x_n + iy_n)e^{-in\varphi} \\ &= \frac{x_0}{2\pi} + \frac{1}{\pi}\sum_{n=1}^{\infty}\frac{1}{2}(x_n - iy_n)e^{in\varphi} + \frac{1}{\pi}\sum_{n=-\infty}^{-1}\frac{1}{2}(x_{-n} + iy_{-n})e^{in\varphi}\,. \end{aligned} \tag{1.57}$$

Inserting in above relation the definitions (1.56), it follows immediately:

$$r(\varphi) = \frac{1}{2\pi}\sum_{n=-\infty}^{\infty} v_n e^{in\varphi}\,, \tag{1.58}$$

where v_n is in general complex. To make a further progress we observe that $r(\varphi)$ is real, meaning that $r(\varphi) = r(\varphi)^*$. Applying this equality to (1.58) gives trivially $v_n = v_{-n}^*$. Inserting this result in (1.58) it follows that for a real p.d.f. $r(\varphi)$ the most general Fourier decomposition reads:

$$\begin{aligned} r(\varphi) &= \frac{v_0}{2\pi} + \frac{1}{2\pi}\sum_{n=1}^{\infty} v_n^* e^{-in\varphi} + \frac{1}{2\pi}\sum_{n=1}^{\infty} v_n e^{in\varphi} \\ &= \frac{v_0}{2\pi} + \frac{1}{2\pi}\sum_{n=1}^{\infty} 2\cdot\mathfrak{Re}\left[v_n e^{in\varphi}\right]\,. \end{aligned} \tag{1.59}$$

Since v_n is complex, we can always write it as $v_n \equiv |v_n|\, e^{-in\Psi_n}$, which yields:

$$r(\varphi) = \frac{v_0}{2\pi} + \frac{1}{\pi}\sum_{n=1}^{\infty} |v_n|\,\mathfrak{Re}\left[e^{in(\varphi-\Psi_n)}\right]\,. \tag{1.60}$$

Using $v_n \equiv |v_n|$, we take explicitly the real part in above expression and write our final results as:

$$r(\varphi) = \frac{v_0}{2\pi} + \frac{1}{\pi}\sum_{n=1}^{\infty} v_n \cos[n(\varphi-\Psi_n)]\,. \tag{1.61}$$

From this expression it is obvious that in most general case each type of anisotropy can be defined with its own symmetry plane, the so called *participant plane* Ψ_n. Therefore the complete anisotropic flow analysis requires in the most general case the measurement of both v_n and its symmetry plane Ψ_n. By generalizing the derivation of results (1.51) one can show straightforwardly that:

$$v_n = \langle \cos(n(\varphi - \Psi_n)) \rangle \ , \tag{1.62}$$

and that for a normalized distribution $r(\varphi)$, $v_0 = 1$.

As introduced here, anisotropic flow is a physical observable and can be related to the geometry of colliding heavy-ions. This geometry is determined event-by-event by the positions of the participating nucleons in the initial overlap area. Before proceeding further with its description, we stop for the moment in order to describe one model of the geometry in a heavy-ion collisions, the so-called *Glauber model*, in its Monte Carlo incarnation.

Glauber Monte Carlo Model

By the Glauber model [43] we refer in general to the models used to relate experimental heavy-ion data to the *geometric* quantities characterizing the collision of two heavy-ions, like impact parameter $\mathbf{b}$, inelastic total nucleus-nucleus cross-section σ_{inel}, number of participating nucleons N_{part} and number of binary collisions N_{coll}, none of which can be measured directly. Originally, the Glauber model was developed in the 50's to address high-energy scattering of composite particles, providing for the first time a systematic treatment and description based on quantum mechanical scattering theory. Today, the Glauber model is used regularly in all heavy-ion experiments to determine the collision geometry, in particular the *centrality* of the collision. To get the centrality classes of an heavy-ion data sample, one measures per-event the charged particle multiplicity distribution dN/dM. Once the total integral of the distribution is known, centrality classes are defined by binning the distribution on the basis of the fraction of the total integral[7] [44]. Having obtained centrality classes, all physical observables can be reported as a function of centrality classes.

In the Glauber model the collision of two nuclei is seen as the superposition of consecutive individual interactions of the constituent nucleons. Starting from such a picture, it is natural to expect that the geometry of heavy-ion collision will be strongly related to the geometric quantities $\mathbf{b}$, N_{part} and N_{coll}, that we now define. The impact parameter $\mathbf{b}$ is a vector connecting the centers of two colliding heavy-ions. The number of participating nucleons, N_{part}, is a total number of nucleons which undergo at least one inelastic nucleon-nucleon collision (in literature such nucleons are also called *wounded nucleons*, while on the other hand the nucleons which do not participate in collisions are

[7] As an example, centrality class 10%–20% is defined by the boundaries n_{10} and n_{20} which satisfy:

$$\frac{\int_{\infty}^{n_{10}} \frac{dN}{dM} dM}{\int_{\infty}^{0} \frac{dN}{dM} dM} = 0.1 \qquad \text{and} \qquad \frac{\int_{\infty}^{n_{20}} \frac{dN}{dM} dM}{\int_{\infty}^{0} \frac{dN}{dM} dM} = 0.2 \, . \tag{1.63}$$

With such definition, the head-on collisions (i.e. "most central" collisions) correspond to centrality class 0%–5% [44].

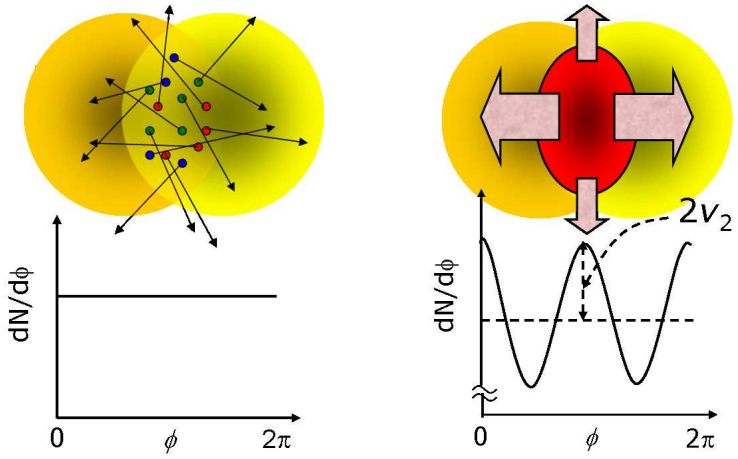

(a) Large mean free path (b) Small mean free path

Figure 1.5: Normalized azimuthal distribution $dN/d\phi$ of a non-central H.I.C.

usually referred to as *spectators*). Finally, N_{coll} is the total number of binary nucleon-nucleon collisions, the quantity which also takes into account the fact that each nucleon can interact a multiple number of times, with different nucleons it encounters on its trajectory though the volume of the opposing nucleus. For head-on collisions in Glauber model, one can show that approximately $N_{\text{coll}} \propto N_{\text{part}}^{4/3}$ irrespectively of the nucleus size [44].

In order to utilize the Glauber model two important inputs from experimental data are needed, both of which can be measured and determined independently in a separate experimental setup. The first one is the nuclear charge density, which is usually parameterized with a Woods-Saxon distribution:

$$\rho(r) = \rho_0 \frac{1 + w(r/R)^2}{1 + \exp\left(\frac{r-R}{a}\right)}, \tag{1.64}$$

where ρ_0 is the nucleon density in the center of nucleus, R is the radius of nucleus, a represents the thickness of the nucleus surface (so-called skin depth), and w describes deviations from a spherical shape (for heavy-ions used in collisions at RHIC and at the LHC, like Au, Cu and Pb, w is zero). All these parameters can be determined independently in low-energy electron scattering experiments [44]. The second input to Glauber model is the inelastic nucleon-nucleon cross section, which serves as an input due to the main assumption in the Glauber model that nucleus-nucleus collisions are treated as a superposition of many nucleon-nucleon collisions [44].

In a *Monte Carlo Glauber* model the nucleus is modeled as a set of uncorrelated nucleons sampled from the measured density distribution given in Eq. (1.64). For this implementation of the Glauber model[8], nucleons are located at specific spatial coordi-

[8]In an alternative approach, in a so-called *optical limit* approximation of Glauber model, nucleus is

nates. Therefore, the two nuclei are composed from sampled nucleons, arranged with a random impact parameter **b** and projected onto the x-y plane. Then the collision among any two nucleons will take place if the distance between nucleons in x-y plane is smaller than $\sqrt{\sigma_{\text{inel}}^{NN}/\pi}$, where $\sigma_{\text{inel}}^{NN}$ is an inelastic nucleon-nucleon cross section obtained independently in a separate measurement and here taken as an input for the model [44].

Physical meaning of v_2

We now focus on one particular harmonic and elaborate in more details about its physical meaning. It is clear that due to the collision geometry the dominant harmonic in non-central collisions will be elliptic flow v_2, so we therefore give it most of our attention. Elliptic flow quantifies how the system responds to the initial spatial ellipsoidal anisotropy [35, 40–42]. Suppose two extreme situations illustrated in Fig. 1.5. In the first case (see Fig. 1.5(a)) the mean free path among the produced particles is much larger than the typical size of the system. In this case the azimuthal distribution of the particles does not depend on azimuthal angle on average due to the symmetry of the production process. The other extreme case, when the mean free path is very small compared to the typical system size, is shown in Fig. 1.5(b). In this case hydrodynamics can be applied to describe the space-time evolution of the system. The pressure gradient along the horizontal axis is much larger than along the vertical axis due to the geometry. So the collective flow is stronger along the horizontal axis compared to the vertical axis and, which in turn, leads to an azimuthal distribution which is not uniform anymore. The amplitude of this oscillation in the normalized azimuthal distribution is exactly the elliptic flow parameter. In this way, the elliptic flow is generated by the spatial anisotropy of the almond shape due to multiple interactions among the produced particles. Therefore a measurement of elliptic flow allows us to extract some information about the mean free path in the created system.

The asymmetry characterized by the eccentricity is a very important quantity to interpret elliptic flow phenomena. To quantify the initial almond shape, the following formula can be used

$$\varepsilon_2 = \frac{\langle y^2 - x^2 \rangle}{\langle y^2 + x^2 \rangle} \,. \tag{1.65}$$

This definition determines the so-called standard eccentricity. The brackets denote an average over the transverse plane with the number density of participants as a weighting function

$$\langle \cdots \rangle = \int dxdy \cdots n_{\text{part}}(x, y) \,. \tag{1.66}$$

represented with continuous density of nucleons, i.e. unlike in Monte Carlo case nucleons are not located at specific spatial coordinates within the nucleus. As a starting point in this approach, it is assumed that at sufficiently high energies nucleons within colliding nuclei continue undeflected as two nuclei intersect each other and remain on independent linear trajectories throughout the collision (to ensure this it is also assumed that the size of the nucleus is large compared to the extent of the nucleon-nucleon force) [44]. Under such assumptions it is possible to derive approximate mathematical expressions which relate all geometric quantities of interest, namely nucleus-nucleus inelastic cross section σ_{inel}, number of participating nucleons N_{part} and number of binary collisions N_{coll}, to the starting, and measured independently, input quantities: nuclear charge densities and inelastic nucleon-nucleon cross section [44].

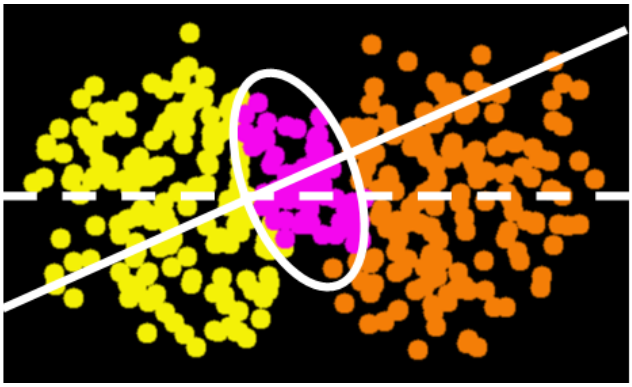

Figure 1.6: An example of participants (magenta) and spectators (yellow and orange) in a H.I.C. from a Monte Carlo Glauber model. Adopted from a presentation file by D. Hofman at Quark Matter 2006, Shanghai, China.

If the system is elongated along the y-axis, the eccentricity is positive. In more realistic situations, the eccentricity fluctuates from event to event. This fluctuation of the initial eccentricity [45–50] is particularly important to understand the elliptic flow in the small system such as Cu+Cu collisions or very peripheral and very central Au+Au collisions. Figure 1.6 shows an example event projected into the transverse plane from a Monte Carlo Glauber model. Participants are shown in magenta and spectators are in yellow and orange. In this case one could misidentify the tilted line as the reaction plane, while the true reaction plane is the horizontal axis (dashed line). The angle of the tilted plane with respect to the true reaction plane fluctuates event-by-event. It is the spatial ellipticity which determines the orientation of the tilted plane, so by taking into account the terminology introduced above this orientation is referred to as the participant plane Ψ_2. Analogously, the event-by-event fluctuations can give rise to event-by-event triangularity in initial geometry which will determine the participant plane Ψ_3, etc. Just as we cannot measure precisely the true reaction plane from experimental data, it is also impossible to measure directly these various participant planes.

Another definition, called the participant eccentricity, takes these fluctuations info account and can be used for quantifying the almond shape on an event-by-event basis:

$$\varepsilon_{\rm part} = \frac{\sqrt{(\sigma_y^2-\sigma_x^2)^2+4\sigma_{xy}^2}}{\sigma_x^2+\sigma_y^2}\,, \tag{1.67}$$

$$\sigma_x^2 = \left\{x^2\right\}-\left\{x\right\}^2\,, \tag{1.68}$$

$$\sigma_y^2 = \left\{y^2\right\}-\left\{y\right\}^2\,, \tag{1.69}$$

$$\sigma_{xy} = \left\{xy\right\}-\left\{x\right\}\left\{y\right\}\,. \tag{1.70}$$

Now the average $\{\cdots\}$ is taken over a single event generated in a Glauber Monte Carlo model.

For example, Fig. 1.7 shows the (standard) eccentricity ε_x and the momentum ec-

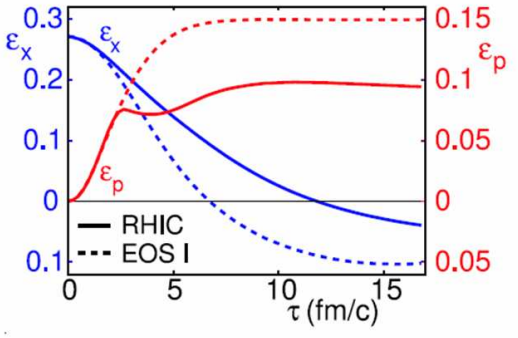

Figure 1.7: The spatial eccentricity ε_x and the momentum eccentricity ε_p as a function of the proper time τ in Au+Au collisions at $b = 7$ fm [51]. Solid and dashed curves correspond to two different sets of the EoS.

centricity

$$\varepsilon_p = \frac{\int dxdy(T_0^{xx} - T_0^{yy})}{\int dxdy(T_0^{xx} + T_0^{yy})} \tag{1.71}$$

as a function of the proper time from a hydrodynamic simulation, assuming Bjorken scaling solution in the longitudinal direction and two different sets of the EoS [51]. The spatial eccentricity ε_x decreases as the system expands and the momentum anisotropy rapidly increases at the same time. So the spatial anisotropy turns into the momentum anisotropy. The momentum anisotropy ε_p is created and saturates in the first several femtometers, so the observed v_2 is expected to be sensitive to the initial stage of the collision.

1.4 Historical snapshot

As discussed in previous sections, v_2/ε can be interpreted as a response of the system to the initial spatial eccentricity. Figure 1.8 shows v_2/ε as a function of the transverse multiplicity density $(1/S)dN_{\rm ch}/dy$ (where S is the area of overlap region, $N_{\rm ch}$ is multiplicity of charged particles, y is rapidity—defined in this way the transverse multiplicity density is Lorentz invariant and the system size independent quantity) from AGS to RHIC energies. Hydrodynamic results in Fig. 1.8 are shown as horizontal lines. The experimental data monotonically increase with particle density, while the ideal hydrodynamic response is almost flat [52]. Ideal hydrodynamics is expected to generate the maximum response among the transport models and experimental data reached this limit for the first time at RHIC.

An historical overview of the experimental results for elliptic flow obtained at experiments prior to the LHC era is presented in Fig. 1.9. We can clearly see the nontrivial dependence of elliptic flow on collision energy; the change in signature at lower energies indicates the change from flow "out-of-plane" (negative signature), to the flow "in-plane"

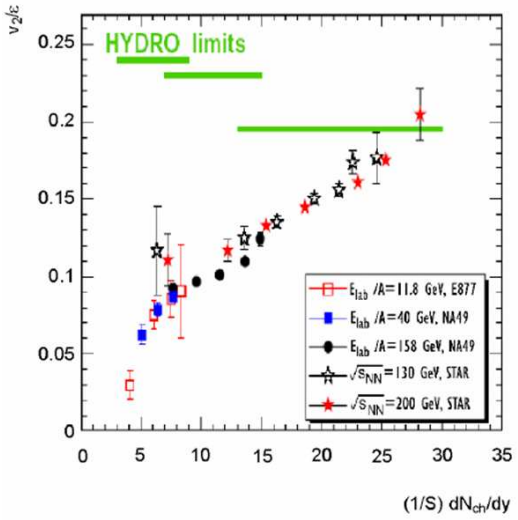

Figure 1.8: v_2/ε as a function of transverse multiplicity density compiled by NA49 Collaboration [53].

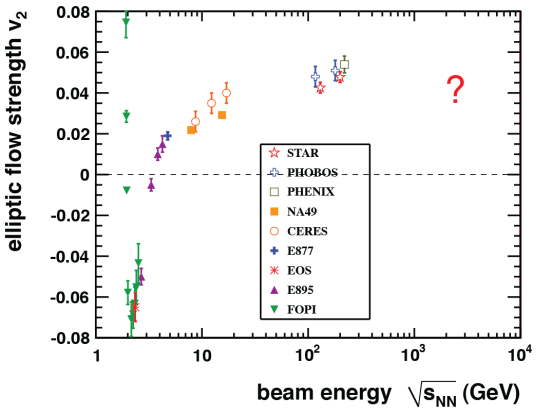

Figure 1.9: Collection of v_2 measurements in 20%-30% centrality class in the experiments prior to LHC era [74, 75].

(positive signature). Sizable values of elliptic flow at larger energies (in particular STAR, PHOBOS and PHENIX results) indicate that produced matter in gold-gold collisions at RHIC *does not* behave as a weakly interacting gas (for which v_2 would be negligible), but instead as a strongly coupled liquid. Whether the produced matter in heavy-ion collisions at LHC energies continues to show the same trend and behaves as a strongly coupled liquid will be answered in the remainder of the thesis.

Chapter 2

Experimental setup

In this chapter we briefly summarize the main aspects of the experimental setup and analysis framework used for the anisotropic flow results presented in the subsequent chapters. We start by introducing the CERN's Large Hadron Collider (LHC) in Section 2.1. In Section 2.2 we focus on one of the LHC's experiments: A Large Ion Collider Experiment (ALICE), with a basic description of the ALICE detectors which were used in the analysis. Finally, in Section 2.3 we, in short, present the offline analysis framework in ALICE.

2.1 Large Hadron Collider (LHC)

The CERN's LHC complex is located close to the French-Swiss border in the suburb of the city of Geneva, Switzerland. The accelerator components and detectors are placed on average about 100 m beneath the Earth's surface in a circular tunnel spanning 27 km in circumference (see Fig. 2.1). Main colliding systems are two: proton-proton (p-p) and lead-lead (Pb-Pb) opposite beams, but asymmetric proton-ion (p-A) collisions and collisions of lighter ions (e.g. argon) are also foreseen. The design maximum energy for p-p collisions is 7 TeV per beam (or 14 TeV centre of mass), while for Pb-Pb collisions the centre of mass energy is 5.5 TeV per nucleon pair (or 1150 TeV total). To achieve the collision energy of 7 TeV for protons in each beam, the protons have to be accelerated to 99.9999991% of the speed of light, which makes them traverse the LHC accelerator ring 11,245 times each second. The protons are grouped within each beam in bunches, where adjacent bunches are separated 25 ns in time (or about 7 m in distance). The design number of bunches per proton beam is 2808, with 1.1×10^{11} protons per bunch, resulting in a design luminosity of 10^{34} cm^{-2}s^{-1}. When two bunches cross each other, due to the smallness of protons there will be only about 20 collisions between 2.2×10^{11} protons in two intersecting bunches [21]. The average crossing rate of bunches is determined by the total number of bunches in accelerator ring, and the total number of turns the bunch makes within the accelerator ring per second, i.e. $2808 \times 11245 = 31.6$ MHz [21]. This results in a total of 20×31.6 MHz ≈ 600 million p-p collisions per second [21].

LHC experiment comprises six detector experiments: ALICE (A Large Ion Collider

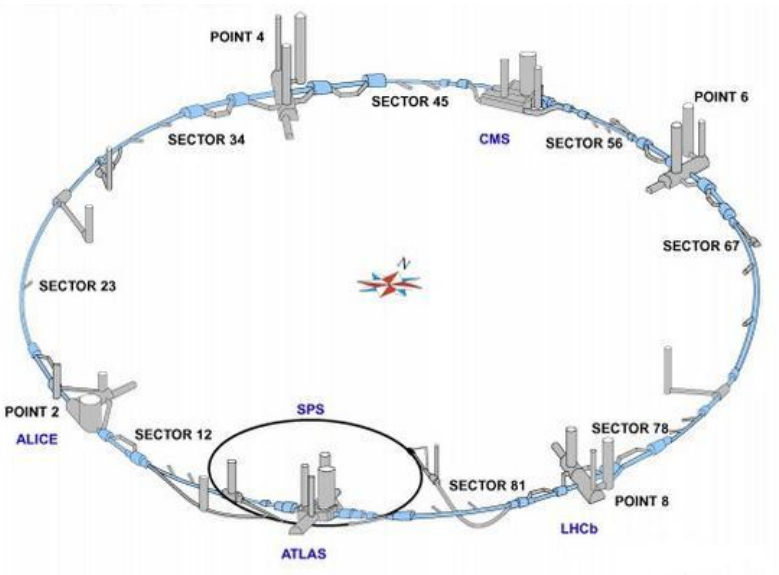

Figure 2.1: LHC complex [22].

Experiment) [23], ATLAS (A Toroidal LHC Apparatus) [24], CMS (Compact Muon Solenoid) [25], LHCb (Large Hadron Collider beauty) [26], LHCf (Large Hadron Collider forward) [27] and TOTEM (TOTal Elastic and diffractive cross section Measurement) [28], bringing together more than 10,000 scientists and engineers from the universities and laboratories from more than 100 countries. The primary physical goals at the LHC are addressing some of the most fundamental open questions in physics:

1. **Existence of Higgs boson.** The postulated elementary particle whose existence can explain the origin of mass of other elementary particles will be either confirmed or disproved at LHC energies by two general purpose experiments ATLAS and/or CMS.

2. **Properties of Quark-Gluon Plasma.** The Quark-Gluon Plasma was already shortly introduced in Section 1.2. Such study will be in particular pursued by ALICE, a dedicated heavy-ion experiment.

3. **Asymmetry between matter and antimatter.** In the observable Universe there is a vast excess of matter over antimatter, while at the time of the Big Bang they were produced at the same rate. Why starting from about 1 second after the Big Bang antimatter had all but disappeared will be addressed in a dedicated experiment LHCb, by focusing mainly on physical processes involving B mesons (composite particles containing a bottom (beauty) quark or its antiquark). To create imbalance between matter and antimatter the violation of CP symmetry must be imposed, which was observed in the decays of B mesons in previous

experiments BaBar and Belle.

4. **Supersymmetry.** Supersymmetry is a hypothesized symmetry which revolves round the idea that for each boson in the Standard Model of elementary particles there exists a corresponding fermion with the same internal quantum numbers and mass, and vice-versa. The reason why we did not see these superpartners in experiments so far is that this symmetry is broken, making all superpartners much heavier and much more difficult to produce. If they indeed exist, the lightest of these massive superpartners might be produced in the collisions at LHC energies for the very first time in controlled environment.

5. **Origin of Dark Matter and Dark Energy.** Experimental evidence shows that the composition of Universe is only about 4% due to ordinary baryonic matter, which gives rise only to the visible part of Universe, while about 23% and about 73% are due to Dark Matter and Dark Energy, respectively. The details of Dark Matter and Dark Energy remain so far unknown and directly unobservable. Discoveries at LHC energies might in particular shed light on the Dark Matter physics, i.e. one or more of so far only hypothesized Dark Matter candidate particles can be produced at LHC.

6. **Extra dimensions.** Currently widespread and popular theories, like for instance String Theory, demand the existence of additional spatial dimensions besides the standard three macroscopic spatial dimensions characterizing the Euclidean space. Such extra spatial dimensions might be detectable at LHC energies.

Although conceived in the early 80's and approved by CERN Council in 1994, the very first collisions at LHC occurred only in 2008, due to the various design challenges and cutting edge new technologies required during its development. In particular, the very first p-p collisions at 900 GeV centre of mass energy were delivered at LHC in September 2008. LHC operations were successfully continued in November 2009 after more than 1 year shutdown due to the serious incident caused by a faulty electrical connection between two magnets, which occurred during the first p-p collisons in 2008. At the end of November 2009, by achieving the energy of 1.18 TeV per proton beam, LHC became the most powerful accelerator in the world. The first p-p collisions at centre of mass energy of 7 TeV were delivered in March 2010, and the first Pb-Pb collisions at centre of mass energy of 2.76 TeV per nucleon pair in November 2010.

2.2 A Large Ion Collider Experiment (ALICE)

The ALICE detector is located in Saint-Genis-Pouilly, France. The ALICE detector has been embedded within the large solenoid magnet existing already at that location in the accelerator ring from the previous L3 experiment from the Large Electron-Positron Collider (LEP) era (see Fig. 2.2). The ALICE detector contains 18 subdetectors most of which were fully completed and operational at LHC startup in 2008. In the subsequent sections we will highlight only four of these 18 subdetectors which were crucial for the analysis pursued in this thesis: the Time Projection Chamber (TPC), the Inner

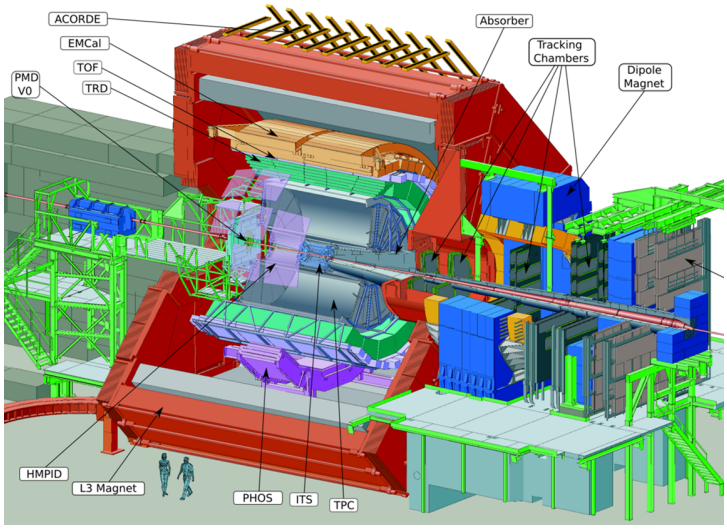

Figure 2.2: ALICE detector.

Tracking System (ITS), the VZERO and the Zero Degree Calorimeter (ZDC) (a detailed description of all ALICE subdetectors can be found in [29]).

The ALICE experiment is a dedicated heavy-ion experiment. Its first primary physical goal is the study of the properties of quark-gluon plasma, the deconfined state of matter which existed shortly after the Big Bang. By colliding heavy ions at LHC energies temperatures are being achieved which are 100,000 times larger than that at the centre of the Sun. At such extreme conditions all composite particles will decompose into quarks, the more fundamental building blocks, which cannot exist deconfined at ordinary temperatures and energy densities. ALICE will try to provide the understanding of the physics behind the quark confinement in hadrons and quark deconfinement in quark-gluon plasma. As a second primary physical goal ALICE will try to answer why the sum of individual quark masses are so much lighter than the masses of composite objects they are building up (e.g. baryons and mesons).

The ALICE collaboration consists of more than 1,000 scientists and engineers from more than 30 countries. ALICE detector is 26 m long, 16 m high and 16 m wide. It weights 10,000 tones and it costed 115 MCHF.

2.2.1 Time Projection Chamber (TPC)

The TPC detector [29, 30] is one of the biggest and one of the most important ALICE systems. It has a cylindrical shape separated in two volumes with a cathode in the middle (see Fig. 2.3), with a longitudinal length (the length alongside beam direction) of 5 m, the innermost radius of 85 cm and outer radius of 250 cm. It is a gaseous detector filled with a 90 m^3 gas mixture of $Ne/CO_2/N_2$ and it is the main tracking device in ALICE. The TPC gas is being ionized by the traversing charged particles, after which

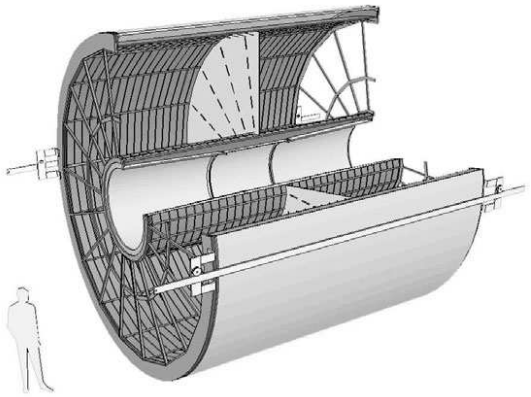

Figure 2.3: ALICE's Time Projection Chamber (TPC).

the liberated electrons drift towards the end plates. The drift time information can be used to determine the z coordinate, while the r and ϕ coordinates are obtained directly from the position of the end plates. It is the TPC's slow drift time of about ~ 90 μs which is the limiting factor for the maximum luminosity ALICE can handle. The TPC was designed to cope with a large number of particles per event in Pb-Pb collisions, which in the most central collisions was expected to reach about 20,000 primary and secondary particles. When it comes to the phase space coverage, the TPC is capable of detecting the particles in the transverse momentum range $0.1 < p_t < 100$ GeV/c, with a transverse momentum resolution of about 6% for $p_t < 20$ GeV/c in central Pb-Pb collisions, and about 4.5% for $p_t < 20$ GeV/c in p-p collisions [29]. For higher transverse momenta the resolution deteriorates, and for instance in interval $60 < p_t < 80$ GeV/c it is about 25% in central Pb-Pb collisions, and about 22% in p-p collisions [29]. On the other hand, the track finding efficiency of TPC saturates at about 90% for $p_t > 1$ GeV/c, both in central Pb-Pb collisions and p-p collisions, which is essentially determined by the size of the TPC dead zones. The TPC covers full azimuth, with the exception of dead zones between the neighboring sectors (there are 16 sectors altogether), which in total adds up to about 10% of the azimuthal angle [29]. The TPC's azimuthal resolution is about $\Delta\varphi = 0.7$ mrad irrespectively of the transverse momentum [31]. Finally, the TPC has a pseudorapidity coverage of $|\eta| < 0.9$ if only the tracks with maximum radial track length are being considered.

Besides the primary usage for tracking, the TPC also provides valuable information about distinct particle species (particle identification (PID)) via standard dE/dx technique. Moreover, TPC is also used as a centrality estimator with a resolution of about 0.5% centrality bin width in the most central collisions [84]. Its uniform azimuthal coverage makes the TPC the ideal detector for anisotropic flow analysis, because any inefficiencies in the detector's azimuthal acceptance would result in non-negligible systematic biases for such an analysis.

2.2.2 Inner Tracking System (ITS)

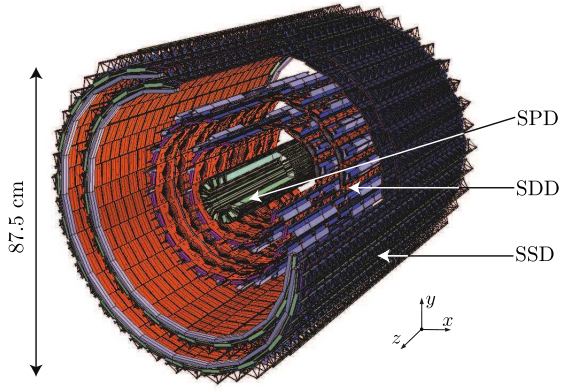

Figure 2.4: ALICE's Inner Tracking System (ITS). The innermost part is Silicon Pixel Detector (SPD), the part in the middle is Silicon Drift Detector (SDD), and the outermost part is Silicon Strip Detector (SSD).

The ALICE Inner Tracking System [29, 32] consists of 6 silicon layers, grouped in three distinct groups of two layers forming three distinct detectors. The innermost two silicon layers are composed of Silicon Pixel Detector (SPD), the third and fourth layer consist of Silicon Drift Detector (SDD), and the outermost two layers are based on Silicon Strip Detector (SSD), see Fig. 2.4. The ITS is placed inside the inner TPC radius and it is the central barrel system closest to the interaction point and beam pipe (see Fig. 2.2). The diameter of beam pipe is 6 cm, providing the lower physical boundary for the innermost radius of ITS. On the other hand, the outermost radius of ITS is bounded by the radius of innermost TPC volume (see Table 2.1 for the summary of the most important sizes of three ITS' detectors [29]).

Table 2.1: Dimensions of the ITS detectors.

Layer	Type	r (cm)	$\pm z$ (cm)
1	pixel	3.9	14.1
2	pixel	7.6	14.1
3	drift	15.0	22.2
4	drift	23.9	29.7
5	strip	38.0	43.1
6	strip	43.0	48.9

The ITS is being used both for primary vertex reconstruction, with a resolution better than 100 μm, and for the reconstruction of secondary vertices [1]. Phase space coverage

of ITS has the following characteristics: Transverse momentum is covered within the range $0.1 < p_t < 3$ GeV/c with a relative momentum resolution better than 2% for pions in this transverse momentum range [29], while for $p_t > 3$ GeV/c ITS still can be used to improve the transverse momentum resolution for the tracks which also traverse the TPC. Coverage in pseudo-rapidity is $|\eta| < 0.9$, while the coverage in azimuth by design is uniform in 360° but in reality due to cooling problems in two innermost layers the resulting azimuthal acceptance is non-uniform. Although ITS has standalone tracking capabilities, which makes it also possible to reconstruct in ALICE the charge particles traversing the dead zones of TPC and to reconstruct the low p_t particles which do not make it into TPC, its main role when it comes to tracking is the improvement of transverse momentum and angle resolution of particles reconstructed by TPC.

The PID capabilities of the ITS rely on standard dE/dx techniques applicable in the 4 outer most layers (SDD and SSD). The SPD detector is being used as a centrality estimator, with a resolution of about 0.5% centrality bin width in the most central collisions [84]. Finally, the SPD detector is also used as an online trigger, but more on this in subsequent sections in this chapter.

2.2.3 VZERO

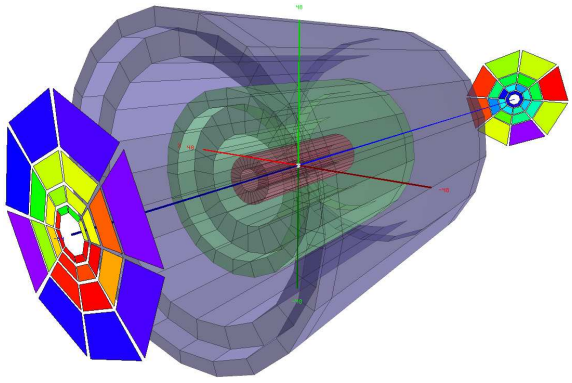

Figure 2.5: VZERO detectors on both sides of ITS.

The VZERO detector [29,33] consists of two separate arrays of scintillator counters, V0A and V0C, placed on different sides of the central barrel detectors along the beam line (see Fig. 2.5). V0A and V0C are placed asymetrically with respect to the interaction point: V0A is located 340 cm from the interaction point on the side opposite to the muon arm (see Fig. 2.2), while V0C is placed 90 cm from the interaction point on the opposite side from V0A. Because of this asymmetry, V0A and V0C have different pseudo-rapidity coverage. V0A covers pseudo-rapidity range $2.8 < \eta < 5.1$, while V0C covers $-3.7 < \eta < -1.7$. Each set of VZERO arrays contains 32 elementary counters arranged in 4 rings and 8 sectors of 45° (see Fig. 2.5).

The VZERO detector serves various purposes within the ALICE experiment. V0A

and V0C each provide one online trigger which is an OR of all scintillator signals above threshold. The pulse shape an arrival times are measured and decoded offline. Next, the VZERO detector is utilized for centrality determination, with a resolution of about 0.5% centrality bin width in the most central collisions, and resolution still better than 2% centrality bin width for peripheral collisions [84].

2.2.4 Zero Degree Calorimeter (ZDC)

The Zero Degree Calorimeter (ZDC) [29, 34] is ALICE's hadron calorimeter used primarily for the determination of the collision centrality. It consists of four separate calorimeters, 2 for protons and 2 for neutrons, placed in groups of two at the distance of about 115 m along the beam line on each side of the interaction point. When two nuclei collide only a fraction of nucleons participate in the collision (so-called "participants"), while other nucleons proceed away from the interaction point unaffected (so-called "spectators"). The ZDC measures the energy of the spectator nucleons, the energy which is correlated with the overlapping region between the two colliding nuclei (larger overlapping region involve more nucleons in the collisions, leaving less spectators to reach ZDC and hence less energy is deposited there in the calorimeters). The LHC magnets will affect in a different way spectator protons and spectator neutrons after the collisions. The spectator protons will be slightly deflected with respect to the beam direction while spectator neutrons will fly away after the collisions basically at zero degree. It is therefore required to place calorimeters for protons and neutrons at slightly different positions with respect to the beam line; proton calorimeters are placed external to the outgoing beam, while neutron calorimeters are placed between the two beams. The centrality estimated in ALICE with ZDC has a resolution of about 1% in most central collisions, which quickly deteriorate to 3% in midcental collisions [84]. ZDC also has trigger capabilities which will be described later in this chapter.

2.3 Offline framework

The ALICE offline framework [1, 76, 77] has been developed in order to reconstruct and analyse the data coming both from simulated and real collisions. The ALICE offline framework is dubbed AliRoot [76] and has been built on top of another less specific framework called ROOT [77]. The ROOT system is an object-oriented framework (written in C++) developed at CERN in the 90's and used by various collaborations worldwide as a starting framework on top of which the specific framework needed for particular collaboration is being built. It provides a full set of features needed for event generation, detector simulation, event reconstruction, data acquisition and data analysis. All features are encoded in a set of about 650 classes grouped in about 40 libraries. A vast majority of ROOT classes inherit from the common base class called `TObject`, which provides default behaviour and protocol (e.g. protocol for the object I/O, error handling, sorting, inspection, printing, drawing, etc.) for all objects in the ROOT system, but the standalone classes which can be used as built-in types (e.g. `TString, TRegExp, TTime`) are also implemented. ROOT offers its own C++ interpreter called CINT, which covers about 95% of ANSI C and about 90% of ANSI C++. ROOT capa-

bilities and functionality are also extended for the needs of parallel computing and have resulted in a product called the PROOF system [78].

The base AliRoot classes are placed in the STEER module. Each detector system forms an independent module containing the detector specific code for simulation and reconstruction. After events are generated via various event generators (e.g. Pythia [79], Hijing [80]) the detector response is simulated via various transport codes (e.g. GEANT3 [81]). The simulation framework is flexible enough to offer the possibility to combine underlying events and rare signal events at the primary particle level (a so-called coctail) and on the digit[1] level (so-called merging). Final state particle correlations are being introduced in a controlled way using afterburners.

2.3.1 Minimum bias event selection

The main requirements of the definition of minumum bias (MB) trigger are large efficiencies for low multiplicity and diffractive events, and a good rejection of beam-backgrounds interactions [82]. The main detectors in ALICE used at hardware level ("online") for this purpose are VZERO and SPD, already introduced in Sections 2.2.2 and 2.2.3, respectively. The VZERO detector is capable of selecting events from real collisions and can also reject the interactions of the beam with the residual gas in the beam pipe. The VZERO detectors are making use of the fact that the arrival time of particles to V0A and V0C is different in beam–beam and in beam-gas interactions. In particular, particles originating from real collisions will arrive at the V0A (V0C) arrays approximately 11.3 ns (3.0 ns) after the time when the bunches coming from opposite directions crossed the nominal interaction point in ALICE [82]. On the other hand, the particles originating from beam-background collisions will arrive V0A and V0C arrays at significantly different times. For the SPD, the FastOR (FO) trigger is formed by trigger signals, one produced for each chip of the SPD [82]. There are 1200 FO trigger signals which can be combined logically to form the FO trigger. In addition to VZERO and SPD, also the ZDC detector is used for minimum bias event selection at reconstruction level ("offline"). In particular, electromagnetically induced interactions are rejected by requiring an energy deposition above 500 GeV in each of the neutron Zero Degree Calorimeters (ZDCs) positioned at $\pm$ 114 m from the interaction point [83].

Based on this, the minimum-bias interaction trigger used in ALICE in the beginning of data taking required at least two out of the following three conditions [85]: (i) two pixel chips hit in the outer layer of the SPD, (ii) a signal in V0A, (iii) a signal in V0C.

2.3.2 Event reconstruction and tracking

The final goal of event reconstruction [1, 29, 31, 76] is to create the output file, so called *Event Summary Data* (ESD), from the starting input digits. The ESD file contains all information needed for a physics analysis (e.g. run number, event number, trigger word, version of the reconstruction, primary vertex, array of ESD tracks, arrays of reconstructed secondary vertexes, etc.). The reconstruction starts with the local reconstruction of clusters in each detector (cluster is a set of adjacent (in space and/or in

[1] Digit is a digitized signal obtained by a sensitive pad of a detector at a certain time.

time) digits that were presumably generated by the same particle crossing the sensitive element of a detector), after which vertexes and tracks are reconstructed and particles types are being identified. The reconstructed track is determined with a set of five parameters (such as the curvature and the angles) of the particles trajectory together with the corresponding covariance matrix estimated at a given point in space. The track reconstruction in each detector can be done independently from the status of other detectors, but the information from other detectors (if useful) can be used as well.

There are three passes which are being performed during tracking.[2] The first pass starts with track finding and fitting in inward direction in the TPC and then in the ITS. This pass starts by finding the track candidates in the outer radius of TPC, where the track density is low, and goes on towards the inner radius of TPC, after which it is continued to the ITS. The primary vertex position is estimated from the clusters of the two innermost layers of ITS, and the ITS tracker is trying to prolong the TPC track as close as possible to the primary vertex. In addition, the ITS performs as a standalone tracker for ITS clusters not having a corresponding match in the TPC (e.g. for the tracks traversing the dead zones on TPC). In the second pass starting from ITS the track reconstruction is performed in the outward direction towards all detectors. At this step also the first estimation of particle type is performed. In the final third pass all the tracks are refitted in the inward direction in order to get the track parameters at the vertex. The tracks which pass this step are also used for the determination of the secondary vertex. Finally, arrays of reconstructed tracks with accompanying physical characteristics are stored in ESD, from which they are used in physics analyses.

[2]The main method used in ALICE for tracking is Kalman filtering introduced in 1983 by P. Billior [99].

Chapter 3

Q-cumulants

Anisotropic flow measurements are based on an analysis of azimuthal correlations and might be biased by contributions from correlations that are not related to the initial geometry, which are called *nonflow*. The most frequently used method in flow analysis is the standard *event plane method* (EP) [58], which will be briefly summarized below. This method is biased by contributions from nonflow. To improve the anisotropic flow measurements advanced methods based on genuine multi-particle correlations (*cumulants*) have been developed which suppress systematically the nonflow contribution [54–56]. These multi-particle correlations can be calculated by looping over all possible multiplets, however this quickly becomes prohibitively CPU intensive. Therefore, the most used technique for cumulant calculations is based on generating functions (GFC) [54–56]. This approach in calculating cumulants involves approximations, which might lead to systematic biases, which complicate the interpretation of the results. In this chapter we present an exact method for direct calculations of multi-particle cumulants using moments of the flow vectors, so-called Q-cumulants (QC) [59]. The detailed description of Q-cumulants will form the bulk of this chapter. Also recently, a Lee-Yang-Zero method (LYZ) [60–63] has been developed to suppress nonflow contribution to all orders. Closely related to that are methods of Fourier and Bessel transforms of the q-distributions [65], and the method of a direct fit of the q-distribution (FQD). In this chapter we will highlight the main characteristics of some of these methods.

Before proceeding further, we define one of the central objects in anisotropic flow analysis, the so called *Q-vector*, or *flow vector*. The Q-vector evaluated in the harmonic n is a complex number denoted by Q_n and is defined as:

$$Q_n \equiv \sum_{i=1}^{M} e^{in\phi_i} \,, \tag{3.1}$$

where M is the number of particles in an event, and ϕ_i labels the azimuthal angle of i-th particle measured in a fixed coordinate system in the laboratory.

3.1 A bit of history

3.1.1 Standard event plane method (EP)

The most commonly used method in the anisotropic flow analysis is the standard event plane method [58]. In this method the true reaction plane angle is estimated and all particle's azimuthal angles are correlated to this estimated plane in order to get the flow harmonics v_n. Taking into account all symmetries of the collision discussed in Section 1.3.3 and neglecting, for simplicity, effects of fluctuations in initial geometry, we have

$$\frac{dN}{d\phi} = \frac{1}{2\pi}\left[1 + \sum_{n=1}^{\infty} 2v_n \cos[n(\phi - \psi_R)]\right], \tag{3.2}$$

from which it follows

$$v_n = \langle \cos[n(\phi - \psi_R)] \rangle \ . \tag{3.3}$$

The reaction plane is a plane spanned by the impact parameter $\mathbf{b}$ and the beam line z (see Fig. 1.4), and its orientation in a laboratory frame is denoted with ψ_R. The orientation of the reaction plane randomly changes event-by-event and it cannot be measured directly. Instead, we use the measured azimuthal angles of the detected particles and for each event we estimate the orientation of reaction plane. This estimate is called *event plane* and it is given by [58]:

$$\psi_R \simeq \psi_{\mathrm{EP}} \equiv \frac{1}{n} \arctan \frac{\sum_i \sin(n\phi_i)}{\sum_i \cos(n\phi_i)} \, . \tag{3.4}$$

Here independent results for ψ_{EP} can be obtained for different harmonics n. In practice, since in each event there is a finite number of created particles, the result for ψ_{EP} will be affected by a limited resolution. This can be corrected for by estimating the event plane resolution from the correlations obtained via two or more independent subevents [58].

The main drawback of the standard event plane method is the fact that the event plane resolution is affected by correlations which do not stem from genuine correlation of all particles with the true reaction plane. This will introduce a bias in the flow estimates. In order to reduce this bias an alternative approach was proposed in the flow analysis—which doesn't require the reaction plane estimation event-by-event—which we introduce in detail in the subsequent sections.

3.1.2 Fitted q-distribution (FQD)

As indicated in the previous section, anisotropic flow is quantified by the values of Fourier harmonics in the Fourier series expansion of azimuthal particle distribution $dN/d\phi$ (see Eq. (3.2)). Direct and precise reconstruction of this distribution via Eq. (3.3) from the measured azimuthal angles of reconstructed particles is not feasible in practice because the orientation of reaction plane Ψ_R cannot be estimated reliably event-by-event. Clearly, by definition the experimental distribution of measured azimuthal angles is sensitive to the flow harmonics v_n in each event. Moreover, any observable which is defined to be a function of measured azimuthal angles will be sensitive to the flow harmonics v_n

as well. The underlying idea now is to come up with an observable which is a function of measured azimuthal angles (hence has indirectly the sensitivity to flow harmonics v_n), and in addition invariant in each event to the orientation of the reaction plane Ψ_R. One example of such an observable is the so-called *modulus of reduced Q-vector*, q_n, which is defined as:

$$q_n \equiv \frac{|Q_n|}{\sqrt{M}}\,. \tag{3.5}$$

In the above definition Q_n is the Q-vector defined in (3.1) and M is the multiplicity of an event. The requirement for the factor $1/\sqrt{M}$ in definition (3.5) can easily be understood as follows. In the case of a data sample consisting of uncorrelated (i.e. randomly sampled) particles, the modulus $|Q_n|$ grows as $\sqrt{M}$. In this case the Q-vector is nothing but the sum of random unit steps in a 2D plane, and the problem is completely equivalent to the famous "random walk problem in 2D", for which it is known that the distance from the origin grows as a $\sqrt{\text{number of steps}}$. In the context of the Q-vector definition, the "new step" is made by adding a new particle to the Q-vector, hence the total number of steps is the multiplicity M, and the "distance from the origin" is $|Q_n|$. This means that, as defined in Eq. (3.5), the modulus of reduced Q-vector, q_n, will not exhibit any trivial dependence on multiplicity, and as a consequence its distribution will not be systematically biased by trivial event-by-event multiplicity fluctuations. In addition q_n is clearly independent of the reaction plane orientation event-by-event, simply because (3.5) only depends on the relative differences between the azimuthal angles.

Having introduced the modulus of the reduced Q-vector as a quantity of interest, what remains is to show how it depends on the anisotropic flow coefficients v_n. This was derived in [36]:

$$\frac{dN}{dq_n} = \frac{q_n}{\sigma_n^2} \exp\left(-\frac{v_n^2 M + q_n^2}{2\sigma_n^2}\right) I_0\left(\frac{q_n v_n \sqrt{M}}{\sigma_n^2}\right)\,. \tag{3.6}$$

In above equation I_0 is a modified Bessel function of the first kind, and M is the multiplicity. We see that the flow harmonic v_n appears as one of the parameters in the above expression, and experimentally can be obtained by fitting the measured dN/dq_n distribution. Another parameter appearing in (3.6) is σ_n^2, which quantifies the systematic bias originating both from nonflow and statistical flow fluctuations [74]. In the ideal case, when only flow correlations are present in a data sample, $\sigma_n^2 = \frac{1}{2}$ [74].

The estimate of v_n obtained by fitting the dN/dq_n distribution with Eq. (3.6) is denoted as $v_n\{\text{FQD}\}$, or alternatively as $v_n\{\text{q-dist}\}$. As an example, using a toy model, we show in Fig. 3.1 the q-distribution and corresponding fit by utilizing theoretical distribution given in Eq. 3.6.

The fitted q-distribution method has four serious limitations: a) it cannot be generalized to obtain differential flow; b) the equation (3.6) is strictly valid only for large multiplicities; c) it is biased when other harmonics are present, in particular when they are larger than the harmonic under study[1]; d) it cannot be used for detectors with poor

[1] As an example, the presence of harmonic v_4 in the data sample will systematically bias the estimated v_2 harmonic, indicating that theoretical result (3.6) needs generalization for the case when multiple harmonics are present in the system.

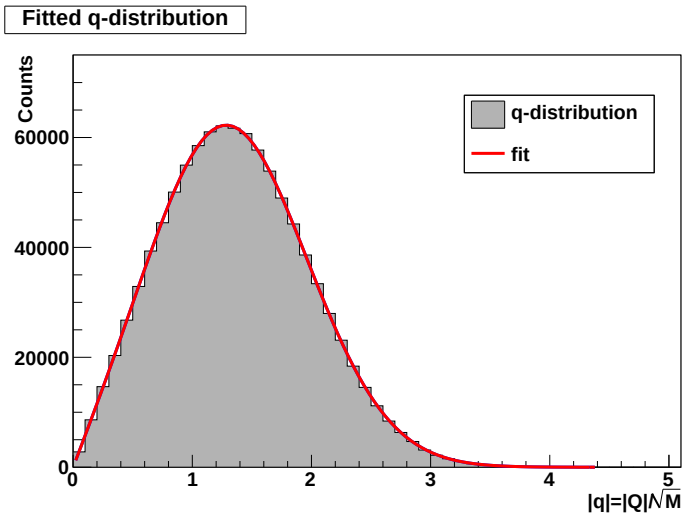

Figure 3.1: Example of a fitted q-distribution. Azimuthal angles of particles were sampled from a Fourier-like p.d.f. given in Eq. (3.2), parameterized with one harmonic $v_2 = 0.05$. The orientation of the reaction plane Ψ_R was randomized uniformly event-by-event. In each event 500 particles were sampled, in a total of 10^6 events. The resulting q-distribution is shown in the solid grey area, while the resulting fit, using Eq. (3.6), is shown as the red curve. From the fit the estimated value of v_2 is $v_2\{\text{FQD}\} = 0.05003 \pm 0.00004$.

azimuthal acceptance.

3.1.3 Lee-Yang Zeroes (LYZ)

In a series of papers [60–63], Bhalerao *et al.* have introduced a new method for anisotropic flow analysis, which they dubbed *Lee-Yang Zeroes (LYZ)* method. The LYZ method provides the genuine collective estimate for the anisotropic flow harmonic v_n. This estimate is by design not sensitive to the contributions from correlations involving only few particles. The theoretical details of the LYZ method are rather sophisticated and will not be presented here, but the interested reader can consult [60, 61]. In this section we will highlight only the basics.

We start by defining the quantity V_n as an all-event average [62]:

$$V_n \equiv \left\langle \sum_{i=1}^{M} \cos[n(\phi_i - \Psi_R)] \right\rangle_{\text{evts}} . \tag{3.7}$$

All symbols on the RHS have the same meaning as in previous two sections. Assuming for simplicity that the multiplicity M in each event is the same, we have $V_n = Mv_n$. The LYZ method gives V_n in the one over the data. To achieve this, for each event the

following complex-valued function is evaluated [62]:

$$g^{\theta}(ir) = \prod_{j=1}^{M} [1 + ir\cos[n(\phi_j - \theta)]]\,, \tag{3.8}$$

by selecting few values of a real positive variable r and few equally spaced angles θ in a laboratory. In the next step for each value of r and θ, the all-event average is being computed [62]:

$$G^{\theta}(ir) \equiv \left\langle g^{\theta}(ir) \right\rangle_{\text{evts}}\,. \tag{3.9}$$

For each value of θ, one determines the first positive minimum of the modulus $\left|G^{\theta}(ir)\right|$. Such a minimum is called the Lee-Yang Zero and it is denoted r_0^{θ}. Finally, V_n, as defined by Eq. (3.7), is estimated as [62]:

$$V_n^{\theta}\{\text{LYZ}\} = \frac{j_{01}}{r_0^{\theta}}\,, \tag{3.10}$$

where $j_{01} = 2.40483$ is the first zero of the Bessel function J_0. In the very last step one averages the result (3.10) over all angles θ, and in this way all systematic biases from trivial anisotropies stemming from a non-uniform azimuthal acceptance are averaged out [62]. The procedure outlined here can be generalized to obtain differential flow estimates [62]. Since the generating function used in Eq. (3.8) is defined as a product, this version of the Lee-Yang Zero method is also being referred to as the *Lee-Yang Zero Product (LYZP)* method.

In an alternative approach, one can start by making the projection to an arbitrary laboratory angle θ of the Q-vector:

$$Q_n^{\theta} = \sum_{i=1}^{M} \cos[n(\phi_i - \theta)]\,, \tag{3.11}$$

and evaluate the following generating function:

$$G_n^{\theta}(ir) = \left|\left\langle e^{irQ_n^{\theta}} \right\rangle_{\text{evts}}\right|\,. \tag{3.12}$$

This is an analogous expression to the one used in Eq. (3.9), and from this point onwards the remaining technical steps which yields Eq. (3.10) are the same. This version of the method is being referred to as the *Lee-Yang Zero Sum (LYZS)* method.

The LYZ method was conceived to provide an estimate for v_n isolating only the genuine collective contribution. From a theoretical point of view, LYZ is therefore the best method to perform anisotropic flow analysis. Automatic correction for non-uniform acceptance is built-in at the level of the generating functions being used. However, in practice the LYZ method has one serious drawback: It requires two passes over the data in order to get the differential flow. In addition, the LYZS version, just like the FQD method, cannot disentangle the interference between various harmonics. On the other hand, the LYZP version was designed to disentangle such interference.

3.1.4 Two- and multi-particle azimuthal correlations

In this section we consider for simplicity only 2- and 4-particle azimuthal correlations—the generalization to azimuthal correlations involving more particles is straightforward. Any correlation involving more than two particles we classify as a multi-particle correlation. In the way we define it, the average 2- and 4-particle azimuthal correlations are obtained through an averaging procedure which consists of two distinct steps.

In the first step we define the *single-event* average 2- and 4-particle azimuthal correlations in the following way:

$$\langle 2\rangle \equiv \left\langle e^{in(\phi_1-\phi_2)}\right\rangle \equiv \frac{1}{\binom{M}{2}2!}\sum_{\substack{i,j=1\\(i\neq j)}}^{M} e^{in(\phi_i-\phi_j)}, \tag{3.13}$$

$$\langle 4\rangle \equiv \left\langle e^{in(\phi_1+\phi_2-\phi_3-\phi_4)}\right\rangle \equiv \frac{1}{\binom{M}{4}4!}\sum_{\substack{i,j,k,l=1\\(i\neq j\neq k\neq l)}}^{M} e^{in(\phi_i+\phi_j-\phi_k-\phi_l)}. \tag{3.14}$$

In the above two equations ϕ_i is the azimuthal angle of the i-th particle measured in the laboratory frame. In order to avoid a trivial and strong contribution coming from autocorrelations we have enforced the constraints $i\neq j$ and $i\neq j\neq k\neq l$ in Eqs. (3.13) and (3.14), respectively.

In the second step we define the final, *all-event*, average 2- and 4-particle azimuthal correlations:

$$\langle\langle 2\rangle\rangle \equiv \left\langle\left\langle e^{in(\phi_1-\phi_2)}\right\rangle\right\rangle \equiv \frac{\sum_{i=1}^{N}(W_{\langle 2\rangle})_i\,\langle 2\rangle_i}{\sum_{i=1}^{N}(W_{\langle 2\rangle})_i}, \tag{3.15}$$

$$\langle\langle 4\rangle\rangle \equiv \left\langle\left\langle e^{in(\phi_1+\phi_2-\phi_3-\phi_4)}\right\rangle\right\rangle \equiv \frac{\sum_{i=1}^{N}(W_{\langle 4\rangle})_i\,\langle 4\rangle_i}{\sum_{i=1}^{N}(W_{\langle 4\rangle})_i}, \tag{3.16}$$

where N is the number of events. In the second step we have introduced the event weights $W_{\langle 2\rangle}$ and $W_{\langle 4\rangle}$. The choice for the event weights in Eqs. (3.15) and (3.16) *is not arbitrary* and, as we will outline now shortly, it has a physical meaning which will render the number of combinations (i.e. number of distinct 2- and 4-particle combinations one can form for an event with multiplicity M) as the only correct event weight.

To see this, consider a data sample consisting of N events, where the multiplicity of the i-th event is denoted by M_i. Equivalently, by reasoning from all-events' point of view we would define naturally the all-event average 2-particle azimuthal correlation directly as

$$\langle\langle 2\rangle\rangle \equiv \frac{\displaystyle\sum_{i=1}^{N}\sum_{\substack{a,b=1\\(a\neq b)}}^{M_i} e^{in(\phi_{i,a}-\phi_{i,b})}}{\displaystyle\sum_{i=1}^{N}\sum_{\substack{a,b=1\\(a\neq b)}}^{M_i}}. \tag{3.17}$$

This definition ensures four important things. First, in each event we have taken into account all possible distinct pairs of particles[2]. Second, by imposing constraint $a \neq b$ we have by definition completely eliminated all contributions from autocorrelations. Third, this definition ensures that we are not correlating two particles belonging to two different events (such correlation would only unneccessarily dilute the genuine physical correlations which exist only among the particles created in the same event). Finally, if we take two distinct pairs of particles, one formed in event A and another formed in event B, then the above definition ensures that these two distinct pairs of particles will be taken into account at equal footing (i.e. a unit weight has being assigned to each distinct pair of particles in any event in Eq. (3.17)). The denominator in definition (3.17) simply counts the total number of all such distinct pairs in all events.

For a data sample consisting only of the i-th event the definition (3.17) reduces to

$$\langle 2 \rangle_i \equiv \frac{\sum\limits_{\substack{a,b=1 \\ (a \neq b)}}^{M_i} e^{in(\phi_{i,a}-\phi_{i,b})}}{\sum\limits_{\substack{a,b=1 \\ (a \neq b)}}^{M_i}}\,, \tag{3.18}$$

where by $\langle 2 \rangle_i$ we denote the average 2-particle azimuthal correlation in the i-th event. The denominator in definition (3.18) counts the total number of distinct pairs in the i-th event and can be evaluated as follows:

$$\sum_{\substack{a,b=1 \\ (a \neq b)}}^{M_i} = \left(\sum_{a=1}^{M_i}\right)\left(\sum_{b=1}^{M_i}\right) - \sum_{a=b=1}^{M_i} = M_i^2 - M_i = M_i(M_i-1)\,. \tag{3.19}$$

We insert this result in both (3.17) and (3.18) and obtain

$$\langle\langle 2 \rangle\rangle = \frac{\sum\limits_{i=1}^{N}\sum\limits_{\substack{a,b=1 \\ (a \neq b)}}^{M_i} e^{in(\phi_{i,a}-\phi_{i,b})}}{\sum\limits_{i=1}^{N} M_i(M_i-1)}\,, \tag{3.20}$$

and

$$\langle 2 \rangle_i = \frac{\sum\limits_{\substack{a,b=1 \\ (a \neq b)}}^{M_i} e^{in(\phi_{i,a}-\phi_{i,b})}}{M_i(M_i-1)}\,. \tag{3.21}$$

[2]By distinct pair of particles we mean a pair (ϕ_a, ϕ_b) in which $\phi_a \neq \phi_b$, and ordering matters.

Having obtained the result (3.21), we see immediately that the definitions (3.17) and (3.13) are consistent. We can now rewrite trivially Eq. (3.20) as

$$\langle\langle 2\rangle\rangle = \frac{\displaystyle\sum_{i=1}^{N} M_i(M_i-1) \times \frac{\displaystyle\sum_{\substack{a,b=1 \\ (a\neq b)}}^{M_i} e^{in(\phi_{i,a}-\phi_{i,b})}}{M_i(M_i-1)}}{\displaystyle\sum_{i=1}^{N} M_i(M_i-1)}\,, \tag{3.22}$$

and finally insert the RHS of Eq. (3.21) into numerator of Eq. (3.22) to obtain

$$\langle\langle 2\rangle\rangle = \frac{\displaystyle\sum_{i=1}^{N} M_i(M_i-1) \times \langle 2\rangle_i}{\displaystyle\sum_{i=1}^{N} M_i(M_i-1)}\,. \tag{3.23}$$

We see immediately from result (3.23) that the event weight number of combinations has to be used to weight single event averages $\langle 2\rangle$ to obtain *exactly* the all event average $\langle\langle 2\rangle\rangle$ as defined in (3.17), which then satisfies all physical requirement imposed upon it and discussed in the text below it. This reasoning trivially generalizes to correlations involving more than two particles[3]. For completeness sake, by using the notation introduced in (3.15) and (3.16) we have

$$W_{\langle 2\rangle} \equiv M(M-1)\,, \tag{3.24}$$

$$W_{\langle 4\rangle} \equiv M(M-1)(M-2)(M-3)\,. \tag{3.25}$$

One concrete example to illustrate the advantage of number of combinations over unit or multiplicity itself as a weight is illustrated in Section 3.2.4 in Fig. 3.4.

Multi-particle azimuthal correlations as introduced above are observables which can be used to estimate flow harmonics v_n *without* requiring the knowledge of the symmetry plane Ψ_n event-by-event (see discussion in Sec. 1.3.3). It is easy to see this connection [64]:

$$\begin{aligned}\langle\langle 2\rangle\rangle \equiv \left\langle\left\langle e^{in(\phi_1-\phi_2)}\right\rangle\right\rangle &= \left\langle\left\langle e^{in(\phi_1-\Psi_n-(\phi_2-\Psi_n))}\right\rangle\right\rangle \\ &= \left\langle\left\langle e^{in(\phi_1-\Psi_n)}\right\rangle\left\langle e^{-in(\phi_2-\Psi_n)}\right\rangle\right\rangle = \left\langle v_n^2\right\rangle\,. \end{aligned} \tag{3.26}$$

In case only flow correlations are present in the system, the correlation among any two particles is induced through the correlation of each particle with the same symmetry

[3]The reasoning outlined here assumed that only flow correlations are present in the system. In general, all correlations measured in practice will be systematically biased due to nonflow. One can attempt to reduce this systematic bias by tuning multiplicity weights based on some Monte Carlo study, but since this cannot be done neither systematically nor in general, we refrain from this idea.

plane Ψ_n [64]. Each of these single particle azimuthal distributions can be related to the flow harmonics via Eq. (1.62) (when colliding nuclei are the same due to the symmetry of collisions all sinus terms vanish). Analogously, one can show that

$$\langle\langle 4\rangle\rangle = \left\langle v_n^4 \right\rangle, \ \langle\langle 6\rangle\rangle = \left\langle v_n^6 \right\rangle, \ \langle\langle 8\rangle\rangle = \left\langle v_n^8 \right\rangle, \text{ etc.} \tag{3.27}$$

Two remarks about the result presented in Eq. (3.26): a) Even in the perfect case when only flow correlations are present in the system, estimates both from 2-particle and multi-particle correlations will be systematically biased due to statistical flow fluctuations, simply because $\langle v_n \rangle^k \neq \langle v_n^k \rangle$; b) In reality two particles can be correlated for various other reasons and not only through the correlation to the symmetry plane, which will in general break the factorization assumption used in derivation (3.26). We will in detail comment on both of these issues in subsequent sections.

3.1.5 Cumulants

In this section we briefly summarize the most important general facts about cumulants [66].

Consider first any two random observables x_1 and x_2 and their joint probability distribution function $f(x_1, x_2)$. In the case x_1 and x_2 are statistically independent the joint probability distribution function factorizes, namely

$$f(x_1, x_2) = f_{x_1}(x_1) f_{x_2}(x_2) \,. \tag{3.28}$$

In case x_1 and x_2 are not statistically independent, i.e. if they are statistically *connected*, than there is a genuine 2-particle correlation in the system which we quantify in terms of a genuine 2-particle probability distribution function $f_c(x_1, x_2)$. For a 2-particle correlation we have in general the following decomposition:

$$f(x_1, x_2) = f_{x_1}(x_1) f_{x_2}(x_2) + f_c(x_1, x_2) \,. \tag{3.29}$$

Written in terms of expectation values this decomposition translates into:

$$E[x_1 x_2] = E[x_1] E[x_2] + E_c[x_1 x_2] \,. \tag{3.30}$$

In practice we rarely know the exact functional form of the p.d.f.'s appearing in Eq. (3.29). However, we can use measured (sampled) values of the random variables x_1 and x_2 to construct unbiased estimators for the expectation values in Eq. (3.30).

The last term on the RHS in Eq. (3.30), $E_c[x_1 x_2]$, is by definition the 2-particle (or 2^{nd} order) cumulant. Clearly, by definition the 2-particle cumulant isolates the contribution to the expectation value $E[x_1 x_2]$ coming only from the genuine 2-particle correlation $f_c(x_1, x_2)$. This procedure can be generalized to any number of observables. For n random observables it is possible to isolate the contribution coming only from the genuine n-particle correlation, which is defined to be the n-particle (or n^{th} order) cumulant $E_c[x_1 x_2 \cdots x_n]$. The n-particle cumulant $E_c[x_1 x_2 \cdots x_n]$ is zero if one of the observables $x_1, x_2, \ldots, x_n$ is statistically independent from the others. Conversely, the cumulant $E_c[x_1 x_2 \cdots x_n]$ is not vanishing if, and only if, all the variables $x_1, x_2, \ldots, x_n$ are statistically connected. For a proof of these statements we refer the reader to [66]. In Appendix J we present how cumulants can be obtained in practice.

3.1.6 Cumulants in flow analysis

The general formalism of cumulants was introduced for flow analysis by Borghini *et al.* in [54–56]. For the two random observables x_1 and x_2 they used

$$\begin{aligned} x_1 &\equiv e^{in\phi_1}\,, \\ x_2 &\equiv e^{-in\phi_2}\,, \end{aligned} \tag{3.31}$$

where ϕ_1 and ϕ_2 are the azimuthal angles of two particles measured in the laboratory frame. With this choice we can write Eq. (3.30) in the following way:

$$E[e^{in(\phi_1-\phi_2)}] = E[e^{in\phi_1}]E[e^{-in\phi_2}] + E_c[e^{in(\phi_1-\phi_2)}]\,, \tag{3.32}$$

i.e.

$$E_c[e^{in(\phi_1-\phi_2)}] = E[e^{in(\phi_1-\phi_2)}] - E[e^{in\phi_1}]E[e^{-in\phi_2}]\,. \tag{3.33}$$

In practice we cannot estimate the cumulant $E_c[e^{in(\phi_1-\phi_2)}]$ directly. Instead, we estimate from the sampled values of random observables ϕ_1 and ϕ_2 the quantities $E[e^{in\phi_1}]$, $E[e^{-in\phi_2}]$ and $E[e^{in(\phi_1-\phi_2)}]$, and then use the relation (3.33) to estimate the 2-particle cumulant $E_c[e^{in(\phi_1-\phi_2)}]$. An immediate consequence of the choice (3.31) is that for a perfect detector (i.e. for a detector with uniform azimuthal acceptance) $E[e^{in\phi_1}]$ and $E[e^{-in\phi_2}]$ vanish [55], so that we have

$$E_c[e^{in(\phi_1-\phi_2)}] = E[e^{in(\phi_1-\phi_2)}]\,. \tag{3.34}$$

Even if we do not know the underlying joint p.d.f. to calculate the true expectation value in the RHS of Eq. (3.34), we can still use the sampled values of the azimuthal angles to estimate it. An unbiased estimator [67] for $E[e^{in(\phi_1-\phi_2)}]$ is an all-event average 2-particle correlation defined in Eq. (3.15), so that we finally have

$$c_n\{2\} = \langle\langle 2\rangle\rangle\,, \tag{3.35}$$

where we have used the notation $c_n\{2\}$ introduced by Borghini *et al.* [55] for the unbiased estimator of the true 2-particle cumulant $E_c[e^{in(\phi_1-\phi_2)}]$.

In order to get the estimate for the 4-particle cumulant we need to decompose the average 4-particle azimuthal correlation into its independent contributions. It was shown for the first time in [55] that for the case of detectors with uniform acceptance (for the general case see [66], for the practical implementation see Appendix J) the average 4-particle correlation decomposes into:

$$\begin{aligned} E[e^{in(\phi_1+\phi_2-\phi_3-\phi_4)}] &= E[e^{in(\phi_1-\phi_3)}]E[e^{in(\phi_2-\phi_4)}] \\ &+ E[e^{in(\phi_1-\phi_4)}]E[e^{in(\phi_2-\phi_3)}] \\ &+ E_c[e^{in(\phi_1+\phi_2-\phi_3-\phi_4)}]\,, \end{aligned} \tag{3.36}$$

which we can invert to isolate the *genuine* 4-particle correlation $E_c[e^{in(\phi_1+\phi_2-\phi_3-\phi_4)}]$, which is by definition the 4-particle (or 4^{th} order) cumulant:

$$\begin{aligned} E_c[e^{in(\phi_1+\phi_2-\phi_3-\phi_4)}] &= E[e^{in(\phi_1+\phi_2-\phi_3-\phi_4)}] \\ &- E[e^{in(\phi_1-\phi_3)}]E[e^{in(\phi_2-\phi_4)}] \\ &- E[e^{in(\phi_1-\phi_4)}]E[e^{in(\phi_2-\phi_3)}]\,. \end{aligned} \tag{3.37}$$

Taking into account the unbiased estimators for 4- and 2-particle correlations given in Eqs. (3.16) and (3.15), respectively, and using that all 2-particle averages in Eq. (3.37) are actually the same physical quantities apart from trivial relabeling of the azimuthal angles, the relation (3.37) can be written as [55]:

$$c_n\{4\} = \langle\langle 4\rangle\rangle - 2 \cdot \langle\langle 2\rangle\rangle^2 \,, \tag{3.38}$$

where now $c_n\{4\}$ stands for the unbiased estimator of the true 4-particle cumulant $E_c[e^{in(\phi_1+\phi_2-\phi_3-\phi_4)}]$. We remark that expressions (3.35) and (3.38) for cumulants are applicable only for detectors with uniform acceptance; these cumulants are generalized in Appendix D. For completeness, we also give the expressions for the 6- and 8-particle cumulants:

$$c_n\{6\} = \langle\langle 6\rangle\rangle - 9 \cdot \langle\langle 2\rangle\rangle \langle\langle 4\rangle\rangle + 12 \cdot \langle\langle 2\rangle\rangle^3 \,, \tag{3.39}$$

$$\begin{aligned} c_n\{8\} &= \langle\langle 8\rangle\rangle - 16 \cdot \langle\langle 6\rangle\rangle \langle\langle 2\rangle\rangle - 18 \cdot \langle\langle 4\rangle\rangle^2 \\ &+ 144 \cdot \langle\langle 4\rangle\rangle \langle\langle 2\rangle\rangle^2 - 144 \cdot \langle\langle 2\rangle\rangle^4 \,. \end{aligned} \tag{3.40}$$

The physical importance of cumulants stems from the fact that *all* particles produced in a heavy-ion collision are correlated to the symmetry plane determined by the geometry of that collision. The correlation of each particle with such a symmetry plane leads to the genuine multi-particle correlation for any number of particles in the correlator (so called *flow correlations*). On the other hand, correlations which do not originate from this correlation (so called *nonflow*) typically involve only few particles. As an example, if there is a genuine 2-particle nonflow correlation in the system (originating for instance from 2-particle resonance decays or from track splitting in the detector), then by definition the 2-particle cumulant is sensitive to it while the 4-particle cumulant is not. Usually the genuine 2-particle nonflow contribution to the 2-particle cumulant is denoted by δ_2 and for an event with multiplicity M its strength can be roughly estimated as:

$$\delta_2 \sim \frac{1}{M-1} \,, \tag{3.41}$$

simply because this is how the probability will scale (the probability that after we have picked up the first particle in the correlator for the second particle in the correlator we will pick up the only particle correlated to it out of remaining $M-1$ particles in the sample). This can be understood from the fact that once we have specified the first particle in the correlator we will pick up as the second correlated particle in the correlator one out of the remaining $M-1$ particles, when there is a genuine 2-particle nonflow correlation in the system. On the other hand, if there are flow correlations in the system, then they will induce contribution to genuine multi-particle correlations for all particles in the correlator and both 2- and 4-particle cumulant will be sensitive to them. Therefore in this particular example only the 4-particle cumulant can disentangle between the contribution coming from flow correlations and from the contribution coming from genuine 2-particle nonflow.

Having obtained estimates for cumulants from the data, one can easily use them to estimate flow harmonics. If all reconstructed particles passing certain track quality

criteria were taken in the analysis, we get reference cumulants and reference flow estimates, respectively, which are needed to perform differential flow analysis, which in turn is our main interest (for instance, the study of transverse momentum dependence of flow harmonics). In particular, after inserting results (3.26) and (3.27) into (3.35) and (3.38) it follows immediately for the ideal case where nonflow correlations and statistical flow fluctuations are absent in the system [55] that,

$$\begin{aligned}\sqrt{c_n\{2\}} &= \sqrt{\langle\langle 2\rangle\rangle} = v_n\,, \\ \sqrt[4]{-c_n\{4\}} &= \sqrt[4]{-\langle\langle 4\rangle\rangle + 2\cdot\langle\langle 2\rangle\rangle^2} = \sqrt[4]{-v_n^4 + 2v_n^4} = v_n\,. \end{aligned} \tag{3.42}$$

So in this ideal case scenario both 2- and 4-particle reference cumulants can be used to independently give the same exact answer for the reference flow harmonic v_n. In reality 2- and 4-particle cumulants will exhibit different systematic biases due to nonflow correlations and statistical flow fluctuations. To make this systematic difference clear, we use a distinct notation for each flow estimate:

$$v_n\{2\} \equiv \sqrt{c_n\{2\}}\,, \tag{3.43}$$

$$v_n\{4\} \equiv \sqrt[4]{-c_n\{4\}}\,, \tag{3.44}$$

where the notation $v_n\{2\}$ is used to denote the reference flow harmonic v_n estimated with the reference 2-particle cumulant $c_n\{2\}$ and $v_n\{4\}$ stands for the reference flow harmonic v_n estimated with the reference 4-particle cumulant $c_n\{4\}$. Starting from Eqs. (3.39) and (3.40) one can show that the 6- and 8-particle estimates are given as:

$$v_n\{6\} \equiv \sqrt[6]{\frac{1}{4}c_n\{6\}}\,, \tag{3.45}$$

$$v_n\{8\} \equiv \sqrt[8]{-\frac{1}{33}c_n\{8\}}\,. \tag{3.46}$$

So far we have provided the general concepts of multi-particle azimuthal correlations, cumulants and flow estimates from cumulants. One of the problems in measuring multi-particle correlations is the computing power needed to go over all possible particle multiplets, which prohibits calculations of correlations involving more than three particles in a central heavy-ion collision. In the next sections we will outline how multi-particle azimuthal correlations and cumulants can be measured in practice.

3.1.7 Generating Function Cumulants (GFC)

To avoid the evaluation of nested loops[4] in the measurement of multi-particle azimuthal correlations, Borghini *et al.* [54–56] in a series of papers have proposed an alternative, which is based on the use of generating functions. Cumulants were for the first time introduced into the flow analysis in [54], where it was suggested to express cumulants in terms of moments of the magnitude of the corresponding Q-vector, Q_n, defined in Eq. (3.1)[5]. For instance, 2- and 4-particle reference cumulants were defined by [54]

$$\begin{aligned} c_n\{2\} &\equiv \left\langle |Q_n|^2 \right\rangle , \\ c_n\{4\} &\equiv \left\langle |Q_n|^4 \right\rangle - 2\left\langle |Q_n|^2 \right\rangle^2 . \end{aligned} \tag{3.47}$$

To define cumulants in such a way is incomplete. Cumulants defined in such a way are systematically biased due to trivial effects of autocorrelations, which stem from the correlation terms in $|Q_n|^2$ and $|Q_n|^4$ having two or more indices which label azimuthal angles the same. For example, as a consequence $|Q_n|^4$ will in general pick-up the contribution coming from the higher harmonic v_{2n}, which is not counterbalanced by the corresponding contribution of harmonic v_{2n} to any other term in the definition of $c_n\{4\}$ in Eq. (3.47) (for a detailed analysis how various expressions involving Q-vectors depend on multiplicity and on the flow harmonics we refer the reader to Appendix E). This means that the 4-particle cumulant $c_n\{4\}$ defined as in Eq. (3.47), and correspondingly the 4-particle estimate of v_n, $v_n\{4\}$, will always be systematically biased due to the presence of a higher harmonic v_{2n}.

An improved cumulant method using the formalism of generating functions suggested in [55, 56] fixed the problem of interfering harmonics. For this improved approach the analytical calculations become rather tedious and therefore the solutions are obtained using interpolation formulae. Unfortunately this introduces numerical uncertainties and requires tuning of interpolating parameters for different values of the flow harmonics v_n and multiplicity M.

[4] In practice, to evaluate the 2-particle azimuthal correlation as defined in Eq. (3.13), and in order to enforce the condition $i \neq j$ one has to come up with the following schematic implementation:

```
for(int i=0;i<M;i++) // loop over first particles in the correlator
{
 for(int j=0;j<M;j++) // loop over second particles in the correlator
 {
  if(i==j){continue;} // if two particles are the same, skip calculation (avoiding autocorrelations)
  .... calculate correlations ....
 }
}
```

Such implementation is often referred to as *two nested loops*, and for large multiplicity M this calculation quickly becomes CPU prohibitive. For instance, we have estimated that to evaluate 8-particle correlations with eight nested loops for events with multiplicities characteristic for heavy-ion collisions at LHC energies, it would last almost as long as the lifetime of the Sun. So, with a bit of luck, such evaluation can in principle be finalized just in time ....

[5] In [54] authors have used additional prefactor $1/\sqrt{M}$ in the definition of Q-vector to suppress trivial contribution from multiplicity fluctuations in $|Q_n|$, and correspondingly in the cumulants.

We now sketch the main idea behind the generating function formalism in the cumulant analysis, and refer reader to Appendix F for more details. We start by introducing the generating functions $G_n(z)$ for multi-particle azimuthal correlations and $C_n(z)$ for the cumulants. The main idea is that all multi-particle azimuthal correlations can be generated after expanding the following complex, real valued function $G_n(z)$ in series of $(z^*)^k z^l$, where $k, l = 0, 1, 2, \ldots M$,

$$G_n(z) \equiv \prod_{j=1}^{M} \left(1 + \frac{z^* e^{in\phi_j} + z e^{-in\phi_j}}{M}\right) . \tag{3.48}$$

The function $G_n(z)$ defined in this way is the generating function for the multi-particle azimuthal correlations and it can be evaluated in a single loop over all particles in each event. For a detector with uniform acceptance the series expansion of $\langle G_n(z)\rangle$, where $\langle\langle\cdot\rangle\rangle$ denotes the average over all events, contains only diagonal terms [55] and it reads,

$$\langle\langle G_n(z)\rangle\rangle \quad = \quad \sum_{k=0}^{M/2} \frac{|z|^{2k}}{M^{2k}} \binom{M}{k} \binom{M-k}{k} \left\langle\left\langle e^{in(\phi_1+\cdots+\phi_k-\phi_{k+1}-\cdots-\phi_{2k})}\right\rangle\right\rangle . \tag{3.49}$$

In the next step we introduce the generating function for the cumulants $\mathcal{C}_n(z)$. We write the series expansion of $\mathcal{C}_n(z)$ in a series of $|z|^{2k}$, where $k = 0, 1, 2, \ldots M$, in the following way,

$$\mathcal{C}_n(z) \; = \sum_{k=1}^{M/2} \frac{|z|^{2k}}{(k!)^2} c_n\{2k\} . \tag{3.50}$$

The generating functions for multi-particle azimuthal correlations (3.48) and cumulants (3.50) are related via the following relation [55]:

$$\left(1 + \frac{\mathcal{C}_n(z)}{M}\right)^M = \langle\langle G_n(z)\rangle\rangle \; , \tag{3.51}$$

which in the limit of large multiplicity reduces to

$$\mathcal{C}_n(z) = \ln \langle\langle G_n(z)\rangle\rangle \; , \tag{3.52}$$

which is the standard definition for the generating function of cumulants used in other areas of physics. By inserting (3.50) into the LHS, and by inserting result (3.49) into the RHS of Eq. (3.51), and after expanding and collecting the terms for each order in expansion, one recovers cumulants expressed in terms of multi-particle azimuthal correlations (see Appendix F for a detailed calculation). The formalism can be generalized also for the calculation of differential flow, and is applicable for detectors with non-uniform acceptance (see Appendix F).

Calculating cumulants from the formalism of generating functions circumvented the problem of evaluating nested loops, however this formalism introduced possible systematic biases which we now summarize:

1. **Results are only approximate.** It is clear that in practice one has to terminate at a certain order the series (3.50) in order to apply the interpolating procedure outlined in Appendix F. Moreover, one will recover the theoretical definitions of cumulants in terms of multi-particle azimuthal correlations *only* in the limit of large multiplicity M (compare Eqs. (F.6)-(F.9) to Eqs. (F.10)).

2. **Multiplicity fluctuations.** In transferring the product in Eq. (3.48) into the sum in Eq. (3.49) we have to use the same multiplicity in each event, meaning that cumulants calculated from generating functions will not use the full number of particles (i.e. exploiting full statistics in each event would introduce systematic bias in this analysis even in the ideal case scenario when only flow correlations are present).

3. **Numerical instability.** In order to set up the interpolating scheme outlined in Appendix F one has to tune parameters, which in general will depend on the multiplicity and the strength of the flow signal itself (see in particular the discussion following Eq. (5) in [56]).

4. **Independent estimates cannot be obtained independently.** Flow estimates from 2-, 4-, 6- and 8-particle cumulants in this formalism are obtained from a system of coupled equations (see Appendix F), meaning that in practice in order to get 2-particle estimate one also has to calculate the remaining higher-order estimates.

All these issues were eventually resolved with the improved version of the cumulant method recently proposed in [59]—in the next section we elaborate in details about it.

3.2 Q-cumulants (QC)

In this section we provide details of an improved cumulant method, so called Q-cumulants (QC), which allows for a fast and exact calculation of all multi-particle cumulants, avoiding the evaluation of nested loops. The method was recently developed in [59] and it was used for the flow analysis in the ALICE experiment [69, 70]. We illustrate all the main improvements over the existing methods with a few examples. At the end we also indicate the remaining open questions and drawbacks.

3.2.1 Main idea and calculating strategy

One can express analytically all multi-particle azimuthal correlations in terms of Q-vectors evaluated (in general) in *different harmonics*[6] $n, 2n, 3n, \ldots$ and build cumulants from these analytical expressions for multi-particle azimuthal correlations. Calculated in this way all multi-particle cumulants are expressed analytically in terms of various expressions depending on Q-vectors, and we name them *Q-cumulants* (QC).

Next we outline the steps of the calculating strategy to obtain the exact expressions for all multi-particle cumulants:

[6] This idea is due to Sergei Voloshin.

Step 1: Decompose expressions like $|Q_n|^2$, $|Q_n|^4$, $|Q_n|^6$, $Q_{2n}Q_n^*Q_n^*$, $Q_{3n}Q_{2n}^*Q_n^*$, $Q_{2n}Q_nQ_{2n}^*Q_n^*$, ..., in terms of $\langle 2\rangle_{n|n}$, $\langle 3\rangle_{2n|n,n}$, $\langle 4\rangle_{n,n|n,n}$, ..., where notation used is understood as follows:

$$\langle k\rangle_{m_1,m_2,\ldots|\ldots,m_{k-1},m_k} \equiv \left\langle e^{i(m_1\phi_1+m_2\phi_2+\ldots-\ldots-m_{k-1}\phi_{k-1}-m_k\phi_k)}\right\rangle,\ \phi_1 \neq \phi_2 \neq \ldots \neq \phi_k,$$

and $\langle\cdot\rangle$ denotes a single-event average.

Step 2: Solve the system of coupled equations obtained in Step 1 for the multi-particle correlations in the *same* harmonic $\langle 2\rangle_{n|n}$, $\langle 4\rangle_{n,n|n,n}$, $\langle 6\rangle_{n,n,n|n,n,n}$, ... At the end of the day you should have $\langle 2\rangle_{n|n}$, $\langle 4\rangle_{n,n|n,n}$, $\langle 6\rangle_{n,n,n|n,n,n}$, ... expressed solely in terms of the various combinations of Q-vectors evaluated (in general) in different harmonics.

Step 3: Use Eqs. (3.15)-(3.16) to get the final results for multi-particle correlations $\langle\langle 2\rangle\rangle_{n|n}$, $\langle\langle 4\rangle\rangle_{n,n|n,n}$, $\langle\langle 6\rangle\rangle_{n,n,n|n,n,n}$, ..., where now $\langle\langle\cdot\rangle\rangle$ denotes an all-event average.

Step 4: Insert the results for $\langle\langle 2\rangle\rangle_{n|n}$, $\langle\langle 4\rangle\rangle_{n,n|n,n}$, $\langle\langle 6\rangle\rangle_{n,n,n|n,n,n}$, ... in the definitions (3.35), (3.38), (3.39) and (3.40) in order to obtain reference Q-cumulants $QC\{2\}$, $QC\{4\}$, $QC\{6\}$ and $QC\{8\}$.

Step 5: Use relations (3.43)-(3.46) to get the final estimates for the reference flow.

3.2.2 Reference flow results

We now outline the analytic results we have obtained for 2- and 4-particle Q-cumulants, both for reference and differential case (the details of the calculations are outlined in Appendix I).

To obtain the 2-particle Q-cumulant, $QC\{2\}$, it suffices to separate diagonal and off-diagonal terms in $|Q_n|^2$ (we remark again that in all summations $'$ means that all indices are taken different):

$$|Q_n|^2 = Q_nQ_n^* = \sum_{i,j=1}^{M} e^{in(\phi_i-\phi_j)} = M + \sum_{i,j}{}' e^{in(\phi_i-\phi_j)}\,, \tag{3.53}$$

which can be trivially solved to obtain $\langle 2\rangle$ defined in (3.13):

$$\langle 2\rangle = \frac{|Q_n|^2 - M}{M(M-1)}\,. \tag{3.54}$$

The event averaging is being performed via Eq. (3.15). The resulting expression for $\langle\langle 2\rangle\rangle$ is then used to estimate the 2-particle cumulant (3.35), the estimate which, when the analytical expression (3.54) is utilized, we name the 2-particle Q-cumulant and denote as $QC\{2\}$. Estimated in this way, $QC\{2\}$ is further used to estimate the reference flow harmonic v_n by making use of Eq. (3.43).

To obtain the 4-particle Q-cumulant we start with identifying the 4-particle correlations in the decomposition of $|Q_n|^4$:

$$|Q_n|^4 = Q_n Q_n Q_n^* Q_n^* = \sum_{i,j,k,l=1}^{M} e^{in(\phi_i+\phi_j-\phi_k-\phi_l)} \,. \tag{3.55}$$

This sum contains terms corresponding to four distinct combinations of the indices i, j, k and l: 1) they are all different (4-particle correlation), 2) three are different, 3) two are different, or 4) they are all the same. Explicit expressions for all the terms are given in Eq. (I.10). Note, that the case of three different indices corresponds to the so-called mixed harmonics 3-particle correlations, of great interest by themselves [71,72]. Analytic equations for 3-particle correlations are provided in Appendix G. Taking everything into account, we obtain the following analytic result for the single-event average 4-particle correlation defined in Eq. (3.14) (for details see Appendix I):

$$\begin{aligned} \langle 4 \rangle &= \frac{|Q_n|^4 + |Q_{2n}|^2 - 2 \cdot \mathfrak{Re}\left[Q_{2n} Q_n^* Q_n^*\right]}{M(M-1)(M-2)(M-3)} \\ &- 2\,\frac{2(M-2)\cdot |Q_n|^2 - M(M-3)}{M(M-1)(M-2)(M-3)} \,. \end{aligned} \tag{3.56}$$

The reason why the originally proposed cumulant analysis based on Q-vectors [54] was systematically biased lies in the fact that the terms consisting of Q-vectors evaluated in *different* harmonics (for instance terms $|Q_{2n}|^2$ and $\mathfrak{Re}\left[Q_{2n} Q_n^* Q_n^*\right]$ in (3.56)) were neglected. If a higher harmonic v_{2n} is non-zero then $|Q_n|^4$ gets an additional contribution of magnitude $v_{2n}^2 M(M-1) + v_n^2 v_{2n} 2M(M-1)(M-2)$, which is exactly canceled out with the contribution of harmonic v_{2n} to $|Q_{2n}|^2$ and $\mathfrak{Re}\left[Q_{2n} Q_n^* Q_n^*\right]$, which read $M v_{2n}^2 (M-1)$ and $M(M-1)(M-2) v_n^2 v_{2n} + M(M-1) v_{2n}^2$, respectively (see Appendix E for a detailed derivation and further clarification). The final, event averaged 4-particle azimuthal correlation, $\langle\langle 4 \rangle\rangle$, is then obtained by making use of Eqs. (3.16), and (3.25). Using $\langle\langle 4 \rangle\rangle$ and $\langle\langle 2 \rangle\rangle$ one can estimate the 4-particle Q-cumulant, $QC\{4\}$, from Eq. (3.38). Finally, the reference flow harmonic v_n is estimated by making use of Eq. (3.44).

The equations so far are applicable for an analysis with a detector with full uniform azimuthal coverage. In a non-ideal case one needs to take into account the acceptance corrections [61, 73]. Acceptance affects the cumulants in three ways: (i) contributions from additional terms, e.g. proportional to $\langle\langle \cos n\phi \rangle\rangle$ or $\langle\langle \sin n\phi \rangle\rangle$, that for a detector with full uniform azimuthal coverage are identical to zero, (ii) contributions from other flow harmonics, and (iii) the cumulant might be rescaled, which at the end can affect the final extracted flow values. We refer to [61, 73] for a more complete discussion of acceptance effects. In practice the most important correction is the first one, for which we provide the full set of equations for a 2- and 4-particle Q-cumulant analysis in Appendix D. The other two we will discuss shortly in Section 3.2.5.

3.2.3 Differential flow results

Once the reference flow has been estimated with the help of the formalism from previous sections, we proceed to the calculation of differential flow. For that, all particles selected

for flow analysis are classified as *Reference Flow Particle*, RFP, or *Particle Of Interest*, POI, or both. These labels are needed because the flow analysis is performed in two steps. In the first step we estimate the reference flow by using only the RFPs, while in the second step we estimate the differential flow of POIs with respect to the reference flow obtained in the first step.

Reduced multi-particle azimuthal correlations

For reduced[7] single-event average 2- and 4-particle azimuthal correlations we use the following notations and definitions:

$$\begin{aligned}\langle 2' \rangle &\equiv \left\langle e^{in(\psi_1-\phi_2)} \right\rangle \\ &\equiv \frac{1}{m_p M - m_q} \sum_{i=1}^{m_p} {\sum_{j=1}^{M}}' e^{in(\psi_i-\phi_j)}, \qquad (3.57)\\ \langle 4' \rangle &\equiv \left\langle e^{in(\psi_1+\phi_2-\phi_3-\phi_4)} \right\rangle \\ &\equiv \frac{1}{(m_p M - 3m_q)(M-1)(M-2)} \\ &\times \sum_{i=1}^{m_p} {\sum_{j,k,l=1}^{M}}' e^{in(\psi_i+\phi_j-\phi_k-\phi_l)}, \qquad (3.58)\end{aligned}$$

where m_p is the total number of particles labeled as POI (some might have been also labeled as RFP), m_q is the total number of particles labeled *both* as RFP and POI, M is the total number of particles labeled as RFP (some might have been also labeled as POI) in the event, ψ_i is the azimuthal angle of the i-th particle labeled as POI (taken even if labeled as RFP), ϕ_j is the azimuthal angle of the j-th particle labeled as RFP (taken even if it was labeled as POI). $\sum'$, as before, denotes that in all occurring sums all indices are taken different.

Finally, event averaged reduced 2- and 4-particle correlations are given by:

$$\begin{aligned}\langle\langle 2' \rangle\rangle &\equiv \frac{\sum_{\text{events}} (w_{\langle 2' \rangle})_i \langle 2' \rangle_i}{\sum_{\text{events}} (w_{\langle 2' \rangle})_i}, \qquad (3.59)\\ \langle\langle 4' \rangle\rangle &\equiv \frac{\sum_{\text{events}} (w_{\langle 4' \rangle})_i \langle 4' \rangle_i}{\sum_{\text{events}} (w_{\langle 4' \rangle})_i}. \qquad (3.60)\end{aligned}$$

[7] By *reduced* azimuthal correlation we indicate that one particle in the correlator, usually the particle of interest (POI), is restricted to belong only to the narrower phase-space window (e.g. to the narrower transverse momentum range).

In our calculations we use event weights $w_{\langle 2' \rangle}$ and $w_{\langle 4' \rangle}$ defined by:

$$w_{\langle 2' \rangle} \equiv m_p M - m_q \,, \tag{3.61}$$
$$w_{\langle 4' \rangle} \equiv (m_p M - 3m_q)(M-1)(M-2) \,. \tag{3.62}$$

As in the case of reference flow, this choice for the event weights reflects the number of distinct combinations of particles one can form when calculating the average reduced 2- and 4-particle correlations.

Differential cumulants

We derive equations for the differential cumulants using p- and q-vectors; p is constructed out of all POIs (m_p in total), and q only from POIs labeled also as RFP (m_q in total):

$$p_n \equiv \sum_{i=1}^{m_p} e^{in\psi_i} \,, \tag{3.63}$$

$$q_n \equiv \sum_{i=1}^{m_q} e^{in\psi_i} \,. \tag{3.64}$$

The q-vector is introduced here to subtract effects of autocorrelations. Using the p- and q-vectors, we obtain[8] the following equations for the average reduced single- and all-event 2-particle correlations:

$$\langle 2' \rangle = \frac{p_n Q_n^* - m_q}{m_p M - m_q} \,, \tag{3.65}$$
$$\langle\langle 2' \rangle\rangle = \frac{\sum_{i=1}^{N} (w_{\langle 2' \rangle})_i \langle 2' \rangle_i}{\sum_{i=1}^{N} (w_{\langle 2' \rangle})_i} \,. \tag{3.66}$$

For detectors with uniform azimuthal acceptance the differential 2$^{\text{nd}}$ order cumulant is given by

$$d_n\{2\} = \langle\langle 2' \rangle\rangle \,, \tag{3.67}$$

where, we use again the notation from Ref. [55]. We present equations for the case of detectors with non-uniform acceptance in Appendix D. Estimates of differential flow v_n' are denoted as $v_n'\{2\}$ and are given by [55]:

$$v_n'\{2\} = \frac{d_n\{2\}}{\sqrt{c_n\{2\}}} \,. \tag{3.68}$$

Before proceeding further, we comment on the above equation. In the ideal case scenario when only flow correlations are present, the numerator in above equation gives $v_n' v_n$, while the denominator gives $\sqrt{v_n v_n}$, so that overall the reference flow harmonic v_n drops out from Eq. (3.68). The point behind the usage of reference particles is only to make

[8] Details of results presented in this section are outlined in Appendix I.

statistically stable both numerator and denominator in (3.68), i.e. direct differential flow analysis using only particles of interest would not be feasible in practice due to limited statistics of particles of interest in majority of the cases. For this reason, reference particles are always selected to be the most abundant particles in an event, usually all charged particles.

Below we present the corresponding formulae for reduced 4-particle correlations:

$$\begin{aligned}\langle 4' \rangle &= \Big[p_n Q_n Q_n^* Q_n^* - q_{2n} Q_n^* Q_n^* - p_n Q_n Q_{2n}^* \\ &- 2 \cdot M p_n Q_n^* - 2 \cdot m_q \left|Q_n\right|^2 + 7 \cdot q_n Q_n^* \\ &- Q_n q_n^* + q_{2n} Q_{2n}^* + 2 \cdot p_n Q_n^* \\ &+ 2 \cdot m_q M - 6 \cdot m_q \Big] \\ &/ \Big[(m_p M - 3 m_q)(M-1)(M-2)\Big], \end{aligned} \tag{3.69}$$

$$\langle\langle 4' \rangle\rangle = \frac{\sum_{i=1}^{N} (w_{\langle 4' \rangle})_i \langle 4' \rangle_i}{\sum_{i=1}^{N} (w_{\langle 4' \rangle})_i}. \tag{3.70}$$

Equation (3.69) is the main equation for differential flow analysis with multi-particle cumulants: It is an analytical result for reduced 4-particle azimuthal correlation, covering all three distinct cases of overlap between RFPs and POIs, namely "full overlap", "no overlap" and "partial overlap." The 4$^{\text{th}}$ order differential cumulant[9] is given by [55]:

$$d_n\{4\} = \langle\langle 4' \rangle\rangle - 2 \cdot \langle\langle 2' \rangle\rangle \langle\langle 2 \rangle\rangle . \tag{3.71}$$

Having obtained estimates for $d_n\{4\}$ and $c_n\{4\}$, we can estimate the differential flow [55]:

$$v_n'\{4\} = -\frac{d_n\{4\}}{(-c_n\{4\})^{3/4}}. \tag{3.72}$$

As for reference flow, we use the notation $v_n'\{4\}$ for the differential flow harmonics v_n' obtained from 4$^{\text{th}}$ order cumulants. $v_n'\{4\}$ and $v_n'\{2\}$ are independent estimates for the same differential flow harmonic v_n'.

3.2.4 List of improvements

In this section we will, with a series of examples, illustrate the advantages of the Q-cumulants over the cumulants obtained with the formalism of generating functions, as well as advantages over other methods for flow analysis.

1. **Complete flow analysis is done in a one pass over the data.** When the formalism of generating functions is used for the cumulant analysis one needs to perform a dedicated run to first get an estimate for the reference flow, which then can be used in the second pass over the data to estimate the differential flow. For

[9] Equations for the case of detectors with non-uniform acceptance are again presented in Appendix D.

the Lee-Yang Zeros (LYZ) method [60,61] one also needs two runs over the data to get the differential flow estimates. Some other methods, like fitted q-distribution (FQD) are capable only of providing the reference flow.

2. **Acceptance effects can be corrected for better or at the same level than with any other method.** To demonstrate that Q-cumulants work well even in case of rather bad acceptance we simulated 10^7 events with $v_2 = 0.05$ for a detector that had two large "holes" (see Fig. 3.2a). Figure 3.2b shows (open squares) the obtained v_2 estimates using Eqs. (3.35) and (3.38) which are valid for detectors with perfect acceptance. Clearly these values are strongly biased, when compared to the true Monte Carlo flow estimates shown in the first bin and denoted as $v_2\{\mathrm{MC}\}$ (only to this estimate we provide event-by-event the information about the reaction plane orientation). The v_2 estimates obtained from the more general equations for Q-cumulants, Eqs. (D.2) and (D.7), which do account for the acceptance effects, are shown as full squares and agree with the Monte Carlo estimate. In Fig. 3.2c we look in more detail at the agreement with the Monte Carlo estimate and, in addition, compare to other methods (generating function cumulants (GFC) and Lee-Yang Zero, sum generating function (LYZS)). The figure clearly shows that detector effects are corrected for at the level of or better than other methods. In section 3.2.5 we will discuss shortly the remaining issues with systematic biases stemming from non-uniform acceptance in a cumulant analysis.

3. **No interference between harmonics.** The first version of the cumulants [54] was biased by the interference between harmonics. This bias was removed in the second version of cumulant method [60,61], however it remains present in other two widely used methods, Lee-Yang Zero (only when using the faster sum generating function, LYZS) and FQD. Figure 3.3 shows the results from a simulation of events with anisotropic flow present in two harmonics, the second and the fourth. The elliptic flow estimated by different methods is shown in the figure. A clear bias is observed in the estimates from fitting of the q-distribution method and the Lee-Yang Zero's Sum method, labeled as $v_2\{\mathrm{FQD}\}$ and $v_2\{\mathrm{LYZS}\}$, respectively. Results obtained with Q-cumulants of different order, labeled as $v_2\{k, \mathrm{QC}\}$, are unaffected by v_4 interference.

4. **Smaller statistical spread.** As it was advocated in Section 3.1.4 in the Q-cumulant analysis the event weight is the number of combinations. This choice for the event weight minimizes the statistical spread. A comparison to two other widely used weights in the cumulant analysis, "unit" and "multiplicity itself," is shown in Fig. 3.4. The choice of multiplicity weight "number of combinations" also makes the statistical spread in the QC analysis sizeably smaller when compared to the statistical spread in the analysis with other methods (see Fig. 3.5).

5. **Numerical stability.** A drawback in the flow analysis with cumulants obtained via the formalism of generating functions is the fact that the tuning parameters needed for the interpolating procedure outlined in Appendix F.2 *cannot* be chosen to be the same for different values of the flow estimates. To illustrate this, we show in Fig. 3.6 the results of the flow estimates obtained from the generating

function cumulants (GFC) for $v_2 = 0.05$ (top panel) and $v_2 = 0.2$ (bottom panel), with the same choice of tuning parameters for both cases ($r_0 = 2.2$ was used, see Eqs. (F.27)). The choice for r_0 which worked well in the case of $v_2 = 0.05$ clearly yields numerically unstable results for the case $v_2 = 0.2$. On the other hand, the estimates from Q-cumulants (QC) are numerically stable in both cases for all cumulant orders. This illustrates that one can utilize the Q-cumulants in the flow analysis *without* a priori assumption about the flow signal strength.

6. **Generalization to multi-particle correlations in mixed harmonics.** With the calculation strategy outlined in Section 3.2.1 not only the multi-particle correlations in the same harmonic can be analytically expressed in terms of Q-vectors, but also the correlations in mixed harmonics for any number of particles in the correlators. Multi-particle azimuthal correlations, both in same and mixed harmonics, expressed analytically in terms of Q-vectors are given in Appendix G. On the contrary, methods based on generating functions (like generating function cumulants or Lee-Yang Zeroes) are not suitable for the evaluation of multi-particle cumulants in mixed harmonics, in a sense that the different starting generating functions have to be utilized each time, depending on the correlators in question. Correlators involving mixed harmonics provide additional information not obtained by correlators involving only the same harmonic: the correlation between the participant planes of different harmonics (e.g. the correlator $\langle\langle\cos[n(4\phi_1-2\phi_2-2\phi_3)]\rangle\rangle$ is also sensitive to the correlation between participant planes ψ_4 and ψ_2 of harmonics v_4 and v_2, respectively).

3.2.5 Open questions

There are three remaining open questions and drawbacks in the flow analysis with Q-cumulants that we are aware of:

1. **Interplay between multiplicity fluctuations and nonflow.** As demonstrated in Fig. 3.4 (black squares), standalone multiplicity fluctuations are not harmful in the Q-cumulant analysis. It is only the interplay between nonflow correlations and multiplicity fluctuations which yields a systematic bias which Q-cumulants (all orders) cannot deal with. This is precisely the case which we encounter in reality. However, one can completely circumvent this systematic bias in practice (at the expense of losing statistics) by selecting for each centrality the event with minimal multiplicity, M_{min}, and then from all other events in this centrality to select randomly only M_{min} particles for the analysis.

2. **Correcting for non-uniform acceptance when multiple harmonics are present.** The automatic procedure to correct for non-uniform acceptance in a Q-cumulant analysis elaborated in detail in Appendix D fails when multiple harmonics are present in the system. As an example, in Fig. 3.7 we indicate the case when the estimate of v_2 remains systematically biased due to the interference between non-uniform acceptance and the higher harmonic v_4, even when the formalism from Appendix D has been applied.

3. **Low sensitivity to small flow values.** As can be seen from the expressions for the statistical errors presented in Appendix C, the statistical spread of flow estimates from Q-cumulants is suppressed with a prefactor of the inverse of estimated flow signal itself raised to a certain power (the power depends on the cumulant order). This means that in the regime where the estimated flow signal is sizeable the prefactor will suppress the statistical spread. On the other hand, when the estimated flow signal is very small such a prefactor will make the flow estimates statistically unstable.

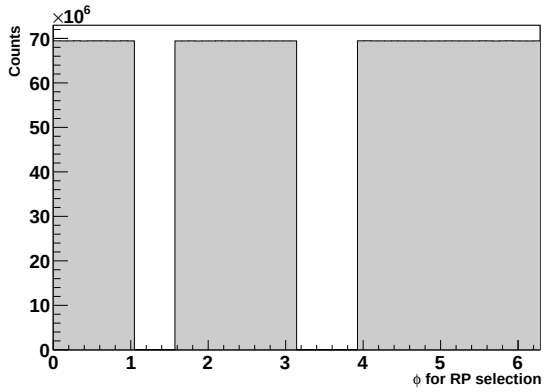

(a)

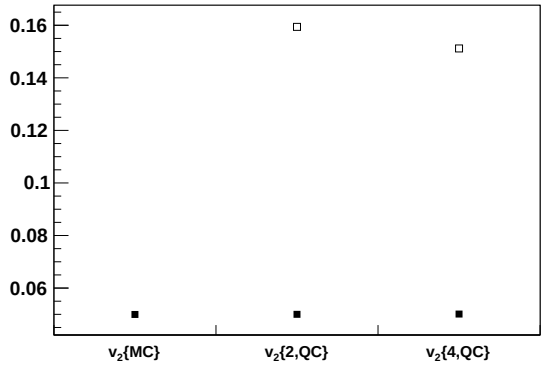

(b)

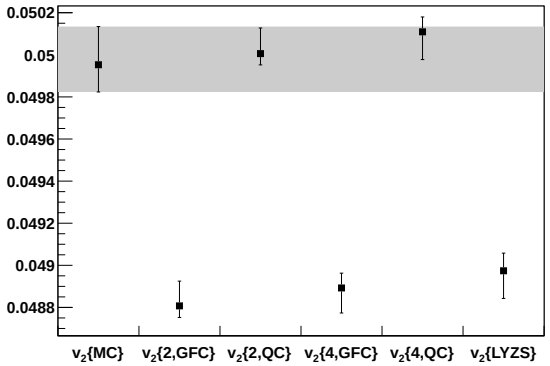

(c)

Figure 3.2: a) The azimuthal distribution of accepted particles. b) Extracted elliptic flow accounting for acceptance effects, closed markers, and without, open markers. c) Extracted elliptic flow accounting for acceptance effects in different methods.

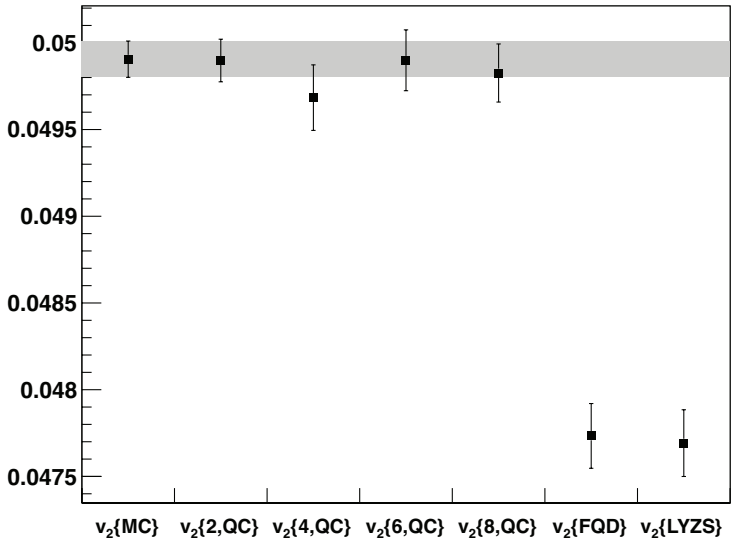

Figure 3.3: Elliptic flow extracted by different methods for 10^5 simulated events with multiplicity $M = 500$, $v_2 = 0.05$ and at the same time $v_4 = 0.1$. MC denotes Monte Carlo estimate for v_2, QC stands for Q-cumulant estimates, FQD denotes estimate obtained from fitted q-distribution and finally LYZS marks estimate from Lee-Yang Zero method (sum generating function).

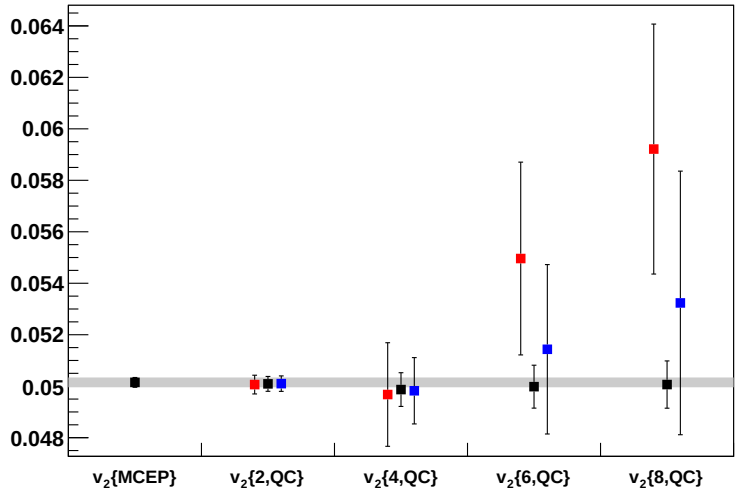

Figure 3.4: Comparison of event (multiplicity) weights introduced in Eqs. (3.15) and (3.16). In this example in total of 50K events multiplicity of an event was sampled uniformly from [50,500]. Particle's azimuthal angles were sampled from a Fourier-like p.d.f. parameterized with harmonic $v_2 = 0.05$. In the first bin is a true Monte Carlo v_2 estimate. In the remaining bins are estimates from Q-cumulants, but obtained with three different multiplicity weights: "number of combinations" (black), "unit" (red) and "multiplicity itself" (blue). The advantage of using "number of combinations" as a multiplicity weight is obvious.

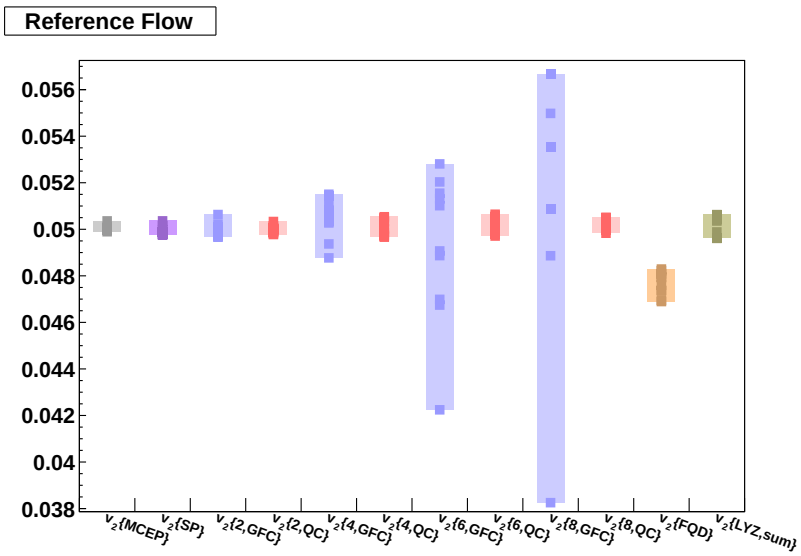

Figure 3.5: Comparison of statistical spread of various methods. In this example the starting dataset was divided in 10 equal subsets of 100 K events each and for each subset flow analysis was performed independently. We have allowed multiplicity to fluctuate in interval [400,600] and particle azimuthal angles were sampled from the Fourier-like p.d.f. parameterized only with $v_2 = 0.05$. For each subset and for each method the estimates are shown with filled squares. The spread of these 10 independent results shows the size of statistical spread for each method (MCEP = true Monte Carlo flow estimate, SP = Scalar Product method, GFC = Generating Function Cumulants ($2^{\text{nd}} - 8^{\text{th}}$ order), QC = Q-cumulants ($2^{\text{nd}} - 8^{\text{th}}$ order), FQD = Fitted q-distribution, LYZ, sum = Lee-Yang Zeroes, sum generating function). When compared to GFC estimates, the statistical spread of QC estimates is clearly smaller.

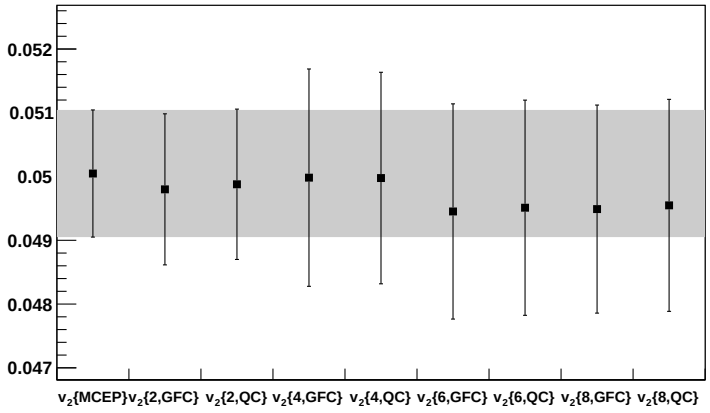

(a)

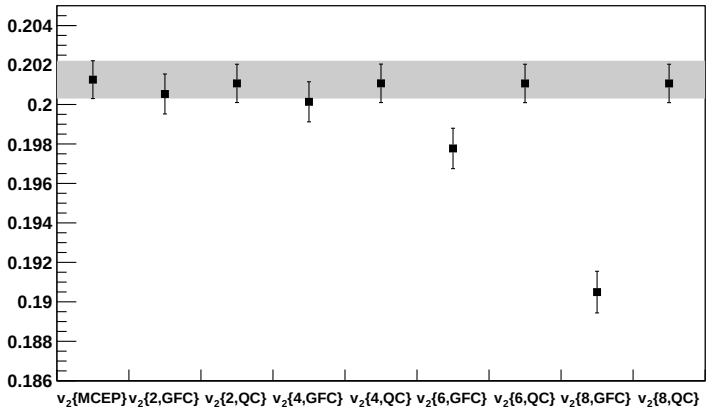

(b)

Figure 3.6: Flow estimates for the example in which particle angles were sampled from Fourier-like p.d.f. parameterized only with (a) $v_2 = 0.05$, and (b) $v_2 = 0.2$. In the first bin in both plots is true Monte Carlo v_2 estimate and the shaded band was obtained after extending its statistical error horizontally over all bins. In the subsequent bins are estimates from generating function cumulants (GFC) and Q-cumulants (QC). Clearly, the set of tuning parameters in the GFC analysis which worked well in the first case becomes numerically unstable in the second case. On the other hand, QC estimates are numerically stable in both cases.

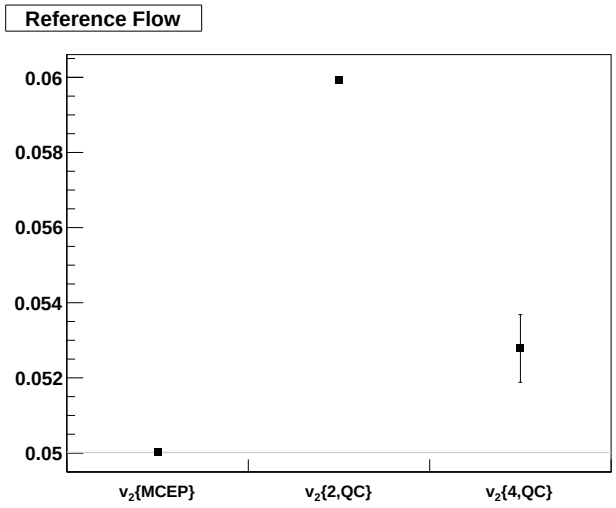

Figure 3.7: Detector's azimuthal non-uniform acceptance was simulated by omitting particles emitted in range $60^0 < \phi < 120^0$ in the analysis. Particle azimuthal angles were sampled from Fourier-like p.d.f. parameterized with two harmonics, $v_2 = 0.05$ and $v_4 = 0.20$. Clearly, estimate of v_2 is systematically biased due to the interference between non-uniform acceptance of detector and the presence of higher harmonic v_4 in the system, even after the formalism from Appendix D has been applied.

Chapter 4

Data selection

In this chapter we outline the selection criteria applied in the analysis. With a series of plots we illustrate the effect of using various cuts on the distributions of physical quantities of interest. We also present at the end on this chapter a few Monte Carlo based results.

1. **Data taking details.** For the first elliptic flow analysis in ALICE published in [69] only the Pb-Pb collisions at $\sqrt{s_{NN}} = 2.76$ TeV from run 137161 ("golden run") were taken into account. This run was taken at Novemeber 9^{th}, 2010, LHC fill number 1483. The duration of the run was 3 hours and 23 minutes, with a minimum-bias trigger rate of 53.07 Hz. The bunch intensity was typically 10^7 Pb ions per bunch and each beam had 4 colliding bunches. The estimated luminosity was 5×10^{23} cm^{-2}s^{-1}, resulting in a total number of $\sim$ 650K reconstructed events. The final data sample of reconstructed events passing all online and offline selection criteria, was $\sim$ 45K events. Elliptic flow analysis was performed in centrality bins, where the width of a centrality bin was typically 10%. The centrality-wise statistics was $\sim$ 6K events per bin.

2. **Electromagnetically induced interactions.** Electromagnetically induced interactions are rejected by requiring an energy deposition above 500 GeV in each of the Zero Degree Calorimeters (ZDCs) positioned at $\pm$ 114 m from the interaction point [83].

3. **Beam-background events.** A removal of background events was carried out off-line using the VZERO timing information and the requirement of two tracks in the central detector.

4. **Tracking detectors.** For the reconstruction of all charged particles in the ALICE detector the Inner Tracking System (ITS) and Time Projection Chamber (TPC) were used as the main tracking devices (see Chapter 2). The relative momentum resolution for tracks used in this analysis was better than 5%, both for the combined ITS-TPC and TPC standalone tracks. Because the ITS does not have uniform acceptance corrections have to be performed when it is used in the

tracking. On the other hand, when only information from the TPC is used in the tracking these corrections are negligible due to its uniform acceptance. In the analysis presented here both approaches for tracking were used. As an example, the uniform acceptance when only TPC standalone tracks are used in the analysis is shown in Fig. 4.1. The non-uniform acceptance of the SPD, is shown in Fig. 4.2. In order to obtain the latter figure, the tracks were reconstructed only from the two hits in two SPD layers.

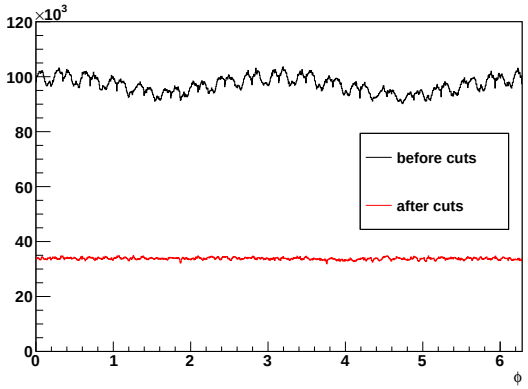

Figure 4.1: Azimuthal distribution of all charged particles reconstructed only with the TPC detector, before and after the track quality cuts, for the centrality class 40–50%.

5. **Kinematic region.** Reference particles (RPs) were selected from the transverse momentum interval $0.2 < p_t < 5$ GeV/c and pseudorapidity range $|\eta| < 0.8$. The lower boundary in transverse momentum is because of the tracking capabilities of the ALICE detector which deteriorate significantly below 200 MeV/c, mostly because the low-p_t tracks do not make it into the TPC (see Fig. 4.10). The upper p_t boundary in the RP selection is set to 5 GeV in order to suppress the contribution to correlations coming from jets (when traversing the medium the energetic partons clusterize, and produce jets of strongly correlated high-p_t particles, the correlations which we classify as nonflow and consider to be a systematic bias in our analysis). Finally, the chosen pseudorapidity range is due to the physical acceptance of TPC in pseudorapidity and the requirement to have a uniform acceptance in the analysis, which is ensured in ALICE only if the TPC standalone tracks are being used. Taking into account all track quality cuts described below, the resulting p_t spectrum is presented in Fig. 4.3, while the resulting pseudorapidity distribution of all charged particles is presented in Fig. 4.4, before and after track quality cuts have been applied.

6. **The primary vertex determination.** Primary vertex position in ALICE is determined with the ITS, in particular with its innermost part the SPD. The resolution in the z-coordinate is at level of 10 μm in heavy-ion collisions and at

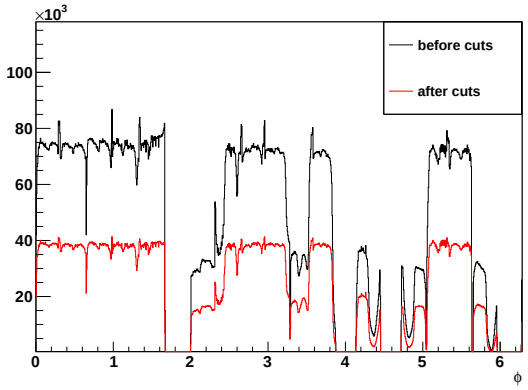

Figure 4.2: Azimuthal distribution of tracklets reconstructed only with the SPD detector, before and after the track quality cuts, for the centrality class 40–50%.

the level of 150 μm in proton-proton collisions [29]. Only events with a primary vertex found in $|z| < 10$ cm were used in this analysis to ensure an uniform acceptance in the central pseudorapidity region $|\eta| < 0.8$ (see Fig. 4.5).

7. **Centrality determination.** The default estimator for centrality determination in ALICE is obtained from the measured multiplicity in the VZERO detectors. Other centrality estimators used in this analysis are based on the multiplicity measured in the SPD and TPC detectors. The resolution in centrality determination based on the VZERO multiplicity is ∼0.5% for the centrality range 0-20%, and remains below 2% for the centrality range 20-80% [84].

8. **Minimum-bias trigger.** The online (hardware level) minimum-bias interaction trigger required at least two out of the following three conditions [85]: (i) two pixel chips hit in the outer layer of the SPD, (ii) a signal in VZERO-A, (iii) a signal in VZERO-C.

9. **DCA cut.** Tracks with a distance of closest approach (DCA) to the primary vertex are rejected if the distance is larger than 3.0 cm, both in the longitudinal (z) and radial (xy) direction, when the TPC standalone track are used in the analysis. If the combined ITS and TPC information is used in the reconstruction, then the DCA cut is set to 0.3 cm, again both in the longitudinal (z) and radial (xy) direction. With this DCA cut the contribution from secondary particles originating from either weak decays or from the interaction of particles with the material is minimized. DCA distributions in the longitudinal and transverse direction for TPC standalone tracks are shown in Figs. 4.6 and 4.7, respectively.

10. **TPC only cuts.** The tracks are required to have at least 70 reconstructed space points out of the maximum 159 in the TPC (see Fig. 4.8) and a $\langle \chi^2 \rangle$ per TPC cluster ≤ 4 (with 2 degrees of freedom per cluster).

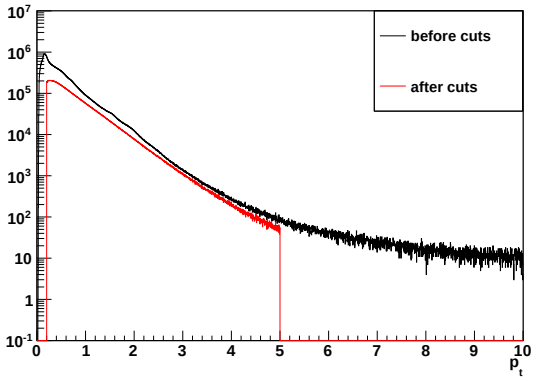

Figure 4.3: Transverse momentum spectrum before and after track quality cuts, for the centrality class 40–50%.

11. **ITS only cuts.** Reconstructed tracks are required to have a hit in at least two out of the six ITS layers. This cut is not applied when only TPC standalone tracks are being used in the analysis.

12. **Acceptance effects.** In an analysis based on azimuthal correlations, e.g. a flow analysis with two- and multi-particle azimuthal correlations, any inefficiencies in the detector's azimuthal acceptance will introduce a non-negligible systematic bias. When the TPC standalone tracks are used in the analysis this bias is negligible due to the uniform azimuthal acceptance of the TPC detector in ALICE. When combined ITS and TPC information is used in the reconstruction, the resulting azimuthal acceptance is not uniform. For this case, the bias was corrected for with the prescription from Appendix D.

13. **Reconstruction efficiency.** When the combined ITS and TPC information is being used in the reconstruction, the reconstruction efficiency for tracks with $0.2 < p_t < 0.7$ GeV/c increases from 67% to 85% after which it stays constant at (85$\pm$5)% (see Fig. 4.9). The efficiency as a function of transverse momentum does not change significantly as a function of multiplicity and is therefore the same for all centrality classes (see Fig. 4.9). On the other hand, when only TPC information is used in the reconstruction the reconstruction efficiency for these tracks with $0.2 < p_t < 0.7$ GeV/c increases from 70% to 87% after which it stays constant at (87 $\pm$ 5)% (see Fig. 4.10). For this track selection the efficiency as a function of transverse momentum also does not depend significantly on the track density and is therefore the same for all centrality classes (see Fig. 4.10).

14. **Contamination from secondary interactions and photon conversions.** For tracks reconstructed using both the ITS and TPC information the contamination from secondary interactions and photon conversions is less than 10% for $p_t = 0.2$

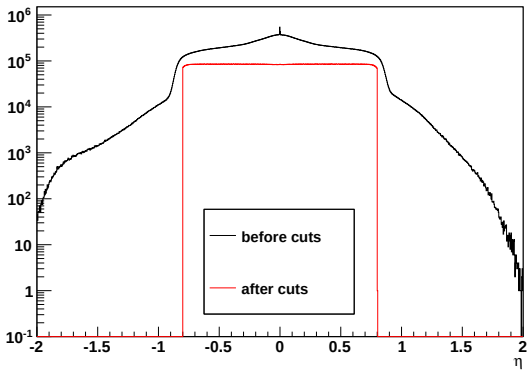

Figure 4.4: Pseudorapidity distribution of all charged particles before and after track quality cuts, for the centrality class 40–50%.

GeV/c and below 4% for $p_t > 1$ GeV/c (see Fig. 4.11). The contamination as a function of transverse momentum does not change significantly as a function of multiplicity and is therefore the same for all centrality classes (see Fig. 4.11). On the other hand, for tracks reconstructed using only TPC information the contamination is less than 20% at $p_t = 0.2$ GeV/c and drops below 10% at $p_t > 1$ GeV/c (see Fig. 4.12). As in the previous case, the contamination is the same for all centrality classes (see Fig. 4.12). To check what the flow is of the tracks coming from various processes we need to plot v_2 as function of process ID for the most dominant contributions. We therefore use for this study THERMINATOR [87, 88] events which do have flow distributions from hydrodynamics and nonflow from the decays. In Fig. 4.13a the differential flow, $v_2(p_t)$, is shown for charged tracks originating from different processes. The $v_2(p_t)$ from decay charged particles is very close to the $v_2(p_t)$ of primary tracks. The $v_2(p_t)$ for tracks from pair production is shifted due to the shift in momentum of the daughter. The yield of pair production is not that large, however at the lowest transverse momentum there is a small bias on $v_2(p_t)$ of all charged tracks compared to the primaries which we take as a systematic uncertainty. The flow of tracks from hadronic interactions is negligible and not shown. Figure 4.13b shows that not only the differential flow but also the p_t-integrated flow of tracks coming from decays is very similar to primary tracks. In addition the p_t-integrated elliptic flow of tracks from Compton scattering and pair production is still close to the value of primaries in THERMINATOR (the pairs from conversions have a flow which is different, however their yield is only a few percent of the total). The p_t-integrated flow of the tracks produced by hadronic interactions is very small, just as their yield.

Having outlined and discussed the selection criteria, finally in the next chapter we present our main results.

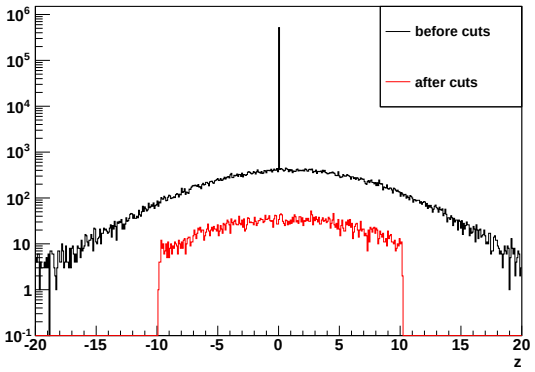

Figure 4.5: Distribution of primary vertex z coordinate, before and after the cut was applied, in the centrality class 40–50%.

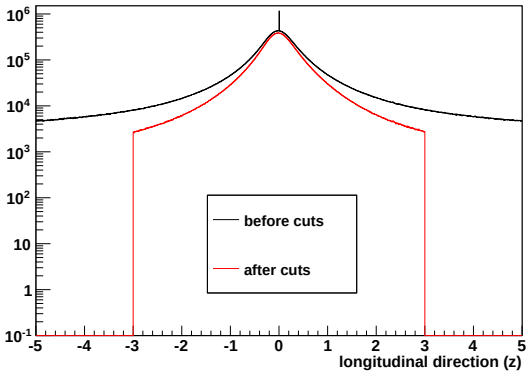

Figure 4.6: The distance of closest approach (DCA) to the primary vertex in the longitudinal direction, before and after the track quality cuts, for the centrality class 40–50%.

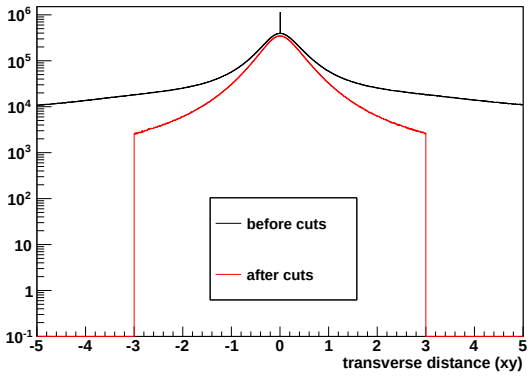

Figure 4.7: Distance of closest approach (DCA) to the primary vertex in transverse direction, before and after the track quality cuts, for the centrality class 40–50%.

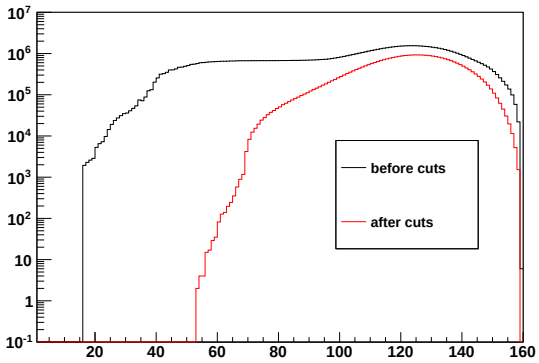

Figure 4.8: Distribution of number of TPC clusters, before and after the cuts, in the centrality class 40–50%. Although we have required to have at least 70 reconstructed space points, the smearing down to 55 points (red curve) occurs. This smearing is due to the fact that the cut was applied on the TPC clusters from the first pass of reconstruction, while the used QA code histogrammed the "standard" number of TPC clusters, in this case after the third reconstruction pass. Clearly, few clusters were rejected in later reconstruction passes.

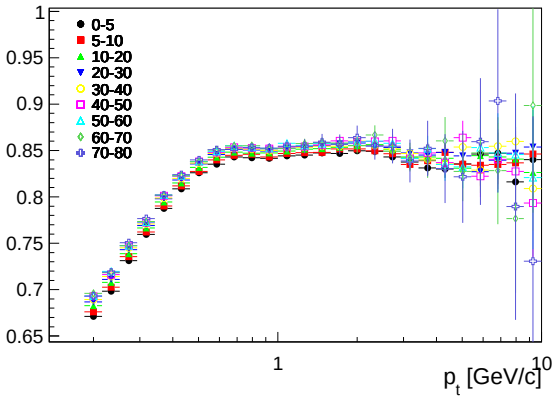

Figure 4.9: Reconstruction efficiency of global tracks (ITC+TPC) as function of transverse momentum for different centrality classes [86].

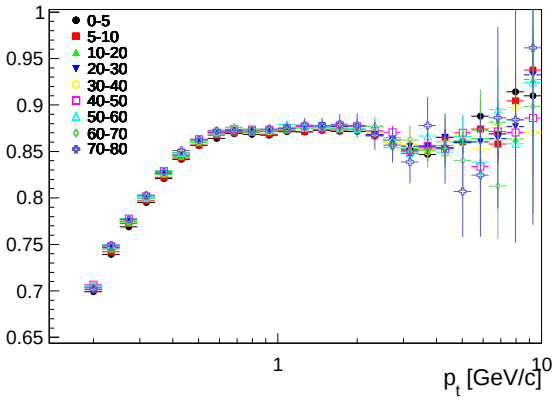

Figure 4.10: Reconstruction efficiency of TPC standalone tracks as a function of transverse momentum for different centrality classes [86].

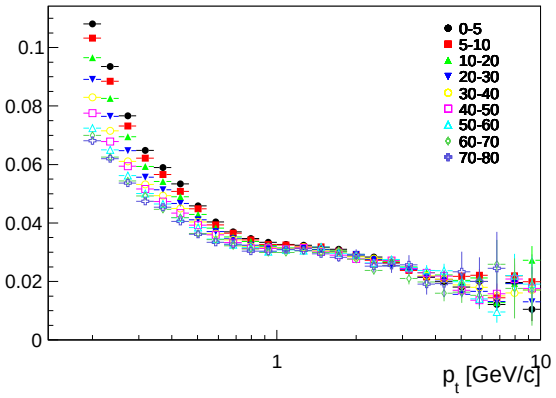

Figure 4.11: Contamination (the number of secondaries in our primary selection) for global tracks as a function of transverse momentum and different centrality classes [86].

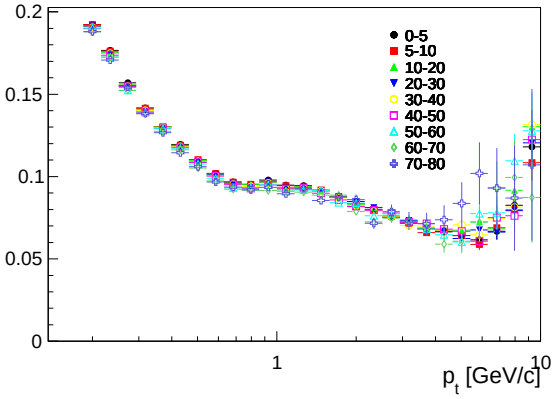

Figure 4.12: Contamination (the number of secondaries in our primary selection) for TPC standalone tracks as a function of transverse momentum and centrality classes [86].

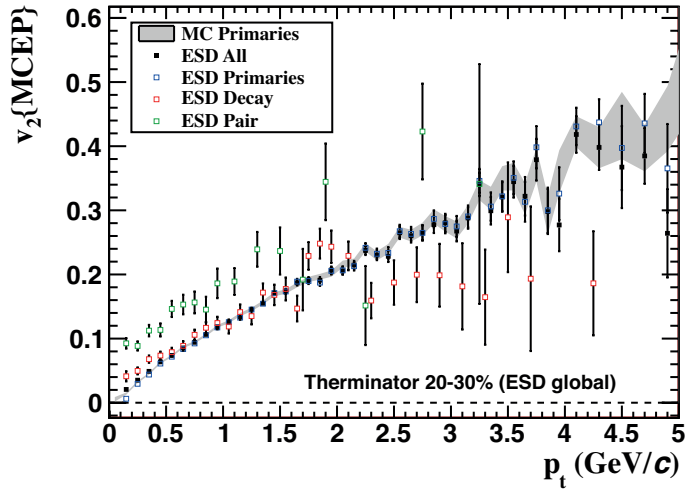

(a)

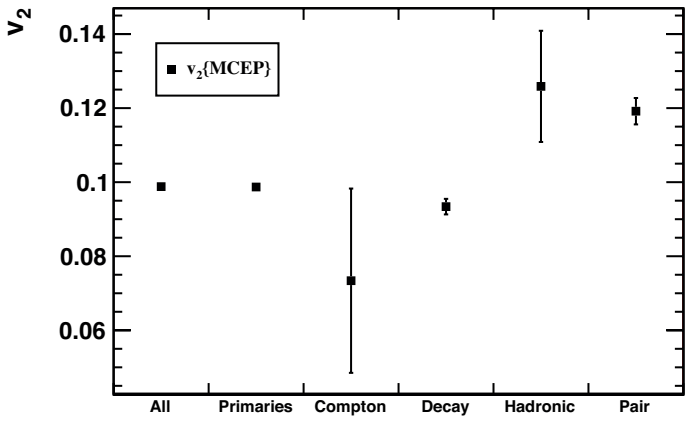

(b)

Figure 4.13: a) The differential flow in THERMINATOR [87, 88] for primary tracks compared to decays and other processes. b) The integrated flow in THERMINATOR [87, 88] for primary tracks compared to decays and other processes.

Chapter 5

Results

In this chapter we present the results of the anisotropic flow analysis of charged particles in the ALICE experiment. We start by outlining the published results of elliptic flow v_2 [69] obtained with limited statistics, accompanied here with plots demonstrating additional systematic cross-checks. Subsequently we show the more detailed and precise results for elliptic flow obtained with much larger statistics. We conclude the chapter with recent results of higher harmonics beyond v_2 published in [70]. The data selection and track cuts used were described in Chapter 4.

5.1 Centrality determination

For the elliptic flow analysis published in [69] a data sample of $\sim$ 45K Pb-Pb collisions was used. The data are analyzed in centrality classes determined by cuts on the uncorrected charged particle multiplicity measured in the pseudorapidity range $|\eta| < 0.8$. Figure 5.1 shows the uncorrected charged particle multiplicity in the TPC for these events and the nine centrality bins used in the analysis. Besides the TPC tracks also the VZERO and SPD information was used in estimating the centrality independently as part of estimating the systematic uncertainty in v_2—the comparison plots with results for elliptic flow will be shown later in Fig. 5.3 for all three cases.

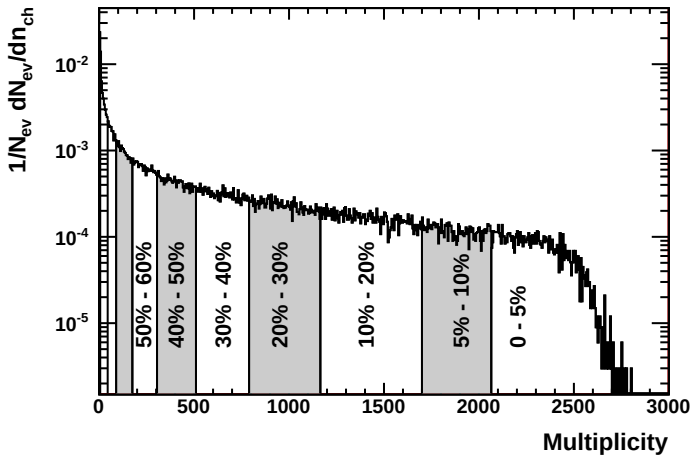

Figure 5.1: The uncorrected multiplicity distribution of charged particles in the TPC ($|\eta| < 0.8$). The centrality bins used in the analysis are shown and the cumulative fraction of the total events is indicated in percent. The bins 60-70% and 70-80% are not labeled.

5.2 Elliptic flow (v_2)

In this section we present first the published results for elliptic flow v_2 [69]. We focus in particular on centrality, transverse momentum and energy dependence of elliptic flow v_2.

5.2.1 Centrality dependence

The centrality dependence of integrated elliptic flow is shown in Fig. 5.2. The integrated elliptic flow is calculated for each centrality class using the measured $v_2(p_t)$ together with the charged particle p_t-differential yield, according to:

$$v_n \equiv \frac{\int_0^\infty v_n(p_t)\frac{dN}{dp_t}dp_t}{\int_0^\infty \frac{dN}{dp_t}dp_t} \,. \tag{5.1}$$

For the determination of the integrated elliptic flow, the magnitude of the charged particle reconstruction efficiency does not play a role, because it appears both in the numerator and the denominator of Eq. (5.1), and to leading order it cancels out. However, the relative change in efficiency as a function of transverse momentum does matter. The correction to the integrated elliptic flow due to the p_t cutoff at 200 MeV/c has been estimated based on HIJING and THERMINATOR simulations. Transverse momentum spectra in HIJING and THERMINATOR are different, which allows us to estimate the uncertainty

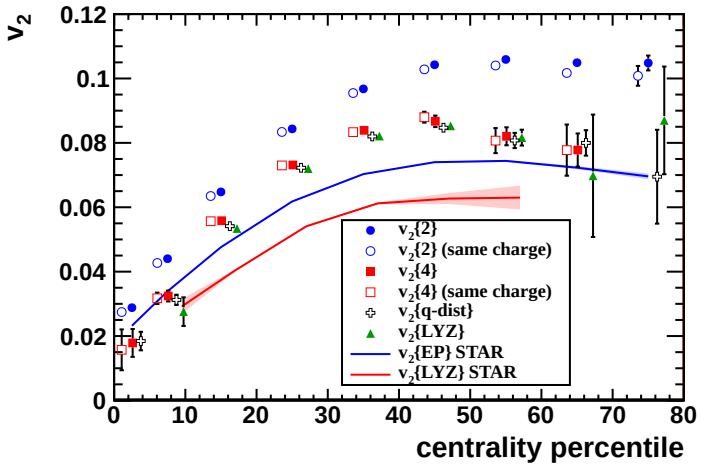

Figure 5.2: Elliptic flow integrated over the p_t range $0.2 < p_t < 5.0$ GeV/c, as a function of event centrality, for the 2- and 4-particle cumulant method, a fit of the distribution of the flow vector, and the Lee-Yang zeros method. For the cumulants the measurements are shown for all charged particles (full markers) and same charge particles (open markers). Data points are shifted horizontally for visibility. RHIC measurements for Au-Au at $\sqrt{s_{NN}} = 200$ GeV, integrated over the p_t range $0.15 < p_t < 2.0$ GeV/c, for the event plane $v_2\{\mathrm{EP}\}$ and Lee-Yang zeros are shown by the full curves.

in the correction. The correction is about 2% with an uncertainty of 1% [86]. In addition, the uncertainty due to the centrality determination results in a relative uncertainty of about 3% on the value of the elliptic flow, see Fig. 5.3. Figure 5.2 shows that the integrated elliptic flow increases from central to peripheral collisions and reaches a maximum value in the 50-60% and 40-50% centrality class of $0.106 \pm 0.001(\mathrm{stat}) \pm 0.004(\mathrm{syst})$ and $0.087 \pm 0.002(\mathrm{stat}) \pm 0.003(\mathrm{syst})$ for the 2- and 4-particle cumulant method, respectively. It is also seen that the measured integrated elliptic flow from the 4-particle cumulant, from fits of the flow vector distribution (FQD), and from the Lee-Yang zeros method (LYZ), are in agreement. The open markers in Fig. 5.2 show the results obtained for the cumulants using particles of the same charge. The 4-particle cumulant results agree within uncertainties for all charged particles and for the same charge particle data sets, indicating that the 4-particle cumulant by construction suppresses very well nonflow contribution from resonance decays, which comes only from the correlation of particles of opposite charge (due to charge conservation at each decay). The 2-particle cumulant results, as expected due to nonflow, depend weakly on the charge combination. The difference is most pronounced for the most peripheral and central events. More detailed results for various charge combinations are presented in Fig. 5.4 for $v_2\{2\}$ and $v_2\{4\}$. The results for higher order cumulants, $v_2\{6\}$ and $v_2\{8\}$, are presented in Fig. 5.5. Elliptic flow results estimated with 6- and 8-particle cumulants are in an excellent agreement

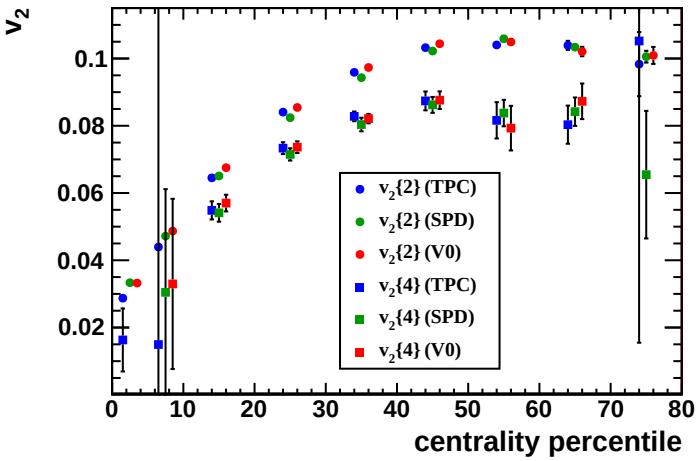

Figure 5.3: Centrality dependence of elliptic flow, where centrality was determined by using three different detectors: TPC (blue markers), SPD (green markers) and VZERO (red markers)

with 4-particle estimate, indicating that few particle nonflow correlations are already significantly suppressed with 4-particle cumulants. In addition, this agreement is also due to the fact that, to leading order, all higher order cumulants experience the same systematic bias due to statistical flow fluctuations (see Appendix A).

The results for integrated flow presented in Fig. 5.2 were obtained using only the events from the "golden run" 137161 (see Chapter 4). In Fig. 5.6 these results are compared with the results obtained by taking events from a subsequent run 137162, with the same selection criteria. As it can be seen in Fig. 5.6 the results of these two independent analyses are in an excellent agreement.

The cumulant results were obtained with Q-cumulants, however the cumulant analysis previously (most notably in the STAR experiment at RHIC) was performed by making use of the generating functions. For the ALICE data the comparison between these two versions of cumulants is presented in Fig. 5.7.

Reference flow particles were selected for the analysis in the transverse momentum range $[0.2, 5]$ GeV/c. The difference between these and when reference flow particles are in the range $[0.2, 2]$ GeV/c is shown in Fig. 5.8. These results are compared to results from the STAR experiment in Fig. 5.9. From this figure we can see that when the reference particles are taken from the transverse momentum interval $[0.2, 5]$ GeV/c, the values of integrated elliptic flow at LHC energies are about 30% larger than the corresponding values are RHIC energies (assuming a negligible importance of a small difference in the low p_t cutoff in the two measurements).

As already mentioned in Chapter 4 the elliptic flow analysis was performed independently by using only the TPC information during reconstruction ("TPC only" tracks)

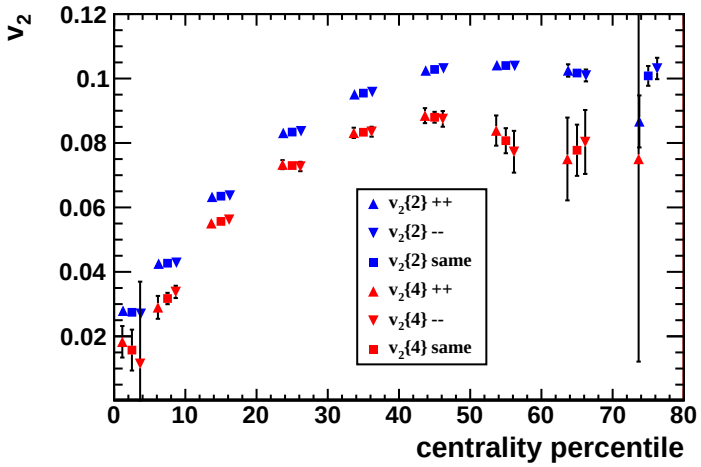

Figure 5.4: Comparison of p_t-integrated elliptic flow, for the 2- and 4-particle cumulant method, obtained for various charge combinations.

and by using the combined ITS-TPC information ("global" tracks). The first has the advantage of a uniform acceptance of reconstructed tracks due to the full azimuthal coverage of TPC, while the combined tracks are plagued by a systematic bias originating from the non-uniform acceptance of the SPD (the innermost part of the ITS). This systematic bias can be corrected for in the cumulant analysis by using the prescription outlined in Appendix D. The comparison of these independent analysis for $v_2\{2\}$ and $v_2\{4\}$ are presented in Fig. 5.10. All results are in agreement, and the results with "TPC only" tracks were used in the publication [69] because of the smaller corrections needed for acceptance effects. The discrepancy between results obtained with "global" tracks corrected and not corrected for non-uniform acceptance (open and filled blue circles, respectively, in Fig. 5.10) is largest in the centrality bins where the elliptic flow signal is smallest, as expected.

Now we present more recent results with higher statistics which allow for binning in much finer centrality ranges. The results were obtained from a data sample of about 5M minimum-bias Pb-Pb collisions, while the previous results were obtained from $\sim$ 45K events. As it was explained in Chapter 3 the flow contribution to cumulants is well understood and quantified by [55, 59]:

$$\begin{aligned} QC\{2\} &= v^2\,, & QC\{4\} &= -v^4\,, \\ QC\{6\} &= 4v^6\,, & QC\{8\} &= -33v^8\,. \end{aligned} \tag{5.2}$$

From the above equations, it is clear that when the measured cumulants are dominated by flow correlations, they will exhibit a characteristic signature $(+,-,+,-)$ irrespective of the order of the harmonic for which the cumulants are measured. In Fig. 5.11,

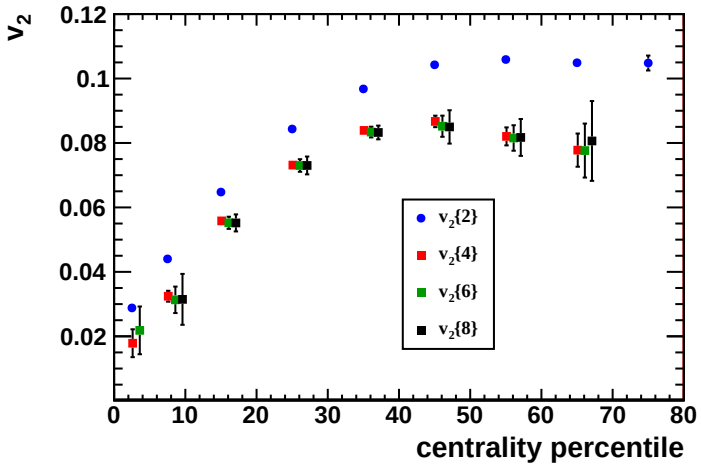

Figure 5.5: Elliptic flow integrated over the p_t range $0.2 < p_t < 5.0$ GeV/c, as a function of event centrality, for the 2-, 4-, 6- and 8-particle cumulant method, for all charged particles. Data points are shifted horizontally for visibility.

cumulants for harmonic $n = 2$ are shown in the centrality range 0-80%. The centrality bin width is 1% for 0-20% centrality and 2% for the range 20-80% centrality [84]. In Fig. 5.12 results for first 10 centralities where the flow signal is smallest are shown. Clearly, the cumulants show the characteristic flow signature. Inversion of Eq. (5.2) yields an independent estimate for the harmonic v_2, denoted as $v_2\{2\}, v_2\{4\}, v_2\{6\}$ and $v_2\{8\}$, respectively.[1] These independent estimates are presented in Fig. 5.13. The 2-particle estimate, $v_2\{2\}$, was obtained by using two different $|\Delta\eta|$ gaps (open and filled blue markers) in order to illustrate the magnitude of the nonflow contribution. The nonflow contribution to the 2-particle cumulant scales as $\sim 1/(M-1)$, where M is the multiplicity of the event, meaning that the relative nonflow contribution will be largest in the peripheral events where M is smallest, as indeed is seen in Fig. 5.13). All estimates from multi-particle cumulants are in an excellent agreement with each other (red, green and black markers) which indicates that already with the 4-particle cumulant nonflow is greatly suppressed, so that there is little gain in suppressing it further by using 6- and 8-particle cumulants. Finally, the difference between 2- and multi-particle estimates can be understood in terms of different (opposite in signature) sensitivity to the fluctuations in the initial geometry (see Appendix A).

The magnitude of multiplicity and trivial flow fluctuations, due to the size of the centrality bins, can be estimated by comparing, for instance, the results of flow analysis in centrality bins of varying width. The systematic bias on v_2 due to the multiplicity and

[1] To suppress nonflow contribution and to eliminate detector effects from reconstruction (e.g. track splitting), a $|\Delta\eta|$ gap was enforced among particles correlated in the measurement of the 2-particle cumulant.

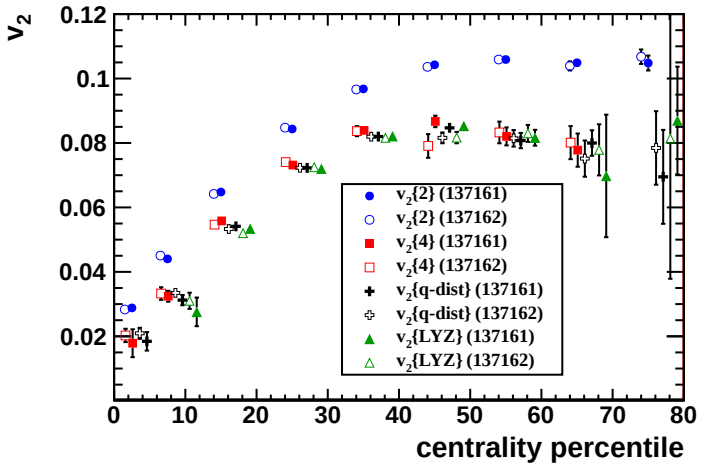

Figure 5.6: Elliptic flow integrated over the p_t range $0.2 < p_t < 5.0$ GeV/c, as a function of event centrality, for the 2- and 4-particle cumulant method, a fit of the distribution of the flow vector, and the Lee-Yang zeros method. Data points are shifted for visibility. With filled markers published results for "golden run" 137161 are shown, and with open markers the results for the subsequent run 137162. Same selection criteria was applied in both cases.

trivial flow fluctuations was estimated and found to be negligible compared to the large event-by-event flow fluctuations already present in small centrality bins, see Fig. 5.14.

When the analysis is performed as is done here in very fine centrality bins the centrality determination itself might yield a non-negligible systematic bias, due to limited resolution of centrality estimators. In order to estimate the magnitude of such bias, the centrality determination was performed by using these three different centrality estimators: VZERO (default), TPC and SPD. Results for the centrality dependence of $v_2\{2\}, v_2\{4\}, v_2\{6\}$ and $v_2\{8\}$, where centrality was determined by using three different centrality estimators, are presented in Figs. 5.15-5.18. These results were used for estimating the systematic uncertainty reported in Fig. 5.13.

5.2.2 Transverse momentum dependence

Having obtained the centrality dependence, we now outline a more differential and detailed anisotropic flow analysis. In particular, we consider the transverse momentum dependence of the flow harmonics v_n within each centrality class. Such analysis, for instance, might indicate precisely the onset of hydrodynamic description failure, which cannot be applicable in high-p_t range where the correlations are dominated by jets. Figure 5.19(a) shows $v_2(p_t)$ for the centrality class 40-50% obtained with different methods. For comparison, we present STAR measurements [90, 91] for the same centrality from

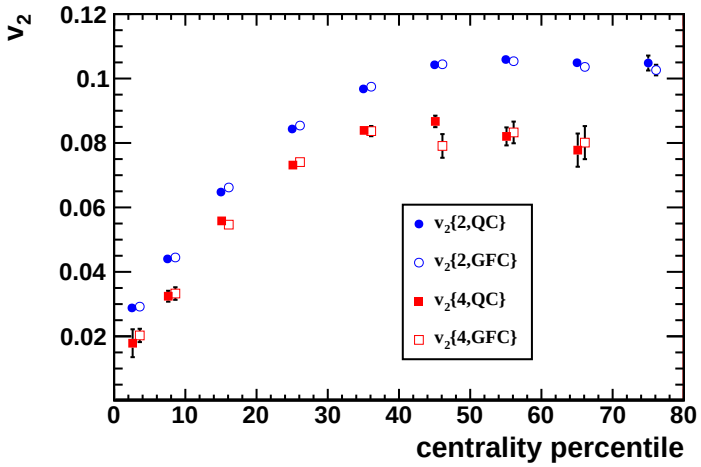

Figure 5.7: Comparison of p_t-integrated elliptic flow, for the 2- and 4-particle cumulant method, obtained via the formalism of generating functions (GFC) and Q-cumulants (QC).

Au-Au collisions at $\sqrt{s_{NN}} = 200$ GeV, indicated by the shaded band. We find that the value of $v_2(p_t)$ does not change within uncertainties from $\sqrt{s_{NN}} = 200$ GeV to 2.76 TeV. Figure 5.19(b) presents $v_2(p_t)$ obtained with the 4- particle cumulant method for three different centralities, compared to STAR measurements. The transverse momentum dependence is qualitatively similar for all three centrality classes.

5.2.3 Energy dependence

Depending on the collision energy the anisotropic flow pattern changes and this was already observed at previous experiments (see Fig. 1.9 and discussion below it). The integrated elliptic flow measured in ALICE in the 20-30% centrality class is compared to results from lower energies in Fig. 5.20. For the comparison the integrated elliptic flow has been corrected for the p_t cutoff of 0.2 GeV/c. The estimated magnitude of this correction is (12 ± 5)% based on calculations with THERMINATOR [86]. The figure shows that there is a continuous increase in the magnitude of the elliptic flow for this centrality region from RHIC to LHC energies. In comparison to the elliptic flow measurements in Au-Au collisions at $\sqrt{s_{NN}} = 200$ GeV, we observe about a 30% increase in the magnitude of v_2 at $\sqrt{s_{NN}} = 2.76$ TeV. The increase of about 30% is larger than in current ideal hydrodynamic calculations at LHC multiplicities [93] but is in agreement with some models that include viscous corrections which at the LHC become less important [94–98].

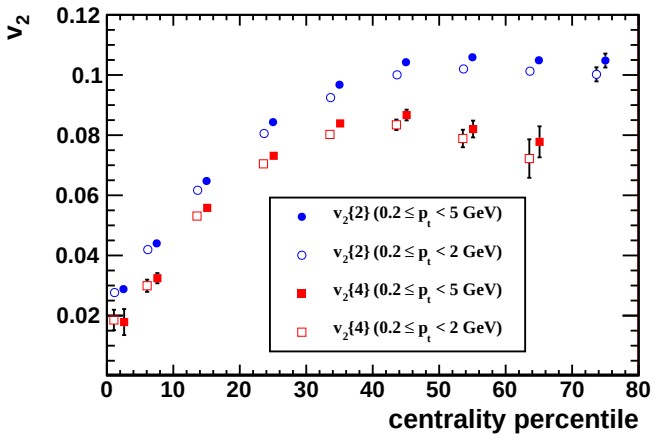

Figure 5.8: Comparison of p_t-integrated elliptic flow, for the 2- and 4-particle cumulant method, obtained for two different p_t ranges. With filled markers are published results where reference particles are selected from the interval $0.2 \leq p_t < 5$ GeV/c, and with open markers results for which transverse momentum of reference particles are constrained to interval $0.2 \leq p_t < 2$ GeV/c.

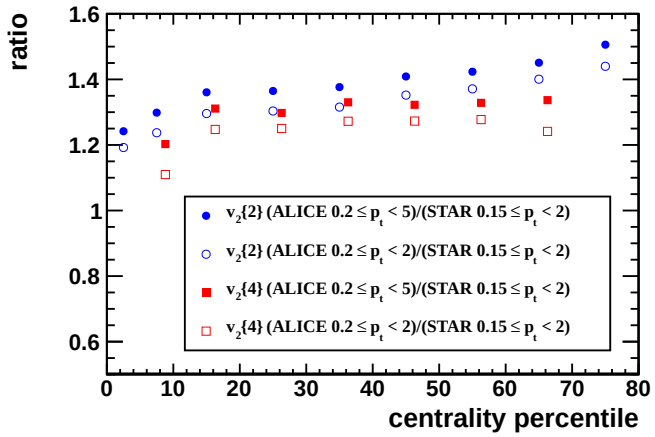

Figure 5.9: Comparison of p_t-integrated elliptic flow, for the 2- and 4-particle cumulant method, obtained for two different p_t ranges and compared to analogous STAR results. We observe that results for 4-particles estimates of v_2 are about 30% larger for midcentral collisions at LHC energy than analogous results at RHIC energy.

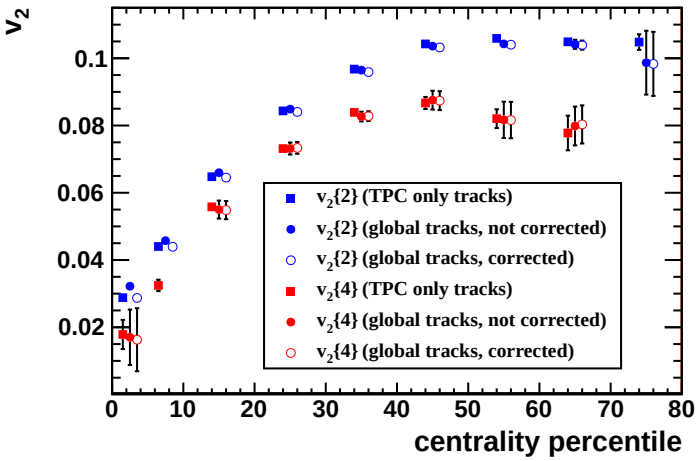

Figure 5.10: Comparison of p_t-integrated elliptic flow, for the 2- and 4-particle cumulant method, obtained for three different cases: a) Only the TPC information was used during reconstruction (filled squares), b) Combined ITS-TPC information was used during reconstruction and results were not corrected for acceptance effects (filled circles), and c) Combined ITS-TPC information was used during reconstruction and results were corrected for acceptance effects (open circles). All results are in an agreement to each other. The agreement between cases b) and c) indicates that acceptance effects are not dominant given the large value of measured v_2 signal.

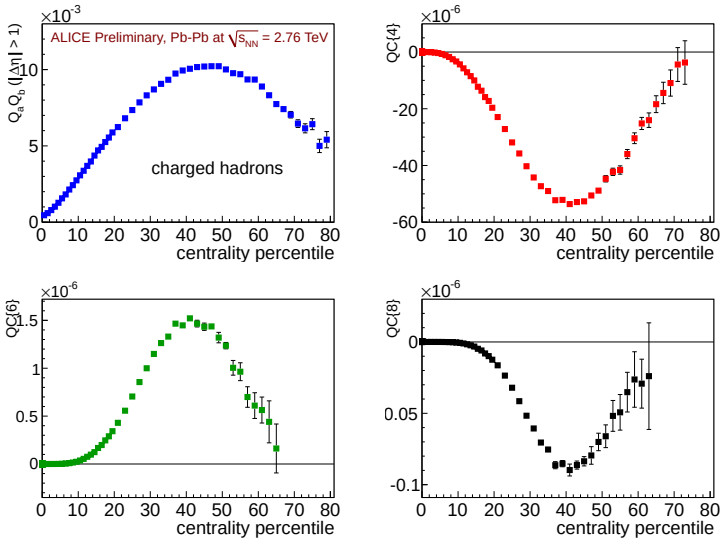

Figure 5.11: The centrality dependence of cumulants measured for harmonic $n = 2$.

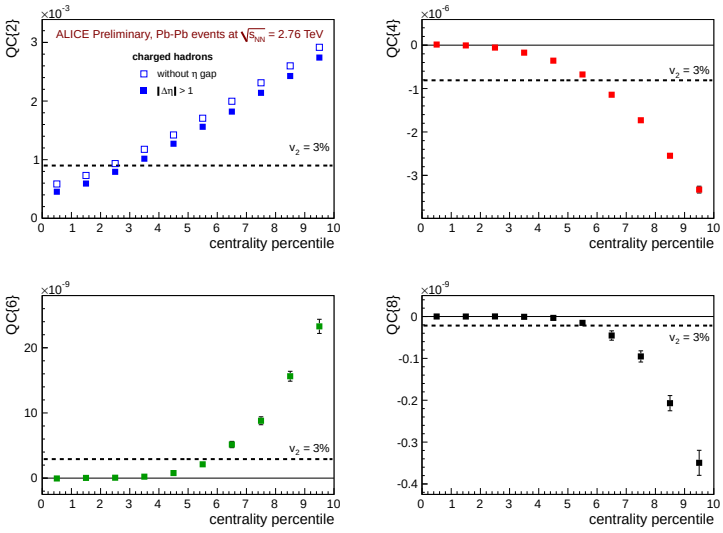

Figure 5.12: The centrality dependence of cumulants measured for harmonic $n = 2$ and zoomed only for ten most central centralities, with centrality bin width of 1%.

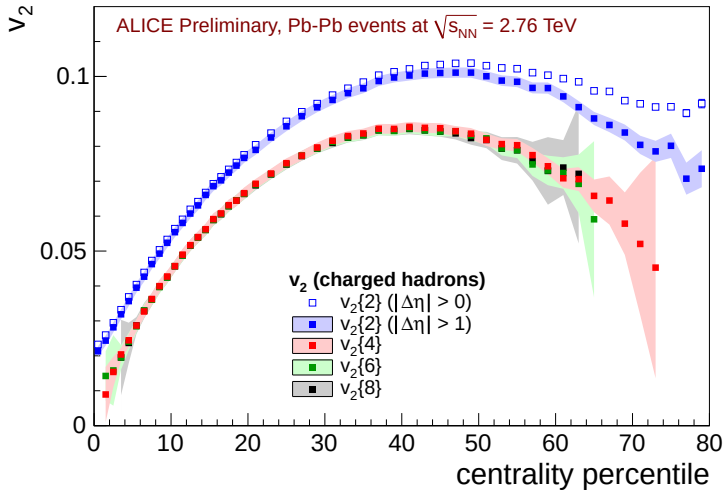

Figure 5.13: The centrality dependence of elliptic flow v_2, estimated with 2- and multi-particle Q-cumulants.

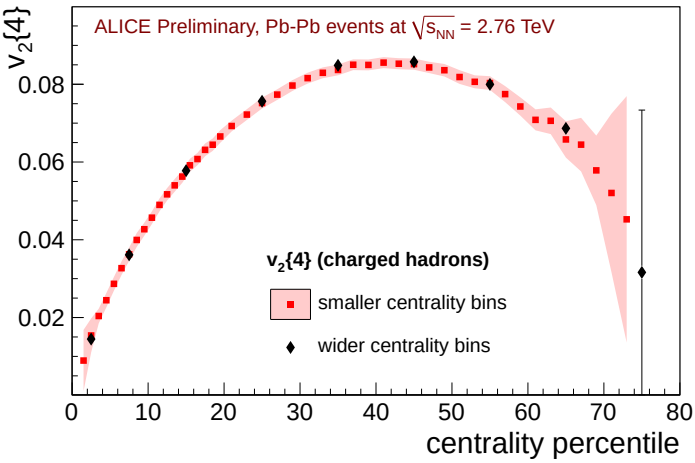

Figure 5.14: Comparison of elliptic flow results in smaller and wider centrality bins.

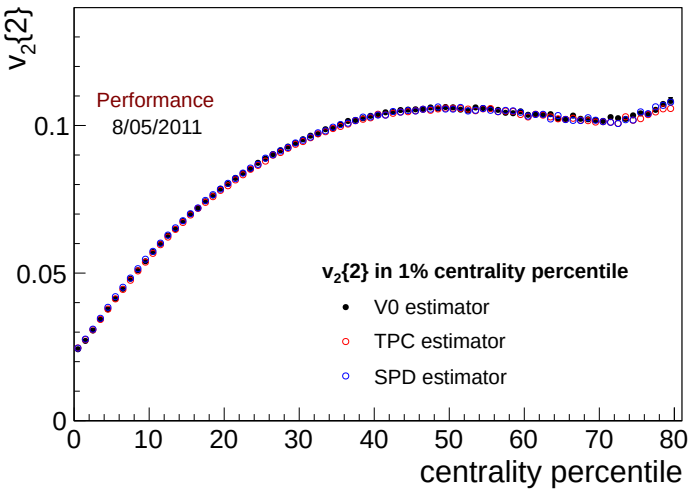

Figure 5.15: Centrality dependence of $v_2\{2\}$, where centrality was determined by using three different centrality estimators (VZERO, TPC and SPD).

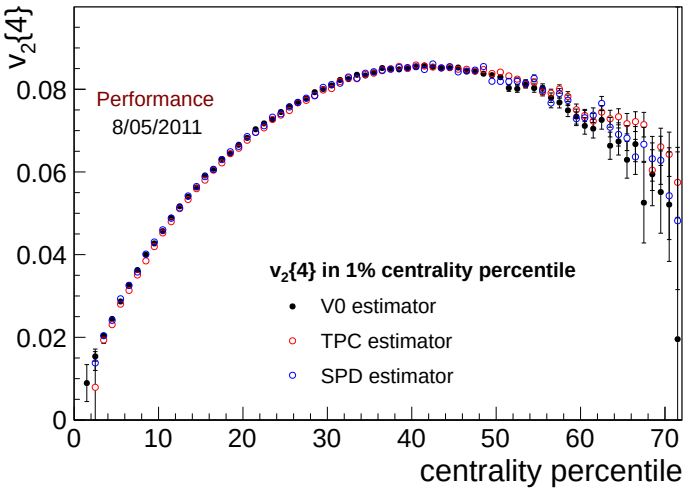

Figure 5.16: Centrality dependence of $v_2\{4\}$, where centrality was determined by using three different centrality estimators (VZERO, TPC and SPD).

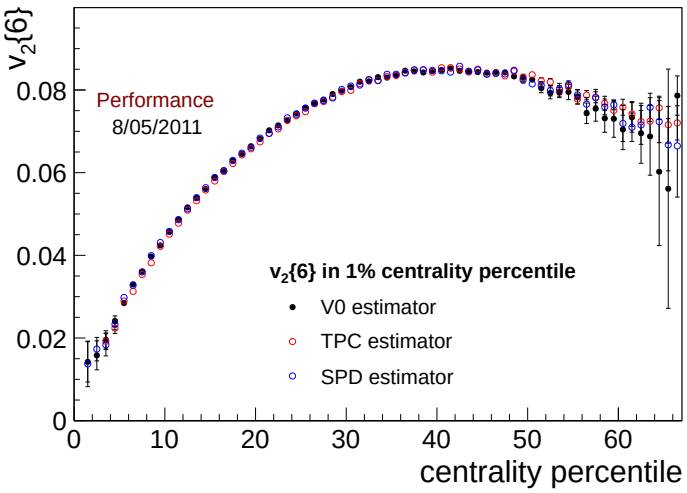

Figure 5.17: Centrality dependence of $v_2\{6\}$, where centrality was determined by using three different centrality estimators (VZERO, TPC and SPD).

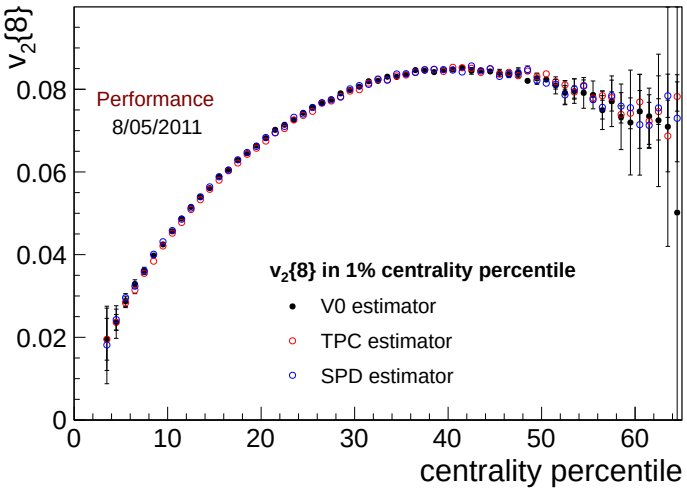

Figure 5.18: Centrality dependence of $v_2\{8\}$, where centrality was determined by using three different centrality estimators (VZERO, TPC and SPD).

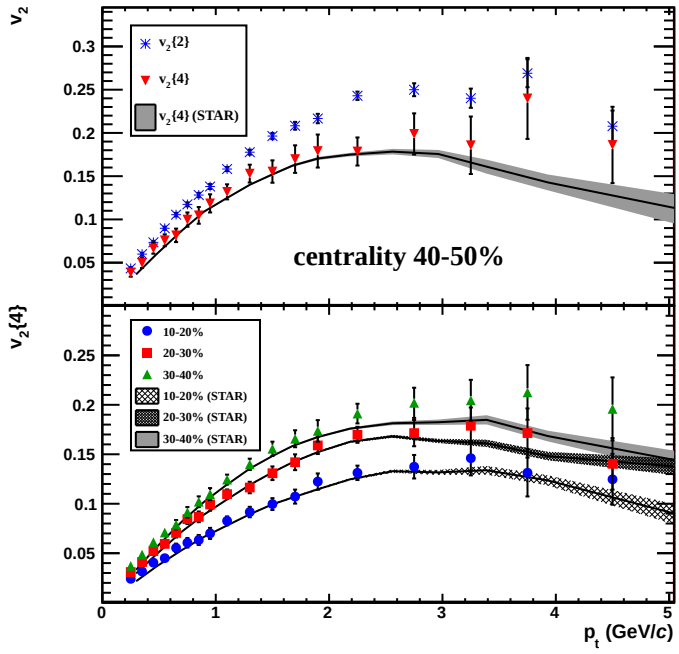

Figure 5.19: (a) $v_2(p_t)$ for the centrality bin 40-50% from the 2- and 4-particle cumulant methods for this measurement and for Au-Au collisions at $\sqrt{s_{NN}} = 200$ GeV. (b) $v_2\{4\}(p_t)$ for various centralities compared to STAR measurements. The data points in the 20-30% centrality bin are shifted in p_t for visibility.

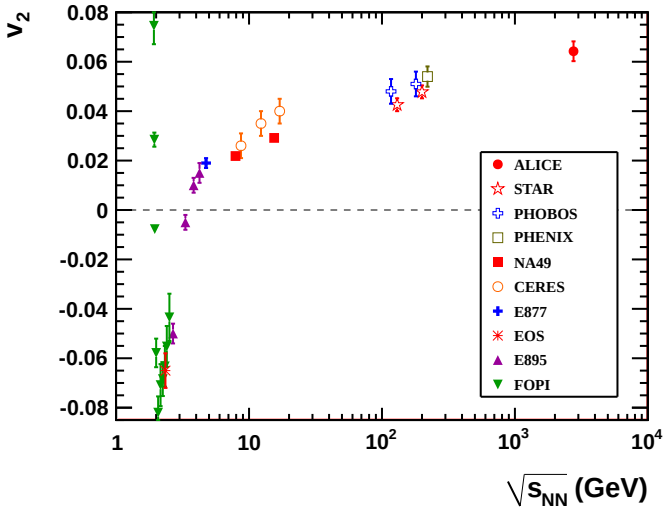

Figure 5.20: Integrated elliptic flow at 2.76 TeV in Pb-Pb 20–30% centrality class compared with results from lower energies taken at similar centralities [74, 75].

5.3 Higher harmonics

After publishing results of elliptic flow in [69] the anisotropic flow analysis within the ALICE collaboration mostly focused on the extraction of higher order harmonics, like v_3 (triangular flow), v_4 (quandrangular flow) and v_5 (pentagonal flow). This analysis was recently published in [70]. In this section we present the most important results.

5.3.1 Centrality dependence

In Fig. 5.21 the results for harmonics beyond v_2 are shown [70]. It can be seen that the triangular flow, v_3, is not zero. Triangular flow v_3 cannot develop as a correlation of all particles with the reaction plane (see discussion in Section 1.3.3), but only as a correlation with the participant plane of v_3 (event-by-event fluctuations in the initial geometry yields event-by-event triangularity in coordinate space which determines a symmetry plane[2]). More generally, each harmonic has its own participant plane, raising the question of the relation between the different participant planes. As an example, in Fig. 5.21 we demonstrate that the participant planes of v_2 and v_3 are uncorrelated (black diamonds)—see Appendix H for the technical details how the relevant measurements were performed. In general, the 5-particle correlator $QC\{5\} = \langle\cos[2\phi_1+2\phi_2+2\phi_3-3\phi_4-3\phi_5]\rangle$ is sensitive to the product $v_2^3 v_3^2$. In Fig. 5.21 we plot the measured $QC\{5\}$ divided by v_2^3. After this division we have obtained v_3^2 measured with respect to the symmetry (participant) plane of v_2, denoted as v_{3/Ψ_2} (multiplied by 100 in Fig. 5.21). We have adopted this notation because the measured 5-particle Q-cumulant can have both signs due to statistical fluctuations around zero. For the centralities where it goes negative we cannot take the square root—this is why we are plotting $100 \times v_{3/\Psi_2}^2$ and demonstrate that this quantity is consistent with zero. Finally, this result leads to the conclusion that the symmetry (participant) planes of v_2 and v_3 are not correlated, from which it follows that they cannot the same. Triangular flow estimated with the 4-particle cumulant (open blue squares) is half as large as the corresponding 2-particle estimate (filled blue squares), in agreement with a recent prediction by Bhalerao *et al* [89].

The nonflow contribution to the results for $v_3\{2\}$ and $v_3\{4\}$ presented in Fig. 5.21 was tested in Fig. 5.22, where is was estimated by: a) Correlating all charged particles in the analysis (filled blue upwards triangles), b) Correlating only particles of the same charge to suppress contribution from resonance decays which predominantly produce nonflow correlation among particles of opposite charge due to charge conservation (blue stars), c) Correlating only particles separated in rapidity, where the separation is larger than 0.2 unit of rapidity (open blue upwards triangles) or 1.0 unit of rapidity (open blue downwards triangles). By enforcing the rapidity separation among the particles being correlated we are suppressing the nonflow contributions from the near-side jets and decays—if the nonflow contribution is significant we will obtain different results for different rapidity separations. As it can be seen clearly from Fig. 5.22 all four results for $v_2\{2\}$ are in reasonable agreement for the 0% to 30% centrality percentile, beyond which nonflow contributions start to become visible. For more peripheral centrality

[2] In this thesis we use terms participant plane and symmetry plane at equal footing.

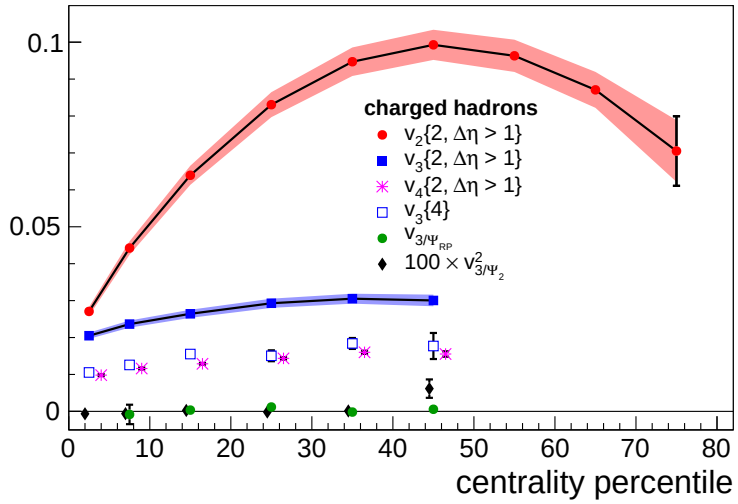

Figure 5.21: Centrality dependence of elliptic flow and higher harmonics.

bins (beyond centrality percentile 50%) the $v_3\{2\}$ estimates start to deviate even more, showing that the nonflow contribution becomes important. In red markers the results for $v_3\{4\}$ are shown. These results were obtained by taking all charged particles in the analysis (filled red squares) or by correlating only the particles of the same charge (open red squares). Within statistical fluctuations these two results are in agreement with each other indicating that nonflow is greatly suppressed by 4-particle cumulants (i.e. we do not observe any systematic difference between these two results).

A remaining important check is whether the v_3 signal shown in Figs. 5.21 and 5.22 is not originating from a trivial systematic bias coming from the interplay between nonflow correlations and multiplicity fluctuations, a bias which even the higher order cumulants cannot suppress well. To test this, all events were binned according to the number of reference particles (RPs), for which the relevant correlators were evaluated, and the flow analysis was performed in each bin separately. In Fig. 5.23 the results for v_2 and v_3 are plotted as a function of the number of RP's, estimated with all Q-cumulants up to order eight. These results as a function of the number of RP's are free from multiplicity fluctuations, and the results in wider bins were obtained after rebinning these results, it turn giving results which are free of multiplicity fluctuations also in wider bins. The resulting estimates in wider multiplicity bins for v_3 are shown in Fig. 5.24. Both 2- and 4-particle estimates are non-vanishing and both are consistent with the flow signature (see discussion following Eq. (5.2)). Taking the Q-cumulant results from Fig. 5.24 we finally obtain the results for $v_3\{2\}$ and $v_3\{4\}$ which are free of systematic bias originating from the interplay between nonflow correlations and multiplicity fluctuations. The results for $v_3\{2\}$ and $v_3\{4\}$ presented in Fig. 5.25 indicate that the corresponding results shown

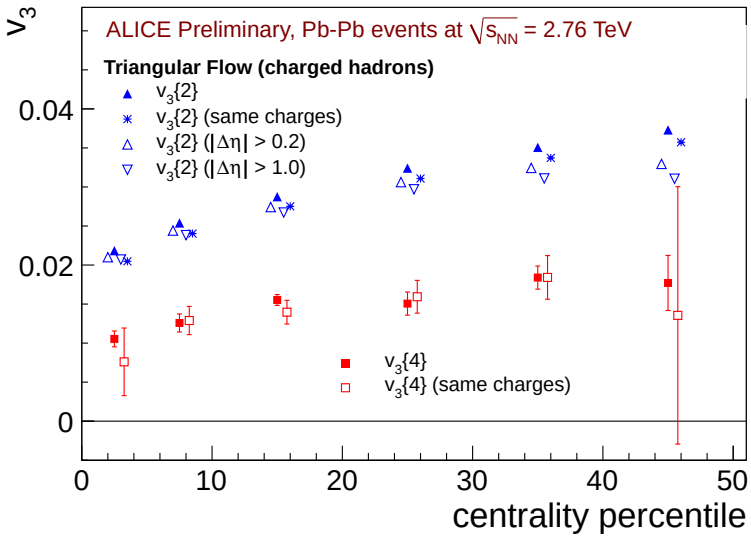

Figure 5.22: Centrality dependence of triangular flow estimated with 2- and 4-particle Q-cumulants, obtained for different charge combinations and different rapidity separation among correlated particles.

in Fig. 5.21 do not have significant contributions from the interplay between nonflow correlations and multiplicity fluctuations.

5.3.2 Transverse momentum dependence

In Fig. 5.26, the p_t dependence of the harmonics v_2, v_3, v_4 and v_5 are presented [70]. The elliptic and triangular flow is compared to model calculations based both on ideal and viscous relativistic hydrodynamics with Glauber initial conditions[3] (taking into account the role of event-by-event fluctuations of the initial conditions) as was proposed in [92]. Within this particular model the overall magnitude of elliptic and triangular flow agrees with the measurement, but the details of the p_t dependence are not well described. In particular, the magnitude of $v_2(p_t)$ is described better with ideal hydro with $\eta/s = 0$, while for $v_3(p_t)$ the model with $\eta/s = 0.08$ provides a better description, indicating that this model fails to describe v_2 and v_3 simultaneously.

[3]See Section 1.3.3 for the short introduction to Glauber model.

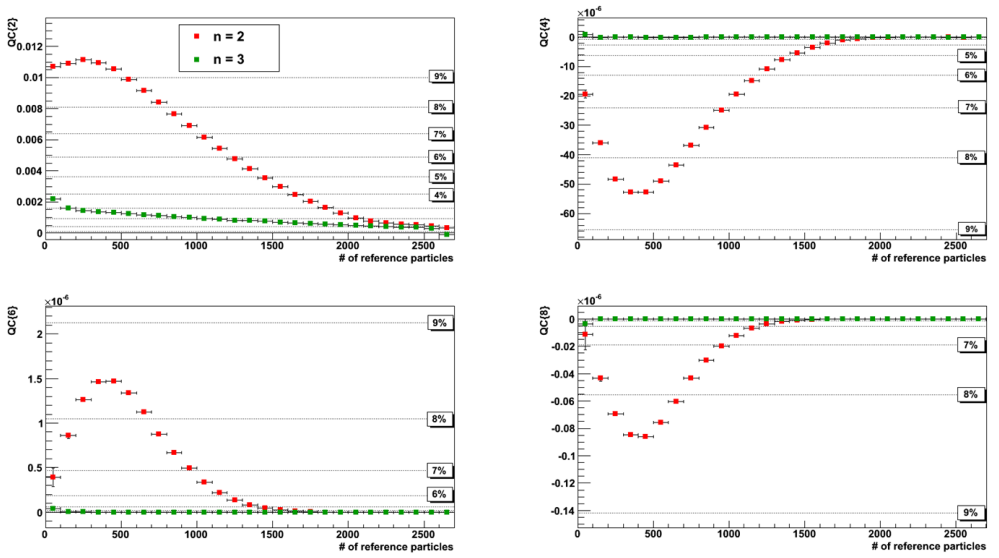

Figure 5.23: 2-, 4-, 6- and 8-particle Q-cumulants measured for harmonics $n = 2$ (red markers) and $n = 3$ (green markers), as a function of the number of reference particles.

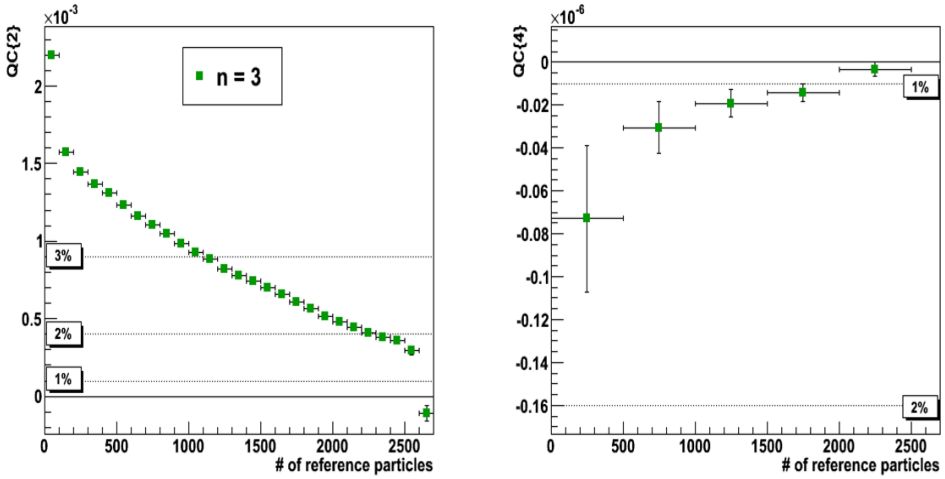

Figure 5.24: 2- and 4-particle Q-cumulants measured for harmonics $n = 3$, as a function of the number of reference particles.

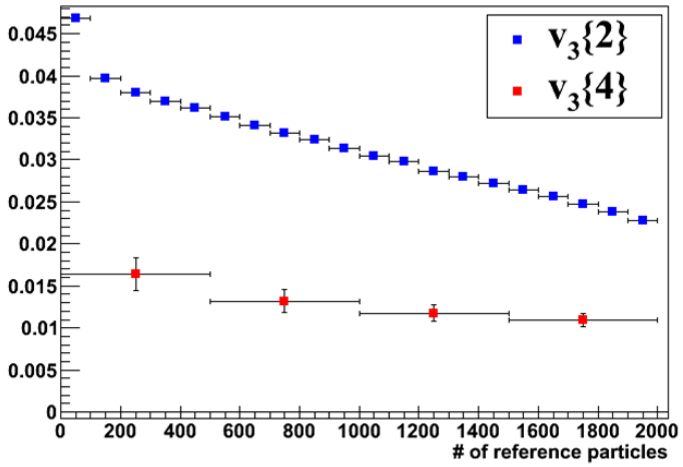

Figure 5.25: $v_3\{2\}$ and $v_3\{4\}$ as a function of the number of reference particles. These results are free from systematic bias coming from the interplay between nonflow correlations and multiplicity fluctuations.

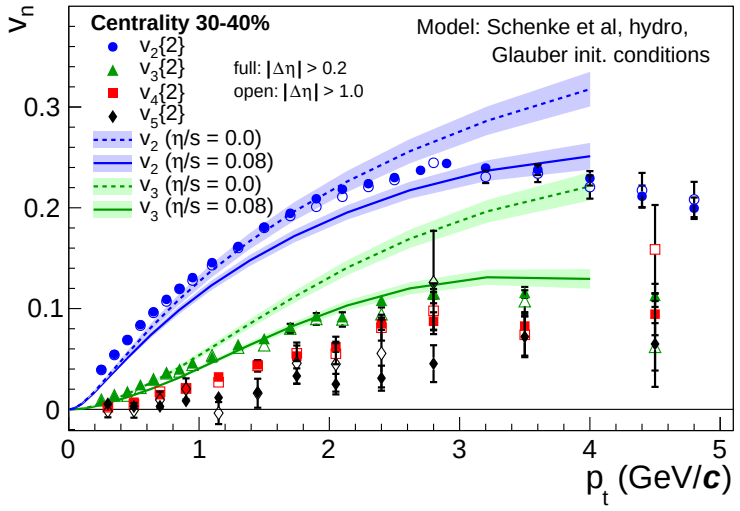

Figure 5.26: Comparison of transverse momentum dependence of measured anisotropic flow harmonic v_2, v_3, v_4 and v_5 with a particular theoretical model [92]. This model fails to describe v_2 and v_3 simultaneously.

5.4 Outlook

In this thesis anisotropic flow results were presented and were compared to theoretical predictions. The anisotropic flow analysis at LHC energies is far from finished. At the end of 2011 the second heavy-ion run will start at the LHC, and with the additional acquired statistics estimating higher order harmonics, like v_4 or v_5, with multi-particle cumulants might become feasible, providing further independent constraints on the nature of these harmonics. Another interesting prospect is the search for signatures of anisotropic flow in high-multiplicity p-p collisions. This direction of research is motivated by the fact that highest multiplicities in p-p collisions at LHC energies are comparable to the multiplicities in Cu-Cu collisions at RHIC for those centralities where sizable anisotropic flow has been reported. At the end of 2012 the LHC will deliver for the first time also p-A collisions. Given the expected sizable multiplicity in these collisions, it is natural to search for signatures of collective effects there as well.

Chapter 6

Epilogue

The most important material presented in this thesis contains the recent anisotropic flow results obtained from lead-lead collisions at LHC energies. The physics of anisotropic flow is a novel and rich field of research both for the experimentalists and the theorists, and this thesis aims to contribute to its better understanding. Clearly, there is still a long way to go before we can claim to have the full knowledge of anisotropic flow and all associated phenomena under our control. Nevertheless, with this thesis we have tried to make a step forward in that direction.

In the last couple of years is was realized that in addition to elliptic flow other harmonics v_n can be measured and can be understood in terms of event-by-event fluctuating initial spatial distributions of the created QGP matter. Therefore the complete anisotropic flow analysis requires the determination of both v_n and Ψ_n for each n—this was discussed in detail in Section 1.3.3.

Since the anisotropic flow phenomenon is closely intertwined with the physics underlying the initial collision geometry, it was important to establish a theoretical model which will relate harmonics v_n to the geometric quantities characterizing the initial geometry of colliding heavy-ions. An example of such a theoretical model is Glauber model, see Section 1.3.3.

Experimental methods developed to measure anisotropic flow harmonics v_n were presented and discussed in Chapter 3. A method which relies on estimating anisotropic flow harmonics by correlating azimuthal angles of two or more particles, and than isolating the contribution only from the genuine correlation involving all correlated particles, so-called cumulants, was presented in this chapter. Multi-particle cumulants (i.e. the genuine multi-particle correlations), are by definition less sensitive to systematic biases originating from correlations which are not determined by the initial geometry (e.g. resonance decays), because such correlations typically involve only few particles. The main issue in calculating multi-particle cumulants was tremendous CPU time required to loop over all distinct multi-particle tuples, prohibiting effectively the calculation of any correlation involving more than three particles. To circumvent this problem, cumulants were calculated via the formalism of generating functions (GFC) in the STAR experiment, and more recently in PHENIX and CMS. This formalism was described in

Section 3.1.7. However, GFC is by design fast but only an approximate way to perform cumulant analysis. The new, fast and exact, way to calculate all multi-particle cumulants, so-called Q-cumulants (QC), was presented in detail in Section 3.2. The list of improvements over other existing methods for anisotropic flow analysis was outlined in Section 3.2.4. The majority of anisotropic flow results presented in this thesis were obtained with these Q-cumulants.

Finally, in Chapter 5 we have presented our final results for the anisotropic flow of charged particles, obtained for Pb-Pb collisions at center of mass energy of 2.76 TeV per nucleon pair. In November 2010, 10 days after the first heavy-ion collisions were delivered by the LHC, the ALICE collaboration reported the initial measurement of elliptic flow v_2 [69]. The observed integrated elliptic flow at LHC energies is about 30% larger than at RHIC energies, while the differential elliptic flow $v_2(p_t)$ almost does not differ from the values measured at RHIC. The observed increase of $\sim$30% in integrated elliptic flow is attributed to larger radial flow at LHC energies [86]. In this thesis we have presented new and more detailed analysis obtained with much larger statistics, which allowed binning in very fine centrality bins of 1%. The elliptic flow measurements suggest that the produced matter in heavy-ion collisions at LHC energies remains to behave as a nearly perfect liquid.

After publishing the results for elliptic flow in [69], our subsequent analysis aimed at the measurement of higher order harmonics, like v_3 (triangular flow), v_4 (quadrangular flow) and v_5 (pentagonal flow). This analysis was recently published in [70], and in Section 5.3 the main results were presented. The analysis shows that odd harmonics, like v_3 and v_5, are not zero. Odd harmonics are sensitive only to the fluctuations in the initial positions of participating nucleons, therefore by measuring them we are probing the very early stages of heavy-ion collisions. The dominant harmonic in all centrality classes is v_2, due to the initial dominant elipsoidal geometry of the overlapping collision region in non-central heavy-ion collision. An exception are the most central collisions where all measured harmonics are comparable in size. This indicates that in the most central collisions the contributions from fluctuations in the initial geometry is the dominant effect. In the regime where flow fluctuations are non-negligible, the complete anisotropic analysis demands the determination of both flow harmonics v_n and associated symmetry (participant) planes Ψ_n (see discussion in Section 1.3.3). In Section 5.3 we have demonstrated, by utilizing 5-particle azimuthal correlations, that the symmetry planes Ψ_2 and Ψ_3 (associated to harmonics v_2 and v_3, respectively) are uncorrelated. The transverse momentum dependence of the harmonics v_2 and v_3 was compared to model calculations from [92]. Within this particular model the overall magnitude of elliptic and triangular flow agrees with the measurement, but the details of the p_t dependence are not well described, indicating that further tuning of theoretical models is required.

Bibliography

[1] F.Carminati, (Ed.) *et al.* [ALICE Collaboration], J. Phys. G **G30** (2004) 1517-1763.

[2] E. V. Shuryak, Zh. Eksp. Teor. Fiz. **74** (1978) 408.

[3] Shuryak, Edward: Structure of Strongly Coupled Quark-Gluon Plasma. Stock, R. (ed.). SpringerMaterials - The Landolt-Brnstein Database (http://www.springermaterials.com). Springer-Verlag Berlin Heidelberg, 2010. DOI: $10.1007/978-3-642-01539-7_19$.

[4] T. D. Lee, G. C. Wick, Phys. Rev. **D9** (1974) 2291.

[5] K. H. Ackermann *et al.* [STAR Collaboration], Phys. Rev. Lett. **86** (2001) 402-407.

[6] T. Hirano, N. van der Kolk, A. Bilandzic, Lect. Notes Phys. **785** (2010) 139-178. [arXiv:0808.2684 [nucl-th]].

[7] http://www.bnl.gov/bnlweb/pubaf/pr/PR_display.asp ?prID=05-38.

[8] L.D. Landau, E.M. Lifshitz: *Fluid Mechanics*, (Pergamon Press, New York, 1959), Sections 133–136.

[9] C. Eckart: Phys. Rev. **58**, 919 (1940).

[10] T. Hirano, *"Hydrodynamics and Flow"*, pages 13-14, http://tkynt2.phys.s.u-tokyo.ac.jp/∼hirano/presentation/08YITPlecture/hirano_2nd.ppt .

[11] U. W. Heinz, in 'Relativistic Heavy Ion Physics', Landolt-Boernstein New Series, I/23, edited by R. Stock (Springer Verlag, New York,2010) Chap. 5 [arXiv:0901.4355 [nucl-th]].

[12] J. D. Bjorken: Phys. Rev. D **27**, 140 (1983).

[13] P. Kovtun, D. T. Son and A. O. Starinets: Phys. Rev. Lett. **94**, 111601 (2005).

[14] A. Nakamura and S. Sakai: Phys. Rev. Lett. **94**, 072305 (2005).

[15] D. Kharzeev, K. Tuchin, JHEP **0809** (2008) 093.

[16] F. Karsch, D. Kharzeev and K. Tuchin: Phys. Lett. B **663**, 217 (2008).

[17] M. Mizutani, S. Muroya and M. Namiki: Phys. Rev. D **37**, 3033 (1988).

[18] W. A. Hiscock, L. Lindblom, Phys. Rev. **D31** (1985) 725-733.

[19] G. S. Denicol, T. Kodama, T. Koide, P. .Mota, J. Phys. G **G35** (2008) 115102.

[20] C. Cattaneo: Atti. Sem. Mat. Univ. Modena **3**, 83 (1948)

[21] http://cdsweb.cern.ch/record/1165534/files/CERN-Brochure-2009-003-Eng.pdf .

[22] CERN public pages (http://public.web.cern.ch/public/) .

[23] ALICE public pages (http://aliceinfo.cern.ch/Public/Welcome.html) .

[24] ATLAS public pages (http://atlas.ch) .

[25] CMS public pages (http://cms.web.cern.ch/cms/index.html) .

[26] LHCb public pages (http://lhcb-public.web.cern.ch/lhcb-public/) .

[27] CERN public pages (http://public.web.cern.ch/public/en/LHC/LHCf-en.html) .

[28] TOTEM public pages (http://totem.web.cern.ch/Totem/) .

[29] K. Aamodt *et al.* [ALICE Collaboration], JINST **3** (2008) S08002.

[30] G. Dellacasa *et al.* [ALICE Collaboration], "ALICE: Technical design report of the time projection chamber."

[31] GAlessandro, (Ed.) *et al.* [ALICE Collaboration], J. Phys. G **G32** (2006) 1295-2040.

[32] G. Dellacasa *et al.* [ALICE Collaboration], "ALICE technical design report of the inner tracking system (ITS)."

[33] PCortese *et al.* [ALICE Collaboration], "ALICE technical design report on forward detectors: FMD, T0 and V0."

[34] G. Dellacasa *et al.* [ALICE Collaboration], "ALICE technical design report of the zero degree calorimeter (ZDC)."

[35] J. Y. Ollitrault, Phys. Rev. D **46** (1992) 229.

[36] S. Voloshin and Y. Zhang, Z. Phys. C **70** (1996) 665.

[37] P. F. Kolb, Phys. Rev. **C68** (2003) 031902.

[38] S. A. Voloshin, A. M. Poskanzer, A. Tang, G. Wang, Phys. Lett. **B659** (2008) 537-541.

[39] E. Butkov, "Mathematical Physics", Addison-Wesley Series in Advanced Physics, 1968.

[40] H. Heiselberg and A. M. Levy: Phys. Rev. C **59**, 2716 (1999).

[41] H. Sorge: Phys. Rev. Lett. **82**, 2048 (1999).

[42] S. A. Voloshin and A. M. Poskanzer: Phys. Lett. B **474**, 27 (2000).

[43] R. J. Glauber, *Lectures in Theoretical Physics*, ed. WE Brittin, LG Dunham, 1:315. New York: Interscience (1959) .

[44] M. L. Miller, K. Reygers, S. J. Sanders, P. Steinberg, Ann. Rev. Nucl. Part. Sci. **57** (2007) 205-243.

[45] M. Miller and R. Snellings: arXiv:nucl-ex/0312008.

[46] X. l. Zhu, M. Bleicher and H. Stoecker: Phys. Rev. C **72**, 064911 (2005).

[47] H. J. Drescher and Y. Nara: Phys. Rev. C **75**, 034905 (2007).

[48] R. Andrade, F. Grassi, Y. Hama, T. Kodama and O. Socolowski Jr.: Phys. Rev. Lett. **97**, 202302 (2006).

[49] W. Broniowski, P. Bozek and M. Rybczynski: Phys. Rev. C **76**, 054905 (2007).

[50] B. Alver *et al.*: Phys. Rev. C **77**, 014906 (2008).

[51] P. F. Kolb, U. W. Heinz, In *Hwa, R.C. (ed.) et al.: Quark gluon plasma* 634-714.

[52] P. F. Kolb, J. Sollfrank and U. W. Heinz: Phys. Rev. C **62**, 054909 (2000).

[53] C. Alt *et al.* [NA49 Collaboration]: Phys. Rev. C **68**, 034903 (2003).

[54] N. Borghini, P. M. Dinh, J. -Y. Ollitrault, Phys. Rev. **C63** (2001) 054906.

[55] N. Borghini, P. M. Dinh, J. -Y. Ollitrault, Phys. Rev. **C64** (2001) 054901.

[56] N. Borghini, P. M. Dinh, J. -Y. Ollitrault, [nucl-ex/0110016].

[57] C. Adler *et al.* [STAR Collaboration], Phys. Rev. C **66**, 034904 (2002).

[58] A. M. Poskanzer, S. A. Voloshin, Phys. Rev. **C58** (1998) 1671-1678.

[59] A. Bilandzic, R. Snellings, S. Voloshin, Phys. Rev. **C83** (2011) 044913.

[60] R. S. Bhalerao, N. Borghini, J. Y. Ollitrault, Phys. Lett. **B580** (2004) 157-162.

[61] R. S. Bhalerao, N. Borghini and J. Y. Ollitrault Nucl. Phys. A **727** (2003) 373.

[62] R. S. Bhalerao, N. Borghini and J. Y. Ollitrault J. Phys. G **30** (2004) S1213.

[63] A. Bilandzic, N. van der Kolk, J. -Y. Ollitrault, R. Snellings, Phys. Rev. **C83** (2011) 014909.

[64] S. Wang, Y. Z. Jiang, Y. M. Liu, D. Keane, D. Beavis, S. Y. Chu, S. Y. Fung, M. Vient *et al.*, Phys. Rev. **C44** (1991) 1091-1095.

[65] S. A. Voloshin, arXiv:nucl-th/0606022.

[66] R. Kubo, "Generalized Cumulant Expansion Method," Journal of the Physical Society of Japan, Vol. 17, No. 7, (1962).

[67] G. Cowan, "Statistical data analysis," *Oxford, UK: Clarendon (1998) 197 p*.

[68] S. Brandt, "Statistical and Computational Methods in Data Analysis," *Amsterdam 1976, 414p*.

[69] Aamodt *et al.* [The ALICE Collaboration], Phys. Rev. Lett. **105** (2010) 252302.

[70] [ALICE Collaboration], Phys. Rev. Lett. **107** (2011) 032301.

[71] J. Adams *et al.* [STAR Collaboration], Phys. Rev. Lett. **92**, 062301 (2004).

[72] N. Borghini, P. M. Dinh and J. Y. Ollitrault, Phys. Rev. C **66**, 014905 (2002).

[73] I. Selyuzhenkov and S. A. Voloshin Phys. Rev. C **77** (2008) 034904.

[74] S. A. Voloshin, A. M. Poskanzer, and R. Snellings, in Landolt-Boernstein, Relativistic Heavy Ion Physics Vol. 1/23 (Springer-Verlag, Berlin, 2010), pp 554.

[75] A. Andronic *et al.* [FOPI Collaboration], Phys. Lett. **B612** (2005) 173-180.

[76] "ALICE Offline pages", http://aliweb.cern.ch/Offline/.

[77] "ROOT System", http://root.cern.ch/.

[78] M. Ballintijn, R. Brun, F. Rademakers and G. Roland "Distributed Parallel Analysis Framework with PROOF," Proc. TUCT004 (2004).

[79] H-U. Bengtsson, T. Sjostrand (1987) Comput. Phys. Commun. **46** 43 (http://www.thep.lu.se/ torbjorn/Pythia.html).

[80] X-N. Wang, M. Gyulassy (1991) Phys. Rev. D 44 3501, M. Gyulassy, X-N. Wang (1994) Comput. Phys. Commun. 83 30731, (http://www-nsdth.lbl.gov/ xnwang/hijing/).

[81] R. Brun, F. Bruyant, M. Maire, A.C. McPherson, P. Zanarini (1985) GEANT3 User Guide CERN Data Handling Division DD/EE/84-1 (http://wwwinfo.cern.ch/asdoc/geantold/GEANTMAIN.html).

[82] J. Conrad *et al* "Minimum bias triggers in proton-proton collisions with VZERO and pixel detectors" ALICE Internal Note ALICE-INT-2005-025, http://cdsweb.cern.ch/record/960438.

[83] C. Loizides, f. t. A. collaboration, "Charged-particle multiplicity and transverse energy in Pb-Pb collisions at sqrt(snn) = 2.76 TeV with ALICE," [arXiv:1106.6324 [nucl-ex]].

[84] A. T. f. Collaboration, arXiv:1107.1973 [nucl-ex].

[85] B. Abelev *et al.* [The ALICE Collaboration], Phys. Rev. Lett. **105** (2010) 252301 .

[86] M. Krzewicki, PhD thesis, *"Anisotropic flow of identifed hadrons in heavy-ion collisions at the LHC — from detector alignment and calibration to measurement,"* Nikhef and Utrecht University, 2011.

[87] A. Kisiel, T. Taluc, W. Broniowski and W. Florkowski, Comput. Phys. Commun. **174**, 669 (2006) .

[88] P. Bozek, M. Chojnacki, W. Florkowski and B. Tomasik, Phys. Lett. B **694**, 238 (2010) .

[89] R. S. Bhalerao, M. Luzum and J. Y. Ollitrault, [arXiv:1104.4740 [nucl-th]].

[90] Y. Bai, Ph.D. thesis, Nikhef and Utrecht University, 2007.

[91] B. I. Abelev *et al.* [STAR Collaboration], Phys. Rev. C **77** (2008) 054901 .

[92] B. Schenke, S. Jeon, C. Gale, [arXiv:1102.0575 [hep-ph]].

[93] G. Kestin, U. W. Heinz, Eur. Phys. J. **C61** (2009) 545-552.

[94] H. Masui, J-Y. Ollitrault, R. Snellings, A. Tang, Nucl. Phys. **A830** (2009) 463C-466C.

[95] M. Luzum, P. Romatschke, Phys. Rev. Lett. **103** (2009) 262302.

[96] T. Hirano, P. Huovinen, Y. Nara, Phys. Rev. **C83** (2011) 021902.

[97] T. Hirano, U. W. Heinz, D. Kharzeev, R. Lacey, Y. Nara, Phys. Lett. **B636** (2006) 299-304.

[98] H. -J. Drescher, A. Dumitru, J. -Y. Ollitrault, [arXiv:0706.1707 [nucl-th]].

[99] P. Billor, "Track Fitting with Multiple Scattering: A New Method," NIM **A225**, 352-366 (1984) .

Appendix A

Flow fluctuations

By using multiparticle correlations to estimate flow harmonics we are actually estimating the averages of various powers of flow harmonics,[1]

$$\langle\langle 2\rangle\rangle = \langle v^2\rangle \,, \tag{A.1}$$
$$\langle\langle 4\rangle\rangle = \langle v^4\rangle \,, \tag{A.2}$$
$$\langle\langle 6\rangle\rangle = \langle v^6\rangle \,, \tag{A.3}$$
$$\langle\langle 8\rangle\rangle = \langle v^8\rangle \,. \tag{A.4}$$

What we are after, however, is $\langle v\rangle$. This means that even in the perfect case scenario ('when only flow correlations are present') the flow estimates obtained from multiparticle correlations will be systematically biased due to the statistical flow fluctuations, which are unavoidable. In what follows we will quantify this systematic bias to the flow estimates from Q-cumulants.

A.1 Some general results

Consider the random observable x sampled from some probability density function (p.d.f.) $f(x)$. The *mean* of x we denote by μ_x and the *variance* of x we denote by σ_x^2 (or equivalently by $V[x]$). Mean and variance of x are given by the following expressions:

$$\mu_x = E[x] = \int_{-\infty}^{\infty} x f(x) dx \,, \tag{A.5}$$
$$\sigma_x^2 = V[x] = E[(x - E[x])^2] = \int_{-\infty}^{\infty} (x - \mu_x)^2 f(x) dx \,, \tag{A.6}$$

where $E[x]$ stands for the *expectation value* of a random variable x.

[1] For simplicity sake in this appendix we suppress the harmonic index and use $v \equiv v_n$ instead.

Now consider any function of a random variable x, $h(x)$, and it's Taylor expansion round mean μ_x up to second order:

$$h(x) = h(\mu_x) + (x - \mu_x)h'(\mu_x) + \frac{(x-\mu_x)^2}{2!}\, h''(\mu_x)\,. \tag{A.7}$$

We are interested to know what is $E[h(x)]$, which we will denote with $\langle h(x)\rangle$. It follows straightforwardly from (A.7),

$$\begin{aligned}
\langle h(x)\rangle \equiv E[h(x)] &= h(\mu_x) + (E[x] - \mu_x)h'(\mu_x) + \frac{1}{2}\, E[(x-\mu_x)^2]h''(\mu_x) \\
&= h(\mu_x) + (\mu_x - \mu_x)h'(\mu_x) + \frac{\sigma_x^2}{2}\, h''(\mu_x) \\
&= h(\mu_x) + \frac{\sigma_x^2}{2}\, h''(\mu_x)\,.
\end{aligned} \tag{A.8}$$

In arriving at last equality we have made use of Eqs. (A.5) and (A.6). In particular, we see that expectation value of the linear term in Taylor's expansion of $h(x)$ round the mean μ_x always vanishes. As an unbiased estimator for the mean μ_x in subsequent sections we will use the sample mean $\langle x\rangle$ of a random variable x.

A.2 $v\{2\}$

Straight from the definitions we have

$$v\{2\} = \left\langle v^2 \right\rangle^{1/2}\,. \tag{A.9}$$

By making use of the Taylor expansion (A.8) for the case $h(v) \equiv v^2$ it follows

$$\left\langle v^2 \right\rangle = \langle v\rangle^2 + \sigma_v^2\,, \tag{A.10}$$

(as it of course should), which can be readily inserted into Eq. (A.9) to obtain

$$\begin{aligned}
v\{2\} &= \left(\langle v\rangle^2 + \sigma_v^2\right)^{1/2} \\
&= \langle v\rangle \left(1 + \frac{\sigma_v^2}{\langle v\rangle^2}\right)^{1/2} \\
&\simeq \langle v\rangle \left(1 + \frac{1}{2}\,\frac{\sigma_v^2}{\langle v\rangle^2}\right)\,,
\end{aligned} \tag{A.11}$$

where in obtaining the last line we have assumed that

$$\sigma_v \ll \langle v\rangle\ , \tag{A.12}$$

and we have used the general result

$$(1+x)^n \simeq 1 + nx\,, \tag{A.13}$$

valid for $x \simeq 0$. Eq. (A.11) can be further simplified to obtain the final result

$$v\{2\} \simeq \langle v \rangle + \frac{1}{2} \frac{\sigma_v^2}{\langle v \rangle} \,. \tag{A.14}$$

From this result we conclude that the flow estimate from 2$^{\text{nd}}$ order Q-cumulant will be always systematically biased with positive signature due to statistical flow fluctuations.

In the next sections we will investigate how this bias looks for the higher order estimates.

A.3 $v\{4\}$

Straight from the definitions we have

$$v\{4\} = \left(- \left\langle v^4 \right\rangle + 2 \left\langle v^2 \right\rangle^2 \right)^{1/4} \,. \tag{A.15}$$

If we use Taylor expansion (A.8) for the case $h(v) \equiv v^4$ we have up to second order in σ_v

$$\left\langle v^4 \right\rangle = \langle v \rangle^4 + 6\sigma_v^2 \langle v \rangle^2 \,. \tag{A.16}$$

Plugging Eqs. (A.10) and (A.16) into (A.15) it follows

$$\begin{aligned} v\{4\} &= \left[- \langle v \rangle^4 - 6\sigma_v^2 \langle v \rangle^2 + 2 \left(\langle v \rangle^2 + \sigma_v^2 \right)^2 \right]^{1/4} \\ &= \left[\langle v \rangle^4 - 2\sigma_v^2 \langle v \rangle^2 + \mathcal{O}(\sigma_v^4) \right]^{1/4} \\ &= \langle v \rangle \left(1 - 2 \frac{\sigma_v^2}{\langle v \rangle^2} \right)^{1/4} \\ &\simeq \langle v \rangle \left(1 - \frac{1}{2} \frac{\sigma_v^2}{\langle v \rangle^2} \right) \,, \end{aligned} \tag{A.17}$$

so that finally we have

$$v\{4\} \simeq \langle v \rangle - \frac{1}{2} \frac{\sigma_v^2}{\langle v \rangle} \,. \tag{A.18}$$

From this expression we conclude that the flow estimate from 4$^{\text{th}}$ order Q-cumulant will be always systematically biased with negative signature due to statistical flow fluctuations, showing thus the *opposite* trend when compared to the systematic bias to flow estimate from 2$^{\text{nd}}$ order Q-cumulant given in Eq. (A.14).

In the next section we will reveal what happens at 6$^{\text{th}}$ order.

A.4 $v\{6\}$

Straight from the definitions we have

$$v\{6\} = \left[\frac{1}{4}\left(\left\langle v^6\right\rangle - 9\left\langle v^2\right\rangle\left\langle v^4\right\rangle + 12\left\langle v^2\right\rangle^3\right)\right]^{1/6} . \tag{A.19}$$

From Taylor formula (A.8) for the case $h(v) \equiv v^6$ we have up to second order is σ_v,

$$\left\langle v^6\right\rangle = \langle v\rangle^6 + 15\sigma_v^2\langle v\rangle^4 . \tag{A.20}$$

Plugging Eqs. (A.10), (A.16) and (A.20) into Eq. (A.19) it follows,

$$\begin{aligned} v\{6\} &= [\frac{1}{4}\big(\langle v\rangle^6 + 15\sigma_v^2\langle v\rangle^4 - 9\big(\langle v\rangle^2 + \sigma_v^2\big)\big(\langle v\rangle^4 + 6\sigma_v^2\langle v\rangle^2\big) \\ &\quad +12\big(\langle v\rangle^2 + \sigma_v^2\big)^3\big)\big]^{1/6} . \end{aligned} \tag{A.21}$$

Keeping within the bracket only terms up to order σ_v^2 it follows

$$\begin{aligned} v\{6\} &= \left[\frac{1}{4}\left(4\langle v\rangle^6 - 12\sigma_v^2\langle v\rangle^4\right)\right]^{1/6} \\ &= \left[\langle v\rangle^6 - 3\sigma_v^2\langle v\rangle^4\right]^{1/6} \\ &= \langle v\rangle\left[1 - 3\frac{\sigma_v^2}{\langle v\rangle^2}\right]^{1/6} \\ &\simeq \langle v\rangle\left[1 - \frac{1}{2}\frac{\sigma_v^2}{\langle v\rangle^2}\right] , \end{aligned} \tag{A.22}$$

so that finally we have

$$v\{6\} \simeq \langle v\rangle - \frac{1}{2}\frac{\sigma_v^2}{\langle v\rangle} , \tag{A.23}$$

which is to leading order the same result as the one obtained for $v\{4\}$ given in Eq. (A.18). In the next section we provide the result for the 8^{th} order estimate.

A.5 $v\{8\}$

Straight from the definitions we have

$$\begin{aligned} v\{8\} &= \Big[-\frac{1}{33}\Big[\left\langle v^8\right\rangle - 16\left\langle v^6\right\rangle\left\langle v^2\right\rangle - 18\left\langle v^4\right\rangle^2 \\ &\quad +144\left\langle v^4\right\rangle\left\langle v^2\right\rangle^2 - 144\left\langle v^2\right\rangle^4\Big]\Big]^{1/8} . \end{aligned} \tag{A.24}$$

Using now the Taylor formula (A.8) for the case $h(v) \equiv v^8$ we have up to second order is σ_v,

$$\left\langle v^8\right\rangle = \langle v\rangle^8 + 28\sigma_v^2\langle v\rangle^6 . \tag{A.25}$$

Plugging Eqs. (A.10), (A.16), (A.20) and (A.25) into Eq. (A.24) it follows,

$$\begin{aligned} v\{8\} &= \left[-\frac{1}{33}\left[\langle v\rangle^8+28\sigma_v^2\langle v\rangle^6-16\left(\langle v\rangle^6+15\sigma_v^2\langle v\rangle^4\right)\left(\langle v\rangle^2+\sigma_v^2\right)\right.\right. \\ &- \left.\left. 18\left(\langle v\rangle^4+6\sigma_v^2\langle v\rangle^2\right)^2+144\left(\langle v\rangle^4+6\sigma_v^2\langle v\rangle^2\right)\left(\langle v\rangle^2+\sigma_v^2\right)^2-144(\langle v\rangle^2+\sigma_v^2)^4\right]\right]^{1/8}. \end{aligned} \tag{A.26}$$

Keeping within the bracket only terms up to order σ_v^2 it follows

$$\begin{aligned} v\{8\} &= \left[-\frac{1}{33}\left[-33\langle v\rangle^8+132\sigma_v^2\langle v\rangle^6\right]\right]^{1/8} \\ &= \left[\langle v\rangle^8-4\sigma_v^2\langle v\rangle^6\right]^{1/8} \\ &= \langle v\rangle\left[1-4\frac{\sigma_v^2}{\langle v\rangle^2}\right]^{1/8} \\ &\simeq \langle v\rangle\left[1-\frac{1}{2}\frac{\sigma_v^2}{\langle v\rangle^2}\right], \end{aligned} \tag{A.27}$$

so that finally we have

$$v\{8\} \simeq \langle v\rangle - \frac{1}{2}\frac{\sigma_v^2}{\langle v\rangle}. \tag{A.28}$$

To leading order this results is the same as the one obtained for $v\{4\}$ and $v\{6\}$ and given in Eqs. (A.18) and (A.23), respectively.

Summary: With the fairly general assumption that $\sigma_v \ll \langle v\rangle$ and by working up to 2^{nd} order in σ_v, we have straight from the formal properties of Taylor expansion obtained the following results:

$$\begin{aligned} v\{2\} &\simeq \langle v\rangle + \frac{1}{2}\frac{\sigma_v^2}{\langle v\rangle}, \\ v\{4\} &\simeq \langle v\rangle - \frac{1}{2}\frac{\sigma_v^2}{\langle v\rangle}, \\ v\{6\} &\simeq \langle v\rangle - \frac{1}{2}\frac{\sigma_v^2}{\langle v\rangle}, \\ v\{8\} &\simeq \langle v\rangle - \frac{1}{2}\frac{\sigma_v^2}{\langle v\rangle}, \end{aligned} \tag{A.29}$$

which are valid *irrespectively* of the details of underlying model of flow fluctuations.[2]

[2] Another regime, namely when $1 \gg \sigma_v \gg \langle v\rangle$, is left for the future exploration.

A.6 Uniform flow fluctuations

In this section as an example we consider the uniform flow distribution. Uniform flow distribution is defined in the following way:

$$f(v) \equiv \begin{cases} \text{const}, & v_{\min} \le v \le v_{\max}\,, \\ 0, & \text{elsewhere}\,. \end{cases} \tag{A.30}$$

In the first step we normalize the distribution. It follows,

$$\begin{aligned} 1 &= \int_{-\infty}^{\infty} f(v)dv \\ &= \int_{v_{\min}}^{v_{\max}} \text{const}\, dv \\ &= \text{const} \cdot (v_{\max} - v_{\min})\,, \end{aligned} \tag{A.31}$$

so that

$$\text{const} = \frac{1}{v_{\max} - v_{\min}}\,. \tag{A.32}$$

The normalized uniform flow distribution is then:

$$f(v) \equiv \begin{cases} \frac{1}{v_{\max} - v_{\min}}, & v_{\min} \le v \le v_{\max}\,, \\ 0, & \text{elsewhere}\,. \end{cases} \tag{A.33}$$

In the second step we determine the true mean μ_v for the normalized uniform flow distribution. By making use of (A.5) it follows

$$\begin{aligned} \mu_v &= \int_{-\infty}^{\infty} v f(v)dv \\ &= \int_{v_{\min}}^{v_{\max}} v\, \frac{1}{v_{\max} - v_{\min}}\, dv \\ &= \frac{1}{v_{\max} - v_{\min}}\, \frac{v^2}{2}\bigg|_{v_{\min}}^{v_{\max}} \\ &= \frac{1}{v_{\max} - v_{\min}}\, \frac{v_{\max}^2 - v_{\min}^2}{2}\,, \end{aligned} \tag{A.34}$$

which can be simplified to obtain the final result:

$$\mu_v = \frac{v_{\max} + v_{\min}}{2}\,. \tag{A.35}$$

In the third step we determine the standard deviation σ_v. By making use of definition (A.6) it follows

$$\begin{aligned} \sigma_v^2 &= \int_{-\infty}^{\infty} (v - \mu_v)^2 f(v)dv \\ &= \int_{v_{\min}}^{v_{\max}} \left(v - \frac{v_{\max} + v_{\min}}{2}\right)^2 \frac{1}{v_{\max} - v_{\min}}\, dv\,, \end{aligned} \tag{A.36}$$

which can me straightforwardly integrated to obtain:

$$\sigma_v^2 = \frac{1}{12}\left(v_{\max} - v_{\min}\right)^2 , \tag{A.37}$$

i.e.

$$\sigma_v = \frac{1}{2\sqrt{3}}\left(v_{\max} - v_{\min}\right) . \tag{A.38}$$

Summary: For the normalized uniform flow distribution

$$f(v) \equiv \begin{cases} \frac{1}{v_{\max}-v_{\min}}, & v_{\min} \leq v \leq v_{\max} , \\ 0, & \text{elsewhere} , \end{cases} \tag{A.39}$$

the true mean μ_v and standard deviation σ_v are given as follows:

$$\mu_v = \frac{v_{\max} + v_{\min}}{2} , \tag{A.40}$$

$$\sigma_v = \frac{1}{2\sqrt{3}}\left(v_{\max} - v_{\min}\right) . \tag{A.41}$$

Plugging these results into the general expression (A.29) we have for the uniform flow fluctuations:

$$\begin{aligned} v\{2\} &= \frac{v_{\max} + v_{\min}}{2} + \frac{\left(v_{\max} - v_{\min}\right)^2}{12\left(v_{\max} + v_{\min}\right)} , \\ v\{4\} &= \frac{v_{\max} + v_{\min}}{2} - \frac{\left(v_{\max} - v_{\min}\right)^2}{12\left(v_{\max} + v_{\min}\right)} , \\ v\{6\} &= \frac{v_{\max} + v_{\min}}{2} - \frac{\left(v_{\max} - v_{\min}\right)^2}{12\left(v_{\max} + v_{\min}\right)} , \\ v\{8\} &= \frac{v_{\max} + v_{\min}}{2} - \frac{\left(v_{\max} - v_{\min}\right)^2}{12\left(v_{\max} + v_{\min}\right)} . \end{aligned} \tag{A.42}$$

These results for uniform flow fluctuations are illustrated on Fig. A.1, together with an example for Gaussian flow fluctuations.

In this Appendix we have quantified the systematic bias to flow estimates from 2- and multi-particle cumulants due to statistical event-by-event flow fluctuations (see Eqs. (A.29)), and demonstrated the validity of these results for two specific models of flow fluctuations (see Fig. A.1).

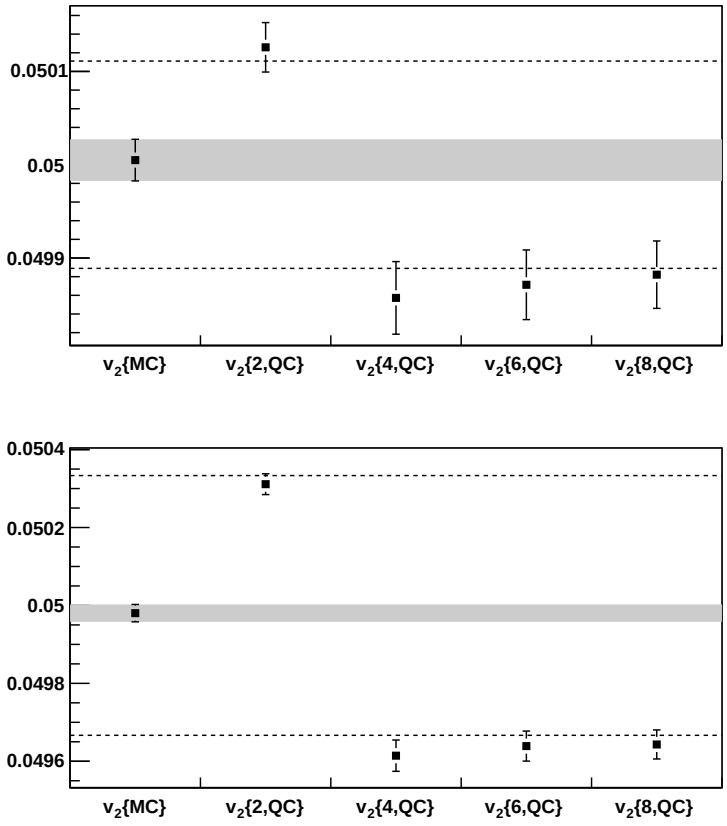

Figure A.1: (*top*) In this example 500 particles per event were sampled from the Fourier-like azimuthal distribution parameterized by a harmonic v_2, where v_2 itself was sampled event-by-event from the Gaussian distribution characterized with mean $\langle v \rangle = 0.05$ and $\sigma_v = 1/300$. The dashed lines indicate theoretical results obtained from the Eqs. (A.29) for these values of $\langle v \rangle$ and σ_v. Total number of events was $N = 2 \times 10^6$. (*bottom*) In this example 500 particles per event were sampled from the Fourier-like azimuthal distribution parameterized by a harmonic v_2, where v_2 itself was event-by-event sampled uniformly from the interval $[0.04, 0.06]$. The dashed lines indicate theoretical results obtained from Eqs. (A.29) for these values of $\langle v \rangle$ and σ_v. Total number of events was $N = 2 \times 10^6$.

Appendix B

Particle weights

In this appendix we provide analytic formulas for the average multiparticle correlations when the most general particle weights are used. Standard examples for particle weights are ϕ-weights, w_ϕ, which are being used to correct for the detector's inefficiencies in azimuth (this technique is applicable only if there is no real gap in the detector's azimuthal acceptance, so that the azimuthal distribution can be inverted and ϕ-weights constructed) and p_t-weights, w_{p_t}, which are being used to optimize the flow signal and correspondingly to reduce the statistical spread of flow estimates.

In general, we denote the particle weight by w and use it only to weigh the contributions of the reference particles (RPs) to generalized (weighted) Q-, p- and q-vectors, to be introduced below shortly. We allow the particle weight w to be the most general function of the RP's azimuth, transverse momentum and rapidity:

$$w = w(\phi, p_t, y)\,. \tag{B.1}$$

In the most cases of interest, however, the particle weight appears in the factorized form,

$$w = w_\phi(\phi) w_{p_t}(p_t) w_y(y)\,. \tag{B.2}$$

We now introduce a weighted Q-vector evaluated in the harmonic n:

$$Q_{n,k} \equiv \sum_{i=1}^{M} w_i^k e^{in\phi_i}\,, \tag{B.3}$$

where w_i is the weight of the i-th particle labeled as RP and M is the total number of RPs in an event. In general, we will need Q-vectors with power k up to the order of multi-particle correlations (i.e. up to the number of correlated particles in a certain correlator). Similarly, we define

$$p_{n,k} \equiv \sum_{i=1}^{m_p} w_i^k e^{in\psi_i}\,. \tag{B.4}$$

Note that only particles which have a RP label have a non-unit weight, while for the particles labeled as particles of interest (POI) *only*, $w_i = 1$. For the subset of POIs which consists of all particles labeled *both* as POI and RP (m_q in total) we introduce

$$q_{n,k} \equiv \sum_{i=1}^{m_q} w_i^k e^{in\psi_i} . \tag{B.5}$$

For RPs we also introduce[1]:

$$S_{p,k} \equiv \left[\sum_{i=1}^{M} w_i^k\right]^p , \tag{B.6}$$

$$\mathcal{M}_{abcd\cdots} \equiv \sum_{i,j,k,l,\ldots=1}^{M}{}' w_i^a w_j^b w_k^c w_l^d \cdots . \tag{B.7}$$

For all particles labeled *both* as RP and POI we evaluate the following quantity:

$$s_{p,k} \equiv \left[\sum_{i=1}^{m_q} w_i^k\right]^p , \tag{B.8}$$

while in the definition below the first sum runs over all POIs in the window of interest and the remaining sums run over all RPs in an event

$$\mathcal{M}'_{abcd\cdots} \equiv \sum_{i=1}^{m_p} \sum_{j,k,l,\ldots=1}^{M}{}' w_i^a w_j^b w_k^c w_l^d \cdots . \tag{B.9}$$

Having introduced these new quantities we are now ready to present the analytic results for weighted multiparticle azimuthal correlations.

B.1 Weighted multiparticle azimuthal correlations

Using the definitions presented above the *weighted* single-event 2- and 4-particle correlations are given by:

$$\langle 2\rangle \equiv \frac{1}{\mathcal{M}_{11}} \sum_{i,j=1}^{M}{}' w_i w_j \, e^{in(\phi_i-\phi_j)} , \tag{B.10}$$

$$\langle 4\rangle \equiv \frac{1}{\mathcal{M}_{1111}} \sum_{i,j,k,l=1}^{M}{}' w_i w_j w_k w_l \, e^{in(\phi_i+\phi_j-\phi_k-\phi_l)} . \tag{B.11}$$

The multiplicity weights, needed to get all-event averages for multiparticle correlations, now read

$$\begin{aligned} W_{\langle 2\rangle} &\equiv \mathcal{M}_{11} , \\ W_{\langle 4\rangle} &\equiv \mathcal{M}_{1111} . \end{aligned} \tag{B.12}$$

[1] In all summations symbol $'$ indicates that all summing indices have to be taken different.

Analogously, the reduced single-event multi-particle correlations are now:

$$\langle 2' \rangle \equiv \frac{1}{\mathcal{M}'_{01}} \sum_{i=1}^{m_p} \sum_{j=1}^{M}{}' w_j \, e^{in(\psi_i - \phi_j)}, \tag{B.13}$$

$$\langle 4' \rangle \equiv \frac{1}{\mathcal{M}'_{0111}} \sum_{i=1}^{m_p} \sum_{j,k,l=1}^{M}{}' w_j w_k w_l \, e^{in(\psi_i + \phi_j - \phi_k - \phi_l)}, \tag{B.14}$$

where the multiplicity weights are:

$$\begin{aligned} w_{\langle 2' \rangle} &\equiv \mathcal{M}'_{01} \,, \\ w_{\langle 4' \rangle} &\equiv \mathcal{M}'_{0111} \,. \end{aligned} \tag{B.15}$$

The weighted average 2-particle correlations are given by the following equations:

$$\begin{aligned} \langle 2 \rangle &= \frac{|Q_{n,1}|^2 - S_{1,2}}{S_{2,1} - S_{1,2}} \,, \\ \langle\langle 2 \rangle\rangle &= \frac{\sum_{i=1}^{N} (\mathcal{M}_{11})_i \langle 2 \rangle_i}{\sum_{i=1}^{N} (\mathcal{M}_{11})_i} \,, \\ \mathcal{M}_{11} &\equiv \sum_{i,j=1}^{M}{}' w_i w_j \\ &= S_{2,1} - S_{1,2} \,, \end{aligned} \tag{B.16}$$

and the weighted average 4-particle correlations are given by:

$$\begin{aligned} \langle 4 \rangle &= \Big[|Q_{n,1}|^4 + |Q_{2n,2}|^2 - 2 \cdot \mathfrak{Re} \left[Q_{2n,2} Q^*_{n,1} Q^*_{n,1} \right] \\ &+ 8 \cdot \mathfrak{Re} \left[Q_{n,3} Q^*_{n,1} \right] - 4 \cdot S_{1,2} \, |Q_{n,1}|^2 \\ &- 6 \cdot S_{1,4} + 2 \cdot S_{2,2} \Big] \Big[\mathcal{M}_{1111} \Big]^{-1} \,, \\ \mathcal{M}_{1111} &\equiv \sum_{i,j,k,l=1}^{M}{}' w_i w_j w_k w_l \\ &= S_{4,1} - 6 \cdot S_{1,2} S_{2,1} + 8 \cdot S_{1,3} S_{1,1} + 3 \cdot S_{2,2} - 6 \cdot S_{1,4} \,, \\ \langle\langle 4 \rangle\rangle &= \frac{\sum_{i=1}^{N} (\mathcal{M}_{1111})_i \, \langle 4 \rangle_i}{\sum_{i=1}^{N} (\mathcal{M}_{1111})_i} \,, \end{aligned} \tag{B.17}$$

where the weighted Q-vector, $Q_{n,k}$, was defined in Eq. (B.3) and $S_{p,k}$ in Eq. (B.6).

Weighted reduced 2- and 4-particle azimuthal correlations are given by the following

formulas:

$$\begin{aligned}
\langle 2' \rangle &= \frac{p_{n,0} Q^*_{n,1} - s_{1,1}}{m_p S_{1,1} - s_{1,1}} \,, \\
\langle\langle 2' \rangle\rangle &= \frac{\sum_{i=1}^{N} (\mathcal{M}'_{01})_i \, \langle 2' \rangle_i}{\sum_{i=1}^{N} (\mathcal{M}'_{01})_i} \,, \\
\mathcal{M}'_{01} &\equiv \sum_{i=1}^{m_p} {\sum_{i,j=1}^{M}}' w_j = m_p S_{1,1} - s_{1,1} \,,
\end{aligned} \tag{B.18}$$

and,

$$\begin{aligned}
\langle 4' \rangle &= \Big[p_{n,0} Q_{n,1} Q^*_{n,1} Q^*_{n,1} \\
&- q_{2n,1} Q^*_{n,1} Q^*_{n,1} - p_{n,0} Q_{n,1} Q^*_{2n,2} \\
&- 2 \cdot S_{1,2} p_{n,0} Q^*_{n,1} - 2 \cdot s_{1,1} \left| Q_{n,1} \right|^2 \\
&+ 7 \cdot q_{n,2} Q^*_{n,1} - Q_{n,1} q^*_{n,2} \\
&+ q_{2n,1} Q^*_{2n,2} + 2 \cdot p_{n,0} Q^*_{n,3} \\
&+ 2 \cdot s_{1,1} S_{1,2} - 6 \cdot s_{1,3} \Big] \Big[\mathcal{M}'_{0111} \Big]^{-1} \,, \\
\langle\langle 4' \rangle\rangle &= \frac{\sum_{i=1}^{N} (\mathcal{M}'_{0111})_i \, \langle 4' \rangle_i}{\sum_{i=1}^{N} (\mathcal{M}'_{0111})_i} \,, \\
\mathcal{M}'_{0111} &\equiv \sum_{i=1}^{m_p} {\sum_{j,k,l=1}^{M}}' w_j w_k w_l \\
&= m_p \left[S_{3,1} - 3 \cdot S_{1,1} S_{1,2} + 2 \cdot S_{1,3} \right] \\
&- 3 \cdot [s_{1,1} (S_{2,1} - S_{1,2}) + 2 \cdot (s_{1,3} - s_{1,2} S_{1,1})] \,.
\end{aligned} \tag{B.19}$$

We note that to evaluate all quantities appearing on the right hand sides in (B.16–B.19) only a single loop over the data is required.

B.1.1 Example for ϕ-weights: Correcting for the bias from non-uniform acceptance of the detector

In this example we sample particles from the Fourier-like azimuthal distribution characterized with a p_t dependent harmonic v_2, namely:

$$v_2(p_t) = \begin{cases} 0.1 p_t & p_t < 2.0 \text{ GeV} \,, \\ 0.2 & p_t \geq 2.0 \text{ GeV} \,. \end{cases} \tag{B.20}$$

The usage of ϕ-weights is illustrated for a detector with two problematic sectors which accepts only 1/2 of the tracks in $60^{\text{o}} \leq \phi < 100^{\text{o}}$ and only 1/3 of the tracks going in $270^{\text{o}} \leq \phi < 330^{\text{o}}$. All particles with azimuthal angles out of these two ranges are

accepted without any loss. In the first step we have to perform a dedicated run over data in order to get the histogram of the azimuthal acceptance. The resulting acceptance histogram for this particular example is presented in Fig. B.1 (top). In the second step from this histogram the ϕ-weights are being constructed. If the average number of particles per ϕ-bin is $\langle N \rangle$ and if the number of particles in particular ϕ-bin is N_ϕ, than the ϕ-weight for that ϕ-bin is simply

$$w_\phi \equiv \frac{\langle N \rangle}{N_\phi} \,. \tag{B.21}$$

The resulting ϕ-weights for the detector in question are presented in Fig. B.1 (bottom). From the Eq. (B.21) it is clear that if there is a gap in the detector's acceptance than there will be a ϕ-bin with zero entries and the ϕ-weight for that bin cannot be constructed—this will limit the applicability of the usage of ϕ-weights in practice. Having constructed in this way the ϕ-weights in a dedicated run, in the subsequent runs over data weighted Q-, p- and q-vectors will be evaluated as defined in Eqs. (B.3), (B.4) and (B.5), respectively. In addition, quantities $S_{p,k}$ and $s_{p,k}$ will be evaluated according to the definitions (B.6) and (B.8). From these quantities by making use of the analytic results presented in Section B.1 all single-event average multiparticle and reduced multiparticle correlations can be obtained, which will be weighted event-by-event with multiplicity weights (B.15) and (B.12), respectively, to get the all-event averages. From this point onwards the procedure to estimate the flow harmonics is the same as outlined in the main part of the thesis for the case of unit particle weights. In Fig. B.2 the estimates for reference flow harmonics are presented and in Figs. B.3 and B.4 the estimates for differential flow harmonics from the 2^{nd} and 4^{th} order differential Q-cumulant, respectively, with (full markers) and without (open markers) using the ϕ-weights.

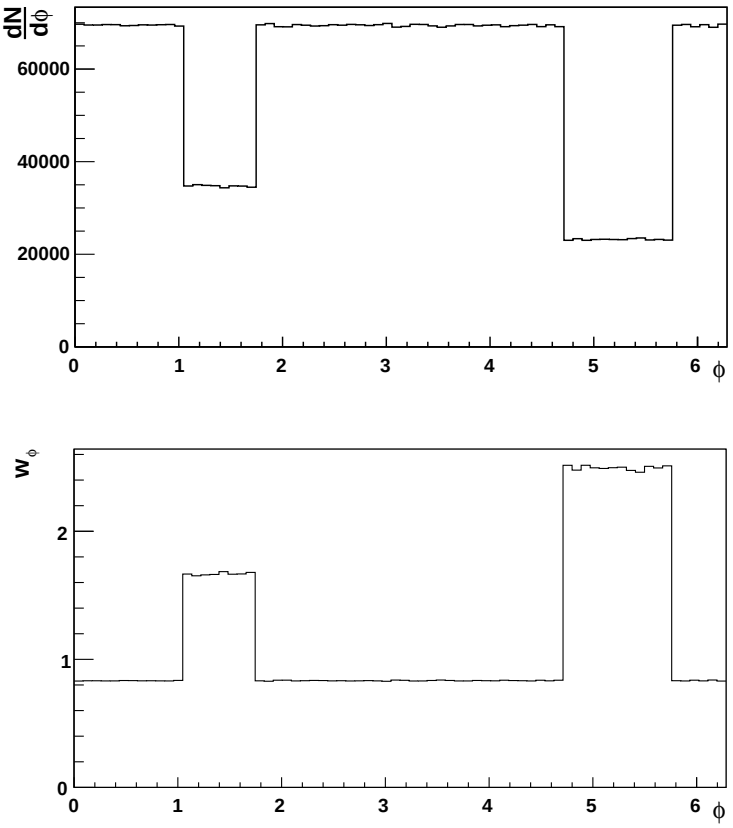

Figure B.1: Azimuthal profile of a detector which accepts 1/2 of the tracks going in $60^{\circ} \leq \phi < 100^{\circ}$ and only 1/3 of the tracks going in $270^{\circ} \leq \phi < 330^{\circ}$ (*top*). Resulting ϕ-weights for the above acceptance profile (*bottom*).

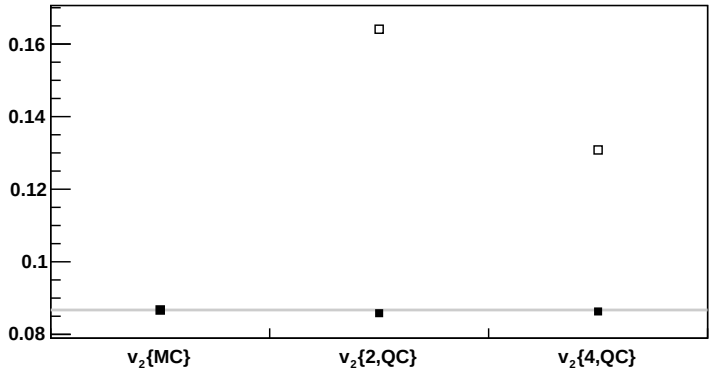

Figure B.2: Estimates for reference flow harmonics for a detector whose acceptance histogram is presented in the top plot of Fig. B.1. In the first bin is given the true Monte Carlo flow estimate (only to this estimate the event-by-event reaction plane orientation is provided, and this estimate is not affected by the non-uniform acceptance). In the second and third bin with open markers are estimates obtained without using ϕ-weights and with closed markers with using ϕ-weights in the analysis with Q-cumulants.

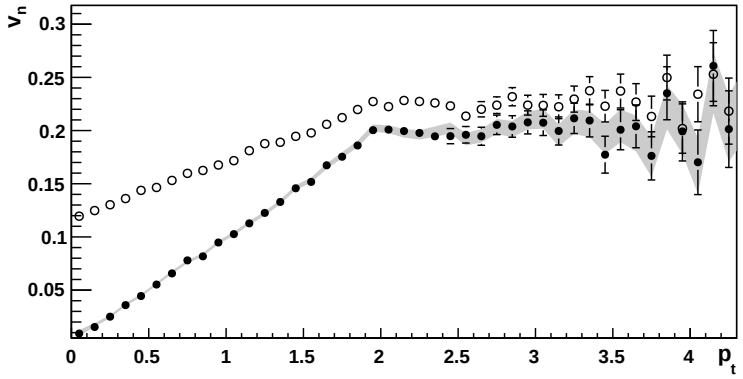

Figure B.3: Estimates for differential flow harmonics from 2$^{\text{nd}}$ order differential Q-cumulant for a detector whose acceptance histogram is presented on the top plot of Fig. B.1. The grey mesh was obtained after joining the ends of error bars of Monte Carlo flow estimates for each p_t bin. With open markers are estimates obtained without using ϕ-weights and with closed markers with using ϕ-weights in the analysis with Q-cumulants.

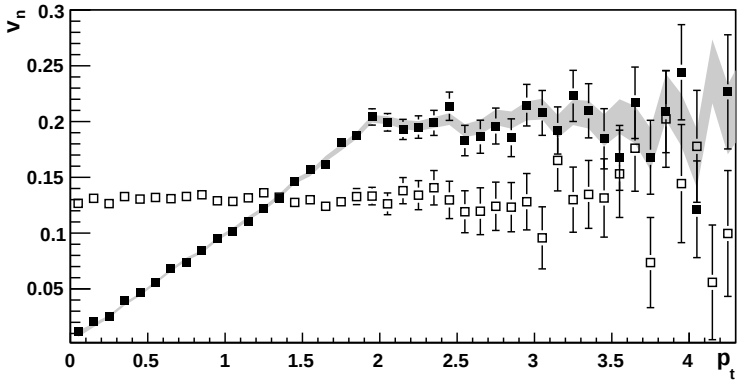

Figure B.4: Estimates for differential flow harmonics from 4^{th} order differential Q-cumulant for a detector whose acceptance histogram is presented on the top plot of Fig. B.1. The grey mesh was obtained after joining the ends of error bars of Monte Carlo flow estimates for each p_t bin. With open markers are estimates obtained without using ϕ-weights and with closed markers with using ϕ-weights in the analysis with Q-cumulants.

Appendix C

Statistical errors

In this appendix we outline the procedure we use to report the statistical errors of the reference and differential flow estimates from Q-cumulants. For simplicity sake in all expressions below we keep only the terms relevant for detectors with uniform acceptance—more general expressions for detectors with non-uniform acceptance can be derived straightforwardly.

C.1 Some general results

Consider[1] the random observable x sampled from some probability density function (p.d.f.) $f(x)$ (for a detailed treatment of what is highlighted here we refer reader to [67]). The *mean* of x we denote by μ_x and the *variance* of x we denote by σ_x^2 (or equivalently by $V[x]$). Mean and variance of x are given by the following expressions:

$$\mu_x = E[x] = \int_{-\infty}^{\infty} x f(x) dx \,, \tag{C.1}$$

$$\sigma_x^2 = V[x] = E[(x - E[x])^2] = \int_{-\infty}^{\infty} (x - \mu_x)^2 f(x) dx \,, \tag{C.2}$$

where $E[x]$ stands for the *expectation value* of a random variable x. We denote by x_i the measured random observable x in the i-th event and by $(w_x)_i$ the observable's weight in that event. Even if the p.d.f. $f(x)$ is completely unknown, we can still use measured values x_i to estimate mean (C.1) and variance (C.2) of a random variable x. In particular, the unbiased estimator[2] for the variance σ_x^2 we denote by s_x^2 and it is given by

$$s_x^2 \equiv \left[\frac{\sum_{i=1}^{N} (w_x)_i (x_i - \langle x \rangle)^2}{\sum_{i=1}^{N} (w_x)_i} \right] \times \left[\frac{1}{1 - \frac{\sum_{i=1}^{N} (w_x)_i^2}{\left[\sum_{i=1}^{N} (w_x)_i\right]^2}} \right] , \tag{C.3}$$

[1] To make this Appendix self-contained we quickly outline at the beginning few general results already presented in Appendix A.

[2] To treat statistical errors in this way was suggested by Evan Warren.

where we have introduced also $\langle x \rangle$ as the unbiased estimator for mean μ_x,

$$\langle x \rangle \equiv \frac{\sum_{i=1}^{N} (w_x)_i x_i}{\sum_{i=1}^{N} (w_x)_i} \,. \tag{C.4}$$

In above two equations N is the number of independent measurements, which in our context corresponds to the number of events.

Since the sample mean, $\langle x \rangle$, is an unbiased estimator for the mean of x, μ_x, we will report the final results and the statistical errors as

$$\langle x \rangle \pm V[\langle x \rangle]^{1/2} \,. \tag{C.5}$$

One can easily show that the variance of the sample mean, $V[\langle x \rangle]$, can be written as

$$V[\langle x \rangle] = \frac{\sum_{i=1}^{N} (w_x)_i^2}{\left[\sum_{i=1}^{N} (w_x)_i\right]^2} V[x] \,, \tag{C.6}$$

i.e.

$$V[\langle x \rangle] = \frac{\sum_{i=1}^{N} (w_x)_i^2}{\left[\sum_{i=1}^{N} (w_x)_i\right]^2} \sigma_x^2 \,. \tag{C.7}$$

Taking into account the unbiased estimator s_x^2 for the variance σ_x^2, we can now write down the expression which we will use to report the final results and statistical errors of a random variable x:

$$\langle x \rangle \pm \frac{\sqrt{\sum_{i=1}^{N} (w_x)_i^2}}{\sum_{i=1}^{N} (w_x)_i} s_x \,, \tag{C.8}$$

where $\langle x \rangle$ is given by Eq. (C.4) and s_x by Eq. (C.3).

Consider now the more general case when we deal with two random variables, x and y, and some other random variable h which is a function of x and y. Then the mean of $h(x, y)$, μ_h, is to first order given by

$$\mu_h \equiv E[h(x, y)] \approx h(\mu_x, \mu_y) \,, \tag{C.9}$$

and the variance of h, σ_h^2 (or equivalently $V[h]$), is to first order given by:

$$\begin{aligned} \sigma_h^2 = V[h] &\equiv E[h^2(x, y)] - E[h(x, y)]^2 \\ &\approx \left[\left(\frac{\partial h}{\partial x}\right)\Big|_{x=\mu_x, y=\mu_y}\right]^2 \sigma_x^2 + \left[\left(\frac{\partial h}{\partial y}\right)\Big|_{x=\mu_x, y=\mu_y}\right]^2 \sigma_y^2 \\ &+ 2 \left(\frac{\partial h}{\partial x}\frac{\partial h}{\partial y}\right)\Big|_{x=\mu_x, y=\mu_y} V_{xy} \,, \end{aligned} \tag{C.10}$$

where V_{xy} is *covariance* of two random variables x and y,

$$\begin{aligned} V_{xy} &\equiv E[(x - \mu_x)(y - \mu_y)] \\ &= E[xy] - E[x]E[y] \\ &= \int_{-\infty}^{\infty}\int_{-\infty}^{\infty} xy f(x, y) dx dy - \mu_x \mu_y \,. \end{aligned} \tag{C.11}$$

If we measure in the i-th event two observables x_i and y_i, whose weights are $(w_x)_i$ and $(w_y)_i$, then the unbiased estimator $\mathrm{Cov}(x,y)$ for their covariance V_{xy} is given by

$$\mathrm{Cov}(x,y) = \frac{\frac{\sum_{i=1}^{N}(w_x)_i(w_y)_i x_i y_i}{\sum_{i=1}^{N}(w_x)_i(w_y)_i} - \frac{\sum_{i=1}^{N}(w_x)_i x_i}{\sum_{i=1}^{N}(w_x)_i}\frac{\sum_{j=1}^{N}(w_y)_j y_j}{\sum_{j=1}^{N}(w_y)_j}}{1-\frac{\sum_{i=1}^{N}(w_x)_i(w_y)_i}{\sum_{i=1}^{N}(w_x)_i\sum_{j=1}^{N}(w_y)_j}}\,. \tag{C.12}$$

We will report the final result and statistical error for $h(x,y)$ as

$$\langle h\rangle \pm s_{\langle h\rangle}\,, \tag{C.13}$$

where $\langle h\rangle$ is the unbiased estimator for the mean of $h(x,y)$ and it is to first order given by

$$\langle h\rangle = h(\langle x\rangle,\langle y\rangle)\,, \tag{C.14}$$

while $s^2_{\langle h\rangle}$ is the unbiased estimator for the variance $V[\langle h\rangle]$. The variance $V[\langle h\rangle]$ can be obtained to first order straightforwardly from Eq. (C.10):

$$\begin{aligned} V[\langle h\rangle] &\approx \left[\left(\frac{\partial h}{\partial x}\right)\Big|_{x=\mu_x,y=\mu_y}\right]^2 V[\langle x\rangle] + \left[\left(\frac{\partial h}{\partial y}\right)\Big|_{x=\mu_x,y=\mu_y}\right]^2 V[\langle y\rangle] \\ &+ 2\left(\frac{\partial h}{\partial x}\frac{\partial h}{\partial y}\right)\Big|_{x=\mu_x,y=\mu_y} V_{\langle x\rangle\langle y\rangle}\,. \end{aligned} \tag{C.15}$$

One can easily show that

$$V_{\langle x\rangle\langle y\rangle} = \frac{\sum_{i=1}^{N}(w_x)_i(w_y)_i}{\sum_{i=1}^{N}(w_x)_i\sum_{j=1}^{N}(w_y)_j}\,V_{xy}\,. \tag{C.16}$$

Then the unbiased estimator $s^2_{\langle h\rangle}$ for variance $V[\langle h\rangle]$ is

$$\begin{aligned} s^2_{\langle h\rangle} &\approx \left[\left(\frac{\partial h}{\partial x}\right)\Big|_{x=\langle x\rangle,y=\langle y\rangle}\right]^2 \frac{\sum_{i=1}^{N}(w_x)_i^2}{\left[\sum_{i=1}^{N}(w_x)_i\right]^2}\,s_x^2 \\ &+ \left[\left(\frac{\partial h}{\partial y}\right)\Big|_{x=\langle x\rangle,y=\langle y\rangle}\right]^2 \frac{\sum_{i=1}^{N}(w_y)_i^2}{\left[\sum_{i=1}^{N}(w_y)_i\right]^2}\,s_y^2 \\ &+ 2\left(\frac{\partial h}{\partial x}\frac{\partial h}{\partial y}\right)\Big|_{x=\langle x\rangle,y=\langle y\rangle} \times \frac{\sum_{i=1}^{N}(w_x)_i(w_y)_i}{\sum_{i=1}^{N}(w_x)_i\sum_{j=1}^{N}(w_y)_j}\,\mathrm{Cov}(x,y)\,. \end{aligned} \tag{C.17}$$

These formulas can be trivially generalized for the case of more than two random variables. We will use these results to report final results and statistical errors for the flow estimates from Q-cumulants in subsequent sections in this Appendix, which were used in the main body of the thesis.

C.2 Statistical errors for reference flow estimates

We start by identifying random variable x in our analysis. We will denote its event-by-event measured (sampled) value by x_i and its weight by $(w_x)_i$.

In what follows we will treat the average multi-particle correlations, $\langle 2\rangle$, $\langle 4\rangle$, $\langle 6\rangle$ and $\langle 8\rangle$ as the measured observables event-by-event. The corresponding event-wise weights are taken to be the "number of combinations." We can calculate then the final averages of multi-particle correlations (i.e. the unbiased estimators for their true mean values), $\langle\langle 2\rangle\rangle$, $\langle\langle 4\rangle\rangle$, $\langle\langle 6\rangle\rangle$ and $\langle\langle 8\rangle\rangle$, and also the unbiased estimators for their variances, $s^2_{\langle 2\rangle}$, $s^2_{\langle 4\rangle}$, $s^2_{\langle 6\rangle}$ and $s^2_{\langle 8\rangle}$, straight from the data by making use of the definitions (C.4) and (C.3), respectively.

Having calculated these quantities from the data, we will report the final results and statistical errors for the average multi-particle azimuthal correlations in the following way:

$$\begin{aligned}
\langle\langle 2\rangle\rangle &\pm \frac{\sqrt{\sum_{i=1}^{N}(w_{\langle 2\rangle})_i^2}}{\sum_{i=1}^{N}(w_{\langle 2\rangle})_i}\, s_{\langle 2\rangle}\,, \\
\langle\langle 4\rangle\rangle &\pm \frac{\sqrt{\sum_{i=1}^{N}(w_{\langle 4\rangle})_i^2}}{\sum_{i=1}^{N}(w_{\langle 4\rangle})_i}\, s_{\langle 4\rangle}\,, \\
\langle\langle 6\rangle\rangle &\pm \frac{\sqrt{\sum_{i=1}^{N}(w_{\langle 6\rangle})_i^2}}{\sum_{i=1}^{N}(w_{\langle 6\rangle})_i}\, s_{\langle 6\rangle}\,, \\
\langle\langle 8\rangle\rangle &\pm \frac{\sqrt{\sum_{i=1}^{N}(w_{\langle 8\rangle})_i^2}}{\sum_{i=1}^{N}(w_{\langle 8\rangle})_i}\, s_{\langle 8\rangle}\,,
\end{aligned} \tag{C.18}$$

where event-wise weights in above equations are the "number of combinations," i.e.:

$$\begin{aligned}
w_{\langle 2\rangle} &= M(M-1)\,, \\
w_{\langle 4\rangle} &= M(M-1)(M-2)(M-3)\,, \\
w_{\langle 6\rangle} &= M(M-1)(M-2)(M-3)(M-4)(M-5)\,, \\
w_{\langle 8\rangle} &= M(M-1)(M-2)(M-3)(M-4)(M-5)(M-6)(M-7)\,,
\end{aligned} \tag{C.19}$$

and M is the number of reference particles (in most cases of interest the multiplicity itself) in the i-th event.

On the other hand, we will report the final results and statistical errors of the flow estimates from Q-cumulants by taking into account their functional dependence on multi-particle correlations. In accordance with the notation introduced in previous section (see Eq. (C.13)) we will report the final results and statistical errors of reference flow

estimates as follows:

$$\begin{aligned}\langle v_n\{2\}\rangle &\pm s_{\langle v_n\{2\}\rangle}\,,\\ \langle v_n\{4\}\rangle &\pm s_{\langle v_n\{4\}\rangle}\,,\\ \langle v_n\{6\}\rangle &\pm s_{\langle v_n\{6\}\rangle}\,,\\ \langle v_n\{8\}\rangle &\pm s_{\langle v_n\{8\}\rangle}\,.\end{aligned} \tag{C.20}$$

Unbiased estimators for the variances of the sample mean of reference flow estimates, $s_{\langle v_n\{2\}\rangle}$, $s_{\langle v_n\{4\}\rangle}$, $s_{\langle v_n\{6\}\rangle}$ and $s_{\langle v_n\{8\}\rangle}$, introduced in Eq. (C.20), can be straightforwardly expressed in terms of unbiased estimators for the variances of the sample mean of multiparticle correlations, $s_{\langle 2\rangle}$, $s_{\langle 4\rangle}$, $s_{\langle 6\rangle}$ and $s_{\langle 8\rangle}$, which as already indicated were obtained straight from the data—these expressions will follow shortly.

But before proceeding further the very important thing to note, however, is that the different average multiparticle correlations measured event-by-event *are not independent quantities*. Due to this, we will also need the unbiased estimators for their covariances (e.g. $\mathrm{Cov}(\langle 2\rangle,\langle 4\rangle)$), which can also be obtained straight from the data by making use of Eq. (C.12).

C.2.1 2-particle estimate

When it comes to the 2-particle reference flow estimate we use the fact that

$$v_n\{2\} = \sqrt{\langle 2\rangle}\,, \tag{C.21}$$

so that we have to first order

$$\langle v_n\{2\}\rangle \approx \sqrt{\langle\langle 2\rangle\rangle}\,. \tag{C.22}$$

By restricting result in Eq. (C.17) to the functional dependence on one variable it follows

$$s^2_{\langle v_n\{2\}\rangle} = \frac{1}{4\,\langle\langle 2\rangle\rangle}\,\frac{\sum_{i=1}^{N}(w_{\langle 2\rangle})_i^2}{\left[\sum_{i=1}^{N}(w_{\langle 2\rangle})_i\right]^2}\,s^2_{\langle 2\rangle}\,, \tag{C.23}$$

i.e.

$$s_{\langle v_n\{2\}\rangle} = \frac{1}{2\sqrt{\langle\langle 2\rangle\rangle}}\,\frac{\sqrt{\sum_{i=1}^{N}(w_{\langle 2\rangle})_i^2}}{\sum_{i=1}^{N}(w_{\langle 2\rangle})_i}\,s_{\langle 2\rangle}\,. \tag{C.24}$$

Equation (C.22) gives the final value of the 2-particle reference flow estimate and Eq. (C.24) the corresponding statistical error.

For completeness sake we also outline the corresponding results for the 2-particle reference Q-cumulant:

$$\begin{aligned}QC\{2\} &= \langle\langle 2\rangle\rangle\,,\\ s_{QC\{2\}} &= \frac{\sqrt{\sum_{i=1}^{N}(w_{\langle 2\rangle})_i^2}}{\sum_{i=1}^{N}(w_{\langle 2\rangle})_i}\,s_{\langle 2\rangle}\,.\end{aligned} \tag{C.25}$$

C.2.2 4-particle estimate

We start from

$$v_n\{4\} = \sqrt[4]{2 \cdot \langle 2\rangle^2 - \langle 4\rangle}\,, \tag{C.26}$$

which gives to first order

$$\langle v_n\{4\}\rangle \approx \sqrt[4]{2 \cdot \langle\langle 2\rangle\rangle^2 - \langle\langle 4\rangle\rangle}\,. \tag{C.27}$$

By applying Eq. (C.17) to equation (C.26) we have obtained

$$\begin{aligned} s^2_{\langle v_n\{4\}\rangle} &= \frac{1}{\left[2 \cdot \langle\langle 2\rangle\rangle^2 - \langle\langle 4\rangle\rangle\right]^{3/2}} \times \left[\langle\langle 2\rangle\rangle^2 \, \frac{\sum_{i=1}^N (w_{\langle 2\rangle})_i^2}{\left[\sum_{i=1}^N (w_{\langle 2\rangle})_i\right]^2} \, s^2_{\langle 2\rangle}\right. \\ &+ \left. \frac{1}{16} \frac{\sum_{i=1}^N (w_{\langle 4\rangle})_i^2}{\left[\sum_{i=1}^N (w_{\langle 4\rangle})_i\right]^2} \, s^2_{\langle 4\rangle} - \frac{1}{2} \, \langle\langle 2\rangle\rangle \frac{\sum_{i=1}^N (w_{\langle 2\rangle})_i (w_{\langle 4\rangle})_i}{\sum_{i=1}^N (w_{\langle 2\rangle})_i \sum_{j=1}^N (w_{\langle 4\rangle})_j} \, \mathrm{Cov}(\langle 2\rangle,\langle 4\rangle)\right]. \end{aligned} \tag{C.28}$$

Equation (C.27) gives the final value of the 4-particle reference flow estimate and Eq. (C.28) the corresponding statistical error.

For completeness sake we also outline the corresponding results for the 4-particle reference Q-cumulant:

$$\begin{aligned} QC\{4\} &= \langle\langle 4\rangle\rangle - 2 \cdot \langle\langle 2\rangle\rangle^2 \,, \\ s^2_{QC\{4\}} &= 16 \cdot \langle\langle 2\rangle\rangle^2 \, \frac{\sum_{i=1}^N (w_{\langle 2\rangle})_i^2}{\left[\sum_{i=1}^N (w_{\langle 2\rangle})_i\right]^2} s^2_{\langle 2\rangle} + \frac{\sum_{i=1}^N (w_{\langle 4\rangle})_i^2}{\left[\sum_{i=1}^N (w_{\langle 4\rangle})_i\right]^2} s^2_{\langle 4\rangle} \\ &- 8 \cdot \langle\langle 2\rangle\rangle \, \frac{\sum_{i=1}^N (w_{\langle 2\rangle})_i (w_{\langle 4\rangle})_i}{\sum_{i=1}^N (w_{\langle 2\rangle})_i \sum_{j=1}^N (w_{\langle 4\rangle})_j} \, \mathrm{Cov}(\langle 2\rangle,\langle 4\rangle)\,. \end{aligned} \tag{C.29}$$

C.2.3 6-particle estimate

We start from

$$v_n\{6\} = 2^{-1/3} \cdot \sqrt[6]{\langle 6\rangle - 9 \cdot \langle 2\rangle \, \langle 4\rangle + 12 \cdot \langle 2\rangle^3}\,, \tag{C.30}$$

which gives to first order

$$\langle v_n\{6\}\rangle \approx 2^{-1/3} \cdot \sqrt[6]{\langle\langle 6\rangle\rangle - 9 \cdot \langle\langle 2\rangle\rangle \, \langle\langle 4\rangle\rangle + 12 \cdot \langle\langle 2\rangle\rangle^3}\,. \tag{C.31}$$

From the extended version of Eq. (C.17) valid for three random variables, we have obtained

$$
\begin{aligned}
s^2_{\langle v_n\{6\}\rangle} &= \frac{1}{2\cdot 2^{2/3}\cdot\left[\langle\langle 6\rangle\rangle - 9\cdot\langle\langle 4\rangle\rangle\langle\langle 2\rangle\rangle + 12\cdot\langle\langle 2\rangle\rangle^3\right]^{5/3}}\times \\
&\Bigg[\frac{9}{2}\cdot\left[4\cdot\langle\langle 2\rangle\rangle^2 - \langle\langle 4\rangle\rangle\right]^2\frac{\sum_{i=1}^N (w_{\langle 2\rangle})_i^2}{\left[\sum_{i=1}^N (w_{\langle 2\rangle})_i\right]^2}s^2_{\langle 2\rangle} \\
&+\frac{9}{2}\cdot\langle\langle 2\rangle\rangle^2\frac{\sum_{i=1}^N (w_{\langle 4\rangle})_i^2}{\left[\sum_{i=1}^N (w_{\langle 4\rangle})_i\right]^2}s^2_{\langle 4\rangle} + \frac{1}{18}\frac{\sum_{i=1}^N (w_{\langle 6\rangle})_i^2}{\left[\sum_{i=1}^N (w_{\langle 6\rangle})_i\right]^2}s^2_{\langle 6\rangle} \\
&-9\cdot\langle\langle 2\rangle\rangle\left[4\cdot\langle\langle 2\rangle\rangle^2 - \langle\langle 4\rangle\rangle\right]\frac{\sum_{i=1}^N (w_{\langle 2\rangle})_i(w_{\langle 4\rangle})_i}{\sum_{i=1}^N (w_{\langle 2\rangle})_i\sum_{j=1}^N (w_{\langle 4\rangle})_j}\mathrm{Cov}(\langle 2\rangle,\langle 4\rangle) \\
&+\left[4\cdot\langle\langle 2\rangle\rangle^2 - \langle\langle 4\rangle\rangle\right]\frac{\sum_{i=1}^N (w_{\langle 2\rangle})_i(w_{\langle 6\rangle})_i}{\sum_{i=1}^N (w_{\langle 2\rangle})_i\sum_{j=1}^N (w_{\langle 6\rangle})_j}\mathrm{Cov}(\langle 2\rangle,\langle 6\rangle) \\
&-\langle\langle 2\rangle\rangle\frac{\sum_{i=1}^N (w_{\langle 4\rangle})_i(w_{\langle 6\rangle})_i}{\sum_{i=1}^N (w_{\langle 4\rangle})_i\sum_{j=1}^N (w_{\langle 6\rangle})_j}\mathrm{Cov}(\langle 4\rangle,\langle 6\rangle)\Bigg]\,. \qquad \text{(C.32)}
\end{aligned}
$$

Equation (C.31) gives the final value of the 6-particle reference flow estimate and Eq. (C.32) the corresponding statistical error.

For completeness sake we also outline the corresponding results for the 6-particle reference Q-cumulant:

$$
\begin{aligned}
QC\{6\} &= \langle\langle 6\rangle\rangle - 9\cdot\langle\langle 2\rangle\rangle\langle\langle 4\rangle\rangle + 12\cdot\langle\langle 2\rangle\rangle^3\,, \\
s^2_{QC\{6\}} &= 81\cdot\left[4\cdot\langle\langle 2\rangle\rangle^2 - \langle\langle 4\rangle\rangle\right]^2\frac{\sum_{i=1}^N (w_{\langle 2\rangle})_i^2}{\left[\sum_{i=1}^N (w_{\langle 2\rangle})_i\right]^2}s^2_{\langle 2\rangle} \\
&+ 81\cdot\langle\langle 2\rangle\rangle^2\frac{\sum_{i=1}^N (w_{\langle 4\rangle})_i^2}{\left[\sum_{i=1}^N (w_{\langle 4\rangle})_i\right]^2}s^2_{\langle 4\rangle} + \frac{\sum_{i=1}^N (w_{\langle 6\rangle})_i^2}{\left[\sum_{i=1}^N (w_{\langle 6\rangle})_i\right]^2}s^2_{\langle 6\rangle} \\
&- 162\cdot\langle\langle 2\rangle\rangle\left[4\cdot\langle\langle 2\rangle\rangle^2 - \langle\langle 4\rangle\rangle\right]\frac{\sum_{i=1}^N (w_{\langle 2\rangle})_i(w_{\langle 4\rangle})_i}{\sum_{i=1}^N (w_{\langle 2\rangle})_i\sum_{j=1}^N (w_{\langle 4\rangle})_j}\mathrm{Cov}(\langle 2\rangle,\langle 4\rangle) \\
&+ 18\cdot\left[4\cdot\langle\langle 2\rangle\rangle^2 - \langle\langle 4\rangle\rangle\right]\frac{\sum_{i=1}^N (w_{\langle 2\rangle})_i(w_{\langle 6\rangle})_i}{\sum_{i=1}^N (w_{\langle 2\rangle})_i\sum_{j=1}^N (w_{\langle 6\rangle})_j}\mathrm{Cov}(\langle 2\rangle,\langle 6\rangle) \\
&- 18\cdot\langle\langle 2\rangle\rangle\frac{\sum_{i=1}^N (w_{\langle 4\rangle})_i(w_{\langle 6\rangle})_i}{\sum_{i=1}^N (w_{\langle 4\rangle})_i\sum_{j=1}^N (w_{\langle 6\rangle})_j}\mathrm{Cov}(\langle 4\rangle,\langle 6\rangle)\,. \qquad \text{(C.33)}
\end{aligned}
$$

C.2.4 8-particle estimate

We start from

$$v_n\{8\} \equiv 33^{-1/8}\sqrt[8]{-\langle 8\rangle+16\langle 6\rangle\langle 2\rangle+18\langle 4\rangle^2-144\langle 4\rangle\langle 2\rangle^2+144\langle 2\rangle^4}, \quad \text{(C.34)}$$

which gives to first order

$$\langle v_n\{8\}\rangle \approx 33^{-1/8}\sqrt[8]{-\langle\langle 8\rangle\rangle+16\langle\langle 6\rangle\rangle\langle\langle 2\rangle\rangle+18\langle\langle 4\rangle\rangle^2-144\langle\langle 4\rangle\rangle\langle\langle 2\rangle\rangle^2+144\langle\langle 2\rangle\rangle^4}. \quad \text{(C.35)}$$

An extended version of Eq. (C.17) valid for four random variables yields

$$\begin{aligned}
s^2_{\langle v_n\{8\}\rangle} = {} & \frac{4\cdot 33^{-1/4}}{\left[-\langle\langle 8\rangle\rangle+16\langle\langle 6\rangle\rangle\langle\langle 2\rangle\rangle+18\langle\langle 4\rangle\rangle^2-144\langle\langle 4\rangle\rangle\langle\langle 2\rangle\rangle^2+144\langle\langle 2\rangle\rangle^4\right]^{7/4}}\times \\
& \Bigg[\left[36\cdot\langle\langle 2\rangle\rangle^3-18\cdot\langle\langle 4\rangle\rangle\langle\langle 2\rangle\rangle+\langle\langle 6\rangle\rangle\right]^2\frac{\sum_{i=1}^N(w_{\langle 2\rangle})_i^2}{\left[\sum_{i=1}^N(w_{\langle 2\rangle})_i\right]^2}s^2_{\langle 2\rangle} \\
& +\frac{81}{16}\cdot\left[4\cdot\langle\langle 2\rangle\rangle^2-\langle\langle 4\rangle\rangle\right]^2\frac{\sum_{i=1}^N(w_{\langle 4\rangle})_i^2}{\left[\sum_{i=1}^N(w_{\langle 4\rangle})_i\right]^2}s^2_{\langle 4\rangle} \\
& +\langle\langle 2\rangle\rangle^2\frac{\sum_{i=1}^N(w_{\langle 6\rangle})_i^2}{\left[\sum_{i=1}^N(w_{\langle 6\rangle})_i\right]^2}s^2_{\langle 6\rangle}+\frac{1}{256}\frac{\sum_{i=1}^N(w_{\langle 8\rangle})_i^2}{\left[\sum_{i=1}^N(w_{\langle 8\rangle})_i\right]^2}s^2_{\langle 8\rangle} \\
& -\frac{9}{2}\left[36\cdot\langle\langle 2\rangle\rangle^3-18\cdot\langle\langle 2\rangle\rangle\langle\langle 4\rangle\rangle+\langle\langle 6\rangle\rangle\right]\left[4\cdot\langle\langle 2\rangle\rangle^2-\langle\langle 4\rangle\rangle\right] \\
& \times\frac{\sum_{i=1}^N(w_{\langle 2\rangle})_i(w_{\langle 4\rangle})_i}{\sum_{i=1}^N(w_{\langle 2\rangle})_i\sum_{j=1}^N(w_{\langle 4\rangle})_j}\mathrm{Cov}(\langle 2\rangle,\langle 4\rangle) \\
& +2\cdot\langle\langle 2\rangle\rangle\left[36\cdot\langle\langle 2\rangle\rangle^3-18\cdot\langle\langle 2\rangle\rangle\langle\langle 4\rangle\rangle+\langle\langle 6\rangle\rangle\right] \\
& \times\frac{\sum_{i=1}^N(w_{\langle 2\rangle})_i(w_{\langle 6\rangle})_i}{\sum_{i=1}^N(w_{\langle 2\rangle})_i\sum_{j=1}^N(w_{\langle 6\rangle})_j}\mathrm{Cov}(\langle 2\rangle,\langle 6\rangle) \\
& -\frac{1}{8}\left[36\langle\langle 2\rangle\rangle^3-18\langle\langle 2\rangle\rangle\langle\langle 4\rangle\rangle+\langle\langle 6\rangle\rangle\right]\frac{\sum_{i=1}^N(w_{\langle 2\rangle})_i(w_{\langle 8\rangle})_i}{\sum_{i=1}^N(w_{\langle 2\rangle})_i\sum_{j=1}^N(w_{\langle 8\rangle})_j}\mathrm{Cov}(\langle 2\rangle,\langle 8\rangle) \\
& -\frac{9}{2}\cdot\langle\langle 2\rangle\rangle\left[4\cdot\langle\langle 2\rangle\rangle^2-\langle\langle 4\rangle\rangle\right]\frac{\sum_{i=1}^N(w_{\langle 4\rangle})_i(w_{\langle 6\rangle})_i}{\sum_{i=1}^N(w_{\langle 4\rangle})_i\sum_{j=1}^N(w_{\langle 6\rangle})_j}\mathrm{Cov}(\langle 4\rangle,\langle 6\rangle) \\
& +\frac{9}{32}\left[4\cdot\langle\langle 2\rangle\rangle^2-\langle\langle 4\rangle\rangle\right]\frac{\sum_{i=1}^N(w_{\langle 4\rangle})_i(w_{\langle 8\rangle})_i}{\sum_{i=1}^N(w_{\langle 4\rangle})_i\sum_{j=1}^N(w_{\langle 8\rangle})_j}\mathrm{Cov}(\langle 4\rangle,\langle 8\rangle) \\
& -\frac{1}{8}\cdot\langle\langle 2\rangle\rangle\frac{\sum_{i=1}^N(w_{\langle 6\rangle})_i(w_{\langle 8\rangle})_i}{\sum_{i=1}^N(w_{\langle 6\rangle})_i\sum_{j=1}^N(w_{\langle 8\rangle})_j}\mathrm{Cov}(\langle 6\rangle,\langle 8\rangle)\Bigg]. \quad \text{(C.36)}
\end{aligned}$$

Equation (C.35) gives the final value of the 8-particle reference flow estimate and Eq. (C.36) the corresponding statistical error.

For completeness sake we also outline the corresponding results for the 8-particle reference Q-cumulant:

$$
\begin{aligned}
QC\{8\} &= \langle\langle 8\rangle\rangle - 16\cdot\langle\langle 6\rangle\rangle\langle\langle 2\rangle\rangle - 18\cdot\langle\langle 4\rangle\rangle^2 + 144\cdot\langle\langle 4\rangle\rangle\langle\langle 2\rangle\rangle^2 - 144\cdot\langle\langle 2\rangle\rangle^4 \,, \\
s^2_{QC\{8\}} &= 256\cdot\Big[36\cdot\langle\langle 2\rangle\rangle^3 - 18\cdot\langle\langle 4\rangle\rangle\langle\langle 2\rangle\rangle + \langle\langle 6\rangle\rangle\Big]^2 \frac{\sum_{i=1}^N (w_{\langle 2\rangle})_i^2}{\Big[\sum_{i=1}^N (w_{\langle 2\rangle})_i\Big]^2} s^2_{\langle 2\rangle} \\
&+ 1296\cdot\Big[4\cdot\langle\langle 2\rangle\rangle^2 - \langle\langle 4\rangle\rangle\Big]^2 \frac{\sum_{i=1}^N (w_{\langle 4\rangle})_i^2}{\Big[\sum_{i=1}^N (w_{\langle 4\rangle})_i\Big]^2} s^2_{\langle 4\rangle} \\
&+ 256\cdot\langle\langle 2\rangle\rangle^2 \frac{\sum_{i=1}^N (w_{\langle 6\rangle})_i^2}{\Big[\sum_{i=1}^N (w_{\langle 6\rangle})_i\Big]^2} s^2_{\langle 6\rangle} + \frac{\sum_{i=1}^N (w_{\langle 8\rangle})_i^2}{\Big[\sum_{i=1}^N (w_{\langle 8\rangle})_i\Big]^2} s^2_{\langle 8\rangle} \\
&- 1152\cdot\Big[36\cdot\langle\langle 2\rangle\rangle^3 - 18\cdot\langle\langle 4\rangle\rangle\langle\langle 2\rangle\rangle + \langle\langle 6\rangle\rangle\Big] \\
&\times \Big[4\cdot\langle\langle 2\rangle\rangle^2 - \langle\langle 4\rangle\rangle\Big] \frac{\sum_{i=1}^N (w_{\langle 2\rangle})_i (w_{\langle 4\rangle})_i}{\sum_{i=1}^N (w_{\langle 2\rangle})_i \sum_{j=1}^N (w_{\langle 4\rangle})_j} \mathrm{Cov}(\langle 2\rangle,\langle 4\rangle) \\
&+ 512\cdot\langle\langle 2\rangle\rangle\Big[36\cdot\langle\langle 2\rangle\rangle^3 - 18\cdot\langle\langle 4\rangle\rangle\langle\langle 2\rangle\rangle + \langle\langle 6\rangle\rangle\Big] \\
&\times \frac{\sum_{i=1}^N (w_{\langle 2\rangle})_i (w_{\langle 6\rangle})_i}{\sum_{i=1}^N (w_{\langle 2\rangle})_i \sum_{j=1}^N (w_{\langle 6\rangle})_j} \mathrm{Cov}(\langle 2\rangle,\langle 6\rangle) \\
&- 32\cdot\Big[36\cdot\langle\langle 2\rangle\rangle^3 - 18\cdot\langle\langle 4\rangle\rangle\langle\langle 2\rangle\rangle + \langle\langle 6\rangle\rangle\Big] \\
&\times \frac{\sum_{i=1}^N (w_{\langle 2\rangle})_i (w_{\langle 8\rangle})_i}{\sum_{i=1}^N (w_{\langle 2\rangle})_i \sum_{j=1}^N (w_{\langle 8\rangle})_j} \mathrm{Cov}(\langle 2\rangle,\langle 8\rangle) \\
&- 1152\cdot\langle\langle 2\rangle\rangle\Big[4\cdot\langle\langle 2\rangle\rangle^2 - \langle\langle 4\rangle\rangle\Big] \frac{\sum_{i=1}^N (w_{\langle 4\rangle})_i (w_{\langle 6\rangle})_i}{\sum_{i=1}^N (w_{\langle 4\rangle})_i \sum_{j=1}^N (w_{\langle 6\rangle})_j} \mathrm{Cov}(\langle 4\rangle,\langle 6\rangle) \\
&+ 72\cdot\Big[4\cdot\langle\langle 2\rangle\rangle^2 - \langle\langle 4\rangle\rangle\Big] \frac{\sum_{i=1}^N (w_{\langle 4\rangle})_i (w_{\langle 8\rangle})_i}{\sum_{i=1}^N (w_{\langle 4\rangle})_i \sum_{j=1}^N (w_{\langle 8\rangle})_j} \mathrm{Cov}(\langle 4\rangle,\langle 8\rangle) \\
&- 32\cdot\langle\langle 2\rangle\rangle \frac{\sum_{i=1}^N (w_{\langle 6\rangle})_i (w_{\langle 8\rangle})_i}{\sum_{i=1}^N (w_{\langle 6\rangle})_i \sum_{j=1}^N (w_{\langle 8\rangle})_j} \mathrm{Cov}(\langle 6\rangle,\langle 8\rangle) \,. \qquad \text{(C.37)}
\end{aligned}
$$

In the next section we provide an analogous treatment for the differential flow estimates.

C.3 Statistical errors for differential flow estimates

We will treat statistical errors of differential flow estimates in analogy to the treatment of statistical errors of reference flow estimates presented in the previous section.

As measured random observables event-by-event we identify the average reduced multiparticle correlations $\langle 2' \rangle$ and $\langle 4' \rangle$. As in the previous section, we will write the final results for the average reduced correlations and report their statistical errors as

$$\begin{aligned} \langle\langle 2' \rangle\rangle &\pm \frac{\sqrt{\sum_{i=1}^{N} (w_{\langle 2' \rangle})_i^2}}{\sum_{i=1}^{N} (w_{\langle 2' \rangle})_i} s_{\langle 2' \rangle} \,, \\ \langle\langle 4' \rangle\rangle &\pm \frac{\sqrt{\sum_{i=1}^{N} (w_{\langle 4' \rangle})_i^2}}{\sum_{i=1}^{N} (w_{\langle 4' \rangle})_i} s_{\langle 4' \rangle} \,, \end{aligned} \tag{C.38}$$

where the weights $w_{\langle 2' \rangle}$ and $w_{\langle 4' \rangle}$ were defined in the main part of this thesis (see Eqs. (3.61) and (3.62), respectively). All quantities in the above two equations can be obtained straight from the data. Having this in mind we will report the final results and statistical errors for the differential flow estimates by taking into account their functional dependence on the multi-particle correlations and by propagating the statistical error from this dependence. In accordance with the notation introduced in previous section (see Eq. (C.13)) we will report the final results and statistical errors of the differential flow estimates:

$$\begin{aligned} \langle v_n'\{2\} \rangle &\pm s_{\langle v_n'\{2\} \rangle} \,, \\ \langle v_n'\{4\} \rangle &\pm s_{\langle v_n'\{4\} \rangle} \,. \end{aligned} \tag{C.39}$$

As in the previous section, the very important thing to note is that the different average multiparticle correlations and the different average reduced multiparticle correlations measured event-by-event *are not mutually independent quantities*. Hence, we also need the unbiased estimators for their covariances Cov($\langle 2 \rangle$,$\langle 2' \rangle$), Cov($\langle 2 \rangle$,$\langle 4' \rangle$), Cov($\langle 4 \rangle$,$\langle 2' \rangle$), Cov($\langle 4 \rangle$,$\langle 4' \rangle$) and Cov($\langle 2' \rangle$,$\langle 4' \rangle$). These unbiased estimators for the covariances can also be obtained straight from the data by making use of Eq. (C.12) .

C.3.1 2-particle estimate

For the 2-particle differential flow estimate we have

$$v_n'\{2\} \equiv \frac{\langle 2' \rangle}{\langle 2 \rangle^{1/2}} \,, \tag{C.40}$$

which yields to first order

$$\langle v_n'\{2\} \rangle \approx \frac{\langle\langle 2' \rangle\rangle}{\langle\langle 2 \rangle\rangle^{1/2}} \,. \tag{C.41}$$

After plugging this functional dependence into Eq. (C.17) we have

$$\begin{aligned} s^2_{\langle v'_n\{2\}\rangle} &= \frac{1}{4\cdot\langle\langle 2\rangle\rangle^3}\times\Bigg[\langle\langle 2'\rangle\rangle^2\,\frac{\sum_{i=1}^N (w_{\langle 2\rangle})_i^2}{\left[\sum_{i=1}^N (w_{\langle 2\rangle})_i\right]^2}\,s^2_{\langle 2\rangle} \\ &+ 4\cdot\langle\langle 2\rangle\rangle^2\,\frac{\sum_{i=1}^N (w_{\langle 2'\rangle})_i^2}{\left[\sum_{i=1}^N (w_{\langle 2'\rangle})_i\right]^2}\,s^2_{\langle 2'\rangle} - 4\cdot\langle\langle 2\rangle\rangle\,\langle\langle 2'\rangle\rangle \\ &\times \frac{\sum_{i=1}^N (w_{\langle 2\rangle})_i (w_{\langle 2'\rangle})_i}{\sum_{i=1}^N (w_{\langle 2\rangle})_i \sum_{j=1}^N (w_{\langle 2'\rangle})_j}\,\mathrm{Cov}(\langle 2\rangle,\langle 2'\rangle)\Bigg]\,. \end{aligned} \tag{C.42}$$

Equation (C.41) gives the final value of the 2-particle differential flow estimate and Eq. (C.42) gives the corresponding statistical error. For the completeness sake we also outline the results for the differential 2-particle Q-cumulant:

$$\begin{aligned} QC\{2'\} &= \langle\langle 2'\rangle\rangle\,, \\ s_{QC\{2'\}} &= \frac{\sqrt{\sum_{i=1}^N (w_{\langle 2'\rangle})_i^2}}{\sum_{i=1}^N (w_{\langle 2'\rangle})_i}\,s_{\langle 2'\rangle}\,. \end{aligned} \tag{C.43}$$

Finally, in the next section we present the results for the 4-particle differential flow.

C.3.2 4-particle estimate

When it comes to the 4-particle differential flow estimate we start from

$$v'_n\{4\} \equiv \frac{2\cdot\langle 2\rangle\langle 2'\rangle - \langle 4'\rangle}{\left[2\cdot\langle 2\rangle^2 - \langle 4\rangle\right]^{3/4}}\,, \tag{C.44}$$

which yields to leading order

$$\langle v'_n\{4\}\rangle \approx \frac{2\cdot\langle\langle 2\rangle\rangle\langle\langle 2'\rangle\rangle - \langle\langle 4'\rangle\rangle}{\left[2\cdot\langle\langle 2\rangle\rangle^2 - \langle\langle 4\rangle\rangle\right]^{3/4}}\,. \tag{C.45}$$

We use again the generalized version of Eq. (C.17) valid for four random variables. After some algebra, it follows straightforwardly:

$$
\begin{aligned}
s^2_{\langle v'_n\{4\}\rangle} \;=\; & \frac{1}{\left[2\cdot\langle\langle 2\rangle\rangle^2-\langle\langle 4\rangle\rangle\right]^{\frac{7}{2}}}\times \qquad\qquad (C.46)\\
& \Bigg\{\left[2\cdot\langle\langle 2\rangle\rangle^2\langle\langle 2'\rangle\rangle-3\cdot\langle\langle 2\rangle\rangle\langle\langle 4'\rangle\rangle+2\cdot\langle\langle 4\rangle\rangle\langle\langle 2'\rangle\rangle\right]^2\\
& \times\frac{\sum_{i=1}^N(w_{\langle 2\rangle})_i^2}{\left[\sum_{i=1}^N(w_{\langle 2\rangle})_i\right]^2}s^2_{\langle 2\rangle}\\
& +\frac{9}{16}\cdot\left[2\cdot\langle\langle 2\rangle\rangle\langle\langle 2'\rangle\rangle-\langle\langle 4'\rangle\rangle\right]^2\frac{\sum_{i=1}^N(w_{\langle 4\rangle})_i^2}{\left[\sum_{i=1}^N(w_{\langle 4\rangle})_i\right]^2}s^2_{\langle 4\rangle}\\
& +4\cdot\langle\langle 2\rangle\rangle^2\left[2\cdot\langle\langle 2\rangle\rangle^2-\langle\langle 4\rangle\rangle\right]^2\frac{\sum_{i=1}^N(w_{\langle 2'\rangle})_i^2}{\left[\sum_{i=1}^N(w_{\langle 2'\rangle})_i\right]^2}s^2_{\langle 2'\rangle}\\
& +\left[2\cdot\langle\langle 2\rangle\rangle^2-\langle\langle 4\rangle\rangle\right]^2\frac{\sum_{i=1}^N(w_{\langle 4'\rangle})_i^2}{\left[\sum_{i=1}^N(w_{\langle 4'\rangle})_i\right]^2}s^2_{\langle 4'\rangle}\\
& -\frac{3}{2}\cdot\left[2\cdot\langle\langle 2\rangle\rangle\langle\langle 2'\rangle\rangle-\langle\langle 4'\rangle\rangle\right]\\
& \times\left[2\cdot\langle\langle 2\rangle\rangle^2\langle\langle 2'\rangle\rangle-3\cdot\langle\langle 2\rangle\rangle\langle\langle 4'\rangle\rangle+2\cdot\langle\langle 4\rangle\rangle\langle\langle 2'\rangle\rangle\right]\\
& \times\frac{\sum_{i=1}^N(w_{\langle 2\rangle})_i(w_{\langle 4\rangle})_i}{\sum_{i=1}^N(w_{\langle 2\rangle})_i\sum_{j=1}^N(w_{\langle 4\rangle})_j}\mathrm{Cov}(\langle 2\rangle,\langle 4\rangle)\\
& -4\cdot\langle\langle 2\rangle\rangle\left[2\cdot\langle\langle 2\rangle\rangle^2-\langle\langle 4\rangle\rangle\right]\\
& \times\left[2\cdot\langle\langle 2\rangle\rangle^2\langle\langle 2'\rangle\rangle-3\cdot\langle\langle 2\rangle\rangle\langle\langle 4'\rangle\rangle+2\cdot\langle\langle 4\rangle\rangle\langle\langle 2'\rangle\rangle\right]\\
& \times\frac{\sum_{i=1}^N(w_{\langle 2\rangle})_i(w_{\langle 2'\rangle})_i}{\sum_{i=1}^N(w_{\langle 2\rangle})_i\sum_{j=1}^N(w_{\langle 2'\rangle})_j}\mathrm{Cov}(\langle 2\rangle,\langle 2'\rangle)\\
& +2\cdot\left[2\cdot\langle\langle 2\rangle\rangle^2-\langle\langle 4\rangle\rangle\right]\\
& \times\left[2\cdot\langle\langle 2\rangle\rangle^2\langle\langle 2'\rangle\rangle-3\cdot\langle\langle 2\rangle\rangle\langle\langle 4'\rangle\rangle+2\cdot\langle\langle 4\rangle\rangle\langle\langle 2'\rangle\rangle\right]\\
& \times\frac{\sum_{i=1}^N(w_{\langle 2\rangle})_i(w_{\langle 4'\rangle})_i}{\sum_{i=1}^N(w_{\langle 2\rangle})_i\sum_{j=1}^N(w_{\langle 4'\rangle})_j}\mathrm{Cov}(\langle 2\rangle,\langle 4'\rangle)\\
& +3\cdot\langle\langle 2\rangle\rangle\left[2\cdot\langle\langle 2\rangle\rangle^2-\langle\langle 4\rangle\rangle\right]\left[2\cdot\langle\langle 2\rangle\rangle\langle\langle 2'\rangle\rangle-\langle\langle 4'\rangle\rangle\right]\\
& \times\frac{\sum_{i=1}^N(w_{\langle 4\rangle})_i(w_{\langle 2'\rangle})_i}{\sum_{i=1}^N(w_{\langle 4\rangle})_i\sum_{j=1}^N(w_{\langle 2'\rangle})_j}\mathrm{Cov}(\langle 4\rangle,\langle 2'\rangle)\\
& -\frac{3}{2}\cdot\left[2\cdot\langle\langle 2\rangle\rangle^2-\langle\langle 4\rangle\rangle\right]\left[2\cdot\langle\langle 2\rangle\rangle\langle\langle 2'\rangle\rangle-\langle\langle 4'\rangle\rangle\right]\\
& \times\frac{\sum_{i=1}^N(w_{\langle 4\rangle})_i(w_{\langle 4'\rangle})_i}{\sum_{i=1}^N(w_{\langle 4\rangle})_i\sum_{j=1}^N(w_{\langle 4'\rangle})_j}\mathrm{Cov}(\langle 4\rangle,\langle 4'\rangle)\\
& -4\cdot\langle\langle 2\rangle\rangle\left[2\cdot\langle\langle 2\rangle\rangle^2-\langle\langle 4\rangle\rangle\right]^2\times\frac{\sum_{i=1}^N(w_{\langle 2'\rangle})_i(w_{\langle 4'\rangle})_i}{\sum_{i=1}^N(w_{\langle 2'\rangle})_i\sum_{j=1}^N(w_{\langle 4'\rangle})_j}\mathrm{Cov}(\langle 2'\rangle,\langle 4'\rangle)\Bigg\}.
\end{aligned}
$$

Equation (C.45) gives the final value of the 4-particle differential flow estimate and Eq. (C.47) the corresponding statistical error. For completeness sake we also outline the results for the 4-particle differential Q-cumulant:

$$
\begin{aligned}
QC\{4'\} &= \langle\langle 4'\rangle\rangle - 2\cdot\langle\langle 2\rangle\rangle\,\langle\langle 2'\rangle\rangle\ , \\
s^2_{QC\{4'\}} &= 4\cdot\langle\langle 2'\rangle\rangle^2\,\frac{\sum_{i=1}^{N}(w_{\langle 2\rangle})_i^2}{\left[\sum_{i=1}^{N}(w_{\langle 2\rangle})_i\right]^2}\,s^2_{\langle 2\rangle} + 4\cdot\langle\langle 2\rangle\rangle^2\,\frac{\sum_{i=1}^{N}(w_{\langle 2'\rangle})_i^2}{\left[\sum_{i=1}^{N}(w_{\langle 2'\rangle})_i\right]^2}\,s^2_{\langle 2'\rangle} \\
&+ \frac{\sum_{i=1}^{N}(w_{\langle 4'\rangle})_i^2}{\left[\sum_{i=1}^{N}(w_{\langle 4'\rangle})_i\right]^2}\,s^2_{\langle 4'\rangle} + 8\,\langle\langle 2\rangle\rangle\,\langle\langle 2'\rangle\rangle\,\frac{\sum_{i=1}^{N}(w_{\langle 2\rangle})_i(w_{\langle 2'\rangle})_i}{\sum_{i=1}^{N}(w_{\langle 2\rangle})_i\sum_{j=1}^{N}(w_{\langle 2'\rangle})_j}\mathrm{Cov}(\langle 2\rangle,\langle 2'\rangle) \\
&- 4\cdot\langle\langle 2'\rangle\rangle\,\frac{\sum_{i=1}^{N}(w_{\langle 2\rangle})_i(w_{\langle 4'\rangle})_i}{\sum_{i=1}^{N}(w_{\langle 2\rangle})_i\sum_{j=1}^{N}(w_{\langle 4'\rangle})_j}\mathrm{Cov}(\langle 2\rangle,\langle 4'\rangle) \\
&- 4\cdot\langle\langle 2\rangle\rangle\,\frac{\sum_{i=1}^{N}(w_{\langle 2'\rangle})_i(w_{\langle 4'\rangle})_i}{\sum_{i=1}^{N}(w_{\langle 2'\rangle})_i\sum_{j=1}^{N}(w_{\langle 4'\rangle})_j}\mathrm{Cov}(\langle 2'\rangle,\langle 4'\rangle)\,. \qquad \text{(C.47)}
\end{aligned}
$$

With this equation we conclude this Appendix.

Appendix D

Non-uniform acceptance

When building cumulants from multi-particle correlations we have so far omitted non-isotropic terms which vanish for detectors with uniform acceptance. For a more general case they have to be kept [54, 55, 66, 73]. Essentially, for a detector with non-uniform azimuthal acceptance one has to take into account *all* terms in the generalized cumulant expansion (see for instance Eqs. (2.8) in [66]). The underlying idea is that the n-particle cumulants isolate the genuine n-particle physical correlation, and under the reasonable assumption that the physical correlation is the same whether or not the acceptance of the detector is uniform, then the cumulants consisting only of isotropic terms and cumulants consisting of both isotropic and non-isotropic terms shall be the same. For the case of uniform acceptance the non-isotropic terms vanish and the cumulants consist only of isotropic terms. This implies that for the case of non-uniform acceptance the non-isotropic terms will counter balance the systematic bias in the isotropic terms, so that the cumulants remain unbiased. In turn, by inspecting only the non-isotropic terms in the generalized cumulant expansion one can *quantify* the systematic bias due to non-uniform azimuthal acceptance of a detector.

The generalized 2-particle cumulant was given in the 3$^{\text{rd}}$ line in Eqs. (2.8) in [66]:

$$\langle X_j X_l \rangle_c = \langle X_j X_l \rangle - \langle X_j \rangle \langle X_l \rangle \ , \tag{D.1}$$

which gives the generalized 2-particle cumulant, $\langle X_j X_l \rangle_c$, for any two random observables X_j and X_l. After making the specific choice for the two random observables relevant for the flow analysis, namely $X_j \equiv e^{in\phi_1}$ and $X_l \equiv e^{-in\phi_2}$, and isolating only the real parts in the resulting expressions, it follows that the generalized 2-particle cumulant in the context of flow analysis reads:

$$c_n\{2\} \quad = \quad \langle\langle 2 \rangle\rangle - \left[\langle\langle \cos n\phi_1 \rangle\rangle^2 + \langle\langle \sin n\phi_1 \rangle\rangle^2 \right] \ , \tag{D.2}$$

where we have switched to the flow analysis specific notation for the 2-particle cumulant, $c_n\{2\}$, and where $\langle\langle 2 \rangle\rangle \equiv \langle\langle \cos[n(\phi_1 - \phi_2)] \rangle\rangle$, $\phi_1 \neq \phi_2$. Terms $\langle\langle \cos n\phi_1 \rangle\rangle^2$ and $\langle\langle \sin n\phi_1 \rangle\rangle^2$ vanish for the case of uniform acceptance—for the case of non-uniform acceptance they do not vanish and they will counterbalance the systematic bias in

$\langle\langle 2\rangle\rangle$, so that the cumulant $c_n\{2\}$ remains unbiased. Correspondingly, the combination $\langle\langle\cos n\phi_1\rangle\rangle^2 + \langle\langle\sin n\phi_1\rangle\rangle^2$ quantifies the systematic bias due to non-uniform acceptance in the flow analysis with 2-particle azimuthal correlations. This idea can be straightforwardly applied also to correlations involving more than two particles to obtain the generalized cumulants at any order. In this section we outline the generalized cumulants up to order four, both for reference and differential flow, together with one concrete example of their performance.

The correction terms in (D.2) can be expressed in terms of the real and imaginary parts of the Q-vector:

$$\langle\langle\cos n\phi_1\rangle\rangle = \frac{\sum_{i=1}^{N}\left(\mathfrak{Re}\left[Q_n\right]\right)_i}{\sum_{i=1}^{N} M_i}\,, \tag{D.3}$$

$$\langle\langle\sin n\phi_1\rangle\rangle = \frac{\sum_{i=1}^{N}\left(\mathfrak{Im}\left[Q_n\right]\right)_i}{\sum_{i=1}^{N} M_i}\,. \tag{D.4}$$

When particle weights are used the average 2-particle correlation $\langle\langle 2\rangle\rangle$ is determined from Eqs. (B.16), while Eqs. (D.3) and (D.4) generalize into:

$$\langle\langle\cos n\phi_1\rangle\rangle = \frac{\sum_{i=1}^{N}\left(\mathfrak{Re}\left[Q_{n,1}\right]\right)_i}{\sum_{i=1}^{N}(S_{1,1})_i}\,, \tag{D.5}$$

$$\langle\langle\sin n\phi_1\rangle\rangle = \frac{\sum_{i=1}^{N}\left(\mathfrak{Im}\left[Q_{n,1}\right]\right)_i}{\sum_{i=1}^{N}(S_{1,1})_i}\,, \tag{D.6}$$

where $Q_{n,1}$ can be determined from the definition of the weighted Q-vector (B.3) and $S_{1,1}$ from definition (B.6).

The generalized 4^{th} order cumulant reads:

$$\begin{aligned}
c_n\{4\} &= \langle\langle 4\rangle\rangle - 2\cdot\langle\langle 2\rangle\rangle^2 - \\
&- 4\cdot\langle\langle\cos n\phi_1\rangle\rangle\langle\langle\cos n(\phi_1-\phi_2-\phi_3)\rangle\rangle \\
&+ 4\cdot\langle\langle\sin n\phi_1\rangle\rangle\langle\langle\sin n(\phi_1-\phi_2-\phi_3)\rangle\rangle \\
&- \langle\langle\cos n(\phi_1+\phi_2)\rangle\rangle^2 - \langle\langle\sin n(\phi_1+\phi_2)\rangle\rangle^2 \\
&+ 4\cdot\langle\langle\cos n(\phi_1+\phi_2)\rangle\rangle \\
&\times \left[\langle\langle\cos n\phi_1\rangle\rangle^2 - \langle\langle\sin n\phi_1\rangle\rangle^2\right] \\
&+ 8\cdot\langle\langle\sin n(\phi_1+\phi_2)\rangle\rangle\langle\langle\sin n\phi_1\rangle\rangle\langle\langle\cos n\phi_1\rangle\rangle \\
&+ 8\cdot\langle\langle\cos n(\phi_1-\phi_2)\rangle\rangle \\
&\times \left[\langle\langle\cos n\phi_1\rangle\rangle^2 + \langle\langle\sin n\phi_1\rangle\rangle^2\right] \\
&- 6\cdot\left[\langle\langle\cos n\phi_1\rangle\rangle^2 + \langle\langle\sin n\phi_1\rangle\rangle^2\right]^2 .
\end{aligned} \tag{D.7}$$

The terms starting from the second line in Eq. (D.7) counter-balance the bias coming from non-uniform acceptance so that $c_n\{4\}$ is unbiased. These terms can be expressed

in terms of Q-vectors:

$$\langle\langle\cos n(\phi_1+\phi_2)\rangle\rangle = \frac{\sum_{i=1}^{N}\left(\mathfrak{Re}\left[Q_nQ_n-Q_{2n}\right]\right)_i}{\sum_{i=1}^{N}M_i(M_i-1)}, \tag{D.8}$$

$$\langle\langle\sin n(\phi_1+\phi_2)\rangle\rangle = \frac{\sum_{i=1}^{N}\left(\mathfrak{Im}\left[Q_nQ_n-Q_{2n}\right]\right)_i}{\sum_{i=1}^{N}M_i(M_i-1)}, \tag{D.9}$$

$$\begin{aligned}\langle\langle\cos n(\phi_1-\phi_2-\phi_3)\rangle\rangle &= \left\{\sum_{i=1}^{N}\left(\mathfrak{Re}\left[Q_nQ_n^*Q_n^*-Q_nQ_{2n}^*\right]\right.\right.\\ &\left.\left.-2(M-1)\mathfrak{Re}\left[Q_n^*\right]\right)_i\right\}\left\{\sum_{i=1}^{N}M_i(M_i-1)(M_i-2)\right\}^{-1},\end{aligned} \tag{D.10}$$

$$\begin{aligned}\langle\langle\sin n(\phi_1-\phi_2-\phi_3)\rangle\rangle &= \left\{\sum_{i=1}^{N}\left(\mathfrak{Im}\left[Q_nQ_n^*Q_n^*-Q_nQ_{2n}^*\right]\right.\right.\\ &\left.\left.-2(M-1)\mathfrak{Im}\left[Q_n^*\right]\right)_i\right\}\left\{\sum_{i=1}^{N}M_i(M_i-1)(M_i-2)\right\}^{-1}.\end{aligned} \tag{D.11}$$

When particle weights are used the average 2-particle correlation $\langle\langle 2\rangle\rangle$ is determined from Eqs. (B.16), the average 4-particle correlation $\langle\langle 4\rangle\rangle$ is determined from Eqs. (B.17), the Eqs. (D.8) and (D.9) generalize into:

$$\begin{aligned}\langle\langle\cos n(\phi_1+\phi_2)\rangle\rangle &= \frac{\sum_{i=1}^{N}\left(\mathfrak{Re}\left[Q_{n,1}Q_{n,1}-Q_{2n,2}\right]\right)_i}{\sum_{i=1}^{N}(\mathcal{M}_{11})_i},\\ \langle\langle\sin n(\phi_1+\phi_2)\rangle\rangle &= \frac{\sum_{i=1}^{N}\left(\mathfrak{Im}\left[Q_{n,1}Q_{n,1}-Q_{2n,2}\right]\right)_i}{\sum_{i=1}^{N}(\mathcal{M}_{11})_i},\\ \mathcal{M}_{11} &\equiv \sum_{i,j=1}^{M}{}' w_iw_j = S_{2,1}-S_{1,2},\end{aligned} \tag{D.12}$$

and the Eqs. (D.10) and (D.11) generalize into

$$\begin{aligned}
\langle\langle\cos n(\phi_1-\phi_2-\phi_3)\rangle\rangle &= \left\{\sum_{i=1}^{N}\left(\mathfrak{Re}\left[Q_{n,1}Q_{n,1}^{*}Q_{n,1}^{*}\right.\right.\right. \\
&\quad \left.\left.\left.-Q_{n,1}Q_{2n,2}^{*}-2\cdot S_{1,2}Q_{n,1}^{*}+2\cdot Q_{n,3}^{*}\right]\right)_i\right\}\left\{\sum_{i=1}^{N}(\mathcal{M}_{111})_i\right\}^{-1}, \\
\langle\langle\sin n(\phi_1-\phi_2-\phi_3)\rangle\rangle &= \left\{\sum_{i=1}^{N}\left(\mathfrak{Im}\left[Q_{n,1}Q_{n,1}^{*}Q_{n,1}^{*}\right.\right.\right. \\
&\quad \left.\left.\left.-Q_{n,1}Q_{2n,2}^{*}-2\cdot S_{1,2}Q_{n,1}^{*}+2\cdot Q_{n,3}^{*}\right]\right)_i\right\}\left\{\sum_{i=1}^{N}(\mathcal{M}_{111})_i\right\}^{-1}, \\
\mathcal{M}_{111}\equiv{\sum_{i,j,k=1}^{M}}' w_i w_j w_k &= S_{3,1}-3\cdot S_{1,2}S_{1,1}+2\cdot S_{1,3}\,. \qquad \text{(D.13)}
\end{aligned}$$

The generalized 2$^{\text{nd}}$ order differential cumulant reads

$$d_n\{2\} = \langle\langle 2'\rangle\rangle - \langle\langle\cos n\psi_1\rangle\rangle\langle\langle\cos n\phi_2\rangle\rangle - \langle\langle\sin n\psi_1\rangle\rangle\langle\langle\sin n\phi_2\rangle\rangle\,. \qquad \text{(D.14)}$$

Expressions for $\langle\langle\cos n\phi_1\rangle\rangle$ and $\langle\langle\sin n\phi_1\rangle\rangle$ were already given in Eqs. (D.3) and (D.4), respectively (when particle weights are being used in Eqs. (D.5) and (D.6), respectively). Similarly:

$$\langle\langle\cos n\psi_1\rangle\rangle = \frac{\sum_{i=1}^{N}\left(\mathfrak{Re}\left[p_n\right]\right)_i}{\sum_{i=1}^{N}(m_p)_i}\,, \qquad \text{(D.15)}$$

$$\langle\langle\sin n\psi_1\rangle\rangle = \frac{\sum_{i=1}^{N}\left(\mathfrak{Im}\left[p_n\right]\right)_i}{\sum_{i=1}^{N}(m_p)_i}\,, \qquad \text{(D.16)}$$

where p_n and m_p were defined in Section 3.2.3. The Eqs. (D.15) and (D.16) remain unchanged when particle weights are being used.

The generalized 4^{th} order differential cumulant reads:

$$
\begin{aligned}
d_n\{4\} &= \langle\langle 4' \rangle\rangle - 2 \cdot \langle\langle 2' \rangle\rangle \langle\langle 2 \rangle\rangle \\
&- \langle\langle \cos n\psi_1 \rangle\rangle \langle\langle \cos n(\phi_1 - \phi_2 - \phi_3) \rangle\rangle \\
&+ \langle\langle \sin n\psi_1 \rangle\rangle \langle\langle \sin n(\phi_1 - \phi_2 - \phi_3) \rangle\rangle \\
&- \langle\langle \cos n\phi_1 \rangle\rangle \langle\langle \cos n(\psi_1 - \phi_2 - \phi_3) \rangle\rangle \\
&+ \langle\langle \sin n\phi_1 \rangle\rangle \langle\langle \sin n(\psi_1 - \phi_2 - \phi_3) \rangle\rangle \\
&- 2 \cdot \langle\langle \cos n\phi_1 \rangle\rangle \langle\langle \cos n(\psi_1 + \phi_2 - \phi_3) \rangle\rangle \\
&- 2 \cdot \langle\langle \sin n\phi_1 \rangle\rangle \langle\langle \sin n(\psi_1 + \phi_2 - \phi_3) \rangle\rangle \\
&- \langle\langle \cos n(\psi_1 + \phi_2) \rangle\rangle \langle\langle \cos n(\phi_1 + \phi_2) \rangle\rangle \\
&- \langle\langle \sin n(\psi_1 + \phi_2) \rangle\rangle \langle\langle \sin n(\phi_1 + \phi_2) \rangle\rangle \\
&+ 2 \cdot \langle\langle \cos n(\phi_1 + \phi_2) \rangle\rangle \\
&\times [\langle\langle \cos n\psi_1 \rangle\rangle \langle\langle \cos n\phi_1 \rangle\rangle - \langle\langle \sin n\psi_1 \rangle\rangle \langle\langle \sin n\phi_1 \rangle\rangle] \\
&+ 2 \cdot \langle\langle \sin n(\phi_1 + \phi_2) \rangle\rangle \\
&\times [\langle\langle \cos n\psi_1 \rangle\rangle \langle\langle \sin n\phi_1 \rangle\rangle + \langle\langle \sin n\psi_1 \rangle\rangle \langle\langle \cos n\phi_1 \rangle\rangle] \\
&+ 4 \cdot \langle\langle \cos n(\phi_1 - \phi_2) \rangle\rangle \\
&\times [\langle\langle \cos n\psi_1 \rangle\rangle \langle\langle \cos n\phi_1 \rangle\rangle + \langle\langle \sin n\psi_1 \rangle\rangle \langle\langle \sin n\phi_1 \rangle\rangle] \\
&+ 2 \cdot \langle\langle \cos n(\psi_1 + \phi_2) \rangle\rangle \\
&\times \left[\langle\langle \cos n\phi_1 \rangle\rangle^2 - \langle\langle \sin n\phi_1 \rangle\rangle^2\right] \\
&+ 4 \cdot \langle\langle \sin n(\psi_1 + \phi_2) \rangle\rangle \langle\langle \cos n\phi_1 \rangle\rangle \langle\langle \sin n\phi_1 \rangle\rangle \\
&+ 4 \cdot \langle\langle \cos n(\psi_1 - \phi_2) \rangle\rangle \left[\langle\langle \cos n\phi_1 \rangle\rangle^2 + \langle\langle \sin n\phi_1 \rangle\rangle^2\right] \\
&- 6 \cdot \left[\langle\langle \cos n\phi_1 \rangle\rangle^2 - \langle\langle \sin n\phi_1 \rangle\rangle^2\right] \\
&\times [\langle\langle \cos n\psi_1 \rangle\rangle \langle\langle \cos n\phi_1 \rangle\rangle - \langle\langle \sin n\psi_1 \rangle\rangle \langle\langle \sin n\phi_1 \rangle\rangle] \\
&- 12 \cdot \langle\langle \cos n\phi_1 \rangle\rangle \langle\langle \sin n\phi_1 \rangle\rangle \\
&\times [\langle\langle \sin n\psi_1 \rangle\rangle \langle\langle \cos n\phi_1 \rangle\rangle + \langle\langle \cos n\psi_1 \rangle\rangle \langle\langle \sin n\phi_1 \rangle\rangle] \ .
\end{aligned}
\tag{D.17}
$$

The terms starting from the second line in Eq. (D.17) counter-balance the bias coming from non-uniform acceptance. Some of the new terms appearing in this expression can be expressed again in products of flow vectors:

$$
\begin{aligned}
\langle\langle \cos n(\psi_1 + \phi_2) \rangle\rangle &= \frac{\sum_{i=1}^{N} (\mathfrak{Re}\left[p_n Q_n - q_{2n}\right])_i}{\sum_{i=1}^{N} (m_p M - m_q)_i} \ , \\
\langle\langle \sin n(\psi_1 + \phi_2) \rangle\rangle &= \frac{\sum_{i=1}^{N} (\mathfrak{Im}\left[p_n Q_n - q_{2n}\right])_i}{\sum_{i=1}^{N} (m_p M - m_q)_i} \ ,
\end{aligned}
\tag{D.18}
$$

$$\begin{aligned}
\langle\langle\cos n(\psi_1+\phi_2-\phi_3)\rangle\rangle &= \Big\{\sum_{i=1}^{N}\Big(\mathfrak{Re}\left[p_n\Big(|Q_n|^2-M\Big)\right] \\
&\quad -\mathfrak{Re}\left[q_{2n}Q_n^*+m_qQ_n-2q_n\right]\Big)_i\Big\}\Big\{\sum_{i=1}^{N}\left[(m_pM-2m_q)(M-1)\right]_i\Big\}^{-1}, \\
\langle\langle\sin n(\psi_1+\phi_2-\phi_3)\rangle\rangle &= \Big\{\sum_{i=1}^{N}\Big(\mathfrak{Im}\left[p_n\Big(|Q_n|^2-M\Big)\right] \\
&\quad -\mathfrak{Im}\left[q_{2n}Q_n^*+m_qQ_n-2q_n\right]\Big)_i\Big\}\Big\{\sum_{i=1}^{N}\left[(m_pM-2m_q)(M-1)\right]_i\Big\}^{-1}, \qquad \text{(D.19)}
\end{aligned}$$

$$\begin{aligned}
\langle\langle\cos n(\psi_1-\phi_2-\phi_3)\rangle\rangle &= \Big\{\sum_{i=1}^{N}\Big(\mathfrak{Re}\left[p_nQ_n^*Q_n^*-p_nQ_{2n}^*\right] \\
&\quad -\mathfrak{Re}\left[2m_qQ_n^*-2q_n^*\right]\Big)_i\Big\}\Big\{\sum_{i=1}^{N}\left[(m_pM-2m_q)(M-1)\right]_i\Big\}^{-1}, \\
\langle\langle\sin n(\psi_1-\phi_2-\phi_3)\rangle\rangle &= \Big\{\sum_{i=1}^{N}\Big(\mathfrak{Im}\left[p_nQ_n^*Q_n^*-p_nQ_{2n}^*\right] \\
&\quad -\mathfrak{Im}\left[2m_qQ_n^*-2q_n^*\right]\Big)_i\Big\}\Big\{\sum_{i=1}^{N}\left[(m_pM-2m_q)(M-1)\right]_i\Big\}^{-1}. \qquad \text{(D.20)}
\end{aligned}$$

When particle weights are used Eqs. (D.18) generalize into:

$$\begin{aligned}
\langle\langle\cos n(\psi_1+\phi_2)\rangle\rangle &= \frac{\sum_{i=1}^{N}\left(\mathfrak{Re}\left[p_nQ_{n,k}-q_{2n,k}\right]\right)_i}{\sum_{i=1}^{N}\left(m_pS_{1,1}-s_{1,1}\right)_i}, \\
\langle\langle\sin n(\psi_1+\phi_2)\rangle\rangle &= \frac{\sum_{i=1}^{N}\left(\mathfrak{Im}\left[p_nQ_{n,k}-q_{2n,k}\right]\right)_i}{\sum_{i=1}^{N}\left(m_pS_{1,1}-s_{1,1}\right)_i}, \qquad \text{(D.21)}
\end{aligned}$$

Eqs. (D.19) generalize into:

$$\begin{aligned}
\langle\langle\cos n(\psi_1+\phi_2-\phi_3)\rangle\rangle &= \left\{\sum_{i=1}^{N}\left(\mathfrak{Re}\left[p_n\left(|Q_{n,1}|^2-S_{1,2}\right)\right]\right.\right. \\
&\left.\left.-\mathfrak{Re}\left[q_{2n,1}Q_{n,1}^{*}+s_{1,1}Q_{n,1}-2q_{n,2}\right]\right)_i\right\}\times \\
&\left\{\sum_{i=1}^{N}\left(m_p(S_{2,1}-S_{1,2})-2\cdot(s_{1,1}S_{1,1}-s_{1,2})\right)_i\right\}^{-1}, \\
\langle\langle\sin n(\psi_1+\phi_2-\phi_3)\rangle\rangle &= \left\{\sum_{i=1}^{N}\left(\mathfrak{Im}\left[p_n\left(|Q_{n,1}|^2-S_{1,2}\right)\right]\right.\right. \\
&\left.\left.-\mathfrak{Im}\left[q_{2n,1}Q_{n,1}^{*}+s_{1,1}Q_{n,1}-2q_{n,2}\right]\right)_i\right\}\times \\
&\left\{\sum_{i=1}^{N}\left(m_p(S_{2,1}-S_{1,2})-2\cdot(s_{1,1}S_{1,1}-s_{1,2})\right)_i\right\}^{-1},
\end{aligned} \tag{D.22}$$

and finally, Eqs. (D.20) generalize into:

$$\begin{aligned}
\langle\langle\cos n(\psi_1-\phi_2-\phi_3)\rangle\rangle &= \left\{\sum_{i=1}^{N}\left(\mathfrak{Re}\left[p_n\left(Q_{n,1}^{*}Q_{n,1}^{*}-Q_{2n,2}^{*}\right)\right]\right.\right. \\
&\left.\left.-2\cdot\mathfrak{Re}\left[s_{1,1}Q_{n,1}^{*}-q_{n,2}^{*}\right]\right)_i\right\}\times \\
&\left\{\sum_{i=1}^{N}\left(m_p(S_{2,1}-S_{1,2})-2\cdot(s_{1,1}S_{1,1}-s_{1,2})\right)_i\right\}^{-1}, \\
\langle\langle\sin n(\psi_1-\phi_2-\phi_3)\rangle\rangle &= \left\{\sum_{i=1}^{N}\left(\mathfrak{Im}\left[p_n\left(Q_{n,1}^{*}Q_{n,1}^{*}-Q_{2n,2}^{*}\right)\right]\right.\right. \\
&\left.\left.-2\cdot\mathfrak{Im}\left[s_{1,1}Q_{n,1}^{*}-q_{n,2}^{*}\right]\right)_i\right\}\times \\
&\left\{\sum_{i=1}^{N}\left(m_p(S_{2,1}-S_{1,2})-2\cdot(s_{1,1}S_{1,1}-s_{1,2})\right)_i\right\}^{-1}.
\end{aligned} \tag{D.23}$$

D.1 Example: Correcting with generalized cumulants for the bias coming from non-uniform acceptance

In this example we sample particles from the Fourier-like azimuthal distribution characterized with p_t dependent harmonic v_2, namely:

$$v_2(p_t)=\begin{cases}0.1\,p_t & p_t<2.0\ \text{GeV}\,,\\ 0.2 & p_t\geq 2.0\ \text{GeV}\,.\end{cases} \tag{D.24}$$

The usage of generalized cumulants outlined in this appendix is illustrated for a detector with two problematic sectors which do not accept tracks going in $60^{\rm o} \leq \phi < 100^{\rm o}$ and also in $270^{\rm o} \leq \phi < 330^{\rm o}$. All particles with azimuthal angles out of these two ranges are accepted without any loss. This is a more extreme case than the one considered in B.1.1 for the usage of ϕ-weights, because here we allow for real holes in the detector acceptance, for which ϕ-weights cannot be constructed.

When generalized cumulants are being used there is no need for a dedicated run over the data to correct for the acceptance effects as in the case of the usage of ϕ-weights—the correction for non-uniform acceptance can be applied automatically in the same run. For the specific example we consider here, the resulting acceptance histogram is presented in Fig. D.1. In Fig. D.2 the estimates for reference flow harmonics are presented. In

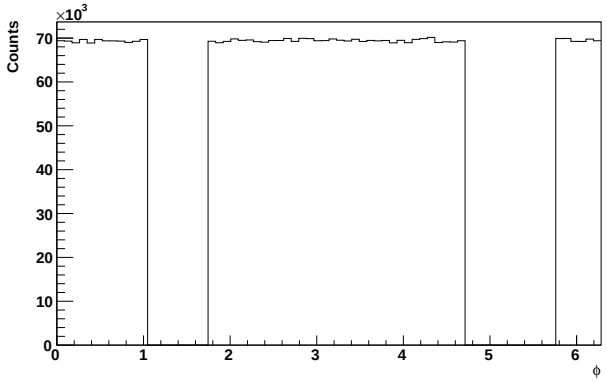

Figure D.1: Azimuthal profile of a detector which do not accepts tracks going in $60^{\rm o} \leq \phi < 100^{\rm o}$ and in $270^{\rm o} \leq \phi < 330^{\rm o}$.

Figs. D.3 and D.4 the estimates for differential flow harmonics are presented from $2^{\rm nd}$ and $4^{\rm th}$ order differential cumulant, respectively. In all figures estimates obtained with cumulants built up only from isotropic terms and applicable only for the case of uniform acceptance are shown with open markers, while the estimates obtained with the generalized cumulants containing also the non-isotropic terms are shown with full markers. The shaded band in each figure was obtained after joining the ends of statistical errors of true Monte Carlo flow estimates. Clearly, in each case the generalized cumulants presented in this section can correct for the systematic bias coming from the non-uniform acceptance of the detector.

In this Appendix we have illustrated that only the generalized cumulants can deal with the systematic bias coming from the non-uniform azimuthal acceptance of a detector.

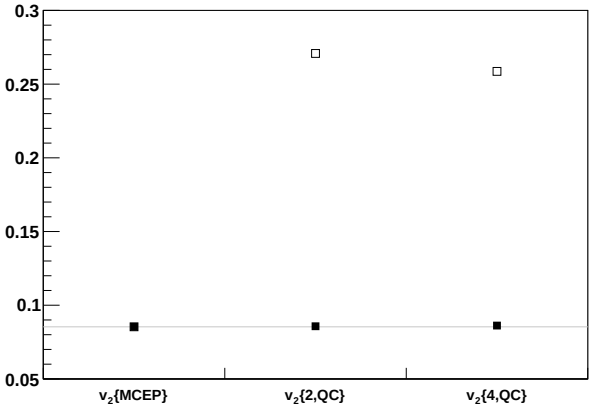

Figure D.2: Estimates for reference flow harmonics for a detector whose acceptance histogram is presented in Fig. D.1. In the first bin is shown the true Monte Carlo flow estimate. In second and third bin with open markers are estimates obtained with cumulants consisting only of isotropic terms (see Eqs. (3.35) and (3.38)), and with closed markers the reference flow estimates obtained with generalized cumulants (see Eqs. (D.2) and (D.7)).

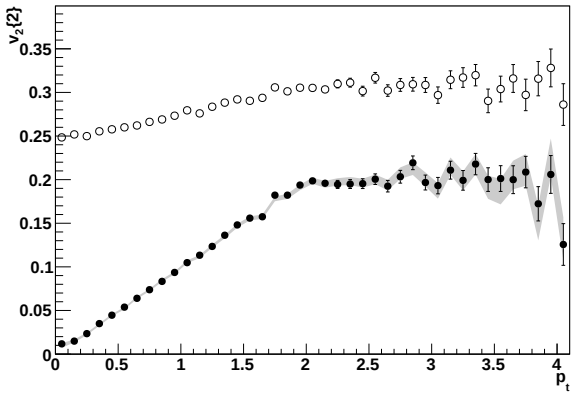

Figure D.3: Estimates for differential flow harmonics from 2^{nd} order differential cumulant for detector whose acceptance histogram is presented in Fig. D.1. The shaded band was obtained after joining the ends of error bars of true Monte Carlo flow estimates for each p_t bin. With open markers are estimates obtained with differential 2-particle cumulants consisting only of isotropic terms (see Eq. (3.67)) and with closed markers the differential flow estimates obtained with generalized differential 2-particle cumulants (see Eq. (D.14)).

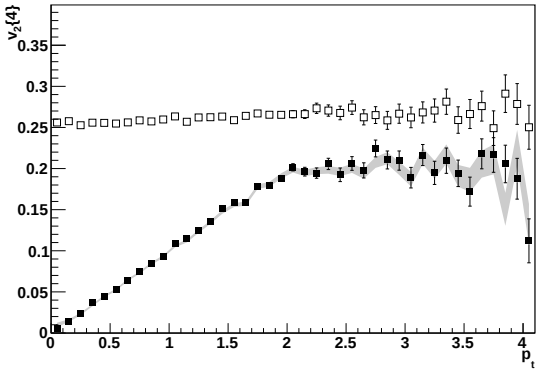

Figure D.4: Estimates for differential flow harmonics from 4^{th} order differential cumulant for detector whose acceptance histogram is presented in Fig. D.1. The shaded band was obtained after joining the ends of error bars of Monte Carlo flow estimates for each p_t bin. With open markers are estimates obtained with differential 4-particle cumulants consisting only of isotropic terms (see Eq. (3.71)) and with closed markers the differential flow estimates obtained with generalized differential 4-particle cumulants (see Eq. (D.17)).

Appendix E

Toy model

The purpose of this appendix is to derive the analytic equations for 2- and 4-particle Q-cumulants in a simple toy model in which, besides existing flow correlations, the strong nonflow correlations are being introduced by taking each particle k times in the analysis.

E.1 Brief summary

To make the exposure in this appendix self-contained we briefly review the main definitions and results needed. The Q-vector evaluated in the harmonic n is a complex quantity denoted by Q_n and is defined as

$$Q_n \equiv \sum_{i=1}^{M} e^{in\phi_i} \,. \tag{E.1}$$

It is possible to express analytically 2-, 3-, 4-, etc, particle azimuthal correlations in terms of Q-vectors evaluated (in general) in different harmonics. In particular:

$$\begin{aligned}
\langle 2 \rangle &\equiv \langle \exp\left[in(\phi_1 - \phi_2)\right] \rangle \,, \quad \phi_1 \neq \phi_2 \\
&= \frac{|Q_n|^2 - M}{M(M-1)} \,, \qquad \text{(E.2)} \\
\langle 3 \rangle &\equiv \langle \exp\left[in(2\phi_1 - \phi_2 - \phi_3)\right] \rangle \,, \quad \phi_1 \neq \phi_2 \neq \phi_3 \\
&= \frac{\mathfrak{Re}\left[Q_{2n}Q_n^*Q_n^*\right] - 2 \cdot |Q_n|^2 - |Q_{2n}|^2 + 2M}{M(M-1)(M-2)} \,, \qquad \text{(E.3)} \\
\langle 4 \rangle &\equiv \langle \exp\left[in(\phi_1 + \phi_2 - \phi_3 - \phi_4)\right] \rangle \,, \quad \phi_1 \neq \phi_2 \neq \phi_3 \neq \phi_4 \\
&= \frac{|Q_n|^4 + |Q_{2n}|^2 - 2 \cdot \mathfrak{Re}\left[Q_{2n}Q_n^*Q_n^*\right]}{M(M-1)(M-2)(M-3)} \\
&- 2\,\frac{2(M-2) \cdot |Q_n|^2 - M(M-3)}{M(M-1)(M-2)(M-3)} \,. \qquad \text{(E.4)}
\end{aligned}$$

Two- and multi-particle azimuthal correlations are being used in the anisotropic flow analysis because they are sensitive to flow harmonics. In the ideal case when only flow correlations are present in the system we have:

$$\begin{aligned} \langle 2 \rangle &= v_n^2 \,, \\ \langle 3 \rangle &= v_{2n} v_n^2 \,, \\ \langle 4 \rangle &= v_n^4 \,. \end{aligned} \tag{E.5}$$

Assuming that statistical flow fluctuations are negligible, we have the following results for the Q-cumulants:

$$QC\{2\} \equiv \langle\langle 2 \rangle\rangle = v_n^2 \,, \tag{E.6}$$

$$QC\{3\} \equiv \langle\langle 3 \rangle\rangle = v_{2n} v_n^2 \,, \tag{E.7}$$

$$QC\{4\} \equiv \langle\langle 4 \rangle\rangle - 2 \cdot \langle\langle 2 \rangle\rangle^2 = -v_n^4 \,. \tag{E.8}$$

In above equations $\langle \cdot \rangle$ denote a single-event average, while $\langle\langle \cdot \rangle\rangle$ denotes an all-event average. In this appendix we will derive a generalization of the idealistic results (E.6-E.8), which are applicable when only flow correlations are present, for the more general case in which strong nonflow correlations are being introduced by taking each particle k times in the analysis. But first we derive few useful results for the simplest example of a random walk, in which both flow and nonflow correlations are absent.

E.2 Random walk

For a random walk both flow and nonflow correlations are absent and we have simply from Eqs. (E.5)

$$\langle 2 \rangle = \langle 3 \rangle = \langle 4 \rangle = 0 \,. \tag{E.9}$$

This result allows us to inspect straightforwardly how various expressions involving Q-vectors depend on multiplicity M for the case of a random walk. From Eq. (E.2) and from $\langle 2 \rangle = 0$ one can easily deduce that

$$|Q_n|^2 = M \,, \tag{E.10}$$

which is valid irrespectively of the harmonic for which Q-vector is being evaluated. Result (E.10) is actually the analogy of the famous result for the distance from the origin of a random walk. Namely, when particle azimuthal angles are sampled randomly the Q-vector from the definition (E.1) is nothing but the sum of random unit steps in a complex plane, for which it is known that the distance from the origin grows as a $\sqrt{\text{number of steps}}$. In the context of Eq. (E.10) a "new step" is being performed by adding a new particle to the Q-vector, hence total number of steps is nothing but multiplicity M and the "distance from origin" is nothing but $|Q_n|$.

On the other hand, from Eq. (E.3) and from $\langle 3 \rangle = 0$ it follows that

$$\mathfrak{Re}\left[Q_{2n} Q_n^* Q_n^*\right] - 2 \cdot |Q_n|^2 - |Q_{2n}|^2 + 2M = 0 \,. \tag{E.11}$$

Taking into account the result (E.10), valid both for $|Q_n|$ and $|Q_{2n}|$, we have

$$\mathfrak{Re}\left[Q_{2n}Q_n^*Q_n^*\right] - 2M - M + 2M = 0\,, \tag{E.12}$$

which gives the following result:

$$\mathfrak{Re}\left[Q_{2n}Q_n^*Q_n^*\right] = M\,. \tag{E.13}$$

Finally, from Eq. (E.4) and from $\langle 4\rangle = 0$ it follows that

$$|Q_n|^4 + |Q_{2n}|^2 - 2\cdot\mathfrak{Re}\left[Q_{2n}Q_n^*Q_n^*\right] - 4(M-2)|Q_n|^2 + 2M(M-3) = 0\,. \tag{E.14}$$

After plugging into this equation the results (E.10) and (E.13) it follows:

$$|Q_n|^4 + M - 2M - 4(M-2)M + 2M(M-3) = 0\,, \tag{E.15}$$

which yields

$$|Q_n|^4 = M(2M-1)\,. \tag{E.16}$$

These results will be used in the subsequent sections.

E.3 Track splitting

In this section we will derive the analytic equations for 2- and multi-particle azimuthal correlations and cumulants for the case in which each track sampled randomly was taken k times in the analysis. Clearly, the equations derived for random walker in previous section are not applicable if $k > 1$. Although at first sight it might look artificial, this example can actually correspond to a realistic scenario in which due to detector inefficiencies each track gets split k times during reconstruction. For simplicity sake in this section we do not yet add flow correlations—they will be added in sections which follow.

If we start with the original sample of M particles in an event and take each particle k times in the analysis, then the new total multiplicity and Q-vector are related to the original ones as

$$\begin{aligned} M_{\mathrm{tot}} &= k\cdot M\,, \\ Q_{n,\mathrm{tot}} &= k\cdot Q_n\,. \end{aligned} \tag{E.17}$$

For a newly created sample consisting of $k\cdot M$ tracks in an event we have by making use of (E.2):

$$\begin{aligned} \langle 2\rangle &= \frac{|k\cdot Q_n|^2 - kM}{kM(kM-1)} \\ &= \frac{k^2|Q_n|^2 - kM}{kM(kM-1)} \\ &= \frac{k^2M - kM}{kM(kM-1)} \\ &= \frac{k-1}{kM-1}\,, \end{aligned} \tag{E.18}$$

where in the 3$^{\text{rd}}$ line we have inserted result (E.10) for $|Q_n|^2$. We remark that (E.10), although derived for a random walk, can be inserted here because Q_n corresponds to the original sample of M tracks in which all tracks were sampled randomly and each track was taken in the analysis once. Clearly, the expression (E.18) gives nonzero value for any $k > 1$, quantifying in turn the nonflow 2-particle correlations we have introduced by taking each particle k times in the analysis.

When it comes to 3-particle azimuthal correlation we have obtained the following result:

$$\begin{aligned}\langle 3\rangle &= \frac{k^3\mathfrak{Re}\left[Q_{2n}Q_n^*Q_n^*\right] - 2k^2|Q_n|^2 - k^2|Q_{2n}|^2 + 2kM}{kM(kM-1)(kM-2)} \\ &= \frac{k^3M - 2k^2M - k^2M + 2kM}{kM(kM-1)(kM-2)} \\ &= \frac{(k-1)(k-2)}{(kM-1)(kM-2)}\,. \end{aligned} \tag{E.19}$$

It is noteworthy to observe that for both $k = 1$ and $k = 2$ this expression is identically 0, which indicates that from the 3-particle correlation's point of view the random walk example and the example with doubled tracks are equivalent.

Analogously, for 4-particle azimuthal correlation we have obtained

$$\langle 4\rangle = \frac{k^3(2M-1) - 2k^2(2M+1) + k(2M+9) - 6}{(kM-1)(kM-2)(kM-3)}\,. \tag{E.20}$$

This expression vanishes for $k = 1$, when this example reduces to a random walk, but unlike 3-particle correlation it does not vanish for $k = 2$, indicating the sensitivity of 4-particle azimuthal correlation to pair-wise correlations in the system.

Equations (E.18) and (E.20) implies the following results for 2- and 4-particle cumulants:

$$QC\{2\} \equiv \langle\langle 2\rangle\rangle = \frac{k-1}{kM-1}\,, \tag{E.21}$$

$$\begin{aligned} QC\{4\} &\equiv \langle\langle 4\rangle\rangle - 2\cdot\langle\langle 2\rangle\rangle^2 \\ &= -\frac{(k-1)\left[k^3M - k^2(5M+1) + k(2M+9) - 6\right]}{(kM-1)^2(kM-2)(kM-3)}\,. \end{aligned} \tag{E.22}$$

In reality we deal with a total multiplicity $M_{\text{tot}} = k \cdot M$ and we do not know k, the number of times the track has split during reconstruction, for instance. It is thus more convenient to express Eqs. (E.21) and (E.22) in terms of M_{tot}:

$$QC\{2\} = \frac{k-1}{M_{\text{tot}}-1}\,, \tag{E.23}$$

$$QC\{4\} = -\frac{(k-1)\left[k^2(M_{\text{tot}}-1) - k(5M_{\text{tot}}-9) + 2(M_{\text{tot}}-3)\right]}{(M_{\text{tot}}-1)^2(M_{\text{tot}}-2)(M_{\text{tot}}-3)}\,. \tag{E.24}$$

Eqs. (E.23) and (E.24) were cross-checked with a simple Monte Carlo study for $k = 2, 3, 4$ and the results are presented in Fig. E.1. We see clearly that the 4-particle

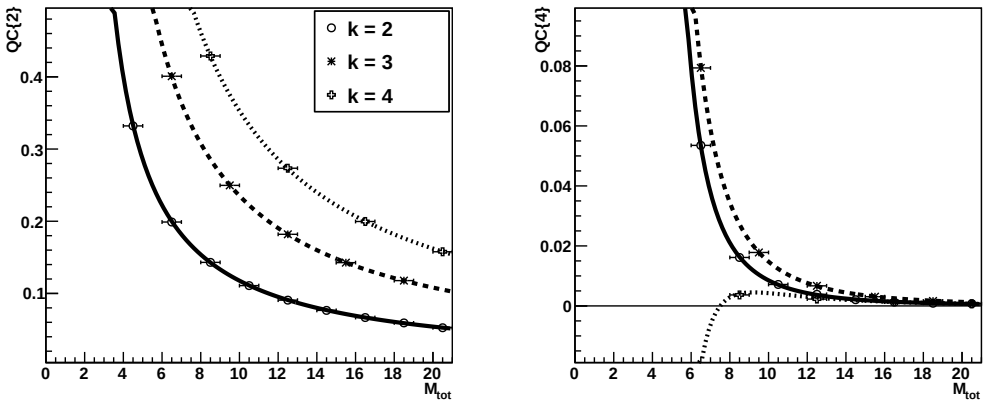

Figure E.1: Lines represent theoretical results Eqs. (E.23) and (E.24) and markers are actual measurements for three independent examples in which tracks were sampled randomly and each track was taken k times ($k = 2, 3, 4$) in the analysis.

cumulant suppresses much faster the contribution from k-particle nonflow correlations as the multiplicity increases than the 2-particle cumulant.

It is interesting to investigate what is the leading contribution to $QC\{2\}$ and $QC\{4\}$ in the limit of large M_{tot}, the regime characteristic for heavy-ion collisions. In this limit we have obtained the following results:

$$QC\{2\} \simeq \frac{k-1}{M_{\mathrm{tot}}}\,, \tag{E.25}$$

$$QC\{4\} \simeq -\frac{(k-1)(k^2-5k+2)}{M_{\mathrm{tot}}^3}\,. \tag{E.26}$$

The contribution of a flow correlation to $QC\{2\}$ comes always with a positive sign (see Eq. (E.6)), meaning that for each k we can misinterpret the nonflow contribution from split tracks, quantified in (E.25), as a flow correlation. On the other hand, since the contribution of a flow correlation to $QC\{4\}$ comes always with a negative sign (see Eq. (E.8)), the first k which gives $QC\{4\}$ with negative sign, that might be misinterpreted as flow in this model, is $k = 5$, namely $QC\{4\} \simeq -8/M_{\mathrm{tot}}^3$. For the cases which correspond close to reality when it comes to the track splitting ($k < 5$), we see that $QC\{2\}$ cannot even in principle distinguish nonflow from flow correlations, while $QC\{4\}$ can be safely used in a sense that it cannot misinterpret the dominant nonflow contribution in this toy example as flow.

In the next section we will generalize the model and allow for the presence of flow correlations due to a single flow harmonic v_n.

E.4 Monochromatic flow and track splitting

In this section we provide the analytic equations which quantify the contributions to 2- and 4-particle cumulants coming from the presence of a single flow harmonic v_n in the system, and simultaneously coming from the nonflow correlations originating from the fact that each particle has been taken k times in the analysis. We start again with the original sample consisting of M particles. Due to the non-vanishing harmonic v_n we have the following results:

$$\langle 2 \rangle = \frac{|Q_n|^2 - M}{M(M-1)} = v_n^2 \,, \tag{E.27}$$

$$\langle 2 \rangle_{2n|2n} = \frac{|Q_{2n}|^2 - M}{M(M-1)} = v_{2n}^2 \,, \tag{E.28}$$

$$\langle 3 \rangle = \frac{\Re\mathfrak{e}\left[Q_{2n}Q_n^*Q_n^*\right] - 2\cdot|Q_n|^2 - |Q_{2n}|^2 + 2M}{M(M-1)(M-2)} = v_{2n}v_n^2 \,, \tag{E.29}$$

$$\begin{aligned} \langle 4 \rangle &= \frac{|Q_n|^4 + |Q_{2n}|^2 - 2\cdot\Re\mathfrak{e}\left[Q_{2n}Q_n^*Q_n^*\right]}{M(M-1)(M-2)(M-3)} \\ &- 2\,\frac{2(M-2)\cdot|Q_n|^2 - M(M-3)}{M(M-1)(M-2)(M-3)} = v_n^4 \,. \end{aligned} \tag{E.30}$$

From the first equation above we can read off the result for the modulus of the Q-vector for the case of a single non-vanishing flow harmonic v_n:

$$|Q_n|^2 = M\left[v_n^2(M-1)+1\right] \,. \tag{E.31}$$

Since we are dealing with monochromatic flow in this section we have $v_{2n} = 0$ and Eq. (E.28) gives simply

$$|Q_{2n}|^2 = M \,, \tag{E.32}$$

i.e. the modulus of the Q-vector evaluated in the harmonic $2n$ is not affected by the presence of v_n. Insertion of (E.31) and (E.32) into (E.29) (taking into account that in this example $v_{2n} = 0$) yields the result:

$$\Re\mathfrak{e}\left[Q_{2n}Q_n^*Q_n^*\right] = M\left[2v_n^2(M-1)+1\right] \,. \tag{E.33}$$

Finally, after inserting (E.31), (E.32) and (E.33) into (E.30) we have obtained the following result:

$$\begin{aligned} |Q_n|^4 &= M(M-1)(M-2)(M-3)v_n^4 \\ &+ 4M(M-1)^2v_n^2 + M(2M-1) \,. \end{aligned} \tag{E.34}$$

The above relations show how various expressions involving Q-vectors depend on monochromatic flow v_n and multiplicity M.

Now let each sampled particle in the analysis be taken k times. Eqs. (E.17) still applies and we have:

$$\begin{aligned}\langle 2\rangle &= \frac{|k\cdot Q_n|^2 - kM}{kM(kM-1)} \\ &= \frac{k^2|Q_n|^2 - kM}{kM(kM-1)} \\ &= \frac{k^2M\left[v_n^2(M-1)+1\right] - kM}{kM(kM-1)} \\ &= \frac{v_n^2k(M-1)+k-1}{kM-1}\,, \end{aligned} \tag{E.35}$$

where in the 3$^{\rm rd}$ line we have inserted (E.31). Analogously, by taking into account (E.31), (E.32) and (E.33), for 3-particle correlation it follows that

$$\begin{aligned}\langle 3\rangle &= \frac{k^3\mathfrak{Re}\left[Q_{2n}Q_n^*Q_n^*\right] - 2\cdot k^2\left|Q_n\right|^2 - k^2\left|Q_{2n}\right|^2 + 2kM}{kM(kM-1)(kM-2)} \\ &= \frac{k^2\left[2v_n^2(M-1)+1\right] - 2k\left[v_n^2(M-1)+1\right] - k + 2}{(kM-1)(kM-2)} \\ &= (k-1)\frac{v_n^2\cdot 2k(M-1)+k-2}{(kM-1)(kM-2)}\,, \end{aligned} \tag{E.36}$$

and finally by following the same procedure for 4-particle correlations we have obtained:

$$\begin{aligned}\langle 4\rangle &= \Big\{v_n^4\left[k^3(M-1)(M-2)(M-3)\right] \\ &\quad + v_n^2\cdot 4k(k-1)(M-1)\left[k(M-1)-2\right] \\ &\quad + (k-1)\left[k^2(2M-1) - k(2M+3) + 6\right]\Big\}\times \\ &\quad \Big\{(kM-1)(kM-2)(kM-3)\Big\}^{-1}\,. \end{aligned} \tag{E.37}$$

Having obtained analytic equations for 2- and 4-particle correlations we can now write also analytic expressions for 2- and 4-particle cumulants:

$$QC\{2\} = \frac{v_n^2k(M-1)+k-1}{kM-1}\,, \tag{E.38}$$

$$\begin{aligned}QC\{4\} &= -\Big\{v^4k^2(M-1)\left[k^2M(M^2+3M-6) - k(9M^2-5M-6) + 12(M-1)\right] \\ &\quad + v^2\cdot 4k(k-1)(M-1)\left[k^2M - k(2M+1) + 4\right] \\ &\quad + (k-1)\left[k^3M - k^2(5M+1) + k(2M+9) - 6\right]\Big\}\times \\ &\quad \Big\{(kM-1)^2(kM-2)(kM-3)\Big\}^{-1}\,. \end{aligned} \tag{E.39}$$

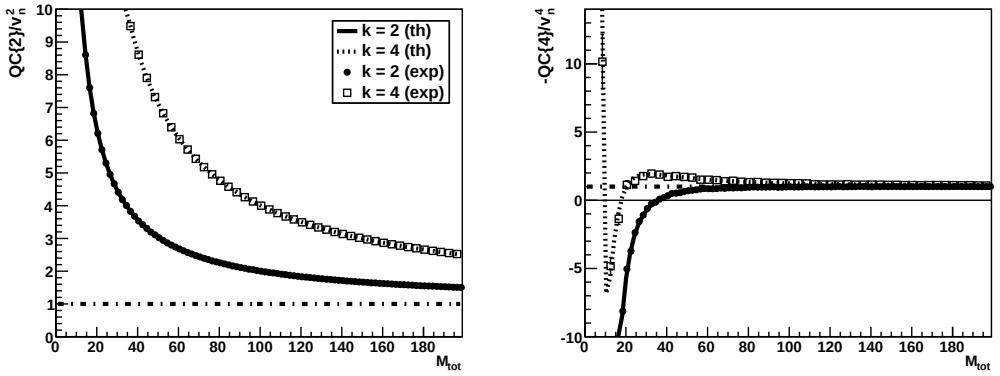

Figure E.2: Lines represent theoretical results Eqs. (E.40) and (E.41) rescaled with v_n^2 and $-v_n^4$, respectively, and markers represent the corresponding measurements for two independent Monte Carlo examples in which tracks were sampled from a Fourier-like p.d.f. parameterized with harmonic $v_2 = 0.1$, and each track was taken two times (solid lines and filled markers) and four times (dashed lines and open markers) in the analysis.

Rewritten in terms of $M_{\rm tot} = k \cdot M$ these equations turn into:

$$QC\{2\} = \frac{v_n^2(M_{\rm tot}-k)+k-1}{M_{\rm tot}-1}\,, \tag{E.40}$$

$$\begin{aligned} QC\{4\} &= -\Big\{ v_n^4(M_{\rm tot}-k) \\ &\times \left[6k^2(1-M_{\rm tot})+k(3M_{\rm tot}^2+5M_{\rm tot}-12)+M_{\rm tot}(M_{\rm tot}^2-9M_{\rm tot}+12)\right] \\ &+ v_n^2\cdot 4(k-1)(M_{\rm tot}-k)\left[k(M_{\rm tot}-1)-2(M_{\rm tot}-2)\right] \\ &+ (k-1)\left[k^2(M_{\rm tot}-1)-k(5M_{\rm tot}-9)+2(M_{\rm tot}-3)\right]\Big\}\times \\ &\Big\{(M_{\rm tot}-1)^2(M_{\rm tot}-2)(M_{\rm tot}-3)\Big\}^{-1}\,. \end{aligned} \tag{E.41}$$

The results (E.40) and (E.41) were cross-checked with a simple Monte Carlo study for $k = 2, 3, 4, 5$ and are presented on Figs. E.2 and E.3. Both figures clearly indicate that the 4-particle cumulant suppresses much faster the k-particle nonflow contribution when compared to 2-particle cumulant as the multiplicity is increased and we are entering the heavy-ion regime.

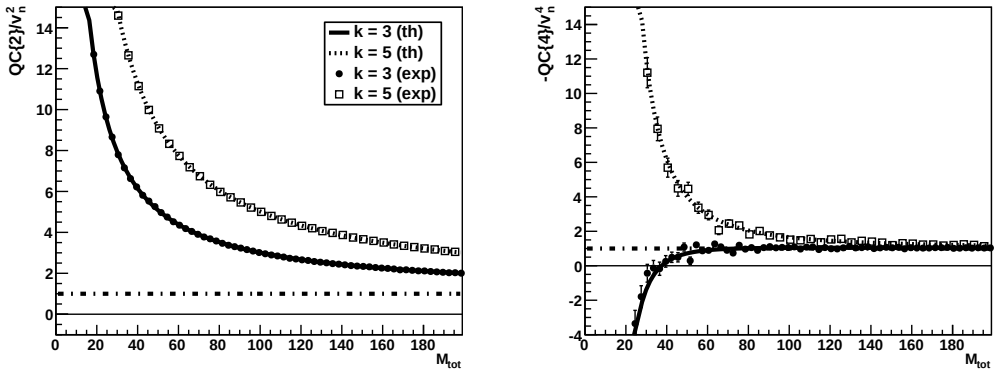

Figure E.3: Lines represent theoretical results Eqs. (E.40) and (E.41) rescaled with v_n^2 and $-v_n^4$, respectively, and markers represent the corresponding measurements for two independent Monte Carlo examples in which tracks were sampled from Fourier-like p.d.f. parameterized with harmonic $v_2 = 0.1$, and each track was taken three times (solid lines and filled markers) and five times (dashed lines and open markers) in the analysis.

Again we investigate the limit of large M_{tot} ($M_{\mathrm{tot}} \gg k$). It follows:

$$QC\{2\} \simeq v_n^2 + \frac{k-1}{M_{\mathrm{tot}}}\,, \tag{E.42}$$

$$QC\{4\} \simeq -v_n^4 - v_n^2 \cdot \frac{4(k-1)(k-2)}{M_{\mathrm{tot}}^2} - \frac{(k-1)(k^2-5k+2)}{M_{\mathrm{tot}}^3}\,. \tag{E.43}$$

We see that in this limit $QC\{2\}$ has two distinct independent contributions, one from flow and a second one from nonflow. However, $QC\{4\}$ has an additional contribution which couples flow and nonflow (middle term, usually in the literature referred to as "flowing clusters"), which complicates the interpretation of the results in the cumulant analysis. The distinct feature both in $QC\{2\}$ and $QC\{4\}$ is that the genuine flow contribution is not scaled with some power of the multiplicity, meaning that in a physical system characterized by large multiplicity (e.g. heavy-ion collisions) only the terms which contain contribution from nonflow correlations will be diluted and suppressed.

E.5 Bichromatic flow and track splitting

In this section we quantify the contribution to $QC\{2\}$ and $QC\{4\}$ coming from the bichromatic flow correlations which originate from the presence of two flow harmonics, namely v_n and v_{2n}, and from the nonflow correlations originating from the k times split tracks. As in the previous section we first outline how various expressions involving Q-vectors behave in the *original* sample of M tracks in the presence of two flow harmonics

v_n and v_{2n}. We have obtained:

$$\begin{aligned}
|Q_n|^2 &= M\left[v_n^2(M-1)+1\right], \\
|Q_{2n}|^2 &= M\left[v_{2n}^2(M-1)+1\right], \\
\mathfrak{Re}\left[Q_{2n}Q_n^*Q_n^*\right] &= 2M(M-1)v_n^2 + M(M-1)(M-2)v_n^2 v_{2n} \\
&+ M(M-1)v_{2n}^2 + M, \\
|Q_n|^4 &= v_n^4 \cdot M(M-1)(M-2)(M-3) + v_n^2 \cdot 4M(M-1)^2 \\
&+ v_{2n}^2 \cdot M(M-1) + v_n^2 v_{2n} \cdot 2M(M-1)(M-2) \\
&+ M(2M-1). \qquad \text{(E.44)}
\end{aligned}$$

These results give rise to the following results for correlations in the resulting sample consisting of k times split tracks:

$$\langle 2\rangle = \frac{v_n^2 k(M-1)+k-1}{kM-1}, \qquad \text{(E.45)}$$

$$\langle 2\rangle_{2n|2n} = \frac{v_{2n}^2 k(M-1)+k-1}{kM-1}, \qquad \text{(E.46)}$$

$$\begin{aligned}
\langle 3\rangle &= \frac{v_n^2 \cdot 2k(k-1)(M-1) + v_n^2 v_{2n} \cdot k^2(M-1)(M-2)}{(kM-1)(kM-2)} \\
&+ \frac{v_{2n}^2 \cdot k(k-1)(M-1) + (k-1)(k-2)}{(kM-1)(kM-2)}, \qquad \text{(E.47)}
\end{aligned}$$

$$\begin{aligned}
\langle 4\rangle &= \frac{v_n^4 \cdot k^3(M-1)(M-2)(M-3) + v_n^2 \cdot 4k(k-1)(M-1)\left[k(M-1)-2\right]}{(kM-1)(kM-2)(kM-3)} \\
&+ \frac{v_n^2 v_{2n} \cdot 2k^2(k-1)(M-1)(M-2) + v_{2n}^2 \cdot k(k-1)^2(M-1)}{(kM-1)(kM-2)(kM-3)} \\
&+ \frac{(k-1)\left[2kM(k-1)+6-3k-k^2\right]}{(kM-1)(kM-2)(kM-3)}. \qquad \text{(E.48)}
\end{aligned}$$

Results for $QC\{2\}$ and $QC\{3\}$ are the same as results for $\langle 2\rangle$ and $\langle 3\rangle$ presented above, whilst the result for $QC\{4\}$ reads:

$$\begin{aligned}
QC\{4\} &= \Big\{ -v_n^4 \cdot k^2(M-1)(-12+6k+12M+5kM-6k^2M-9kM^2+3k^2M^2+k^2M^3) \\
&- v_n^2 \cdot 4(k-1)(4-k-2kM+k^2M) + v_{2n}^4 \cdot (k-1)^2(kM-1) \\
&+ v_n^2 v_{2n} \cdot 2k(k-1)(M-2)(kM-1) \\
&- (k-1)(-6+9k-k^2+2kM-5k^2M+k^3M) \Big\} \\
&\times \Big\{ (kM-1)^2(kM-2)(kM-3) \Big\}^{-1}. \qquad \text{(E.49)}
\end{aligned}$$

We rewrite our results for Q-cumulants in terms of total multiplicity $M_{\rm tot} = k \cdot M$ of resulting sample:

$$QC\{2\} = \frac{v_n^2(M_{\rm tot}-k)+k-1}{M_{\rm tot}-1}\,, \tag{E.50}$$

$$\begin{aligned} QC\{3\} &= \frac{v_n^2(M_{\rm tot}-k)\left[2(k-1)+v_{2n}(M_{\rm tot}-2k)\right]}{(M_{\rm tot}-1)(M_{\rm tot}-2)} \\ &+ \frac{(k-1)\left[v_{2n}^2(M_{\rm tot}-k)+k-2\right]}{(M_{\rm tot}-1)(M_{\rm tot}-2)}\,, \end{aligned} \tag{E.51}$$

$$\begin{aligned} QC\{4\} &= -\Big\{ v_n^4 \cdot (M_{\rm tot}-k) \\ &\times \left[6k^2(1-M_{\rm tot})+k(3M_{\rm tot}^2+5M_{\rm tot}-12)+M_{\rm tot}(M_{\rm tot}^2-9M_{\rm tot}+12)\right] \\ &+ v_n^2 \cdot 4(k-1)(M_{\rm tot}-k)\left[k(M_{\rm tot}-1)-2(M_{\rm tot}-2)\right] \\ &- v_n^2 v_{2n} \cdot 2(M_{\rm tot}-1)(k-1)(M_{\rm tot}-k)(M_{\rm tot}-2k) \\ &- v_{2n}^2 \cdot (k-1)^2(M_{\rm tot}-1)(M_{\rm tot}-k) \\ &+ (k-1)\left[k^2(M_{\rm tot}-1)-k(5M_{\rm tot}-9)+2(M_{\rm tot}-3)\right] \Big\} \\ &\times \Big\{ (M_{\rm tot}-1)^2(M_{\rm tot}-2)(M_{\rm tot}-3) \Big\}^{-1}\,. \end{aligned} \tag{E.52}$$

The above results were cross-checked with a simple Monte Carlo study for $k = 2, 3, 4, 5$ and are presented in Figs. E.4 and E.5. Again, both figures clearly indicate that the 4-particle cumulant suppresses much faster the k-particle nonflow contribution when compared to the 2-particle cumulant as multiplicity is increased.

Finally, in the limit of large $M_{\rm tot} \gg k$ to leading order we have:

$$QC\{2\} \simeq v_n^2 + \frac{k-1}{M_{\rm tot}}\,, \tag{E.53}$$

$$QC\{3\} \simeq v_n^2 v_{2n} + v_n^2 \cdot \frac{2(k-1)}{M_{\rm tot}} + v_{2n}^2 \cdot \frac{k-1}{M_{\rm tot}^2} + \frac{(k-1)(k-2)}{M_{\rm tot}^2}\,, \tag{E.54}$$

$$\begin{aligned} QC\{4\} &\simeq -v_n^4 - v_n^2 \cdot \frac{4(k-1)(k-2)}{M_{\rm tot}^2} + v_n^2 v_{2n} \cdot \frac{2(k-1)}{M_{\rm tot}} \\ &+ v_{2n}^2 \cdot \frac{(k-1)^2}{M_{\rm tot}^2} - \frac{(k-1)(k^2-5k+2)}{M_{\rm tot}^3}\,. \end{aligned} \tag{E.55}$$

We see again that only the terms having contribution from nonflow correlations are being suppressed and diluted with some power of the multiplicity, making them subdominant in a system with large multiplicity.

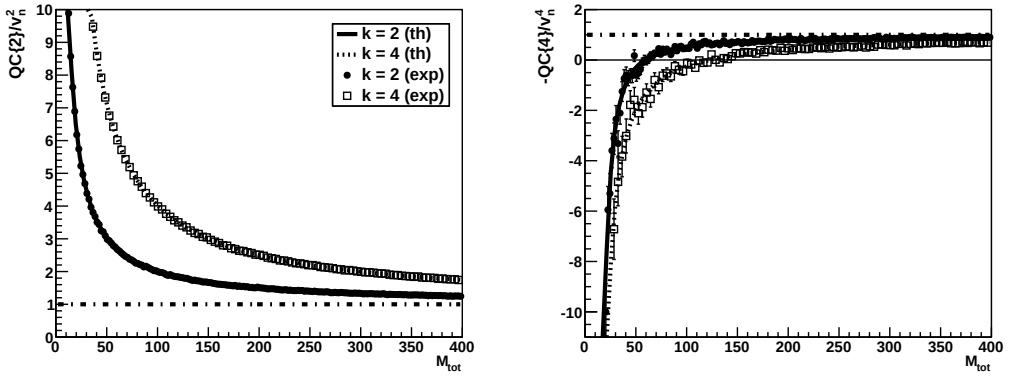

Figure E.4: Lines represent theoretical results Eqs. (E.50) and (E.52) rescaled with v_n^2 and $-v_n^4$, respectively, and markers represent the corresponding measurements for two independent Monte Carlo runs in which tracks were sampled from a Fourier-like p.d.f. parameterized with harmonics $v_2 = 0.1$ and $v_4 = 0.2$, and each track was taken two times (solid lines and filled markers) and four times (dashed line and open markers) in the analysis.

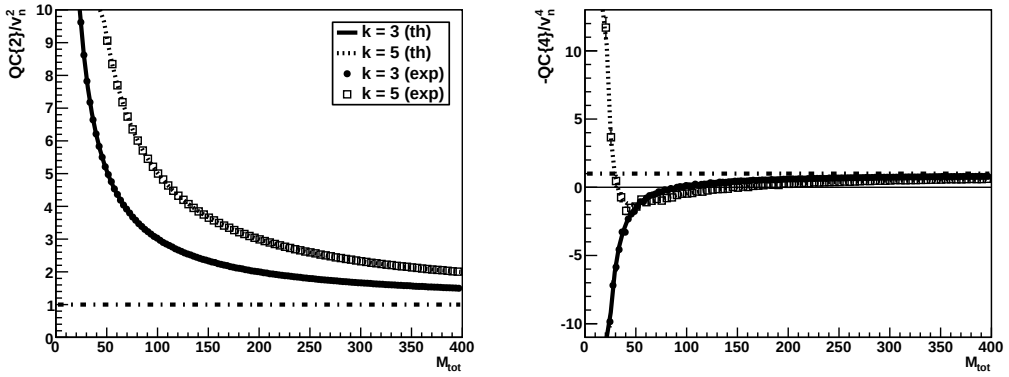

Figure E.5: Lines represent theoretical results Eqs. (E.50) and (E.52) rescaled with v_n^2 and $-v_n^4$, respectively, and markers represent the corresponding measurements for two independent Monte Carlo runs in which tracks were sampled from a Fourier-like p.d.f. parameterized with harmonics $v_2 = 0.1$ and $v_4 = 0.2$, and each track was taken three times (solid lines and filled markers) and five times (dashed line and open markers) in the analysis.

Appendix F

Generating Function Cumulants

In this appendix we provide a detailed derivation of the cumulants calculated from the formalism of generating functions, as originally proposed in [55]. The formalism presented in this appendix is somewhat more general than the one presented in [55] in a sense that we derive some of the results without assuming the multiplicity to be large, in turn extending the applicability of the results also for the case of most peripheral collisions (which produce in general events with small multiplicity). In addition, we allow for the presence of more flow harmonics simultaneously in the system.

F.1 Reference flow

We start by introducing the generating functions $G_n(z)$ for multi-particle azimuthal correlations and $C_n(z)$ for the cumulants. The essence of the idea lies in the fact that all multi-particle azimuthal correlations can be generated after expanding the following complex, real valued function $G_n(z)$ in series of $(z^*)^k z^l$, where $k, l = 0, 1, 2, \ldots M$,

$$G_n(z) \equiv \prod_{j=1}^{M} \left(1 + \frac{z^* e^{in\phi_j} + z e^{-in\phi_j}}{M}\right) . \tag{F.1}$$

The function $G_n(z)$ defined in this way is the generating function for the multi-particle azimuthal correlations and it can be evaluated in a single loop over all particles in each event. For a detector with uniform acceptance the series expansion of $\langle G_n(z)\rangle$, where $\langle\cdot\rangle$ denotes now the average over *all-events*, contains only diagonal terms [55] and it reads,

$$\langle G_n(z)\rangle \;=\; \sum_{k=0}^{M/2} \frac{|z|^{2k}}{M^{2k}} \binom{M}{k} \binom{M-k}{k} \left\langle e^{in(\phi_1+\cdots+\phi_k-\phi_{k+1}-\cdots-\phi_{2k})} \right\rangle . \tag{F.2}$$

We observe immediately that in transferring the product in Eq. (F.1) into the sum in Eq. (F.2) we have to assume that multiplicity is the same in each event, meaning that

cumulants calculated from generating functions will not be able to deal with multiplicity fluctuations in reality, where the multiplicity differs event-by-event. In the next step we introduce the generating function for the cumulants $\mathcal{C}_n(z)$. We write the series expansion of $\mathcal{C}_n(z)$ in a series of $|z|^{2k}$, where $k = 0, 1, 2, \ldots M$, in the following way,

$$\mathcal{C}_n(z) \; = \sum_{k=1}^{M/2} \frac{|z|^{2k}}{(k!)^2} c_n\{2k\} \, . \tag{F.3}$$

The generating function for multi-particle azimuthal correlations (F.1) and cumulants (F.3) are related by [55]:

$$\left(1 + \frac{\mathcal{C}_n(z)}{M}\right)^M = \langle G_n(z) \rangle \; , \tag{F.4}$$

which in the limit of large multiplicity reduces to

$$\mathcal{C}_n(z) = \ln \langle G_n(z) \rangle \; , \tag{F.5}$$

which is the standard definition for the generating function of cumulants used in other areas of physics. By inserting (F.3) into the LHS, and (F.2) into the RHS of Eq. (F.4), and collecting the terms for each order in the expansion in $|z|$, one recovers the cumulants expressed in terms of multi-particle azimuthal correlations. In particular, after some algebra we arrive, order by order, at the following equalities:

$$c_n\{2\} \;=\; \frac{M-1}{M} \left\langle e^{in(\phi_1 - \phi_2)} \right\rangle \, , \tag{F.6}$$

$$\begin{aligned} c_n\{4\} \;&=\; \frac{(M-1)(M-2)(M-3)}{M^3} \left\langle e^{in(\phi_1 + \phi_2 - \phi_3 - \phi_4)} \right\rangle \\ &-\; 2 \left(\frac{M-1}{M}\right)^3 \left\langle e^{in(\phi_1 - \phi_2)} \right\rangle^2 \, , \end{aligned} \tag{F.7}$$

$$\begin{aligned} c_n\{6\} \;&=\; \frac{(M-1)(M-2)(M-3)(M-4)(M-5)}{M^5} \left\langle e^{in(\phi_1 + \phi_2 + \phi_3 - \phi_4 - \phi_5 - \phi_6)} \right\rangle \\ &-\; 9 \, \frac{(M-1)^3(M-2)(M-3)}{M^5} \left\langle e^{in(\phi_1 + \phi_2 - \phi_3 - \phi_4)} \right\rangle \left\langle e^{in(\phi_1 - \phi_2)} \right\rangle \\ &+\; 6 \, \frac{(M-1)^4(2M-1)}{M^5} \left\langle e^{in(\phi_1 - \phi_2)} \right\rangle^3 \, , \end{aligned} \tag{F.8}$$

$$
\begin{aligned}
c_n\{8\} &= \frac{(M-1)(M-2)(M-3)(M-4)(M-5)(M-6)(M-7)}{M^7} \\
&\times \left\langle e^{in(\phi_1+\phi_2+\phi_3+\phi_4-\phi_5-\phi_6-\phi_7-\phi_8)} \right\rangle \\
&- 16\,\frac{(M-1)^3(M-2)(M-3)(M-4)(M-5)}{M^7} \\
&\times \left\langle e^{in(\phi_1+\phi_2+\phi_3-\phi_4-\phi_5-\phi_6)} \right\rangle \left\langle e^{in(\phi_1-\phi_2)} \right\rangle \\
&- 18\,\frac{(M-1)^3(M-2)^2(M-3)^2}{M^7} \left\langle e^{in(\phi_1+\phi_2-\phi_3-\phi_4)} \right\rangle^2 \\
&+ 72\,\frac{(M-1)^4(2M-1)(M-2)(M-3)}{M^7} \\
&\times \left\langle e^{in(\phi_1+\phi_2-\phi_3-\phi_4)} \right\rangle \left\langle e^{in(\phi_1-\phi_2)} \right\rangle^2 \\
&- 24\frac{(M-1)^5(6M^2-5M+1)}{M^7} \left\langle e^{in(\phi_1-\phi_2)} \right\rangle^4 . \qquad \text{(F.9)}
\end{aligned}
$$

In the limit of large multiplicity, the above expressions for the cumulants reduce to

$$
\begin{aligned}
c_n\{2\} &\simeq \left\langle e^{in(\phi_1-\phi_2)} \right\rangle , \\
c_n\{4\} &\simeq \left\langle e^{in(\phi_1+\phi_2-\phi_3-\phi_4)} \right\rangle - 2\left\langle e^{in(\phi_1-\phi_2)} \right\rangle^2 , \\
c_n\{6\} &\simeq \left\langle e^{in(\phi_1+\phi_2+\phi_3-\phi_4-\phi_5-\phi_6)} \right\rangle - 9\left\langle e^{in(\phi_1+\phi_2-\phi_3-\phi_4)} \right\rangle \left\langle e^{in(\phi_1-\phi_2)} \right\rangle \\
&+ 12\left\langle e^{in(\phi_1-\phi_2)} \right\rangle^3 , \\
c_n\{8\} &\simeq \left\langle e^{in(\phi_1+\phi_2+\phi_3+\phi_4-\phi_5-\phi_6-\phi_7-\phi_8)} \right\rangle \\
&- 16\left\langle e^{in(\phi_1+\phi_2+\phi_3-\phi_4-\phi_5-\phi_6)} \right\rangle \left\langle e^{in(\phi_1-\phi_2)} \right\rangle \\
&- 18\left\langle e^{in(\phi_1+\phi_2-\phi_3-\phi_4)} \right\rangle^2 + 144\left\langle e^{in(\phi_1+\phi_2-\phi_3-\phi_4)} \right\rangle \left\langle e^{in(\phi_1-\phi_2)} \right\rangle^2 \\
&- 144\left\langle e^{in(\phi_1-\phi_2)} \right\rangle^4 , \qquad \text{(F.10)}
\end{aligned}
$$

which are the theoretical definitions of cumulants in terms of multi-particle azimuthal correlations. We observe that only in the limit of large multiplicity cumulants obtained via the formalism of generating functions, Eqs. (F.6-F.9) will correspond to the theoretical definitions in Eqs. (F.10).

Having obtained the relations (F.6-F.9) for the cumulants, we present in the next section how the values of reference flow harmonics v_n can be estimated from them.

F.1.1 Estimating the reference flow harmonics v_n from the cumulants

We start this section by introducing some new notation. The average value of the quantity x obtained only from events with the same reaction plane angle Φ_R we denote

by,[1]

$$\langle x\rangle|_{\Phi_R}\,. \tag{F.11}$$

To get the final average value $\langle x\rangle$ of the quantity x one has to average over all angles Φ_R,

$$\langle x\rangle \equiv \frac{1}{2\pi}\int_0^{2\pi} \langle x\rangle|_{\Phi_R}\, d\Phi_R\,. \tag{F.12}$$

It is important to note that when the average is taken with respect to a fixed value of Φ_R for the case of a detector with uniform acceptance we have

$$\left\langle e^{in\phi}\right\rangle\Big|_{\Phi_R} = \left\langle e^{in(\phi-\Phi_R)}\right\rangle\Big|_{\Phi_R} e^{in\Phi_R} = v_n e^{in\Phi_R}\,. \tag{F.13}$$

By making use of this notation it follows,

$$\begin{aligned}
\langle G_n(z)\rangle|_{\Phi_R} &= \left\langle \prod_{j=1}^{M}\left(1+\frac{z^* e^{in\phi_j}+ze^{-in\phi_j}}{M}\right)\right\rangle\Bigg|_{\Phi_R} \\
&= \prod_{j=1}^{M}\left\langle 1+\frac{z^* e^{in\phi_j}+ze^{-in\phi_j}}{M}\right\rangle\Big|_{\Phi_R} \\
&= \prod_{j=1}^{M}\left(1+\frac{z^*\left\langle e^{in\phi_j}\right\rangle\big|_{\Phi_R}+z\left\langle e^{-in\phi_j}\right\rangle\big|_{\Phi_R}}{M}\right)\,.
\end{aligned} \tag{F.14}$$

In obtaining the second line in the above relation we have assumed that the nonflow correlations are much smaller than the flow correlations [55]. After inserting (F.13) in the last line of (F.14), it follows,

$$\begin{aligned}
\langle G_n(z)\rangle|_{\Phi_R} &= \prod_{j=1}^{M}\left(1+\frac{z^* v_n e^{in\Phi_R}+zv_n e^{-in\Phi_R}}{M}\right) \\
&= \left(1+\frac{z^* v_n e^{in\Phi_R}+zv_n e^{-in\Phi_R}}{M}\right)^M\,.
\end{aligned} \tag{F.15}$$

To get the final average value for the generating function $G_n(z)$ we integrate the above expression for $\langle G_n(z)\rangle|_{\Phi_R}$ over Φ_R,

$$\langle G_n(z)\rangle = \frac{1}{2\pi}\int_0^{2\pi}\left(1+\frac{z^* v_n e^{in\Phi_R}+zv_n e^{-in\Phi_R}}{M}\right)^M d\Phi_R\,. \tag{F.16}$$

To proceed further, we make use of the relation:

$$(1+a)^n = \sum_{q=0}^{n}\binom{n}{q}a^q\,. \tag{F.17}$$

[1]Note that this notation is slightly different compared to the one used in [55].

It follows,

$$\begin{aligned}\langle G_n(z)\rangle &= \frac{1}{2\pi}\sum_{q=0}^{M}\binom{M}{q}\int_0^{2\pi}\left(\frac{z^* v_n e^{in\Phi_R}}{M}+\frac{z v_n e^{-in\Phi_R}}{M}\right)^q d\Phi_R \\ &= \frac{1}{2\pi}\sum_{q=0}^{M}\binom{M}{q}\frac{1}{M^q}\int_0^{2\pi}\left(z^* v_n e^{in\Phi_R}+z v_n e^{-in\Phi_R}\right)^q d\Phi_R\,. \quad \text{(F.18)}\end{aligned}$$

In the next step we use

$$(a+b)^q=\sum_{k=0}^{q}\binom{q}{k}a^{q-k}b^k\,. \quad \text{(F.19)}$$

It follows,

$$\begin{aligned}\langle G_n(z)\rangle &= \frac{1}{2\pi}\sum_{q=0}^{M}\binom{M}{q}\frac{1}{M^q}\int_0^{2\pi}\sum_{k=0}^{q}\binom{q}{k}\left(z^* v_n e^{in\Phi_R}\right)^{q-k}\left(z v_n e^{-in\Phi_R}\right)^k \\ &= \frac{1}{2\pi}\sum_{q=0}^{M}\sum_{k=0}^{q}\frac{1}{M^q}\binom{M}{q}\binom{q}{k}(z^*)^{q-k}z^k v_n^q\int_0^{2\pi}e^{in\Phi_R(q-2k)}\,d\Phi_R\,. \quad \text{(F.20)}\end{aligned}$$

The integral above can be evaluated trivially and yields,

$$\int_0^{2\pi}e^{in(q-2k)\Phi_R}\,d\Phi_R=\begin{cases}0 & \text{for } 2k\neq q\,,\\ 2\pi & \text{for } 2k=q\,.\end{cases} \quad \text{(F.21)}$$

This implies that in the summation over k in (F.20) only the terms for which $2k=q$ will be non-vanishing. This in turn implies that in the first summation only terms for which q is even can remain. Taking this into account we obtain:

$$\langle G_n(z)\rangle=\sum_{q=0,2,4\ldots}^{M}\frac{1}{M^q}\binom{M}{q}\binom{q}{q/2}|z|^q v_n^q\,. \quad \text{(F.22)}$$

After introducing $j\equiv q/2$ and after expanding the two binomial coefficients above it follows finally,

$$\langle G_n(z)\rangle=\sum_{j=0,1,2,\ldots}^{M/2}\frac{1}{M^{2j}}\frac{M!}{(M-2j)!(j!)^2}v_n^{2j}|z|^{2j}\,. \quad \text{(F.23)}$$

In order to obtain relations between the flow v_n and cumulants $c_n\{2k\}$ we follow the same strategy which has been used to obtain the relations (F.6-F.9) between cumulants and multi-particle azimuthal correlations. After some algebra, we arrive at the following

relations valid for *arbitrary* multiplicity M,

$$\begin{aligned} v_n^2 &= \frac{M}{M-1}\, c_n\{2\}\,, \\ v_n^4 &= -\frac{M^3}{(M-1)(M^2+M-4)}\, c_n\{4\}\,, \\ v_n^6 &= \frac{M^5}{(M-1)(4M^4+7M^3-28M^2-31M+72)}\, c_n\{6\}\,, \\ v_n^8 &= -\frac{M^7}{(M-1)(33M^6+83M^5-315M^4-655M^3+1362M^2+1652M-2880)}\, c_n\{8\}\,. \end{aligned} \tag{F.24}$$

The various multiplicity dependent prefactors in the above equations are artifacts of using formalism of generating functions in the cumulant analysis and form the part of unavoidable systematic bias characteristic only for this formalism. Only for the case of a large multiplicity M, the relations (F.24) reduce to the theoretical expressions:

$$\begin{aligned} v_n^2 &= c_n\{2\}\,, \\ v_n^4 &= -c_n\{4\}\,, \\ v_n^6 &= \frac{1}{4} c_n\{6\}\,, \\ v_n^8 &= -\frac{1}{33} c_n\{8\}\,. \end{aligned} \tag{F.25}$$

In practice we will restrict ourselves to the analysis up to 8-particle cumulants.[2]

The question which remains to be answered is for which values of the multiplicity M the difference between theoretical relations (F.25) and the ones obtained within the formalism of generating functions, (F.24), is negligible. We have plotted the ratio of these estimates in Fig. F.1. We see clearly that the difference is smaller than 1% for multiplicities larger than 50 for all order estimates.

All the equations derived in this section are applicable only for the case of detector with uniform acceptance—generalization for the case of non-uniform acceptance is provided in [55, 56].

[2] If necessary, even the higher order estimates can be obtained in a straightforward way. For instance, the next four estimates read (for the case of a very large multiplicity),

$$\begin{aligned} v_n^{10} &= \frac{1}{456} c_n\{10\}\,, \\ v_n^{12} &= -\frac{1}{9460} c_n\{12\}\,, \\ v_n^{14} &= \frac{1}{274800} c_n\{14\}\,, \\ v_n^{16} &= -\frac{1}{10643745} c_n\{16\}\,. \end{aligned}$$

These estimates beyond 8-th order are rarely used in practice.

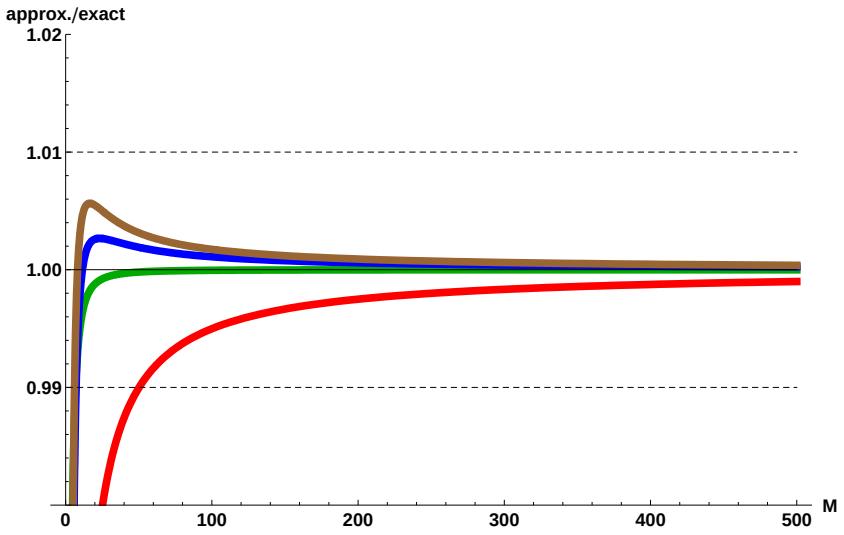

Figure F.1: The ratio of the results (F.25) and (F.24) in the formalism of generating functions. In red is the 2^{nd} order estimate, in green the 4^{th}, in blue the 6^{th} and in brown the 8^{th} order estimate.

F.2 Numerical approach to calculating reference cumulants

The interpolating procedure used in this appendix is an approximate way to circumvent the problem of evaluating multi-particle azimuthal correlations with nested loops which is not feasible in practice for correlators involving four or more particles. Bellow are the steps needed to evaluate the cumulants numerically which involves an evaluation of only one loop over all particles in all events [55, 56]:

Step 1: Bin all events in centrality and for each bin determine the event with minimum multiplicity M_{min}. Then from all events with multiplicity larger than M_{min} in a given centrality bin one has to take *randomly* only M_{min} particles in the analysis. This step is needed in order to justify the transition from the product in the Eq. (F.1) to the summation in Eq. (F.2). In addition, by performing the analysis in this way one is completely removing the systematic bias which stems from the interplay between multiplicity fluctuations and nonflow correlations.

Step 2: Evaluate the generating function for multi-particle azimuthal correlations,

$$G_n(z) \equiv \prod_{j=1}^{M_{\text{min}}} \left(1 + \frac{z^* e^{in\phi_j} + z e^{-in\phi_j}}{M_{\text{min}}}\right), \tag{F.26}$$

at points $z_{p,q} = x_{p,q} + iy_{p,q}$ in a complex plane, where

$$\begin{aligned} x_{p,q} &\equiv r_0\sqrt{p}\cos\left(\frac{2q\pi}{q_{\max}}\right), \\ y_{p,q} &\equiv r_0\sqrt{p}\sin\left(\frac{2q\pi}{q_{\max}}\right), \end{aligned} \tag{F.27}$$

and

$$\begin{aligned} p &= 1, 2, 3 \text{ and } 4, \\ q &= 0, \ldots, q_{\max} - 1, \qquad q_{\max} > 8. \end{aligned} \tag{F.28}$$

We denote the numerical values $G_n(z_{p,q})$ as G_{npq} in what follows. By making use of the above relations for $x_{p,q}$ and $y_{p,q}$, after some algebra from relation (F.26) it follows,

$$\begin{aligned} G_{npq} &\equiv G_n(z_{p,q}) \\ &= \prod_{j=1}^{M_{\min}} \left[1 + \frac{2r_0\sqrt{p}}{M_{\min}}\left(\cos\left(\frac{2q\pi}{q_{\max}}\right)\cos(n\phi_j) + \sin\left(\frac{2q\pi}{q_{\max}}\right)\sin(n\phi_j)\right)\right], \end{aligned} \tag{F.29}$$

i.e.

$$G_{npq} = \prod_{j=1}^{M_{\min}} \left[1 + \frac{2r_0\sqrt{p}}{M_{\min}}\cos\left(\frac{2q\pi}{q_{\max}} - n\phi_j\right)\right]. \tag{F.30}$$

Step 3: Evaluate the average $\langle G_{npq}\rangle$ for each centrality bin as,

$$\langle G_{npq}\rangle = \frac{1}{N}\sum_{i=1}^{N} G_{npq}, \tag{F.31}$$

where N is the number of events in a particular centrality bin.

Step 4: For each multiplicity bin evaluate the generating function for the cumulants $\mathcal{C}_n(z)$ at points $z_{p,q}$ according to,

$$\mathcal{C}_n(z_{p,q}) = M_{\min}\left[\langle G_{npq}\rangle^{1/M_{\min}} - 1\right] \equiv (\mathcal{C}_n)_{p,q}. \tag{F.32}$$

Step 5: Average over the phase of z (in this step the systematic bias due to inefficiencies in the azimuthal acceptance is being averaged out),

$$(\mathcal{C}_n)_p \equiv \frac{1}{q_{\max}}\sum_{q=0}^{q_{\max}-1} (\mathcal{C}_n)_{p,q}. \tag{F.33}$$

Step 6: Solve the following linear system of four equations for the cumulants,

$$(\mathcal{C}_n)_p = \sum_{k=1}^{4} \frac{(r_0\sqrt{p})^{2k}}{(k!)^2} c_n\{2k\}, \qquad 1 \le p \le 4. \tag{F.34}$$

Solution of (F.34) gives:

$$\begin{aligned} c_n\{2\} &= \frac{1}{r_0^2}\left[4(\mathcal{C}_n)_1 - 3(\mathcal{C}_n)_2 + \frac{4}{3}(\mathcal{C}_n)_3 - \frac{1}{4}(\mathcal{C}_n)_4\right], \\ c_n\{4\} &= \frac{1}{r_0^4}\left[-\frac{52}{3}(\mathcal{C}_n)_1 + 19(\mathcal{C}_n)_2 - \frac{28}{3}(\mathcal{C}_n)_3 + \frac{11}{6}(\mathcal{C}_n)_4\right], \\ c_n\{6\} &= \frac{3}{r_0^6}\left[18(\mathcal{C}_n)_1 - 24(\mathcal{C}_n)_2 + 14(\mathcal{C}_n)_3 - 3(\mathcal{C}_n)_4\right], \\ c_n\{8\} &= \frac{24}{r_0^8}\left[-4(\mathcal{C}_n)_1 + 6(\mathcal{C}_n)_2 - 4(\mathcal{C}_n)_3 + (\mathcal{C}_n)_4\right], \end{aligned} \tag{F.35}$$

and the reference flow harmonics v_n can then be estimated by making use of relations (F.25).

In the next step we provide the prescription for estimating differential flow harmonics from cumulants obtained via the formalism of generating functions.

F.3 Differential flow

In this section we present the results relevant to the differential flow analysis with cumulants using the formalism of generating functions. To proceed further we introduce some new terminology. We denote the azimuthal angle of a particle belonging to the window of inerest by ψ and its differential flow harmonics by v_p', where

$$v_p' \equiv \left\langle e^{ip(\psi - \Phi_R)} \right\rangle . \tag{F.36}$$

For the reaction plane angle we continue to use Φ_R. The azimuthal angles of reference particles, which were used to estimate the reference flow v_n, we label with ϕ_j. In order to measure the differential flow of the particles belonging to the window of interest, we correlate their azimuthal angles ψ with the azimuthal angles of reference particles ϕ [55]. In this way the differential flow can be estimated with respect to the reference flow estimated independently. However, we will show later that the previous statement is not true in general—it holds true only if one wants to extract the differential flow harmonic of order which is a multiple of the order of the estimated reference flow harmonic.[3] The reconstructed differential flow harmonic of order p from the reference flow harmonic of order n we denote by $v_{p/n}'$.

Analogous to the strategy we used in previous sections, we construct a generating function of measured azimuthal correlations between the particle belonging to the window of interest and all other particles. This generating function we denote by $\mathcal{G}_{p/n}$ (index indicating that we want to reconstruct $v_{p/n}'$) and it is given by [55],

$$\mathcal{G}_{p/n}(z) \equiv \left\langle e^{ip\psi} G_n(z) \right\rangle , \tag{F.37}$$

[3]For instance, one *can* reconstruct the differential elliptic flow v_2' from the reference directed flow v_1, but one *cannot* reconstruct the differential directed flow v_1' from the reference elliptic flow v_2.

where $G_n(z)$ is the same function as defined previously in (F.1). The angular brackets in (F.37) stand for an average which has to be performed in two steps: One first averages over all particles belonging to the window of interest within the same event, and then in the second step one has to average over all events in which there are particles belonging to the window of interest [55, 56].

The generating function $\mathcal{D}_{p/n}$ for the differential cumulants of azimuthal correlations between particles belonging to the window of interest and all other particles is given by,

$$\mathcal{D}_{p/n}(z) \equiv \frac{\mathcal{G}_{p/n}}{\langle G_n(z)\rangle} = \frac{\left\langle e^{ip\psi}G_n(z)\right\rangle}{\langle G_n(z)\rangle}\,, \tag{F.38}$$

and the differential cumulants are by definition the coefficients $\langle\langle\cdot\rangle\rangle$ in the power-series expansion of this function [55],

$$\mathcal{D}_{p/n}(z) \equiv \sum_{k,l} \frac{z^{*k}z^l}{k!l!} \left\langle\!\left\langle e^{ip\psi+in(\phi_1+\cdots+\phi_k-\phi_{k+1}\cdots-\phi_{k+l})}\right\rangle\!\right\rangle\,. \tag{F.39}$$

In general, the function $\mathcal{D}_{p/n}(z)$ is a complex-valued function of a complex variable z, which implies that in general the differential cumulants defined in (F.39) are complex. However, for a detector with uniform azimuthal acceptance it can be shown that the only non-vanishing cumulants in expansion (F.39) are those for which $l = k + m$, where m is an integer, and all of them are real [55].

To proceed further, we first calculate $\mathcal{G}_{p/n}(z)$. We do this in two steps: First we calculate $\left\langle e^{ip\psi}G_n(z)\right\rangle\big|_{\Phi_R}$ for the events with the same reaction plane angle Φ_R and in the second step we avarage over all reaction plane angles Φ_R. It follows,

$$\begin{aligned}
\mathcal{G}_{p/n}(z) &= \frac{1}{2\pi}\int_0^{2\pi} \left\langle e^{ip\psi}G_n(z)\right\rangle\big|_{\Phi_R}\, d\Phi_R \\
&= \frac{1}{2\pi}\int_0^{2\pi} \left\langle e^{ip(\psi-\Phi_R)}e^{ip\Phi_R}G_n(z)\right\rangle\Big|_{\Phi_R}\, d\Phi_R \\
&= \frac{v'_{p/n}}{2\pi}\int_0^{2\pi} e^{ip\Phi_R}\,\langle G_n(z)\rangle|_{\Phi_R}\, d\Phi_R\,,
\end{aligned} \tag{F.40}$$

where we have used the definition (F.36) and we have assumed that the nonflow correlations are negligible. The average $\langle G_n(z)\rangle|_{\Phi_R}$ was calculated in previous sections and the result is given in relation (F.14). By following the same reasoning we have used in the calculations following the relation (F.14), we here arrive at the following result:

$$\begin{aligned}
\mathcal{G}_{p/n}(z) &= \left\langle e^{ip\psi}G_n(z)\right\rangle \qquad\qquad (F.41) \\
&= \frac{v'_{p/n}}{2\pi}\sum_{q=0}^{M}\sum_{k=0}^{q}\frac{1}{M^q}\binom{M}{q}\binom{q}{k}(z^*)^{q-k}z^k v_n^q\int_0^{2\pi} e^{ip\Phi_R}e^{in\Phi_R(q-2k)}\,d\Phi_R\,.
\end{aligned}$$

The integral in the above equality is zero *unless* the following condition is satisfied,

$$p + n(q-2k) = 0\,, \tag{F.42}$$

i.e.

$$\frac{p}{n} = 2k - q\,. \tag{F.43}$$

It is important to note that on the RHS in above equality we have an integer expression, which implies that on the LHS we also must have an integer expression. This is only possible if p is a multiple of n, i.e. if we can write $p = mn$, where m is an integer. This proves our starting statement in this section, namely that we can reconstruct differential flow v'_p from the reference flow v_n only if p is a multiple of n. From now on in each expression we write mn instead of p.

Taking previous conclusions into account, it follows from relation (F.42),

$$\mathcal{G}_{mn/n}(z) \;=\; v'_{mn/n} \sum_{q=0}^{M} \frac{1}{M^q} \frac{M!}{(M-q)!} \frac{1}{(\frac{q+m}{2})!(\frac{q-m}{2})!} (z^*)^{\frac{q-m}{2}} z^{\frac{q+m}{2}} v_n^q\,, \tag{F.44}$$

which, after introducing $l \equiv (q-m)/2$, can be rewritten as,

$$\mathcal{G}_{mn/n}(z) \;=\; v'_{mn/n} \sum_{l=0,1,2,\ldots}^{\frac{M-m}{2}} \frac{M!}{(M-m-2l)!\,l!\,(l+m)!} (z^*)^l z^{l+m} \Big(\frac{v_n}{M}\Big)^{2l+m}\,. \tag{F.45}$$

For a detector with uniform acceptance we can rewrite expansion (F.39) in the following way,

$$\mathcal{D}_{mn/n}(z) \equiv \sum_{k=0} \frac{z^{*k} z^{k+m}}{k!\,(k+m)!}\, d_{mn/n}\{2k+m+1\}\,, \tag{F.46}$$

where we have introduced notation $d_{mn/n}\{2k+m+1\}$ for the relevant differential cumulants [55]. After expanding $1/\langle G_n(z)\rangle$ in powers of z in relation (F.38) we can write down the following relation,

$$\begin{aligned} & v'_{mn/n} \sum_{l=0,1,2,\ldots}^{\frac{M-m}{2}} \frac{M!}{(M-m-2l)!\,l!\,(l+m)!} (z^*)^l z^{l+m} \Big(\frac{v_n}{M}\Big)^{2l+m} \times \\ & \left[1 - \sum_{j=0,1,2,\ldots}^{M/2} \frac{1}{M^{2j}} \frac{M!}{(M-2j)!(j!)^2} v_n^{2j} |z|^{2j}\right] \\ = \;& \sum_{k=0} \frac{z^{*k} z^{k+m}}{k!\,(k+m)!}\, d_{mn/n}\{2k+m+1\}\,. \end{aligned} \tag{F.47}$$

From this relation, order by order, we can extract a set of equations and solve them for $v'_{mn/n}$. In this way we arrive at various relations between differential flow harmonics, reference flow harmonics and cumulants. When only the flow correlations are present these relations are exact. In reality, for instance due to systematic biases stemming from nonflow correlations or statistical flow fluctuations, these relations are approximate and provide only an estimate for the differential flow harmonics which we denote by $v'_{mn/n}\{2k+m+1\}$. We now outline our final results.

For $m = 1$ we have obtained:

$$\begin{aligned}
v'_{n/n}\{2\} &= \frac{d_{n/n}\{2\}}{v_n}\,, \qquad \text{(F.48)}\\
v'_{n/n}\{4\} &= -\frac{M^2}{M^2+M-2}\,\frac{d_{n/n}\{4\}}{v_n^3}\,,\\
v'_{n/n}\{6\} &= \frac{1}{4}\,\frac{M^4}{M^4+2M^3-4M^2-5M+6}\,\frac{d_{n/n}\{6\}}{v_n^5}\,,\\
v'_{n/n}\{8\} &= -\frac{1}{3}\,\frac{M^6}{11M^6-33M^5-59M^4-173M^3+168M^2+260M-240)}\,\frac{d_{n/n}\{8\}}{v_n^7}\,.
\end{aligned}$$

For a very large multiplicity M the above relations reduce to,

$$\begin{aligned}
v'_{n/n}\{2\} &= \frac{d_{n/n}\{2\}}{v_n}\,,\\
v'_{n/n}\{4\} &= -\frac{d_{n/n}\{4\}}{v_n^3}\,,\\
v'_{n/n}\{6\} &= \frac{d_{n/n}\{6\}}{4v_n^5}\,,\\
v'_{n/n}\{8\} &= -\frac{d_{n/n}\{8\}}{33v_n^7}\,. \qquad \text{(F.49)}
\end{aligned}$$

For $m = 2$ we have obtained the following results,

$$\begin{aligned}
v'_{2n/n}\{3\} &= \frac{M}{M-1}\,\frac{d_{2n/n}\{3\}}{v_n^2}\,, \qquad \text{(F.50)}\\
v'_{2n/n}\{5\} &= -\frac{1}{2}\,\frac{M^3}{M^3-4M+3}\,\frac{d_{2n/n}\{5\}}{v_n^4}\,,\\
v'_{2n/n}\{7\} &= \frac{M^5}{11M^5+11M^4-81M^3-11M^2+190M-120}\,\frac{d_{2n/n}\{7\}}{v_n^6}\,,\\
v'_{2n/n}\{9\} &= -\frac{1}{6}\,\frac{d_{2n/n}\{9\}}{v_n^8}M^7\\
&\quad / \quad (19M^7+38M^6-187M^5-225M^4+826M^3+187M^2-1498M+840)\,,
\end{aligned}$$

which in the limit of very large multiplicity M reduce to

$$\begin{aligned}
v'_{2n/n}\{3\} &= \frac{d_{2n/n}\{3\}}{v_n^2}\,,\\
v'_{2n/n}\{5\} &= -\frac{d_{2n/n}\{5\}}{2v_n^4}\,,\\
v'_{2n/n}\{7\} &= \frac{d_{2n/n}\{7\}}{11v_n^6}\,,\\
v'_{2n/n}\{9\} &= -\frac{d_{2n/n}\{9\}}{114v_n^8}\,. \qquad \text{(F.51)}
\end{aligned}$$

For $m = 3$ we have obtained the following results,

$$
\begin{aligned}
v'_{3n/n}\{4\} &= \frac{M^2}{M^2-3M+2}\,\frac{d_{3n/n}\{4\}}{v_n^3}\,, \qquad \text{(F.52)}\\
v'_{3n/n}\{6\} &= -\frac{1}{3}\,\frac{M^4}{M^4-2M^3-5M^2+14M-8}\,\frac{d_{3n/n}\{6\}}{v_n^5}\,,\\
v'_{3n/n}\{8\} &= \frac{1}{3}\,\frac{M^6}{7M^6-7M^5-75M^4+115M^3+188M^2-468M+240}\,\frac{d_{3n/n}\{8\}}{v_n^7}\,,\\
v'_{3n/n}\{10\} &= -\frac{1}{2}\,M^8/(131M^8-2004M^6+1218M^5+11049M^4-13650M^3\\
&\quad -19256M^2+42672M-20160)\,\frac{d_{3n/n}\{10\}}{v_n^9}\,,
\end{aligned}
$$

which in the limit of a very large multiplicity M reduce to

$$
\begin{aligned}
v'_{3n/n}\{4\} &= \frac{d_{3n/n}\{4\}}{v_n^3}\,,\\
v'_{3n/n}\{6\} &= -\frac{d_{3n/n}\{6\}}{3v_n^5}\,,\\
v'_{3n/n}\{8\} &= \frac{d_{3n/n}\{8\}}{21v_n^7}\,,\\
v'_{3n/n}\{10\} &= -\frac{d_{3n/n}\{10\}}{262v_n^9}\,. \qquad \text{(F.53)}
\end{aligned}
$$

For $m = 4$ we have obtained the following results,

$$
\begin{aligned}
v'_{4n/n}\{5\} &= \frac{M^3}{M^3-6M^2+11M-6}\,\frac{d_{4n/n}\{5\}}{v_n^4}\,, \qquad \text{(F.54)}\\
v'_{4n/n}\{7\} &= -\frac{1}{4}\,\frac{M^5}{M^5-5M^4+35M^2-61M+30}\,\frac{d_{4n/n}\{7\}}{v_n^6}\,,\\
v'_{4n/n}\{9\} &= \frac{1}{2}\,\frac{d_{4n/n}\{9\}}{v_n^8}M^7\\
&\quad / \quad (17M^7-68M^6-154M^5+940M^4-367M^3-3392M^2+5544M-2520)\,,\\
v'_{4n/n}\{11\} &= -\frac{1}{16}\,M^9/(31M^9-93M^8-519M^7+1890M^6+2205M^5-13797M^4\\
&\quad +6059M^3+34680M^2-53136M+22680)\,\frac{d_{3n/n}\{10\}}{v_n^{10}}\,,
\end{aligned}
$$

which in the limit of very large multiplicity M reduce to

$$\begin{aligned} v'_{4n/n}\{5\} &= \frac{d_{4n/n}\{5\}}{v_n^4}\,, \\ v'_{4n/n}\{7\} &= -\frac{d_{4n/n}\{7\}}{4v_n^6}\,, \\ v'_{4n/n}\{9\} &= \frac{d_{4n/n}\{9\}}{34v_n^8}\,, \\ v'_{4n/n}\{11\} &= -\frac{d_{4n/n}\{11\}}{496v_n^{10}}\,. \end{aligned} \tag{F.55}$$

In this Appendix we have highlighted the formalism of generating functions in the flow analysis with cumulants. For the treatment of statistical errors we refer the reader to [55].

Appendix G

Multi-particle azimuthal correlations

In this section we provide the analytic equations for all multi-particles correlators in terms of Q-vectors, which enable the evaluation of all multi-particles correlators with a single loop over all particles. It is assumed that from all final results bellow only the real part is taken, whenever the final results are complex.

G.1 2-particle azimuthal correlations

$$\begin{aligned} \langle 2 \rangle_{k\cdot n|k\cdot n} &\equiv \langle \cos(k \cdot n(\phi_1 - \phi_2)) \rangle \\ &= \frac{1}{\binom{M}{2} 2!} \sum_{\substack{i,j=1 \\ (i \neq j)}}^{M} e^{ik\cdot n(\phi_i - \phi_j)} \\ &= \frac{1}{\binom{M}{2} 2!} \times \left[|Q_{k\cdot n}|^2 - M \right]. \end{aligned} \tag{G.1}$$

G.2 3-particle azimuthal correlations

$$\begin{aligned} \langle 3 \rangle_{2n|n,n} &\equiv \langle \cos(n(2\phi_1 - \phi_2 - \phi_3)) \rangle \\ &= \frac{1}{\binom{M}{3} 3!} \sum_{\substack{i,j,k=1 \\ (i \neq j \neq k)}}^{M} e^{in(2\phi_i - \phi_j - \phi_k)} \\ &= \frac{1}{\binom{M}{3} 3!} \times \left[Q_{2n} Q_n^* Q_n^* - 2 \cdot |Q_n|^2 - |Q_{2n}|^2 + 2M \right]. \end{aligned} \tag{G.2}$$

$$\begin{aligned}\langle 3\rangle_{3n|2n,n} &\equiv \langle\cos(n(3\phi_1-2\phi_2-\phi_3))\rangle \\ &= \frac{1}{\binom{M}{3}3!}\sum_{\substack{i,j,k=1\\(i\neq j\neq k)}}^{M} e^{in(3\phi_i-2\phi_j-\phi_k)} \\ &= \frac{1}{\binom{M}{3}3!}\times\left[Q_{3n}Q_{2n}^{*}Q_{n}^{*}-|Q_{3n}|^2-|Q_{2n}|^2-|Q_n|^2+2M\right].\end{aligned} \tag{G.3}$$

$$\begin{aligned}\langle 3\rangle_{4n|3n,n} &\equiv \langle\cos(n(4\phi_1-3\phi_2-\phi_3))\rangle \\ &= \frac{1}{\binom{M}{3}3!}\sum_{\substack{i,j,k=1\\(i\neq j\neq k)}}^{M} e^{in(4\phi_i-3\phi_j-\phi_k)} \\ &= \frac{1}{\binom{M}{3}3!}\times\left[Q_{4n}Q_{3n}^{*}Q_{n}^{*}-|Q_{4n}|^2-|Q_{3n}|^2-|Q_n|^2+2M\right].\end{aligned} \tag{G.4}$$

$$\begin{aligned}\langle 3\rangle_{5n|3n,2n} &\equiv \langle\cos(n(5\phi_1-3\phi_2-2\phi_3))\rangle \\ &= \frac{1}{\binom{M}{3}3!}\sum_{\substack{i,j,k=1\\(i\neq j\neq k)}}^{M} e^{in(5\phi_i-3\phi_j-2\phi_k)} \\ &= \frac{1}{\binom{M}{3}3!}\times\left[Q_{5n}Q_{3n}^{*}Q_{2n}^{*}-|Q_{5n}|^2-|Q_{3n}|^2-|Q_{2n}|^2+2M\right].\end{aligned} \tag{G.5}$$

$$\begin{aligned}\langle 3\rangle_{5n|4n,n} &\equiv \langle\cos(n(5\phi_1-4\phi_2-\phi_3))\rangle \\ &= \frac{1}{\binom{M}{3}3!}\sum_{\substack{i,j,k=1\\(i\neq j\neq k)}}^{M} e^{in(5\phi_i-4\phi_j-\phi_k)} \\ &= \frac{1}{\binom{M}{3}3!}\times\left[Q_{5n}Q_{4n}^{*}Q_{n}^{*}-|Q_{5n}|^2-|Q_{4n}|^2-|Q_n|^2+2M\right].\end{aligned} \tag{G.6}$$

$$\begin{aligned}\langle 3\rangle_{6n|5n,n} &\equiv \langle\cos(n(6\phi_1-5\phi_2-\phi_3))\rangle \\ &= \frac{1}{\binom{M}{3}3!}\sum_{\substack{i,j,k=1\\(i\neq j\neq k)}}^{M} e^{in(6\phi_i-5\phi_j-\phi_k)} \\ &= \frac{1}{\binom{M}{3}3!}\times\left[Q_{6n}Q_{5n}^{*}Q_{n}^{*}-|Q_{6n}|^2-|Q_{5n}|^2-|Q_n|^2+2M\right].\end{aligned} \tag{G.7}$$

G.3 4-particle azimuthal correlations

$$\begin{aligned}\langle 4\rangle_{n,n|n,n} &\equiv \langle\cos(n(\phi_1+\phi_2-\phi_3-\phi_4))\rangle \qquad \text{(G.8)}\\ &= \frac{1}{\binom{M}{4}4!}\sum_{\substack{i,j,k,l=1\\(i\neq j\neq k\neq l)}}^{M} e^{in(\phi_i+\phi_j-\phi_k-\phi_l)}\\ &= \frac{1}{\binom{M}{4}4!}\times\big[\,|Q_n|^4+|Q_{2n}|^2-2\cdot\mathfrak{Re}\left[Q_{2n}Q_n^*Q_n^*\right]-4(M-2)\,|Q_n|^2\\ &\quad +2M(M-3)\big]\,.\end{aligned}$$

$$\begin{aligned}\langle 4\rangle_{2n,n|2n,n} &\equiv \langle\cos(n(2\phi_1+\phi_2-2\phi_3-\phi_4))\rangle \qquad \text{(G.9)}\\ &= \frac{1}{\binom{M}{4}4!}\sum_{\substack{i,j,k,l=1\\(i\neq j\neq k\neq l)}}^{M} e^{in(2\phi_i+\phi_j-2\phi_k-\phi_l)}\\ &= \frac{1}{\binom{M}{4}4!}\times\big[\,|Q_{2n}|^2\,|Q_n|^2-2\cdot\mathfrak{Re}\left[Q_{3n}Q_{2n}^*Q_n^*\right]-2\cdot\mathfrak{Re}\left[Q_{2n}Q_n^*Q_n^*\right]\\ &\quad +|Q_{3n}|^2-(M-4)\cdot|Q_{2n}|^2-(M-5)\cdot|Q_n|^2+M(M-6)\big]\,.\end{aligned}$$

$$\begin{aligned}\langle 4\rangle_{3n|n,n,n} &\equiv \langle\cos(n(3\phi_1-\phi_2-\phi_3-\phi_4))\rangle \qquad \text{(G.10)}\\ &= \frac{1}{\binom{M}{4}4!}\sum_{\substack{i,j,k,l=1\\(i\neq j\neq k\neq l)}}^{M} e^{in(3\phi_i-\phi_j-\phi_k-\phi_l)}\\ &= \frac{1}{\binom{M}{4}4!}\times\big[Q_{3n}Q_n^*Q_n^*Q_n^*-3\cdot Q_{3n}Q_{2n}^*Q_n^*-3\cdot Q_{2n}Q_n^*Q_n^*\\ &\quad +2\cdot|Q_{3n}|^2+3\cdot|Q_{2n}|^2+6\cdot|Q_n|^2-6M\big]\,.\end{aligned}$$

$$\begin{aligned}\langle 4\rangle_{4n|2n,n,n} &\equiv \langle\cos(n(4\phi_1-2\phi_2-\phi_3-\phi_4))\rangle \qquad \text{(G.11)}\\ &= \frac{1}{\binom{M}{4}4!}\sum_{\substack{i,j,k,l=1\\(i\neq j\neq k\neq l)}}^{M} e^{in(4\phi_i-2\phi_j-\phi_k-\phi_l)}\\ &= \frac{1}{\binom{M}{4}4!}\times\big[Q_{4n}Q_{2n}^*Q_n^*Q_n^*-2\cdot Q_{4n}Q_{3n}^*Q_n^*-Q_{4n}Q_{2n}^*Q_{2n}^*\\ &\quad -2\cdot Q_{3n}Q_{2n}^*Q_n^*-Q_{2n}Q_n^*Q_n^*+2\cdot|Q_{4n}|^2+2\cdot|Q_{3n}|^2\\ &\quad +3\cdot|Q_{2n}|^2+4\cdot|Q_n|^2-6M\big]\,.\end{aligned}$$

$$\begin{aligned}\langle 4\rangle_{3n,n|2n,2n} &\equiv \langle\cos(n(3\phi_1+\phi_2-2\phi_3-2\phi_4))\rangle \\ &= \frac{1}{\binom{M}{4}4!}\sum_{\substack{i,j,k,l=1\\(i\neq j\neq k\neq l)}}^{M} e^{in(3\phi_i+\phi_j-2\phi_k-2\phi_l)} \\ &= \frac{1}{\binom{M}{4}4!}\times\big[Q_{3n}Q_nQ_{2n}^*Q_{2n}^*-Q_{4n}Q_{2n}^*Q_{2n}^*-Q_{3n}Q_nQ_{4n}^* \\ &\quad -2\cdot Q_{3n}Q_{2n}^*Q_n^*-2\cdot Q_nQ_nQ_{2n}^*+|Q_{4n}|^2+2\cdot|Q_{3n}|^2 \\ &\quad +4\cdot|Q_{2n}|^2+4\cdot|Q_n|^2-6M\big]\,.\end{aligned} \tag{G.12}$$

$$\begin{aligned}\langle 4\rangle_{3n,n|3n,n} &\equiv \langle\cos(n(3\phi_1+\phi_2-3\phi_3-\phi_4))\rangle \\ &= \frac{1}{\binom{M}{4}4!}\sum_{\substack{i,j,k,l=1\\(i\neq j\neq k\neq l)}}^{M} e^{in(3\phi_i+\phi_j-3\phi_k-\phi_l)} \\ &= \frac{1}{\binom{M}{4}4!}\times\big[\,|Q_{3n}|^2\,|Q_n|^2-2\cdot\mathfrak{Re}\,[Q_{4n}Q_{3n}^*Q_n^*] \\ &\quad -2\cdot\mathfrak{Re}\,[Q_{3n}Q_{2n}^*Q_n^*]+|Q_{4n}|^2-(M-4)\cdot|Q_{3n}|^2 \\ &\quad +|Q_{2n}|^2+4\cdot|Q_n|^2+M(M-6)\big]\,.\end{aligned} \tag{G.13}$$

$$\begin{aligned}\langle 4\rangle_{4n,2n|3n,3n} &\equiv \langle\cos(n(4\phi_1+2\phi_2-3\phi_3-3\phi_4))\rangle \\ &= \frac{1}{\binom{M}{4}4!}\sum_{\substack{i,j,k,l=1\\(i\neq j\neq k\neq l)}}^{M} e^{in(4\phi_i+2\phi_j-3\phi_k-3\phi_l)} \\ &= \frac{1}{\binom{M}{4}4!}\times\big[Q_{4n}Q_{2n}Q_{3n}^*Q_{3n}^*-Q_{4n}Q_{2n}Q_{6n}^*-Q_{6n}Q_{3n}^*Q_{3n}^* \\ &\quad -2Q_{4n}Q_{3n}^*Q_n^*-2Q_nQ_{2n}Q_{3n}^*+|Q_{6n}|^2+2|Q_{4n}|^2 \\ &\quad +2\cdot(2|Q_{3n}|^2+|Q_{2n}|^2+|Q_n|^2-3M)\big]\,.\end{aligned} \tag{G.14}$$

$$\begin{aligned}\langle 4\rangle_{6n|3n,2n,n} &\equiv \langle\cos(n(6\phi_1-3\phi_2-2\phi_3-\phi_4))\rangle \\ &= \frac{1}{\binom{M}{4}4!}\sum_{\substack{i,j,k,l=1\\(i\neq j\neq k\neq l)}}^{M} e^{in(6\phi_i-3\phi_j-2\phi_k-\phi_l)} \\ &= \frac{1}{\binom{M}{4}4!}\times\big[Q_{6n}Q_{3n}^*Q_{2n}^*Q_n^*-Q_{6n}Q_{4n}^*Q_{2n}^*-Q_{6n}Q_{3n}^*Q_{3n}^* \\ &\quad -Q_{6n}Q_{5n}^*Q_n^*-Q_{5n}Q_{3n}^*Q_{2n}^*-Q_{4n}Q_{3n}^*Q_n^*-Q_{3n}Q_{2n}^*Q_n^* \\ &\quad +2|Q_{6n}|^2+|Q_{5n}|^2+|Q_{4n}|^2+3|Q_{3n}|^2+2|Q_{2n}|^2 \\ &\quad +2|Q_n|^2-6M\big]\,.\end{aligned} \tag{G.15}$$

$$\begin{aligned}
\langle 4\rangle_{3n,2n|3n,2n} &\equiv \langle\cos(n(3\phi_1+2\phi_2-3\phi_3-2\phi_4))\rangle \qquad \text{(G.16)}\\
&= \frac{1}{\binom{M}{4}4!}\sum_{\substack{i,j,k,l=1\\(i\neq j\neq k\neq l)}}^{M} e^{in(3\phi_i+2\phi_j-3\phi_k-2\phi_l)}\\
&= \frac{1}{\binom{M}{4}4!}\times\big[|Q_{3n}|^2|Q_{2n}|^2-2\cdot Q_{5n}Q_{3n}^*Q_{2n}^*-2\cdot Q_{3n}Q_{2n}^*Q_n^*\\
&\quad +|Q_{5n}|^2-(M-4)(|Q_{3n}|^2+|Q_{2n}|^2)+M(M-6)\big]\,.
\end{aligned}$$

$$\begin{aligned}
\langle 4\rangle_{4n,n|3n,2n} &\equiv \langle\cos(n(4\phi_1+\phi_2-3\phi_3-2\phi_4))\rangle \qquad \text{(G.17)}\\
&= \frac{1}{\binom{M}{4}4!}\sum_{\substack{i,j,k,l=1\\(i\neq j\neq k\neq l)}}^{M} e^{in(4\phi_i+\phi_j-3\phi_k-2\phi_l)}\\
&= \frac{1}{\binom{M}{4}4!}\times\big[Q_{4n}Q_nQ_{3n}^*Q_{2n}^*-Q_{5n}Q_{4n}^*Q_n^*-Q_{5n}Q_{3n}^*Q_{2n}^*\\
&\quad -Q_{4n}Q_{3n}^*Q_n^*-Q_{4n}Q_{2n}^*Q_{2n}^*-Q_{3n}Q_{2n}^*Q_n^*-Q_{2n}Q_n^*Q_n^*\\
&\quad +|Q_{5n}|^2+2(|Q_{4n}|^2+|Q_{3n}|^2)+3(|Q_{2n}|^2+|Q_n|^2)-6M\big]\,.
\end{aligned}$$

$$\begin{aligned}
\langle 4\rangle_{5n,n|3n,3n} &\equiv \langle\cos(n(5\phi_1+\phi_2-3\phi_3-3\phi_4))\rangle \qquad \text{(G.18)}\\
&= \frac{1}{\binom{M}{4}4!}\sum_{\substack{i,j,k,l=1\\(i\neq j\neq k\neq l)}}^{M} e^{in(5\phi_i+\phi_j-3\phi_k-3\phi_l)}\\
&= \frac{1}{\binom{M}{4}4!}\times\big[Q_{5n}Q_nQ_{3n}^*Q_{3n}^*-Q_{6n}Q_{5n}^*Q_n^*-Q_{6n}Q_{3n}^*Q_{3n}^*\\
&\quad -2\cdot Q_{5n}Q_{3n}^*Q_{2n}^*-2\cdot Q_{3n}Q_{2n}^*Q_n^*+|Q_{6n}|^2\\
&\quad +2(|Q_{5n}|^2+2|Q_{3n}|^2+|Q_{2n}|^2+|Q_n|^2-3M)\big]\,.
\end{aligned}$$

$$\begin{aligned}
\langle 4\rangle_{5n,n|4n,2n} &\equiv \langle\cos(n(5\phi_1+\phi_2-4\phi_3-2\phi_4))\rangle \qquad \text{(G.19)}\\
&= \frac{1}{\binom{M}{4}4!}\sum_{\substack{i,j,k,l=1\\(i\neq j\neq k\neq l)}}^{M} e^{in(5\phi_i+\phi_j-4\phi_k-2\phi_l)}\\
&= \frac{1}{\binom{M}{4}4!}\times\big[Q_{5n}Q_nQ_{4n}^*Q_{2n}^*-Q_{6n}Q_{5n}^*Q_n^*-Q_{6n}Q_{4n}^*Q_{2n}^*\\
&\quad -Q_{5n}Q_{4n}^*Q_n^*-Q_{5n}Q_{3n}^*Q_{2n}^*-Q_{4n}Q_{3n}^*Q_n^*-Q_{2n}Q_n^*Q_n^*+|Q_{6n}|^2\\
&\quad +2|Q_{5n}|^2+2|Q_{4n}|^2+|Q_{3n}|^2+2|Q_{2n}|^2+3|Q_n|^2-6M\big]\,.
\end{aligned}$$

$$\begin{aligned}
\langle 4\rangle_{5n|3n,n,n} &\equiv \langle\cos(n(5\phi_1-3\phi_2-\phi_3-\phi_4))\rangle \qquad \text{(G.20)}\\
&= \frac{1}{\binom{M}{4}4!}\sum_{\substack{i,j,k,l=1\\(i\neq j\neq k\neq l)}}^{M} e^{in(5\phi_i-3\phi_j-\phi_k-\phi_l)}\\
&= \frac{1}{\binom{M}{4}4!}\times\big[Q_{5n}Q^*_{3n}Q^*_nQ^*_n-2\cdot Q_{5n}Q^*_{4n}Q^*_n-Q_{5n}Q^*_{3n}Q^*_{2n}\\
&\quad -2\cdot Q_{4n}Q^*_{3n}Q^*_n-Q_{2n}Q^*_nQ^*_n+2|Q_{5n}|^2+2|Q_{4n}|^2\\
&\quad +2|Q_{3n}|^2+|Q_{2n}|^2+4|Q_n|^2-6M\big]\,.
\end{aligned}$$

$$\begin{aligned}
\langle 4\rangle_{5n|2n,2n,n} &\equiv \langle\cos(n(5\phi_1-2\phi_2-2\phi_3-\phi_4))\rangle \qquad \text{(G.21)}\\
&= \frac{1}{\binom{M}{4}4!}\sum_{\substack{i,j,k,l=1\\(i\neq j\neq k\neq l)}}^{M} e^{in(5\phi_i-2\phi_j-2\phi_k-\phi_l)}\\
&= \frac{1}{\binom{M}{4}4!}\times\big[Q_{5n}Q^*_{2n}Q^*_{2n}Q^*_n-Q_{5n}Q^*_{4n}Q^*_n-2\cdot Q_{5n}Q^*_{3n}Q^*_{2n}\\
&\quad -Q_{4n}Q^*_{2n}Q^*_{2n}-2\cdot Q_{3n}Q^*_{2n}Q^*_n+2|Q_{5n}|^2+|Q_{4n}|^2\\
&\quad +2|Q_{3n}|^2+4|Q_{2n}|^2+2|Q_n|^2-6M\big]\,.
\end{aligned}$$

$$\begin{aligned}
\langle 4\rangle_{5n,n|5n,n} &\equiv \langle\cos(n(5\phi_1-\phi_2-5\phi_3-\phi_4))\rangle \qquad \text{(G.22)}\\
&= \frac{1}{\binom{M}{4}4!}\sum_{\substack{i,j,k,l=1\\(i\neq j\neq k\neq l)}}^{M} e^{in(5\phi_i-\phi_j-5\phi_k-\phi_l)}\\
&= \frac{1}{\binom{M}{4}4!}\times\big[|Q_{5n}|^2|Q_n|^2-2\cdot Q_{6n}Q^*_{5n}Q^*_n-2\cdot Q_{5n}Q^*_{4n}Q^*_n\\
&\quad +|Q_{6n}|^2-(M-4)|Q_{5n}|^2+|Q_{4n}|^2-(M-4)|Q_n|^2+M(M-6)\big]\,.
\end{aligned}$$

G.4 5-particle azimuthal correlations

$$\begin{aligned}\langle 5\rangle_{2n,n|n,n,n} &\equiv \langle\cos(n(2\phi_1+\phi_2-\phi_3-\phi_4-\phi_5))\rangle \qquad \text{(G.23)}\\ &= \frac{1}{\binom{M}{5}5!}\sum_{\substack{i,j,k,l,m=1\\(i\neq j\neq k\neq l\neq m)}}^{M} e^{in(2\phi_i+\phi_j-\phi_k-\phi_l-\phi_m)}\\ &= \frac{1}{\binom{M}{5}5!}\times\big[Q_{2n}Q_nQ_n^*Q_n^*Q_n^*-Q_{3n}Q_n^*Q_n^*Q_n^*+5\cdot Q_{3n}Q_{2n}^*Q_n^*\\ &\quad -3(M-5)Q_{2n}Q_n^*Q_n^*-2\left|Q_{3n}\right|^2-3\left|Q_{2n}\right|^2\left|Q_n\right|^2+3(M-4)\left|Q_{2n}\right|^2\\ &\quad -3\left|Q_n\right|^4+6(2M-5)\left|Q_n\right|^2-6M(M-4)\big].\end{aligned}$$

$$\begin{aligned}\langle 5\rangle_{2n,2n|2n,n,n} &\equiv \langle\cos(n(2\phi_1+2\phi_2-2\phi_3-\phi_4-\phi_5))\rangle \qquad \text{(G.24)}\\ &= \frac{1}{\binom{M}{5}5!}\sum_{\substack{i,j,k,l,m=1\\(i\neq j\neq k\neq l\neq m)}}^{M} e^{in(2\phi_i+2\phi_j-2\phi_k-\phi_l-\phi_m)}\\ &= \frac{1}{\binom{M}{5}5!}\times\big[Q_{2n}Q_{2n}Q_{2n}^*Q_n^*Q_n^*-Q_{4n}Q_{2n}^*Q_n^*Q_n^*-2\cdot Q_{3n}Q_nQ_{2n}^*Q_{2n}^*\\ &\quad +3\cdot Q_{4n}Q_{2n}^*Q_{2n}^*+8\cdot Q_{3n}Q_{2n}^*Q_n^*+2\cdot Q_{4n}Q_{3n}Q_n^*\\ &\quad -2(M-6)Q_{2n}Q_n^*Q_n^*\\ &\quad -2\left|Q_{4n}\right|^2-4\left|Q_{3n}\right|^2-\left|Q_{2n}\right|^4+2(3M-10)\left|Q_{2n}\right|^2\\ &\quad -4\left|Q_n\right|^2\left|Q_{2n}\right|^2+4(M-5)\cdot\left|Q_n\right|^2-4M(M-6)\big].\end{aligned}$$

$$\begin{aligned}\langle 5\rangle_{4n|n,n,n,n} &\equiv \langle\cos(n(4\phi_1-\phi_2-\phi_3-\phi_4-\phi_5))\rangle \qquad \text{(G.25)}\\ &= \frac{1}{\binom{M}{5}5!}\sum_{\substack{i,j,k,l,m=1\\(i\neq j\neq k\neq l\neq m)}}^{M} e^{in(4\phi_i-\phi_j-\phi_k-\phi_l-\phi_m)}\\ &= \frac{1}{\binom{M}{5}5!}\times\big[Q_{4n}Q_n^*Q_n^*Q_n^*Q_n^*-6\cdot Q_{4n}Q_{2n}^*Q_n^*Q_n^*-4\cdot Q_{3n}Q_n^*Q_n^*Q_n^*\\ &\quad +8\cdot Q_{4n}Q_{3n}^*Q_n^*+3\cdot Q_{4n}Q_{2n}^*Q_{2n}^*+12\cdot Q_{3n}Q_{2n}^*Q_n^*+12\cdot Q_{2n}Q_n^*Q_n^*\\ &\quad -6\left|Q_{4n}\right|^2-8\left|Q_{3n}\right|^2-12\left|Q_{2n}\right|^2-24\left|Q_n\right|^2+24M\big].\end{aligned}$$

$$\begin{aligned}
\langle 5\rangle_{3n,n|2n,n,n} &\equiv \langle\cos(n(3\phi_1+\phi_2-2\phi_3-\phi_4-\phi_5))\rangle \qquad \text{(G.26)}\\
&= \frac{1}{\binom{M}{5}5!}\sum_{\substack{i,j,k,l,m=1\\(i\neq j\neq k\neq l\neq m)}}^{M} e^{in(3\phi_i+\phi_j-2\phi_k-\phi_l-\phi_m)}\\
&= \frac{1}{\binom{M}{5}5!}\times\big[Q_{3n}Q_nQ_{2n}^*Q_n^*Q_n^*-Q_{4n}Q_{2n}^*Q_n^*Q_n^*-Q_{3n}Q_n^*Q_n^*Q_n^*\\
&\quad -Q_{3n}Q_nQ_{2n}^*Q_{2n}^*+4\cdot Q_{4n}Q_{3n}^*Q_n^*+Q_{4n}Q_{2n}^*Q_{2n}^*\\
&\quad -(2M-13)Q_{3n}Q_{2n}^*Q_n^*+7\cdot Q_{2n}Q_n^*Q_n^*\\
&\quad -2\left|Q_{4n}\right|^2+2(M-5)\left|Q_{3n}\right|^2-2\left|Q_{3n}\right|^2\left|Q_n\right|^2+2(M-6)\left|Q_{2n}\right|^2\\
&\quad -2\left|Q_{2n}\right|^2\left|Q_n\right|^2-\left|Q_n\right|^4+2(3M-11)\left|Q_n\right|^2-4M(M-6)\big].
\end{aligned}$$

$$\begin{aligned}
\langle 5\rangle_{4n,2n|3n,2n,n} &\equiv \langle\cos(n(4\phi_1+2\phi_2-3\phi_3-2\phi_4-\phi_5))\rangle \qquad \text{(G.27)}\\
&= \frac{1}{\binom{M}{5}5!}\sum_{\substack{i,j,k,l,m=1\\(i\neq j\neq k\neq l\neq m)}}^{M} e^{in(4\phi_i+2\phi_j-3\phi_k-2\phi_l-\phi_m)}\\
&= \frac{1}{\binom{M}{5}5!}\times\big[Q_{4n}Q_{2n}Q_{3n}^*Q_{2n}^*Q_n^*-Q_{6n}Q_{3n}^*Q_{2n}^*Q_n^*-Q_{5n}Q_nQ_{4n}^*Q_{2n}^*\\
&\quad -Q_{4n}Q_nQ_{3n}^*Q_{2n}^*-Q_{4n}Q_{2n}Q_{3n}^*Q_{3n}^*+Q_{6n}Q_{5n}^*Q_n^*\\
&\quad -Q_{4n}Q_{2n}^*Q_n^*Q_n^*-Q_{3n}Q_nQ_{2n}^*Q_{2n}^*\\
&\quad +3\cdot Q_{6n}Q_{4n}^*Q_{2n}^*+Q_{6n}Q_{3n}^*Q_{3n}^*+Q_{5n}Q_{4n}^*Q_n^*\\
&\quad +3\cdot Q_{5n}Q_{3n}^*Q_{2n}^*-(M-7)Q_{4n}Q_{3n}^*Q_n^*+3\cdot Q_{4n}Q_{2n}^*Q_{2n}^*\\
&\quad +7\cdot Q_{3n}Q_{2n}^*Q_n^*+4\cdot Q_{2n}Q_n^*Q_n^*-\left|Q_{3n}\right|^2\left|Q_{2n}\right|^2\\
&\quad -\left|Q_{4n}\right|^2\left|Q_{2n}\right|^2-\left|Q_{2n}\right|^2\left|Q_n\right|^2-2\left|Q_{6n}\right|^2\\
&\quad -2\left|Q_{5n}\right|^2+(M-8)\left|Q_{4n}\right|^2+(M-10)\left|Q_{3n}\right|^2\\
&\quad +2(M-7)\left|Q_{2n}\right|^2+(M-12)\left|Q_n\right|^2-2M(M-12)\big].
\end{aligned}$$

$$\begin{aligned}
\langle 5\rangle_{3n,2n|3n,n,n} &\equiv \langle\cos(n(3\phi_1+2\phi_2-3\phi_3-\phi_4-\phi_5))\rangle \qquad \text{(G.28)}\\
&= \frac{1}{\binom{M}{5}5!}\sum_{\substack{i,j,k,l,m=1\\(i\neq j\neq k\neq l\neq m)}}^{M} e^{in(3\phi_i+2\phi_j-3\phi_k-\phi_l-\phi_m)}\\
&= \frac{1}{\binom{M}{5}5!}\times\big[Q_{3n}Q_{2n}Q^*_{3n}Q^*_nQ^*_n-Q_{5n}Q^*_{3n}Q^*_nQ^*_n-2\cdot Q_{4n}Q_nQ^*_{3n}Q^*_{2n}\\
&\quad -Q_{3n}Q^*_nQ^*_nQ^*_n-2\cdot Q_{3n}Q_nQ^*_{2n}Q^*_{2n}+2\cdot Q_{5n}Q^*_{4n}Q^*_n\\
&\quad +3\cdot Q_{5n}Q^*_{3n}Q^*_{2n}+6\cdot Q_{4n}Q^*_{3n}Q^*_n+2\cdot Q_{4n}Q^*_{2n}Q^*_{2n}+9\cdot Q_{3n}Q^*_{2n}Q^*_n\\
&\quad -(M-8)Q_{2n}Q^*_nQ^*_n-|Q_{3n}|^2|Q_{2n}|^2-2|Q_{3n}|^2|Q_n|^2-2|Q_{5n}|^2\\
&\quad -4|Q_{4n}|^2+2(M-6)|Q_{3n}|^2+(M-12)|Q_{2n}|^2\\
&\quad +2(M-9)|Q_n|^2-2M(M-12)\big]\,.
\end{aligned}$$

$$\begin{aligned}
\langle 5\rangle_{3n,3n|3n,2n,n} &\equiv \langle\cos(n(3\phi_1+3\phi_2-3\phi_3-2\phi_4-\phi_5))\rangle \qquad \text{(G.29)}\\
&= \frac{1}{\binom{M}{5}5!}\sum_{\substack{i,j,k,l,m=1\\(i\neq j\neq k\neq l\neq m)}}^{M} e^{in(3\phi_i+3\phi_j-3\phi_k-2\phi_l-\phi_m)}\\
&= \frac{1}{\binom{M}{5}5!}\times\big[Q_{3n}Q_{3n}Q^*_{3n}Q^*_{2n}Q^*_n-Q_{6n}Q^*_{3n}Q^*_{2n}Q^*_n-Q_{5n}Q_nQ^*_{3n}Q^*_{3n}\\
&\quad -Q_{4n}Q_{2n}Q^*_{3n}Q^*_{3n}+3\cdot Q_{6n}Q^*_{3n}Q^*_{3n}+Q_{6n}Q^*_{4n}Q^*_{2n}+Q_{6n}Q^*_{5n}Q^*_n\\
&\quad +4\cdot Q_{5n}Q^*_{3n}Q^*_{2n}+4\cdot Q_{4n}Q^*_{3n}Q^*_n-2(M-6)Q_{3n}Q^*_{2n}Q^*_n\\
&\quad -2|Q_{3n}|^2|Q_{2n}|^2-2|Q_{6n}|^2-2|Q_{5n}|^2-2|Q_{4n}|^2\\
&\quad -|Q_{3n}|^4-2|Q_{3n}|^2|Q_n|^2+2(3M-10)|Q_{3n}|^2\\
&\quad +2(M-5)|Q_{2n}|^2+2(M-5)|Q_n|^2-4M(M-6)\big]\,.
\end{aligned}$$

$$\begin{aligned}
\langle 5\rangle_{3n,2n|2n,2n,n} &\equiv \langle\cos(n(3\phi_1+2\phi_2-2\phi_3-2\phi_4-\phi_5))\rangle \qquad \text{(G.30)}\\
&= \frac{1}{\binom{M}{5}5!}\sum_{\substack{i,j,k,l,m=1\\(i\neq j\neq k\neq l\neq m)}}^{M} e^{in(3\phi_i+2\phi_j-2\phi_k-2\phi_l-\phi_m)}\\
&= \frac{1}{\binom{M}{5}5!}\times\big[Q_{3n}Q_{2n}Q^*_{2n}Q^*_{2n}Q^*_n-Q_{5n}Q^*_{2n}Q^*_{2n}Q^*_n-Q_{3n}Q_nQ^*_{2n}Q^*_{2n}\\
&\quad -Q_{4n}Q_nQ^*_{3n}Q^*_{2n}+Q_{5n}Q^*_{4n}Q^*_n+4\cdot Q_{5n}Q^*_{3n}Q^*_{2n}+Q_{4n}Q^*_{3n}Q^*_n\\
&\quad +3\cdot Q_{4n}Q^*_{2n}Q^*_{2n}+4\cdot Q_{2n}Q^*_nQ^*_n-2(M-6)Q_{3n}Q^*_{2n}Q^*_n\\
&\quad -2|Q_{3n}|^2|Q_{2n}|^2-2|Q_{5n}|^2-2|Q_{4n}|^2\\
&\quad +2(M-5)|Q_{3n}|^2-2|Q_{2n}|^2|Q_n|^2-|Q_{2n}|^4\\
&\quad +2(3M-10)|Q_{2n}|^2+2(M-6)|Q_n|^2-4M(M-6)\big]\,.
\end{aligned}$$

$$
\begin{aligned}
\langle 5\rangle_{5n,n|3n,2n,n} &\equiv \langle \cos(n(5\phi_1+\phi_2-3\phi_3-2\phi_4-\phi_5))\rangle \qquad \text{(G.31)}\\
&= \frac{1}{\binom{M}{5}5!} \sum_{\substack{i,j,k,l,m=1\\(i\neq j\neq k\neq l\neq m)}}^{M} e^{in(5\phi_i+\phi_j-3\phi_k-2\phi_l-\phi_m)}\\
&= \frac{1}{\binom{M}{5}5!}\times\big[Q_{5n}Q_nQ^*_{3n}Q^*_{2n}Q^*_n-Q_{6n}Q^*_{3n}Q^*_{2n}Q^*_n-Q_{5n}Q_nQ^*_{3n}Q^*_{3n}\\
&\quad -Q_{4n}Q_nQ^*_{3n}Q^*_{2n}-Q_{5n}Q^*_{3n}Q^*_nQ^*_n-Q_{5n}Q^*_{2n}Q^*_{2n}Q^*_n\\
&\quad -Q_{5n}Q_nQ^*_{4n}Q^*_{2n}+3\cdot Q_{6n}Q^*_{5n}Q^*_n+Q_{6n}Q^*_{4n}Q^*_{2n}\\
&\quad +Q_{6n}Q^*_{3n}Q^*_{3n}+4\cdot Q_{5n}Q^*_{4n}Q^*_n-(M-7)Q_{5n}Q^*_{3n}Q^*_{2n}\\
&\quad +4\cdot Q_{4n}Q^*_{3n}Q^*_n+Q_{4n}Q^*_{2n}Q^*_{2n}+6\cdot Q_{3n}Q^*_{2n}Q^*_n\\
&\quad +3\cdot Q_{2n}Q^*_nQ^*_n-|Q_n|^2\,|Q_{3n}|^2-|Q_n|^2\,|Q_{5n}|^2-|Q_n|^2\,|Q_{2n}|^2\\
&\quad -2\,|Q_{6n}|^2+(M-8)\,|Q_{5n}|^2-4\,|Q_{4n}|^2+(M-10)\,|Q_{3n}|^2\\
&\quad +(M-10)\,|Q_{2n}|^2+2(M-7)\,|Q_n|^2-2M(M-12)\big]\,.
\end{aligned}
$$

G.5 6-particle azimuthal correlations

$$\begin{aligned}
\langle 6\rangle_{n,n,n|n,n,n} &\equiv \langle\cos(n(\phi_1+\phi_2+\phi_3-\phi_4-\phi_5-\phi_6))\rangle \qquad \text{(G.32)}\\
&= \frac{1}{\binom{M}{6}6!}\sum_{\substack{i,j,k,l,m,n=1\\(i\neq j\neq k\neq l\neq m\neq n)}}^{M} e^{in(\phi_i+\phi_j+\phi_k-\phi_l-\phi_m-\phi_n)}\\
&= \frac{1}{\binom{M}{6}6!}\times\big[\,|Q_n|^6+9\cdot|Q_{2n}|^2\,|Q_n|^2-6\cdot\mathfrak{Re}\,[Q_{2n}Q_nQ_n^*Q_n^*Q_n^*]\\
&\quad +4\cdot\mathfrak{Re}\,[Q_{3n}Q_n^*Q_n^*Q_n^*]-12\cdot\mathfrak{Re}\,[Q_{3n}Q_{2n}^*Q_n^*]\\
&\quad +18(M-4)\mathfrak{Re}\,[Q_{2n}Q_n^*Q_n^*]+4\cdot|Q_{3n}|^2\\
&\quad -9(M-4)(|Q_n|^4+|Q_{2n}|^2)+18(M-2)(M-5)\,|Q_n|^2\\
&\quad -6M(M-4)(M-5)\big]\,.
\end{aligned}$$

$$\begin{aligned}
\langle 6\rangle_{2n,n,n|2n,n,n} &\equiv \langle\cos(n(2\phi_1+\phi_2+\phi_3-2\phi_4-\phi_5-\phi_6))\rangle \qquad \text{(G.33)}\\
&= \frac{1}{\binom{M}{6}6!}\sum_{\substack{i,j,k,l,m,n=1\\(i\neq j\neq k\neq l\neq m\neq n)}}^{M} e^{in(2\phi_i+\phi_j+\phi_k-2\phi_l-\phi_m-\phi_n)}\\
&= \frac{1}{\binom{M}{6}6!}\times\big[\,|Q_n|^4\,|Q_{2n}|^2-4\cdot Q_{3n}Q_nQ_{2n}^*Q_n^*Q_n^*-2\cdot Q_{2n}Q_{2n}Q_{2n}^*Q_n^*Q_n^*\\
&\quad -4\cdot Q_{2n}Q_nQ_n^*Q_n^*Q_n^*+4\cdot Q_{3n}Q_n^*Q_n^*Q_n^*\\
&\quad +4\cdot Q_{4n}Q_{2n}^*Q_n^*Q_n^*+4\cdot Q_{3n}Q_nQ_{2n}^*Q_{2n}^*-8\cdot Q_{4n}Q_{3n}^*Q_n^*\\
&\quad -4\cdot Q_{4n}Q_{2n}^*Q_{2n}^*+4(2M-13)Q_{3n}Q_{2n}^*Q_n^*+2(7M-34)Q_{2n}Q_n^*Q_n^*\\
&\quad +4\,|Q_{4n}|^2+4\,|Q_{3n}|^2\,|Q_n|^2-4(M-6)\,|Q_{3n}|^2\\
&\quad +|Q_{2n}|^4-4(M-7)\,|Q_{2n}|^2\,|Q_n|^2\\
&\quad +(2M^2-27M+76)\,|Q_{2n}|^2+4(M^2-15M+34)\,|Q_n|^2\\
&\quad -(M-12)\,|Q_n|^4-2M(M^2-17M+60)\big]\,.
\end{aligned}$$

$$\begin{aligned}
\langle 6\rangle_{2n,2n|n,n,n,n} &\equiv \langle\cos(n(2\phi_1+2\phi_2-\phi_3-\phi_4-\phi_5-\phi_6))\rangle \qquad \text{(G.34)}\\
&= \frac{1}{\binom{M}{6}6!}\sum_{\substack{i,j,k,l,m,n=1\\(i\neq j\neq k\neq l\neq m\neq n)}}^{M} e^{in(2\phi_i+2\phi_j-\phi_k-\phi_l-\phi_m-\phi_n)}\\
&= \frac{1}{\binom{M}{6}6!}\times\big[Q_{2n}Q_{2n}Q_n^*Q_n^*Q_n^*Q_n^*-6\cdot Q_{2n}Q_{2n}Q_{2n}^*Q_n^*Q_n^*\\
&\quad -8\cdot Q_{2n}Q_nQ_n^*Q_n^*Q_n^*-Q_{4n}Q_n^*Q_n^*Q_n^*Q_n^*+8\cdot Q_{3n}Q_n^*Q_n^*Q_n^*\\
&\quad +6\cdot Q_{4n}Q_{2n}^*Q_n^*Q_n^*+8\cdot Q_{3n}Q_nQ_{2n}^*Q_{2n}^*-9\cdot Q_{4n}Q_{2n}^*Q_{2n}^*\\
&\quad -8\cdot Q_{4n}Q_{3n}^*Q_n^*-40\cdot Q_{3n}Q_{2n}^*Q_n^*+24(M-4)Q_{2n}Q_n^*Q_n^*\\
&\quad +6\left|Q_{4n}\right|^2+16\left|Q_{3n}\right|^2+3\left|Q_{2n}\right|^4+24\left|Q_n\right|^2\left|Q_{2n}\right|^2\\
&\quad -12(2M-7)\left|Q_{2n}\right|^2+12\left|Q_n\right|^4-48(M-3)\left|Q_n\right|^2+24M(M-5)\big].
\end{aligned}$$

$$\begin{aligned}
\langle 6\rangle_{3n,n|n,n,n,n} &\equiv \langle\cos(n(3\phi_1+\phi_2-\phi_3-\phi_4-\phi_5-\phi_6))\rangle \qquad \text{(G.35)}\\
&= \frac{1}{\binom{M}{6}6!}\sum_{\substack{i,j,k,l,m,n=1\\(i\neq j\neq k\neq l\neq m\neq n)}}^{M} e^{in(3\phi_i+\phi_j-\phi_k-\phi_l-\phi_m-\phi_n)}\\
&= \frac{1}{\binom{M}{6}6!}\times\big[Q_{3n}Q_nQ_n^*Q_n^*Q_n^*Q_n^*-4\cdot Q_{2n}Q_nQ_n^*Q_n^*Q_n^*\\
&\quad -Q_{4n}Q_n^*Q_n^*Q_n^*Q_n^*-6\cdot Q_{3n}Q_nQ_{2n}^*Q_n^*Q_n^*+6\cdot Q_{4n}Q_{2n}^*Q_n^*Q_n^*\\
&\quad +3\cdot Q_{3n}Q_nQ_{2n}^*Q_{2n}^*-4(M-5)\cdot Q_{3n}Q_n^*Q_n^*Q_n^*-14\cdot Q_{4n}Q_{3n}^*Q_n^*\\
&\quad -3\cdot Q_{4n}Q_{2n}^*Q_{2n}^*-4(3M-17)Q_{3n}Q_{2n}^*Q_n^*+12(M-6)Q_{2n}Q_n^*Q_n^*\\
&\quad +8\left|Q_{3n}\right|^2\left|Q_n\right|^2+12\left|Q_{2n}\right|^2\left|Q_n\right|^2+6\left|Q_{4n}\right|^2\\
&\quad -8(M-5)\left|Q_{3n}\right|^2-12(M-5)\left|Q_{2n}\right|^2-48(M-3)\left|Q_n\right|^2\\
&\quad +12\left|Q_n\right|^4+24M(M-5)\big].
\end{aligned}$$

$$
\begin{aligned}
\langle 6\rangle_{3n,2n,n|3n,2n,n} &\equiv \langle\cos(n(3\phi_1+2\phi_2+\phi_3-3\phi_4-2\phi_5-\phi_6))\rangle \qquad \text{(G.36)}\\
&= \frac{1}{\binom{M}{6}6!}\sum_{\substack{i,j,k,l,m,n=1\\(i\neq j\neq k\neq l\neq m\neq n)}}^{M} e^{in(3\phi_i+2\phi_j+\phi_k-3\phi_l-2\phi_m-\phi_n)}\\
&= \frac{1}{\binom{M}{6}6!}\times\big[\,|Q_{3n}|^2\,|Q_{2n}|^2\,|Q_n|^2-2\cdot Q_{5n}Q_nQ_{3n}^*Q_{2n}^*Q_n^*\\
&\quad -2\cdot Q_{4n}Q_{2n}Q_{3n}^*Q_{2n}^*Q_n^*-2\cdot Q_{3n}Q_{3n}Q_{3n}^*Q_{2n}^*Q_n^*\\
&\quad -2\cdot Q_{3n}Q_{2n}Q_{2n}^*Q_{2n}^*Q_n^*-2\cdot Q_{3n}Q_nQ_{2n}^*Q_n^*Q_n^*\\
&\quad -2\cdot Q_{3n}Q_{2n}Q_{3n}^*Q_n^*Q_n^*+4\cdot Q_{6n}Q_{3n}^*Q_{2n}^*Q_n^*\\
&\quad +2\cdot Q_{4n}Q_{2n}Q_{3n}^*Q_{3n}^*+6\cdot Q_{4n}Q_nQ_{3n}^*Q_{2n}^*+2\cdot Q_{5n}Q_nQ_{4n}^*Q_{2n}^*\\
&\quad +2\cdot Q_{5n}Q_nQ_{3n}^*Q_{3n}^*+2\cdot Q_{5n}Q_{2n}^*Q_{2n}^*Q_n^*+2\cdot Q_{5n}Q_{3n}^*Q_n^*Q_n^*\\
&\quad +6\cdot Q_{3n}Q_nQ_{2n}^*Q_{2n}^*+2\cdot Q_{4n}Q_{2n}^*Q_n^*Q_n^*+2\cdot Q_{3n}Q_n^*Q_n^*Q_n^*\\
&\quad -4\cdot Q_{6n}Q_{5n}^*Q_n^*-4\cdot Q_{6n}Q_{4n}^*Q_{2n}^*-6\cdot Q_{5n}Q_{4n}^*Q_n^*\\
&\quad -4\cdot Q_{6n}Q_{3n}^*Q_{3n}^*+2(M-11)Q_{5n}Q_{3n}^*Q_{2n}^*+2(M-13)Q_{4n}Q_{3n}^*Q_n^*\\
&\quad -8\cdot Q_{4n}Q_{2n}^*Q_{2n}^*+2(5M-32)Q_{3n}Q_{2n}^*Q_n^*+2(M-13)Q_{2n}Q_n^*Q_n^*\\
&\quad -(M-10)\,|Q_{3n}|^2\,|Q_{2n}|^2+|Q_{5n}|^2\,|Q_n|^2+|Q_{4n}|^2\,|Q_{2n}|^2\\
&\quad -(M-11)\,|Q_{3n}|^2\,|Q_n|^2-(M-10)\,|Q_{2n}|^2\,|Q_n|^2\\
&\quad +4\,|Q_{6n}|^2-(M-12)\,|Q_{5n}|^2-(M-16)\,|Q_{4n}|^2+|Q_{3n}|^4+|Q_{2n}|^4\\
&\quad +|Q_n|^4+(M^2-19M+68)\,|Q_{3n}|^2+(M^2-19M+72)\,|Q_{2n}|^2\\
&\quad +(M^2-20M+80)\,|Q_n|^2-M(M-12)(M-10)\big]\,.
\end{aligned}
$$

G.6 7-particle azimuthal correlations

$$
\begin{aligned}
\langle 7\rangle_{2n,n,n|n,n,n,n} &\equiv \langle\cos(n(2\phi_1+\phi_2+\phi_3-\phi_4-\phi_5-\phi_6-\phi_7))\rangle \qquad \text{(G.37)}\\
&= \frac{1}{\binom{M}{7}7!}\sum_{\substack{i,j,k,l,m,n,o=1\\(i\neq j\neq k\neq l\neq m\neq n\neq o)}}^{M} e^{in(2\phi_i+\phi_j+\phi_k-\phi_l-\phi_m-\phi_n-\phi_o)}\\
&= \frac{1}{\binom{M}{7}7!}\times\big[Q_{2n}Q_nQ_nQ_n^*Q_n^*Q_n^*Q_n^*+9\cdot Q_{2n}Q_{2n}Q_{2n}^*Q_n^*Q_n^*\\
&\quad +20\cdot Q_{3n}Q_nQ_{2n}^*Q_n^*Q_n^*-Q_{2n}Q_{2n}Q_n^*Q_n^*Q_n^*Q_n^*\\
&\quad -8(M-8)\cdot Q_{2n}Q_nQ_n^*Q_n^*Q_n^*\\
&\quad -2\cdot Q_{3n}Q_nQ_n^*Q_n^*Q_n^*Q_n^*+2\cdot Q_{4n}Q_n^*Q_n^*Q_n^*Q_n^*\\
&\quad -18\cdot Q_{4n}Q_{2n}^*Q_n^*Q_n^*-14\cdot Q_{3n}Q_nQ_{2n}^*Q_{2n}^*+8(M-7)Q_{3n}Q_n^*Q_n^*Q_n^*\\
&\quad +28\cdot Q_{4n}Q_{3n}^*Q_n^*+12\cdot Q_{4n}Q_{2n}^*Q_{2n}^*-8(5M-31)Q_{3n}Q_{2n}^*Q_n^*\\
&\quad +12(M^2-15M+46)Q_{2n}Q_n^*Q_n^*-12\,|Q_{4n}|^2-16\,|Q_{3n}|^2\,|Q_n|^2\\
&\quad +16(M-6)\,|Q_{3n}|^2-3\,|Q_{2n}|^4-6\,|Q_n|^4\,|Q_{2n}|^2\\
&\quad +12(2M-13)\,|Q_{2n}|^2\,|Q_n|^2-12(M-8)(M-4)\,|Q_{2n}|^2-4\,|Q_n|^6\\
&\quad +12(3M-14)\,|Q_n|^4-24(3M-7)(M-6)\,|Q_n|^2+24M(M-5)(M-6)\big]\,.
\end{aligned}
$$

G.7 8-particle azimuthal correlations

$$
\begin{aligned}
\langle 8\rangle_{n,n,n,n|n,n,n,n} &\equiv \langle\cos(n(\phi_1+\phi_2+\phi_3+\phi_4-\phi_5-\phi_6-\phi_7-\phi_8))\rangle \qquad \text{(G.38)}\\
&= \frac{1}{\binom{M}{8}8!}\sum_{\substack{i,j,k,l,m,n,o,p=1\\(i\neq j\neq k\neq l\neq m\neq n\neq o\neq p)}}^{M} e^{in(\phi_i+\phi_j+\phi_k+\phi_l-\phi_m-\phi_n-\phi_o-\phi_p)}\\
&= \frac{1}{\binom{M}{8}8!}\times\big[\,|Q_n|^8-12\cdot Q_{2n}Q_nQ_nQ_n^*Q_n^*Q_n^*Q_n^*\\
&\quad +6\cdot Q_{2n}Q_{2n}Q_n^*Q_n^*Q_n^*Q_n^*+16\cdot Q_{3n}Q_nQ_n^*Q_n^*Q_n^*Q_n^*\\
&\quad -96\cdot Q_{3n}Q_nQ_{2n}^*Q_n^*Q_n^*-12\cdot Q_{4n}Q_n^*Q_n^*Q_n^*Q_n^*\\
&\quad -36\cdot Q_{2n}Q_{2n}Q_{2n}^*Q_n^*Q_n^*+96(M-6)\cdot Q_{2n}Q_nQ_n^*Q_n^*Q_n^*\\
&\quad +72\cdot Q_{4n}Q_{2n}^*Q_n^*Q_n^*+48\cdot Q_{3n}Q_nQ_{2n}^*Q_{2n}^*\\
&\quad -64(M-6)\cdot Q_{3n}Q_n^*Q_n^*Q_n^*+192(M-6)\cdot Q_{3n}Q_{2n}^*Q_n^*\\
&\quad -96\cdot Q_{4n}Q_{3n}^*Q_n^*-36\cdot Q_{4n}Q_{2n}^*Q_{2n}^*\\
&\quad -144(M-7)(M-4)Q_{2n}Q_n^*Q_n^*+36\,|Q_{4n}|^2+64\,|Q_{3n}|^2\,|Q_n|^2\\
&\quad -64(M-6)\,|Q_{3n}|^2+9\,|Q_{2n}|^4+36\,|Q_n|^4\,|Q_{2n}|^2-144(M-6)\,|Q_{2n}|^2\,|Q_n|^2\\
&\quad +72(M-7)(M-4)(|Q_{2n}|^2+|Q_n|^4)-16(M-6)\,|Q_n|^6\\
&\quad -96(M-7)(M-6)(M-2)\,|Q_n|^2\\
&\quad +24M(M-7)(M-6)(M-5)\big]\,.
\end{aligned}
$$

Appendix H

$v_3\{5\}$

In this Appendix we will use particular 5-particle Q-cumulant to measure the strength of correlation between symmetry (participant) planes ψ_2 and ψ_3 of harmonics v_2 and v_3, respectively. We start from the observation that

$$QC\{5\} = \left\langle\left\langle e^{i(2\phi_1+2\phi_2+2\phi_3-3\phi_4-3\phi_5)}\right\rangle\right\rangle = v_2^3 v_3^2\,, \tag{H.1}$$

for the hypothetical case in which the symmetry planes of the harmonics v_2 and v_3 are the same. To demonstrate this, we use a Fourier-like p.d.f. parameterized only with harmonics v_2 and v_3:

$$f(\phi) = \frac{1}{2\pi}\left[1+2v_2\cos[2(\phi-\psi)]+2v_3\cos[3(\phi-\psi)]\right], \tag{H.2}$$

where ψ is the common hypothetical symmetry plane of harmonics v_2 and v_3. As an input to the simulation we set in the above p.d.f. $v_2 = 8.5\%$ and $v_3 = 2\%$, so that theoretically:

$$QC\{5\} = v_2^3 v_3^2 = 0.085^3 \cdot 0.02^2 = 2.4565 \cdot 10^{-7}\,. \tag{H.3}$$

After sampling from Eq. (H.2) azimuthal angles of 500 particles per event in a total of 10M events, taking each sampled particle in the analysis once and averaging over all distinct 5-particle tuples[1] according to Eq. (H.1), we have obtained:

$$QC\{5\} = (2.4408 \pm 0.0103) \cdot 10^{-7}\,. \tag{H.4}$$

In the second example we sample from Eq. (H.2) azimuthal angles of 250 particles per event in a total of 10M events and we take each sampled particle twice in the analysis in order to simulate a strong 2-particle nonflow correlation. After averaging over all distinct 5-particle tuples we have obtained:

$$QC\{5\} = (2.4104 \pm 0.0299) \cdot 10^{-7}\,. \tag{H.5}$$

[1] By distinct 5-particle tuple we mean a tuple $(\phi_1, \phi_2, \phi_3, \phi_4, \phi_5)$ where each angle in the tuple belongs to a different particle and ordering of angles within tuple matters.

Both results (H.4) and (H.5) are in an excellent agreement with the theoretical result (H.3). Result (H.4) indicates that the starting 5-particle correlator in Eq. (H.1) is indeed sensitive *only* to the product $v_2^3 v_3^2$ for the hypothetical case that v_2 and v_3 are sharing the same symmetry plane ψ, while result (H.5) indicates that for a detector with uniform acceptance this 5-particle correlator is also automatically the relevant 5-particle cumulant, as it correctly suppressed the added 2-particle nonflow correlation. In general, the symmetry planes of v_2 and v_3 are not the same and the 5-particle cumulant introduced here will also have a contribution from the correlation between ψ_2 and ψ_3, the symmetry planes of v_2 and v_3. Hence by measuring directly $QC\{5\}$ and estimating independently v_2 and v_3 (for instance via 4-particle cumulants), we have enough ingredients to isolate the value of correlation between ψ_2 and ψ_3 from the measured value of $QC\{5\}$. In particular, if $v_2\{4\}$ and $v_3\{4\}$ are not zero and if $QC\{5\}$ measured directly via 5-particle correlation techniques vanishes, this would immediately imply that the correlation between ψ_2 and ψ_3 is zero, meaning for instance that ψ_2 and ψ_3 are not the same symmetry planes.

Two additional remarks are in order, however. Firstly, for completeness sake we outline the generalized 5-particle cumulant applicable also for the case of the detector not having a uniform acceptance:

$$
\begin{aligned}
QC\{5\} &= 24\left\langle\left\langle e^{i2n\phi_1}\right\rangle\right\rangle^3\left\langle\left\langle e^{-i3n\phi_1}\right\rangle\right\rangle^2 \\
&-6\times\Big[3\left\langle\left\langle e^{i2n\phi_1}\right\rangle\right\rangle\left\langle\left\langle e^{-i3n\phi_1}\right\rangle\right\rangle^2\left\langle\left\langle e^{i2n(\phi_1+\phi_2)}\right\rangle\right\rangle \\
&+6\left\langle\left\langle e^{i2n\phi_1}\right\rangle\right\rangle^2\left\langle\left\langle e^{-i3n\phi_1}\right\rangle\right\rangle\left\langle\left\langle e^{in(2\phi_1-3\phi_2)}\right\rangle\right\rangle+\left\langle\left\langle e^{i2n\phi_1}\right\rangle\right\rangle^3\left\langle\left\langle e^{-i3n(\phi_1+\phi_2)}\right\rangle\right\rangle\Big] \\
&-\left\langle\left\langle e^{-i3n(\phi_1+\phi_2)}\right\rangle\right\rangle\left\langle\left\langle e^{i2n(\phi_1+\phi_2+\phi_3)}\right\rangle\right\rangle-6\left\langle\left\langle e^{in(2\phi_1-3\phi_2)}\right\rangle\right\rangle\left\langle\left\langle e^{in(2\phi_1+2\phi_2-3\phi_3)}\right\rangle\right\rangle \\
&-3\left\langle\left\langle e^{i2n(\phi_1+\phi_2)}\right\rangle\right\rangle\left\langle\left\langle e^{in(2\phi_1-3\phi_2-3\phi_3)}\right\rangle\right\rangle \\
&+2\times\Big[6\left\langle\left\langle e^{-i3n\phi_1}\right\rangle\right\rangle\left\langle\left\langle e^{in(2\phi_1-3\phi_2)}\right\rangle\right\rangle\left\langle\left\langle e^{i2n(\phi_1+\phi_2)}\right\rangle\right\rangle \\
&+6\left\langle\left\langle e^{i2n\phi_1}\right\rangle\right\rangle\left\langle\left\langle e^{in(2\phi_1-3\phi_2)}\right\rangle\right\rangle^2+3\left\langle\left\langle e^{i2n\phi_1}\right\rangle\right\rangle\left\langle\left\langle e^{i2n(\phi_1+\phi_2)}\right\rangle\right\rangle\left\langle\left\langle e^{-i3n(\phi_1+\phi_2)}\right\rangle\right\rangle \\
&+\left\langle\left\langle e^{-i3n\phi_1}\right\rangle\right\rangle^2\left\langle\left\langle e^{i2n(\phi_1+\phi_2+\phi_3)}\right\rangle\right\rangle+6\left\langle\left\langle e^{i2n\phi_1}\right\rangle\right\rangle\left\langle\left\langle e^{-i3n\phi_1}\right\rangle\right\rangle\left\langle\left\langle e^{in(2\phi_1+2\phi_2-3\phi_3)}\right\rangle\right\rangle \\
&+3\left\langle\left\langle e^{i2n\phi_1}\right\rangle\right\rangle^2\left\langle\left\langle e^{in(2\phi_1-3\phi_2-3\phi_3)}\right\rangle\right\rangle\Big] \\
&-2\left\langle\left\langle e^{-i3n\phi_1}\right\rangle\right\rangle\left\langle\left\langle e^{in(2\phi_1+2\phi_2+2\phi_3-3\phi_4)}\right\rangle\right\rangle-3\left\langle\left\langle e^{i2n\phi_1}\right\rangle\right\rangle\left\langle\left\langle e^{in(2\phi_1+2\phi_2-3\phi_3-3\phi_4)}\right\rangle\right\rangle \\
&+\left\langle\left\langle e^{in(2\phi_1+2\phi_2+2\phi_3-3\phi_4-3\phi_5)}\right\rangle\right\rangle . \qquad \text{(H.6)}
\end{aligned}
$$

Clearly, the only isotropic term in the above expression is the very last term, which means that for detectors with uniform acceptance for this particular case the 5-particle cumulant is identical to the starting 5-particle correlator in Eq. (H.1), i.e:

$$QC\{5\}=\left\langle\left\langle e^{in(2\phi_1+2\phi_2+2\phi_3-3\phi_4-3\phi_5)}\right\rangle\right\rangle . \qquad \text{(H.7)}$$

Secondly, we express analytically the single event 5-particle correlator,

$$\langle 5\rangle_{2n,2n,2n|3n,3n} \equiv \left\langle e^{in(2\phi_1+2\phi_2+2\phi_3-3\phi_4-3\phi_5)}\right\rangle \,, \tag{H.8}$$

in terms of Q-vectors in order to measure it with a single loop over all particles. To achieve this we start to decompose a product $Q_{2n}Q_{2n}Q_{2n}Q^*_{3n}Q^*_{3n}$. In its decomposition the following correlations occur with corresponding combinatorial coefficients:

$$\begin{aligned}
5-\text{particle} \quad &: \quad \langle 5\rangle_{2n,2n,2n|3n,3n} \times \binom{M}{5} 5!\,, \\
4-\text{particle} \quad &: \quad \langle 4\rangle_{2n,2n|n,3n} \times \binom{M}{3}(M-4)3\cdot 3!2!\,, \\
&\qquad\quad \langle 4\rangle_{4n,2n|3n,3n} \times \binom{M}{2}\binom{M-2}{2}2!\frac{3!}{2!}2!\,, \\
&\qquad\quad \langle 4\rangle_{2n,2n,2n|6n} \times \binom{M}{3}(M-4)3!\,, \\
3-\text{particle} \quad &: \quad \langle 3\rangle_{2n,2n|4n} \times \binom{M}{3}3\cdot 3!\,, \\
&\qquad\quad \langle 3\rangle_{n,2n|3n} \times \binom{M}{2}(M-2)2\frac{3!}{2!}2!\,, \\
&\qquad\quad \langle 3\rangle_{6n|3n,3n} \times \binom{M}{2}(M-2)2!\,, \\
&\qquad\quad \langle 3\rangle_{4n,2n|6n} \times \binom{M}{2}2(M-2)\frac{3!}{2!}\,, \\
&\qquad\quad \langle 3\rangle_{2n|n,n} \times \binom{M}{2}(M-2)3!2!\,, \\
&\qquad\quad \langle 3\rangle_{4n|n,3n} \times \binom{M}{2}(M-2)2\frac{3!}{2!}2!\,, \\
2-\text{particle} \quad &: \quad \langle 2\rangle_{3n|3n} \times \binom{M}{2}2\cdot 2!\,, \\
&\qquad\quad \langle 2\rangle_{2n|2n} \times \binom{M}{2}2\frac{3!}{2!}\,, \\
&\qquad\quad \langle 2\rangle_{6n|6n} \times M(M-1)\,, \\
&\qquad\quad \langle 2\rangle_{n|n} \times \binom{M}{2}2\frac{3!}{2!}2!\,, \\
&\qquad\quad \langle 2\rangle_{4n|4n} \times \binom{M}{2}2\frac{3!}{2!}\,, \\
1-\text{particle} \quad &: \quad 1\times M\,.
\end{aligned} \tag{H.9}$$

Working out all the combinatorial coefficients and solving the above decomposition for $\langle 5\rangle_{2n,2n,2n|3n,3n}$ it follows:

$$\begin{aligned}
\langle 5\rangle_{2n,2n,2n|3n,3n} &= \frac{Q_{2n}Q_{2n}Q_{2n}Q_{3n}^*Q_{3n}^*}{M(M-1)(M-2)(M-3)(M-4)} \\
&- \frac{1}{M-4}\Big[6\cdot\langle 4\rangle_{2n,2n|n,3n} + 3\cdot\langle 4\rangle_{4n,2n|3n,3n} + \langle 4\rangle_{2n,2n,2n|6n}\Big] \\
&- \frac{1}{(M-3)(M-4)}\Big[3\cdot\langle 3\rangle_{2n,2n|4n} + 6\cdot\langle 3\rangle_{n,2n|3n} \\
&+ \langle 3\rangle_{6n|3n,3n} + 3\cdot\langle 3\rangle_{4n,2n|6n} + 6\cdot\langle 3\rangle_{2n|n,n} + 6\cdot\langle 3\rangle_{4n|n,3n}\Big] \\
&- \frac{1}{(M-2)(M-3)(M-4)}\Big[2\cdot\langle 2\rangle_{3n|3n} + 3\cdot\langle 2\rangle_{2n|2n} \\
&+ \langle 2\rangle_{6n|6n} + 6\cdot\langle 2\rangle_{n|n} + 3\cdot\langle 2\rangle_{4n|4n}\Big] \\
&- \frac{1}{(M-1)(M-2)(M-3)(M-4)}\,. \qquad \text{(H.10)}
\end{aligned}$$

What remains to be done is to express each correlator in the above expression in terms of Q-vectors. The only new correlator here is $\langle 4\rangle_{4n,2n|3n,3n}$, the other ones can be related to the correlators obtained in the decomposition of $|Q_n|^8$, which was relevant for the calculation of the 8-particle cumulant. For correlation $\langle 4\rangle_{4n,2n|3n,3n}$ we have obtained the following analytic results:

$$\begin{aligned}
\langle 4\rangle_{4n,2n|3n,3n} &= \frac{Q_{4n}Q_{2n}Q_{3n}^*Q_{3n}^*}{M(M-1)(M-2)(M-3)} \\
&-\frac{1}{M-3}\Big[2\cdot\langle 3\rangle_{n,2n|3n} + \langle 3\rangle_{6n|3n,3n} + 2\cdot\langle 3\rangle_{4n|3n,n} + \langle 3\rangle_{4n,2n|6n}\Big] \\
&-\frac{1}{(M-2)(M-3)}\Big[2\cdot\langle 2\rangle_{3n|3n} + \langle 2\rangle_{2n|2n} + \langle 2\rangle_{4n|4n} + \langle 2\rangle_{6n|6n} + 2\cdot\langle 2\rangle_{n|n}\Big] \\
&-\frac{1}{(M-1)(M-2)(M-3)}\,, \qquad \text{(H.11)}
\end{aligned}$$

which gives, after inserting for each correlation the corresponding result in terms of Q-vectors (see Appendix G), the final relation for 4-particle correlator:

$$\begin{aligned}
\langle 4\rangle_{4n,2n|3n,3n} &= \frac{Q_{4n}Q_{2n}Q_{3n}^*Q_{3n}^* - Q_{4n}Q_{2n}Q_{6n}^* - Q_{6n}Q_{3n}^*Q_{3n}^*}{M(M-1)(M-2)(M-3)} \\
&- \frac{2Q_{4n}Q_{3n}^*Q_n^* + 2Q_nQ_{2n}Q_{3n}^* - |Q_{6n}|^2 - 2|Q_{4n}|^2}{M(M-1)(M-2)(M-3)} \\
&+ 2\frac{2|Q_{3n}|^2 + |Q_{2n}|^2 + |Q_n|^2 - 3M}{M(M-1)(M-2)(M-3)}\,. \qquad \text{(H.12)}
\end{aligned}$$

Inserting all results in Eq. (H.10) we have finally:

$$\begin{aligned}\langle 5\rangle_{2n,2n,2n|3n,3n} &= \frac{Q_{2n}Q_{2n}Q_{2n}Q^*_{3n}Q^*_{3n} - Q_{2n}Q_{2n}Q_{2n}Q^*_{6n} - 3Q_{4n}Q_{2n}Q^*_{3n}Q^*_{3n}}{M(M-1)(M-2)(M-3)(M-4)} \\ &- \frac{6Q_{2n}Q_{2n}Q^*_{n}Q^*_{3n} - 2Q_{6n}Q^*_{3n}Q^*_{3n} - 3Q_{4n}Q_{2n}Q^*_{6n}}{M(M-1)(M-2)(M-3)(M-4)} \\ &+ 6\frac{Q_{4n}Q^*_{n}Q^*_{3n} + Q_{2n}Q_{2n}Q^*_{4n} + 2Q_{2n}Q_{n}Q^*_{3n} + Q_{2n}Q^*_{n}Q^*_{n}}{M(M-1)(M-2)(M-3)(M-4)} \\ &- 2\frac{|Q_{6n}|^2 + 3|Q_{4n}|^2 + 6|Q_{3n}|^2 + 9|Q_{2n}|^2 + 6|Q_{n}|^2 - 12M}{M(M-1)(M-2)(M-3)(M-4)}\,. \end{aligned} \tag{H.13}$$

This is the analytic equation which enables the evaluation of $\langle 5\rangle_{2n,2n,2n|3n,3n}$, and correspondingly $QC\{5\}$, in a single loop over all particles. The example measurement of $QC\{5\}$, which was used in obtaining the results for Fig. 5.21 in Section 5.2.1, is presented in Fig. H.1.

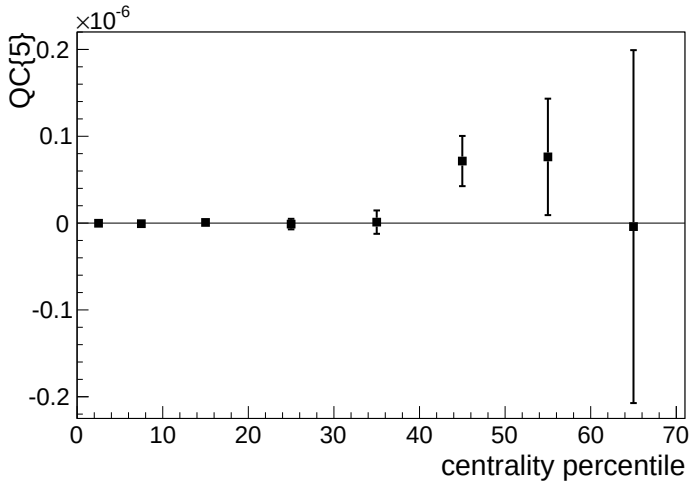

Figure H.1: Centrality dependence of $QC\{5\}$ for the ALICE Pb-Pb data.

Appendix I

Detailed derivations

In this appendix we provide detailed derivations for some of the results presented in the main part of the thesis. For convenience sake we repeat the definition of the Q-vector: In a single loop over all particles one has to evaluate:

$$Q_{k\cdot n} \equiv \sum_{i=1}^{M} e^{ik\cdot n\phi_i} \ (k = 1, 2, 3, \ldots)\,, \tag{I.1}$$

and all multi-particle azimuthal correlations can be expressed analytically it terms of Q-vectors evaluated (in general) in different harmonics, as now will be explicitly proven. The notation to be used in derivations bellow is understood as follows:

$$\langle k \rangle_{m_1,m_2,\ldots|\ldots,m_{k-1},m_k} \equiv \left\langle e^{i(m_1\phi_1+m_2\phi_2+\ldots-\ldots-m_{k-1}\phi_{k-1}-m_k\phi_k)} \right\rangle,\ \phi_1 \neq \phi_2 \neq \ldots \neq \phi_k, \tag{I.2}$$

and $\langle\cdot\rangle$ denotes a single-event average.

I.1 $\langle 2 \rangle$

To obtain $\langle 2 \rangle$ it suffices to decompose $|Q_n|^2$ which is straightforward from the definition (I.1) and is given by

$$|Q_n|^2 = \sum_{i,j=1}^{M} e^{in(\phi_i-\phi_j)}\,. \tag{I.3}$$

It is clear that the two summing indices i and j can be either the same or different in the above relation. Physically, when the indices are different we are correlating two different particles and when the indices are the same we are correlating particle to itself (autocorrelation). Hence in the decomposition of $|Q_n|^2$ we have 2-particle and 1-particle contributions with the following combinatorial coefficients:

$$\begin{aligned} 2-\text{particle} &: \langle 2 \rangle \cdot \binom{M}{2} 2!\,, \\ 1-\text{particle} &: 1 \cdot M\,. \end{aligned} \tag{I.4}$$

Written explicitly,

$$|Q_n|^2 = \langle 2 \rangle \cdot \binom{M}{2} 2! + 1 \cdot M \,, \tag{I.5}$$

which can be trivially solved to obtain $\langle 2 \rangle$. It follows that the average 2-particle azimuthal correlation event-by-event is given by

$$\langle 2 \rangle = \frac{|Q_n|^2 - M}{M(M-1)} \,, \tag{I.6}$$

where Q_n and M are the Q-vector and multiplicity of an event.

As a side remark we observe that the relation (I.6) can be trivially generalized to obtain the following result

$$\langle 2 \rangle_{kn|kn} = \frac{|Q_{kn}|^2 - M}{M(M-1)} \,, \qquad k = 1, 2, 3, \ldots \tag{I.7}$$

In the next section we outline the derivation for the 4-particle azimuthal correlation $\langle 4 \rangle$.

I.2 $\langle 4 \rangle$

This section we start by decomposing $|Q_n|^4$. From definition (I.1),

$$|Q_n|^4 = \sum_{i,j,k,l=1}^{M} e^{in(\phi_i + \phi_j - \phi_k - \phi_l)} \,. \tag{I.8}$$

In the above summation we can have four distinct cases for the indices i, j, k and l—either they are all different (4-particle correlation), either there are three different indices, either there are two different indices, or all indices are the same (autocorrelation). A very important thing to note, however, is that for instance for the case of three different indices we can end up either with a 3-particle correlation if the two indices which are the same are on the same side of the correlator (e.g. $\phi_i + \phi_i - \phi_k - \phi_l = 2\phi_i - \phi_k - \phi_l$) or with the 2-particle correlation if the two indices which are the same are on the opposite side of the correlator (e.g. $\phi_i + \phi_j - \phi_k - \phi_i = \phi_j - \phi_k$). Having this in mind, it follows that in the decomposition of $|Q_n|^4$ we have the following multi-particle correlations with

corresponding combinatorial coefficients:

$$\begin{aligned}
4-\text{particle} &: \langle 4 \rangle_{n,n|n,n} \cdot \binom{M}{4} 4!\,, \\
3-\text{particle} &: \langle 3 \rangle_{2n|n,n} \cdot M \binom{M-1}{2} 2!\,, \\
&\quad \langle 3 \rangle_{n,n|2n} \cdot M \binom{M-1}{2} 2!\,, \\
&\quad \langle 2 \rangle_{n|n} \cdot M(M-1)2!(M-2)2!\,, \\
2-\text{particle} &: \langle 2 \rangle_{n|n} \cdot M(M-1)2!2!\,, \\
&\quad \langle 2 \rangle_{2n|2n} \cdot M(M-1)\,, \\
&\quad 1 \cdot \binom{M}{2} 2!2!\,, \\
1-\text{particle} &: 1 \cdot M\,.
\end{aligned} \tag{I.9}$$

Written explicitly (after grouping some terms),

$$\begin{aligned}
|Q_n|^4 &= \langle 4 \rangle_{n,n|n,n} \cdot \binom{M}{4} 4! \\
&+ \left[\langle 3 \rangle_{2n|n,n} + \langle 3 \rangle_{n,n|2n} \right] \cdot M \binom{M-1}{2} 2! \\
&+ \langle 2 \rangle_{n|n} \cdot [(M(M-1)2!(M-2)2! + M(M-1)2!2!] \\
&+ \langle 2 \rangle_{2n|2n} \cdot M(M-1) + 1 \cdot \left[\binom{M}{2} 2!2! + M \right] .
\end{aligned} \tag{I.10}$$

The 2-particle correlations $\langle 2 \rangle_{n|n}$ and $\langle 2 \rangle_{2n|2n}$ were already expressed in terms of Q-vectors evaluated in harmonics n and $2n$, respectively (see Eq. (I.7)). What remained to be done here is to express $\langle 3 \rangle_{2n|n,n}$ and $\langle 3 \rangle_{n,n|2n}$ in analogous way. In order to accomplish this goal, we must decompose the terms which consist of Q-vectors evaluated in *different* harmonics. In particular, for $\langle 3 \rangle_{2n|n,n}$ and $\langle 3 \rangle_{n,n|2n}$ we have to decompose $Q_{2n}Q_n^*Q_n^*$ and $Q_nQ_nQ_{2n}^*$, respectively. It follows

$$\begin{aligned}
Q_{2n}Q_n^*Q_n^* &= \langle 3 \rangle_{2n|n,n} \cdot M \binom{M}{2} 2! + \langle 2 \rangle_{n|n} \cdot M(M-1)2! \\
&+ \langle 2 \rangle_{2n|2n} \cdot M(M-1) + 1 \cdot M\,.
\end{aligned} \tag{I.11}$$

After inserting from (I.7) the results for $\langle 2 \rangle_{n|n}$ and $\langle 2 \rangle_{2n|2n}$ we obtain

$$\langle 3 \rangle_{2n|n,n} = \frac{Q_{2n}Q_n^*Q_n^* - 2 \cdot |Q_n|^2 - |Q_{2n}|^2 + 2M}{M(M-1)(M-2)}\,. \tag{I.12}$$

Analogously,

$$\langle 3 \rangle_{n,n|2n} = \frac{Q_nQ_nQ_{2n}^* - 2 \cdot |Q_n|^2 - |Q_{2n}|^2 + 2M}{M(M-1)(M-2)}\,. \tag{I.13}$$

It is easy to see that

$$Q_n Q_n Q_{2n}^* = \left(Q_{2n} Q_n^* Q_n^* \right)^* \,, \tag{I.14}$$

so that

$$Q_n Q_n Q_{2n}^* + \left(Q_{2n} Q_n^* Q_n^* \right)^* = 2 \cdot \mathfrak{Re} \left[Q_{2n} Q_n^* Q_n^* \right] \,. \tag{I.15}$$

Taking into account this result we arrive at the following equality

$$\langle 3 \rangle_{n,n|2n} + \langle 3 \rangle_{2n|n,n} = 2 \, \frac{\mathfrak{Re} \left[Q_{2n} Q_n^* Q_n^* \right] - 2 \cdot |Q_n|^2 - |Q_{2n}|^2 + 2M}{M(M-1)(M-2)} \,, \tag{I.16}$$

which can be readily inserted in (I.10). We are now in a position to express the 4-particle correlation $\langle 4 \rangle \equiv \langle 4 \rangle_{n,n|n,n}$ in terms of Q-vectors. It follows,

$$\begin{aligned} \langle 4 \rangle &= \frac{|Q_n|^4 + |Q_{2n}|^2 - 2 \cdot \mathfrak{Re} \left[Q_{2n} Q_n^* Q_n^* \right]}{M(M-1)(M-2)(M-3)} \\ &- 2 \, \frac{2(M-2) \cdot |Q_n|^2 - M(M-3)}{M(M-1)(M-2)(M-3)} \,. \end{aligned} \tag{I.17}$$

In the next section we will climb up to the 6^{th} order.

I.3 $\langle 6 \rangle$

We start here by decomposing $|Q_n|^6$. By definition

$$|Q_n|^6 = \sum_{i,j,k,l,m,n=1}^{M} e^{in(\phi_i + \phi_j + \phi_k - \phi_l - \phi_m - \phi_n)} \,. \tag{I.18}$$

By following the same strategy as in the calculation of 4-particle azimuthal correlation in the previous section, the decomposition of $|Q_n|^6$ yields the following terms:

$$
\begin{aligned}
6-\text{particle} \quad &: \quad \langle 6 \rangle_{n,n,n|n,n,n} \cdot \binom{M}{6} 6!\,, \\
5-\text{particle} \quad &: \quad \langle 5 \rangle_{2n,n|n,n,n} \cdot \binom{M}{3} 3! \binom{M-3}{2} 2! \frac{3!}{2!}\,, \\
&\quad\;\; \langle 5 \rangle_{n,n,n|n,2n} \cdot \binom{M}{3} 3! \binom{M-3}{2} 2! \frac{3!}{2!}\,, \\
&\quad\;\; \langle 4 \rangle_{n,n|n,n} \cdot \binom{M}{4} 4!(M-4) \frac{3!}{2!} \frac{3!}{2!}\,, \\
4-\text{particle} \quad &: \quad \langle 4 \rangle_{3n|n,n,n} \cdot \binom{M}{3} 3!(M-3)\,, \\
&\quad\;\; \langle 4 \rangle_{n,n,n|3n} \cdot \binom{M}{3} 3!(M-3)\,, \\
&\quad\;\; \langle 4 \rangle_{2n,n|2n,n} \cdot \binom{M}{4} 4! \frac{3!}{2!} \frac{3!}{2!}\,, \\
&\quad\;\; \langle 4 \rangle_{n,n|n,n} \cdot \binom{M}{2} 2! \frac{3!}{2!} \binom{M-2}{2} 3!2!\,, \\
&\quad\;\; \langle 3 \rangle_{2n|n,n} \cdot M(M-1) \binom{M-2}{2} \frac{3!}{2!} 3!\,, \\
&\quad\;\; \langle 3 \rangle_{n,n|2n} \cdot M(M-1) \binom{M-2}{2} \frac{3!}{2!} 3!\,, \\
&\quad\;\; \langle 2 \rangle_{n|n} \cdot \binom{M}{2} (M-2)(M-3) 3!3!\,.
\end{aligned}
$$

Before writing down the remaining terms in the decomposition of $|Q_n|^6$ we remark that by correlating three or two different particles we can have the *same* type of correlation originating from completely different correlators. As an example for three different particles, both $\phi_i + \phi_i + \phi_i - \phi_i - \phi_j - \phi_k$ and $\phi_i + \phi_i + \phi_j - \phi_j - \phi_j - \phi_k$ are actually the same 3-particle correlation $\langle 3 \rangle_{2n|n,n}$ but with *different* combinatorial coefficients.

Having this in mind, the remaining terms in the decomposition of $|Q_n|^6$ are:

$$
\begin{aligned}
3-\text{particle} \quad : \quad & \langle 3\rangle_{3n|2n,n} \cdot \binom{M}{2} 2! \frac{3!}{2!}(M-2)\,, \\
& \langle 3\rangle_{2n,n|3n} \cdot \binom{M}{2} 2! \frac{3!}{2!}(M-2)\,, \\
& \langle 3\rangle_{2n|n,n} \cdot \left[\binom{M}{3} 3\cdot 3! + M(M-1)(M-2)\frac{3!}{2!}\frac{3!}{2!}\right]\,, \\
& \langle 3\rangle_{n|n,2n} \cdot \left[\binom{M}{3} 3\cdot 3! + M(M-1)(M-2)\frac{3!}{2!}\frac{3!}{2!}\right]\,, \\
& \langle 2\rangle_{2n|2n} \cdot \binom{M}{2} 2! \frac{3!}{2!}(M-2)\frac{3!}{2!}\,, \\
& \langle 2\rangle_{n|n} \cdot \left[M(M-1)(M-2)\frac{3!}{2!}\frac{3!}{2!} + M(M-1)(M-2)\frac{3!}{2!}3!2!\right]\,, \\
& 1 \cdot \binom{M}{3} 3!3!\,, \\
2-\text{particle} \quad : \quad & \langle 2\rangle_{3n|3n} \cdot M(M-1)\,, \\
& \langle 2\rangle_{2n|2n} \cdot M(M-1)\frac{3!}{2!}2!\,, \\
& \langle 2\rangle_{n|n} \cdot \left[M(M-1)\frac{3!}{2!}2! + M(M-1)\frac{3!}{2!}\frac{3!}{2!}\right]\,, \\
& 1 \cdot M(M-1)\frac{3!}{2!}\frac{3!}{2!}\,, \\
1-\text{particle} \quad : \quad & 1\cdot M\,.
\end{aligned}
\tag{I.19}
$$

We are just a half-way through. In the above decomposition the new terms which appear are[1] $\langle 5\rangle_{2n,n|n,n,n}$, $\langle 4\rangle_{3n|n,n,n}$, $\langle 4\rangle_{2n,n|2n,n}$ and $\langle 3\rangle_{3n|2n,n}$. In order to express these multi-particle correlations in terms of Q-vectors we must consider the decompositions of $Q_{2n}Q_nQ_n^*Q_n^*Q_n^*$, $Q_{3n}Q_n^*Q_n^*Q_n^*$, $Q_{2n}Q_nQ_{2n}^*Q_n^*$ and $Q_{3n}Q_{2n}^*Q_n^*$, respectively. Since this calculation is analogous to the calculations presented so far, we here just present the final results. But before doing so, we rewrite the decomposition of $|Q_n|^6$ (after grouping

[1] It is easy to see that

$$
\begin{aligned}
\langle 5\rangle_{n,n,n|n,2n} &= \langle 5\rangle^*_{2n,n|n,n,n}\,, \\
\langle 4\rangle_{n,n,n|3n} &= \langle 4\rangle^*_{3n|n,n,n}\,, \\
\langle 3\rangle_{2n,n|3n} &= \langle 3\rangle^*_{3n|2n,n}\,.
\end{aligned}
\tag{I.20}
$$

some terms),

$$
\begin{aligned}
|Q_n|^6 &= \binom{M}{6} 6!\, \langle 6 \rangle_{n,n,n|n,n,n} \\
&+ 3\binom{M}{5} 5! \left[\langle 5 \rangle_{2n,n|n,n,n} + \langle 5 \rangle_{n,n,n|n,2n} \right] \\
&+ \binom{M}{4} 4! \left[\langle 4 \rangle_{3n|n,n,n} + \langle 4 \rangle_{n,n,n|3n} + 9 \cdot \langle 4 \rangle_{2n,n|2n,n} + 9(M-2) \cdot \langle 4 \rangle_{n,n|n,n} \right] \\
&+ 3\binom{M}{3} 3! \left[\langle 3 \rangle_{3n|2n,n} + \langle 3 \rangle_{2n,n|3n} + (3M-5)(\langle 3 \rangle_{2n|n,n} + \langle 3 \rangle_{n,n|2n}) \right] \\
&+ \binom{M}{2} 2! \left[\langle 2 \rangle_{3n|3n} + 3(3M-4) \cdot \langle 2 \rangle_{2n|2n} + (18M^2 - 45M + 33) \cdot \langle 2 \rangle_{n|n} \right] \\
&+ M(6M^2 - 9M + 4)\,. \qquad \text{(I.21)}
\end{aligned}
$$

The required expressions for $\langle 5 \rangle_{2n,n|n,n,n}$, $\langle 4 \rangle_{3n|n,n,n}$, $\langle 4 \rangle_{2n,n|2n,n}$ and $\langle 3 \rangle_{3n|2n,n}$ are given as follows:

$$
\begin{aligned}
\langle 3 \rangle_{3n|2n,n} &= \frac{Q_{3n} Q_{2n}^* Q_n^* - M(M-1) \left[\langle 2 \rangle_{3n|3n} + \langle 2 \rangle_{2n|2n} + \langle 2 \rangle_{n|n} \right] - M}{M(M-1)(M-2)} \\
&= \frac{Q_{3n} Q_{2n}^* Q_n^* - |Q_{3n}|^2 - |Q_{2n}|^2 - |Q_n|^2 + 2M}{M(M-1)(M-2)}\,, \qquad \text{(I.22)}
\end{aligned}
$$

$$
\begin{aligned}
\langle 4 \rangle_{3n|n,n,n} &= \frac{Q_{3n} Q_n^* Q_n^* Q_n^*}{M(M-1)(M-2)(M-3)} - 3\,\frac{\langle 3 \rangle_{3n|2n,n} + \langle 3 \rangle_{2n|n,n}}{M-3} \\
&\quad - \frac{\langle 2 \rangle_{3n|3n} + 3 \cdot \langle 2 \rangle_{2n|2n} + 3 \cdot \langle 2 \rangle_{n|n}}{(M-2)(M-3)} - \frac{1}{(M-1)(M-2)(M-3)} \\
&= \frac{Q_{3n} Q_n^* Q_n^* Q_n^* - 3 \cdot Q_{3n} Q_{2n}^* Q_n^* - 3 \cdot Q_{2n} Q_n^* Q_n^*}{M(M-1)(M-2)(M-3)} \\
&\quad + \frac{2 \cdot |Q_{3n}|^2 + 3 \cdot |Q_{2n}|^2 + 6 \cdot |Q_n|^2 - 6M}{M(M-1)(M-2)(M-3)}\,, \qquad \text{(I.23)}
\end{aligned}
$$

$$
\begin{aligned}
\langle 4\rangle_{2n,n|2n,n} &= \frac{Q_{2n}Q_n^*Q_{2n}^*Q_n^*}{M(M-1)(M-2)(M-3)} \\
&\quad - \frac{\langle 3\rangle_{3n|2n,n} + \langle 3\rangle_{2n,n|3n} + \langle 3\rangle_{2n|n,n} + \langle 3\rangle_{n,n|2n}}{M-3} \\
&\quad - \frac{\langle 2\rangle_{3n|3n} + M\cdot\langle 2\rangle_{2n|2n} + (M+1)\cdot\langle 2\rangle_{n|n}}{(M-2)(M-3)} \\
&\quad - \frac{M}{(M-1)(M-2)(M-3)} \\
&= \frac{|Q_{2n}|^2\,|Q_n|^2 - 2\cdot\mathfrak{Re}\left[Q_{3n}Q_{2n}^*Q_n^*\right] - 2\cdot\mathfrak{Re}\left[Q_{2n}Q_n^*Q_n^*\right]}{M(M-1)(M-2)(M-3)} \\
&\quad + \frac{|Q_{3n}|^2 - (M-4)\cdot|Q_{2n}|^2 - (M-5)\cdot|Q_n|^2}{M(M-1)(M-2)(M-3)} \\
&\quad + \frac{M-6}{(M-1)(M-2)(M-3)}\,,
\end{aligned}
\tag{I.24}
$$

$$
\begin{aligned}
\langle 5\rangle_{2n,n|n,n,n} &= \frac{Q_{2n}Q_nQ_n^*Q_n^*Q_n^*}{M(M-1)(M-2)(M-3)(M-4)} \\
&\quad - \frac{\langle 4\rangle_{3n|n,n,n} + 3\cdot\langle 4\rangle_{2n,n|2n,n} + 3\cdot\langle 4\rangle_{n,n|n,n}}{(M-4)} \\
&\quad - \frac{3(M-1)\cdot\langle 3\rangle_{2n|n,n} + 3\cdot\langle 3\rangle_{n,n|2n} + 3\cdot\langle 3\rangle_{3n|2n,n} + \langle 3\rangle_{2n,n|3n}}{(M-3)(M-4)} \\
&\quad - \frac{\langle 2\rangle_{3n|3n} + (3M-2)\cdot\langle 2\rangle_{2n|2n} + (9M-11)\cdot\langle 2\rangle_{n|n}}{(M-2)(M-3)(M-4)} \\
&\quad - \frac{3M-2}{(M-1)(M-2)(M-3)(M-4)} \\
&= \frac{Q_{2n}Q_nQ_n^*Q_n^*Q_n^* - Q_{3n}Q_n^*Q_n^*Q_n^* + 6\cdot Q_{3n}Q_{2n}^*Q_n^*}{M(M-1)(M-2)(M-3)(M-4)} \\
&\quad - \frac{Q_{2n}Q_nQ_{3n}^* + 3(M-6)Q_{2n}Q_n^*Q_n^* + 3\cdot Q_nQ_nQ_{2n}^*}{M(M-1)(M-2)(M-3)(M-4)} \\
&\quad - \frac{2\cdot|Q_{3n}|^2 + 3\cdot|Q_{2n}|^2\,|Q_n|^2 - 3(M-4)\,|Q_{2n}|^2}{M(M-1)(M-2)(M-3)(M-4)} \\
&\quad - 3\,\frac{|Q_n|^4 - 2(2M-5)\,|Q_n|^2 + 2M(M-4)}{M(M-1)(M-2)(M-3)(M-4)}
\end{aligned}
\tag{I.25}
$$

Inserting all these results in the decomposition of $|Q_n|^6$ given in Eq. (I.21) and solving the resulting equation for $\langle 6 \rangle \equiv \langle 6 \rangle_{n,n,n|n,n,n}$ it follows,

$$\begin{aligned}
\langle 6 \rangle &= \frac{|Q_n|^6 + 9 \cdot |Q_{2n}|^2 |Q_n|^2 - 6 \cdot \mathfrak{Re}\left[Q_{2n} Q_n Q_n^* Q_n^* Q_n^*\right]}{M(M-1)(M-2)(M-3)(M-4)(M-5)} \\
&+4 \frac{\mathfrak{Re}\left[Q_{3n} Q_n^* Q_n^* Q_n^*\right] - 3 \cdot \mathfrak{Re}\left[Q_{3n} Q_{2n}^* Q_n^*\right]}{M(M-1)(M-2)(M-3)(M-4)(M-5)} \\
&+2 \frac{9(M-4) \cdot \mathfrak{Re}\left[Q_{2n} Q_n^* Q_n^*\right] + 2 \cdot |Q_{3n}|^2}{M(M-1)(M-2)(M-3)(M-4)(M-5)} \\
&-9 \frac{|Q_n|^4 + |Q_{2n}|^2}{M(M-1)(M-2)(M-3)(M-5)} \\
&+18 \frac{|Q_n|^2}{M(M-1)(M-3)(M-4)} \\
&-\frac{6}{(M-1)(M-2)(M-3)} \,. \qquad \text{(I.26)}
\end{aligned}$$

This relation completes the story at sixth order.

I.4 $\langle 8 \rangle$

In order to obtain the analytic expression for 8-particle azimuthal correlations we start by decomposing $|Q_n|^8$. By definition

$$|Q_n|^8 = \sum_{i,j,k,l,m,n,o,p=1}^{M} e^{in(\phi_i + \phi_j + \phi_k + \phi_l - \phi_m - \phi_n - \phi_o - \phi_p)} \,. \qquad \text{(I.27)}$$

By following the same strategy as in the calculation in previous sections we have obtained the following final result:

$$\begin{aligned}
\langle 8 \rangle &= \frac{1}{\binom{M}{8} 8!} \times \big[|Q_n|^8 - 12 \cdot Q_{2n} Q_n Q_n Q_n^* Q_n^* Q_n^* Q_n^* \\
&+6 \cdot Q_{2n} Q_{2n} Q_n^* Q_n^* Q_n^* Q_n^* + 16 \cdot Q_{3n} Q_n Q_n^* Q_n^* Q_n^* Q_n^* \\
&-96 \cdot Q_{3n} Q_n Q_{2n}^* Q_n^* Q_n^* - 12 \cdot Q_{4n} Q_n^* Q_n^* Q_n^* Q_n^* \\
&-36 \cdot Q_{2n} Q_{2n} Q_{2n}^* Q_n^* Q_n^* + 96(M-6) \cdot Q_{2n} Q_n Q_n^* Q_n^* Q_n^* \\
&+72 \cdot Q_{4n} Q_{2n}^* Q_n^* Q_n^* + 48 \cdot Q_{3n} Q_n Q_{2n}^* Q_{2n}^* \\
&-64(M-6) \cdot Q_{3n} Q_n^* Q_n^* Q_n^* + 192(M-6) \cdot Q_{3n} Q_{2n}^* Q_n^* \\
&-96 \cdot Q_{4n} Q_{3n}^* Q_n^* - 36 \cdot Q_{4n} Q_{2n}^* Q_{2n}^* \\
&-144(M-7)(M-4) Q_{2n} Q_n^* Q_n^* + 36 |Q_{4n}|^2 + 64 |Q_{3n}|^2 |Q_n|^2 \\
&-64(M-6) |Q_{3n}|^2 + 9 |Q_{2n}|^4 + 36 |Q_n|^4 |Q_{2n}|^2 - 144(M-6) |Q_{2n}|^2 |Q_n|^2 \\
&+72(M-7)(M-4)(|Q_{2n}|^2 + |Q_n|^4) - 16(M-6) |Q_n|^6 \\
&-96(M-7)(M-6)(M-2) |Q_n|^2 \\
&+24M(M-7)(M-6)(M-5) \big] \,. \qquad \text{(I.28)}
\end{aligned}$$

In the next section we outline the calculations for reduced multi-particle azimuthal correlations relevant for the differential flow.

I.5 $\langle 2' \rangle$ and $\langle 4' \rangle$

In this section we will outline the detailed calculation only for the most difficult case, namely when there is a full overlap between reference flow particles (RP) and particles of interest (POI). The other two cases, "no overlap" and "partial overlap," can be derived straightforwardly. But first we start by introducing some new notation and terminology.

By *reduced multi-particle azimuthal correlations* we mean the multi-particle correlations obtained after restricting one particle to belong only to the phase window of interest. For instance, later on we will have the reduced 2-particle azimuthal correlation denoted by $\langle 2' \rangle_{\underline{n}|n}$, where $'$ indicates that in the 2-particle correlator one particle will be taken *only* from the phase window of interest and $\underline{n}$ indicates the position of that particle in the correlator. Also, we will have $\langle 2' \rangle_{\underline{\underline{n}}|n}$, where $\underline{\underline{n}}$ indicates that in the 2-particle correlator we will have one particle necessarily out of the specified phase window interest. In order to distinguish which particles belong to the phase window of interest we introduce the following scheme:

1. when we are referring to any particle within an event, we label them by $i_1, i_2, ...$, where each of the indices runs from 1 to M (M is the multiplicity of that event);

2. subset of all particles from the phase window of interest we denote by A and particles belonging to that subset we label by $a_1, a_2, ...$, where each of the indices now runs from 1 to m (m is the number of particles in that subset);

3. subset of all particles not belonging to the phase window of interest we denote by B and label them by $b_1, b_2, ...$, where each of the indices here runs from 1 to $M - m$ ($M - m$ is the number of particles out of the phase window of interest).

In practice, phase window of interest can be a particular transverse momentum or rapidity bin, a subset filled only with identified particles (pions, protons, kaons), etc. Finally, the Q-vector built-up *only* from the particles belonging to the phase window of interest we denote by q_n. With the scheme outline above, it follows

$$q_n \equiv \sum_{a_1=1}^{m} e^{in\phi_{a_1}} \,. \tag{I.29}$$

There are several types of $2'$-particle correlations that we will use in this section.

Here are the corresponding definitions:

$$\langle 2' \rangle_{\underline{n}|n} \equiv \frac{1}{m(M-1)} \sum_{a_1=1}^{m} \sum_{\substack{i_1=1 \\ (i_1 \neq a_1)}}^{M} e^{in(\phi_{a_1} - \phi_{i_1})} , \tag{I.30}$$

$$\langle 2' \rangle_{n|\underline{n}} \equiv \langle 2' \rangle^*_{\underline{n}|n} , \tag{I.31}$$

$$\langle 2' \rangle_{\underline{n}|\underline{n}} \equiv \frac{1}{m(m-1)} \sum_{\substack{a_1,a_2=1 \\ (a_1 \neq a_2)}}^{m} e^{in(\phi_{a_1} - \phi_{a_2})} , \tag{I.32}$$

$$\langle 2' \rangle_{\underline{\underline{n}}|\underline{\underline{n}}} \equiv \frac{1}{(M-m)(M-m-1)} \sum_{\substack{b_1,b_2=1 \\ (b_1 \neq b_2)}}^{M-m} e^{in(\phi_{b_1} - \phi_{b_2})} , \tag{I.33}$$

$$\langle 2' \rangle_{\underline{\underline{n}}|\underline{n}} \equiv \frac{1}{(M-m)m} \sum_{b_1=1}^{M-m} \sum_{a_1=1}^{m} e^{in(\phi_{b_1} - \phi_{a_1})} , \tag{I.34}$$

$$\langle 2' \rangle_{\underline{n}|\underline{\underline{n}}} \equiv \langle 2' \rangle^*_{\underline{\underline{n}}|\underline{n}} . \tag{I.35}$$

All these $2'$-particle correlations can be expressed analytically in terms of Q_n's and q_n's. For instance, in order to get $\langle 2' \rangle_{\underline{n}|n}$ we consider the product $q_n Q_n^*$. From definitions (I.1) and (I.29) it follows,

$$q_n Q_n^* = \sum_{a_1=1}^{m} \sum_{i_1=1}^{M} e^{in(\phi_{a_1} - \phi_{i_1})} . \tag{I.36}$$

Two summing indices a_1 and i_1 in the above expression can be either the same or different. Separating these two distinct cases it follows,

$$q_n Q_n^* = m + \sum_{a_1=1}^{m} \sum_{\substack{i_1=1 \\ (i_1 \neq a_1)}}^{M} e^{in(\phi_{a_1} - \phi_{i_1})} . \tag{I.37}$$

Taking into account the definition (I.30) of $\langle 2' \rangle_{\underline{n}|n}$, it follows

$$q_n Q_n^* = m + m(M-1) \, \langle 2' \rangle_{\underline{n}|n} , \tag{I.38}$$

so that

$$\langle 2' \rangle_{\underline{n}|n} = \frac{q_n Q_n^* - m}{m(M-1)} . \tag{I.39}$$

Analogously,

$$\langle 2' \rangle_{n|\underline{n}} = \frac{Q_n q_n^* - m}{m(M-1)}\,, \tag{I.40}$$

$$\langle 2' \rangle_{\underline{n}|\underline{n}} = \frac{|q_n|^2 - m}{m(m-1)}\,, \tag{I.41}$$

$$\langle 2' \rangle_{\underline{\underline{n}}|\underline{\underline{n}}} = \frac{|Q_n - q_n|^2 - M + m}{(M-m)(M-m-1)}\,, \tag{I.42}$$

$$\langle 2' \rangle_{\underline{\underline{n}}|\underline{n}} = \frac{(Q_n - q_n)q_n^*}{(M-m)m}\,, \tag{I.43}$$

$$\langle 2' \rangle_{\underline{n}|\underline{\underline{n}}} = \frac{q_n(Q_n^* - q_n^*)}{(M-m)m}\,. \tag{I.44}$$

Now we move on to the reduced 3-particle correlations.

The reduced 3-particle correlations that we will need in the subsequent sections are defined in the following way:

$$\langle 3' \rangle_{\underline{2n}|n,n} \equiv \frac{1}{m(M-1)(M-2)} \sum_{a_1=1}^{m} \sum_{\substack{i_1,i_2=1 \\ (i_1 \neq i_2 \neq a_1)}}^{M} e^{in(2\phi_{a_1} - \phi_{i_1} - \phi_{i_2})}\,, \tag{I.45}$$

$$\langle 3' \rangle_{\underline{n},n|2n} \equiv \frac{1}{m(M-1)(M-2)} \sum_{a_1=1}^{m} \sum_{\substack{i_1,i_2=1 \\ (i_1 \neq i_2 \neq a_1)}}^{M} e^{in(\phi_{a_1} + \phi_{i_1} - 2\phi_{i_2})}\,. \tag{I.46}$$

In order to get $\langle 3' \rangle_{\underline{2n}|n,n}$ expressed solely in terms of Q_n's and q_n's, we consider the decomposition of $q_{2n}Q_n^*Q_n^*$. It follows,

$$\begin{aligned} q_{2n}Q_n^*Q_n^* &= m(M-1)(M-2)\,\langle 3' \rangle_{\underline{2n}|n,n} + m(M-1)2!\,\langle 2' \rangle_{\underline{n}|n} \\ &+ m(M-1)\,\langle 2' \rangle_{\underline{2n}|2n} + m\,. \end{aligned} \tag{I.47}$$

Relation (I.39) can be trivially generalized to obtain

$$\langle 2' \rangle_{\underline{2n}|2n} = \frac{q_{2n}Q_{2n}^* - m}{m(M-1)}\,. \tag{I.48}$$

After inserting (I.39) and (I.48) into (I.47) and solving for $\langle 3' \rangle_{\underline{2n}|n,n}$ we arrive at

$$\langle 3' \rangle_{\underline{2n}|n,n} = \frac{q_{2n}Q_n^*Q_n^* - q_{2n}Q_{2n}^* - 2q_nQ_n^* + 2m}{m(M-1)(M-2)}\,. \tag{I.49}$$

On the other hand, in order to get the analogous expression for $\langle 3' \rangle_{\underline{n},n|2n}$ we decompose $q_nQ_n^*Q_{2n}^*$. It follows,

$$\begin{aligned} q_nQ_n^*Q_{2n}^* &= m(M-1)(M-2)\,\langle 3' \rangle_{\underline{n},n|2n} + m(M-1)\,\langle 2' \rangle_{\underline{2n}|2n} \\ &+ m(M-1)\,\langle 2' \rangle_{\underline{n}|n} + m(M-1)\,\langle 2' \rangle_{n|\underline{n}} + m\,. \end{aligned} \tag{I.50}$$

Inserting here the required expressions for reduced 2-particle correlations obtained before and solving for $\langle 3' \rangle_{\underline{n},n|2n}$ we obtain,

$$\langle 3' \rangle_{\underline{n},n|2n} = \frac{q_n Q_n Q_{2n}^* - q_{2n} Q_{2n}^* - 2 \cdot \mathfrak{Re}\left[q_n Q_n^*\right] + 2m}{m(M-1)(M-2)} \,. \tag{I.51}$$

Finally, we outline now the detailed calculation for the reduced 4-particle correlation.

The reduced four-particle correlation that we will use to calculate differential flow is defined as

$$\langle 4' \rangle_{\underline{n},n|n,n} \equiv \frac{1}{m(M-1)(M-2)(M-3)} \sum_{a_1=1}^{m} \sum_{\substack{i_1,i_2,i_3=1 \\ (a_1 \neq i_1 \neq i_2 \neq i_3)}}^{M} e^{in(\phi_{a_1} + \phi_{i_1} - \phi_{i_2} - \phi_{i_3})}. \tag{I.52}$$

To express the reduced four-particle correlation $\langle 4' \rangle_{\underline{n},n|n,n}$ in terms of Q_n's and q_n's, we start by decomposing the product $q_n Q_n Q_n^* Q_n^*$. From the definitions (I.1) and (I.29) it follows,

$$q_n Q_n Q_n^* Q_n^* = \sum_{a_1=1}^{m} \sum_{i_1,i_2,i_3=1}^{M} e^{in(\phi_{a_1} + \phi_{i_1} - \phi_{i_2} - \phi_{i_3})} \,. \tag{I.53}$$

When all four summing indices in above relation are different we have

$$4-\text{particle} \quad : \quad \langle 4' \rangle_{\underline{n},n|n,n} \cdot m(M-1)(M-2)(M-3) \,. \tag{I.54}$$

When there are three different indices in (I.53) we can have four distinct cases in the correlator, namely $\phi_{a_1} + \phi_{a_1} - \phi_{i_1} - \phi_{i_2}$, $\phi_{a_1} + \phi_{i_1} - \phi_{i_2} - \phi_{i_2}$, $\phi_{a_1} + \phi_{i_1} - \phi_{i_1} - \phi_{i_2}$ and $\phi_{a_1} + \phi_{i_1} - \phi_{a_1} - \phi_{i_2}$. First three cases are straightforward to calculate, but the last one is more tricky and deserves a special treatment. Naïvely one would immediately cancel ϕ_{a_1} on both sides of the correlator, but that is *wrong*.[2] More careful analysis of this particular correlator reveals that we must disentangle it in four distinct sub-cases, each of which gives a *different* reduced 2-particle correlation. In particular:

$$\begin{aligned}
i_1, i_2 \in A \quad &: \quad (m-2)m(m-1) \cdot \langle 2' \rangle_{\underline{n}|\underline{n}} \,, \\
i_1 \in A, i_2 \in B \quad &: \quad (m-1)m(M-m) \cdot \langle 2' \rangle_{\underline{n}|\underline{\underline{n}}} \,, \\
i_1 \in B, i_2 \in A \quad &: \quad (m-1)(M-m)m \cdot \langle 2' \rangle_{\underline{\underline{n}}|\underline{n}} \,, \\
i_1, i_2 \in B \quad &: \quad m(M-m)(M-m-1) \cdot \langle 2' \rangle_{\underline{\underline{n}}|\underline{\underline{n}}} \,.
\end{aligned} \tag{I.55}$$

Taking into account these subtleties, for the case of three different indices in (I.50) we

[2] One must keep in mind that here we are dealing with a *constrained summations*.

have finally:

$$\begin{aligned}
3-\text{particle} \quad : \quad & \langle 3' \rangle_{\underline{2n}|n,n} \cdot m(M-1)(M-2)\,, \\
& \langle 3' \rangle_{\underline{n},n|2n} \cdot m(M-1)(M-2)\,, \\
& \langle 2' \rangle_{\underline{n}|n} \cdot (M-2)m(M-1)2!\,, \\
& \langle 2' \rangle_{\underline{n}|\underline{n}} \cdot (m-2)m(m-1)2!\,, \\
& \langle 2' \rangle_{\underline{n}|\underline{\underline{n}}} \cdot (m-1)m(M-m)2!\,, \\
& \langle 2' \rangle_{\underline{\underline{n}}|\underline{n}} \cdot (m-1)(M-m)m\,2!\,, \\
& \langle 2' \rangle_{\underline{\underline{n}}|\underline{\underline{n}}} \cdot m(M-m)(M-m-1)2!\,.
\end{aligned} \tag{I.56}$$

When there are two different indices in (I.53) the only tricky thing to note is that correlators $\phi_{a_1}+\phi_{a_1}-\phi_{a_1}-\phi_{i_1}$ and $\phi_{a_1}+\phi_{i_1}-\phi_{i_1}-\phi_{i_1}$ give rise to the same correlation $\langle 2' \rangle_{\underline{n}|n}$ but with a different combinatorial coefficient. Hence,

$$\begin{aligned}
2-\text{particle} \quad : \quad & \langle 2' \rangle_{\underline{n}|n} \cdot [m(M-1)2! + m(M-1)]\ , \\
& \langle 2' \rangle_{n|\underline{n}} \cdot m(M-1)\,, \\
& \langle 2' \rangle_{\underline{2n}|2n} \cdot m(M-1)\,, \\
& 1 \cdot m(M-1)2!\,.
\end{aligned} \tag{I.57}$$

Finally, when all indices in (I.53) are the same it follows trivially

$$1-\text{particle} \quad : \quad 1 \cdot m\,. \tag{I.58}$$

After inserting in the above decomposition all reduced 2- and 3-particle azimuthal correlations expressed in terms of Q_n's and q_n's and after solving the resulting equation for $\langle 4' \rangle_{\underline{n},n|n,n}$ we arrive at the final expression,

$$\begin{aligned}
\langle 4' \rangle_{\underline{n},n|n,n} \quad = \quad & \frac{q_n Q_n Q_n^* Q_n^* - q_{2n} Q_n^* Q_n^* - q_n Q_n Q_{2n}^* + q_{2n} Q_{2n}^*}{m(M-1)(M-2)(M-3)} \\
- \quad & 2\,\frac{m|Q_n|^2 + (M-3) q_n Q_n^* - Q_n q_n^*}{m(M-1)(M-2)(M-3)} \\
+ \quad & \frac{2}{(M-1)(M-2)}\,.
\end{aligned} \tag{I.59}$$

Eq. (I.59) is the analytic expression for reduced 4-particle correlations for the case of full overlap between RPs and POIs—the generalization to the expression which will also cover the cases of "no overlap" and "partial overlap" is straightforward.

Appendix J

Isolating cumulants from correlations

In this Appendix we present how from any multi-particle correlation one can isolate the corresponding multi-particle cumulant, i.e. the contribution to the correlation involving *all* particles in the correlator. First we demonstrate the explicit calculation, which eventually we abandon because it becomes rather tedious already for correlations involving four random observables. Due to this we present and utilize the analytic expression which generates cumulants for any number of random observables. Finally, we provide the implementation of this analytic expression in MATHEMATICA, which shall be used in practice to quickly isolate cumulants from correlations. The reader not interested in the details, but only in the final outcome can immediately move to Fig. J.1 and skip the rest of this Appendix. In what follows we use notation and conventions introduced in Kubo's paper [66], and we start by considering the simplest case, namely the correlation of two random observables (to which we will equivalently refer to as 2-particle correlation, and analogously for correlations involving more than two random observables).

In the most general case the correlation of two random observables X_1 and X_2 can be decomposed as follows:

$$\langle X_1 X_2 \rangle = \langle X_1 \rangle \langle X_2 \rangle + \langle X_1 X_2 \rangle_c \, . \tag{J.1}$$

If two random observables X_1 and X_2 are statistically independent, then their joint p.d.f. factorizes which translates into

$$\langle X_1 X_2 \rangle = \langle X_1 \rangle \langle X_2 \rangle \, , \quad X_1, X_2 \text{ independent} \, . \tag{J.2}$$

Hence the term $\langle X_1 X_2 \rangle_c$ in Eq. (J.1) quantifies only the *genuine* 2-particle correlation which cannot be decomposed further. By definition this term is the 2-particle cumulant. Trivially,

$$\langle X_1 X_2 \rangle_c = \langle X_1 X_2 \rangle - \langle X_1 \rangle \langle X_2 \rangle \, . \tag{J.3}$$

All quantities on the RHS in (J.3) are accessible experimentally, and in this way one can from any 2-particle correlation, $\langle X_1 X_2 \rangle$, isolate the genuine 2-particle correlation,

i.e. the 2-particle cumulant $\langle X_1 X_2 \rangle_c$. When it comes to 3-particle correlations, in the most general case we have:

$$\begin{aligned} \langle X_1 X_2 X_3 \rangle &= \langle X_1 \rangle \langle X_2 \rangle \langle X_3 \rangle \\ &+ \langle X_1 X_2 \rangle_c \langle X_3 \rangle + \langle X_1 X_3 \rangle_c \langle X_2 \rangle + \langle X_2 X_3 \rangle_c \langle X_1 \rangle \\ &+ \langle X_1 X_2 X_3 \rangle_c \,. \end{aligned} \tag{J.4}$$

The term in the first line in above equation corresponds to the case when three random observables X_1, X_2 and X_3 are statistically independent, i.e. their joint p.d.f. factorizes. The three distinct terms in the second line in Eq. (J.4) correspond to the case when there is some genuine 2-particle correlation in the system, and the three distinct terms originate from the fact that the genuine 2-particle correlation can occur in three distinct ways among the starting three random observables. Finally, the last line in Eq. (J.4) denotes the genuine 3-particle correlation which cannot be decomposed any further—by definition this term is the 3-particle cumulant. To determine the 3-particle cumulant experimentally, one cannot utilize Eq. (J.4) directly. Instead, one has to insert result (J.3) for the genuine 2-particle correlations and solve the resulting expression for 3-particle cumulant $\langle X_1 X_2 X_3 \rangle_c$. After some algebra it follows:

$$\begin{aligned} \langle X_1 X_2 X_3 \rangle_c &= \langle X_1 X_2 X_3 \rangle \\ &- \langle X_1 X_2 \rangle \langle X_3 \rangle - \langle X_1 X_3 \rangle \langle X_2 \rangle - \langle X_2 X_3 \rangle \langle X_1 \rangle \\ &+ 2 \langle X_1 \rangle \langle X_2 \rangle \langle X_3 \rangle \,. \end{aligned} \tag{J.5}$$

All expressions in the RHS in the above equation are accessible experimentally, and in this way from the starting three particle correlation, $\langle X_1 X_2 X_3 \rangle$, one can isolate the corresponding 3-particle cumulant $\langle X_1 X_2 X_3 \rangle_c$. Clearly, by following the above procedure, for any number of particles in the correlator there will be always a unique, well defined, term in the decomposition which cannot be decomposed further—by definition this is cumulant—and such term can be expressed in terms of correlations consisting of same number and fewer number of random variables, the terms all of which are accessible experimentally.

However, it is rather tedious and impractical to isolate cumulants from correlations by following the prescription outlined above for correlations involving four and more random observables. Luckily, mathematicians came before us and provided us with an expression which automatically isolates cumulants from correlations, for any number of random observables. Now we outline and discuss that expression. We start by taking Eq. (2.9) from Kubo's paper [66]:

$$\kappa\{n\} = \sum (l-1)! \, (-)^{l-1} \sum_{\sum_{i=1}^{l} \{m_i\} = \{n\}} \prod_{i=1}^{l} \mu\{m_i\} \,. \tag{J.6}$$

This cryptic equation apparently has to be decrypted first. We start from the LHS. $\kappa\{n\}$ is the n-particle cumulant, which previously was denoted as $\langle X_1 X_2 \cdots X_n \rangle_c$. The first summation on the RHS goes from $l=1$ to $l=n$, where n stands for the total number

of random observables. One forms the set from the available n random observables:

$$\{n\} \equiv (X_1, X_2, \ldots, X_n)\,. \tag{J.7}$$

With such construction the index l in Eq. (J.6) labels all distinct partitions of set $\{n\}$ into its subsets. For instance, the set of three elements can be partitioned in three distinct ways: a) in three subsets, each containing one element; b) in two subsets, first containing two elements and second containing one element, and c) in one subset containing all elements. Each distinct partition can have few instances. For example, due to permutations, in case b) we can out of starting three elements form the subset having two elements in three different ways. In another example, if original set is having four elements and we consider distinct partition of it in two subsets, than in one case we can have first subset containing one element and second three elements, or in another case we can have both subsets containing two elements. For each distinct partition, labeled with index l, its different instances are encapsulated with the expression $\sum_{i=1}^{l}\{m_i\} = \{n\}$ in the index of second summation in Eq. (J.6). For instance, for $n=3$, we have three distinct partitions, depending on the value of index l: a) $l = 1 \Rightarrow \{m_1\} = \{3\}$, i.e. original set is its own subset; b) $l = 2 \Rightarrow \{m_1\} + \{m_2\} = \{3\}$, i.e. original set is split in two subsets, the first one containing m_1 elements and the seconds one m_2 elements; and c) $l = 3 \Rightarrow \{m_1\} + \{m_2\} + \{m_3\} = \{3\}$, i.e. original set is split in three subsets, containing m_1, m_2 and m_3 elements, respectively. The index i in Eq. (J.6) labels i-th subset in the particular instance of particular partition of the starting set $\{n\}$. m_i is the number of elements in such i-th subset, and $\{m_i\}$ is notation for such subset. Hence the second summation in Eq. (J.6) runs first over all subsets in particular instance of particular partition of the starting set $\{n\}$, and than over all instances. Finally, $\mu\{m_i\}$ is correlation of all random variables in subset $\{m_i\}$. In order to clarify this further, we evaluate expression (J.6) explicitly for two simplest cases, namely $n = 2$ and $n = 3$.

- $\mathbf{n = 2}$. This is the case of 2-particle correlations. One starts by forming a set $\{2\} \equiv (X_1, X_2)$, where X_1 and X_2 are two random observables. There are two distinct partitions of set $\{2\}$, each of which we label with different index l:

$$\begin{aligned} l = 1: &\qquad (X_1, X_2) = (X_1, X_2)\,, \\ l = 2: &\qquad (X_1, X_2) = (X_1) + (X_2)\,. \end{aligned}$$

  In this particular example, for each distinct partition there is always a unique way to form it, which means that for each l the second summation in Eq. (J.6) will be evaluated only once. For $l = 1$ the index i in Eq. (J.6) runs only over subset (X_1, X_2) (each set is automatically its own subset), so that $\{m_1\} = (X_1, X_2)$, and $\mu\{m_1\} = \langle X_1 X_2\rangle$. For $l=2$ the index i in Eq. (J.6) runs over two subsets, namely (X_1) and (X_2), so that $\{m_1\} = (X_1)$ and $\{m_2\} = (X_2)$, i.e. $\mu\{m_1\} = \langle X_1\rangle$ and $\mu\{m_2\} = \langle X_2\rangle$. It follows:

$$\kappa\{2\} \;=\; 0!(-1)^0\mu\{m_1\} + 1!(-1)^1\mu\{m_1\}\mu\{m_2\}\,, \tag{J.8}$$

  i.e.

$$\langle X_1 X_2\rangle_c = \langle X_1 X_2\rangle - \langle X_1\rangle\langle X_2\rangle\,, \tag{J.9}$$

  in agreement with result (J.3) derived explicitly.

- $\mathbf{n = 3}$. This is the case of 3-particle correlations. One starts by forming a set $\{3\} \equiv (X_1, X_2, X_3)$, where X_1, X_2 and X_3 are three random observables of interest. Distinct partitions of set $\{3\}$ are:

$$\begin{aligned} l = 1: \quad & (X_1, X_2, X_3) = (X_1, X_2, X_3)\,, \\ l = 2: \quad & (X_1, X_2, X_3) = (X_1, X_2) + (X_3)\,, \\ & (X_1, X_2, X_3) = (X_1, X_3) + (X_2)\,, \\ & (X_1, X_2, X_3) = (X_2, X_3) + (X_1)\,, \\ l = 3: \quad & (X_1, X_2, X_3) = (X_1) + (X_2) + (X_3)\,. \end{aligned}$$

We see that due to permutations the partition labeled with $l = 2$ allows three different instances. This means that now for $l = 2$ the second summation in Eq. (J.6) will be evaluated three times, each time for different instance. On the other hand, for partitions labeled with $l = 1$ and $l = 3$, the second summation in Eq. (J.6) will be evaluated only once, because these partitions have only one instance. It follows:

$$\begin{aligned} \kappa\{3\} &= 0!(-1)^0 \mu\{m_1\} \\ &+ 1!(-1)^1 \times [\mu\{m_1\}\mu\{m_2\} + \mu\{m_1\}\mu\{m_2\} + \mu\{m_1\}\mu\{m_2\}] \\ &+ 2!(-1)^2 \mu\{m_1\}\mu\{m_2\}\mu\{m_3\}\,. \end{aligned} \tag{J.10}$$

Each subset $\{m_i\}$ in the above expression corresponds to a different subset on the RHS of decomposition (J.10). Replacing each $\{m_i\}$ with the corresponding subset, we have:

$$\begin{aligned} \kappa\{3\} &= \mu\{X_1, X_2, X_3\} \\ &+ (-1) \times [\mu\{X_1, X_2\}\mu\{X_3\} + \mu\{X_1, X_3\}\mu\{X_2\} + \mu\{X_2, X_3\}\mu\{X_1\}] \\ &+ 2\mu\{X_1\}\mu\{X_2\}\mu\{X_3\}\,, \end{aligned} \tag{J.11}$$

or utilizing the previous notation for cumulants and correlations

$$\begin{aligned} \langle X_1 X_2 X_3 \rangle_c &= \langle X_1 X_2 X_3 \rangle \\ &- \langle X_1 X_2 \rangle \langle X_3 \rangle - \langle X_1 X_3 \rangle \langle X_2 \rangle - \langle X_2 X_3 \rangle \langle X_1 \rangle \\ &+ 2 \langle X_1 \rangle \langle X_2 \rangle \langle X_3 \rangle\,, \end{aligned} \tag{J.12}$$

in agreement with (J.5) derived explicitly.

Clearly, this way of calculating cumulants is also somewhat tedious and impractical. The main breakthrough in isolating cumulants from correlations came with the implementation of Eq. (J.6) in MATHEMATICA, which can easily be used in practice to get cumulants in principle for any number of random observables. This implementation is presented in Fig. J.1.

```
n = 4; (* set here the cumulant order *)

Needs["Combinatorica`"];
observables = Table[x_i, {i, 1, n}];
partitions = SetPartitions[observables];
Array[subpartitions, n];
For[i = 1, i ≤ n, i++, subpartitions[i] = {}];
Table[For[i = 1, i ≤ Length[partitions], i++, If[Length[Part[partitions, i]] == j,
    AppendTo[subpartitions[j], Part[partitions, i]]]], {j, 1, n}];

(* For[i=1,i≤n,i++,Print[i,":  ",subpartitions[i]]]; *)

nthCumulant =
  Sum_{l=1}^{n} Factorial[l - 1] (-1)^(l-1) Sum_{d=1}^{Length[subpartitions[l]]} Product_{i=1}^{l} Av[Part[Part[Part[subpartitions[l], d], i]]];

Print[c, "{", n, "} = ", nthCumulant]
```

```
c{4} = -6 Av[{x1}] Av[{x2}] Av[{x3}] Av[{x4}] -
  Av[{x1, x4}] Av[{x2, x3}] - Av[{x1, x3}] Av[{x2, x4}] - Av[{x1, x2}] Av[{x3, x4}] +
  2 (Av[{x3}] Av[{x4}] Av[{x1, x2}] + Av[{x2}] Av[{x4}] Av[{x1, x3}] + Av[{x2}] Av[{x3}] Av[{x1, x4}] +
    Av[{x1}] Av[{x4}] Av[{x2, x3}] + Av[{x1}] Av[{x3}] Av[{x2, x4}] + Av[{x1}] Av[{x2}] Av[{x3, x4}]) -
  Av[{x4}] Av[{x1, x2, x3}] - Av[{x3}] Av[{x1, x2, x4}] - Av[{x2}] Av[{x1, x3, x4}] -
  Av[{x1}] Av[{x2, x3, x4}] + Av[{x1, x2, x3, x4}]
```

Figure J.1: Simple MATHEMATICA code which can be used to isolate cumulants from correlations, in principle for any number of random observables. In the first line one has to specify the number of random observables (i.e. the cumulant order), and execute the code. The resulting cumulant is printed in the last line.

Samenvatting

In zware-ionen botsingen bij de 'Large Hadron Collider' (LHC) wordt een nieuwe toestand van materie geproduceerd. Er wordt aangenomen dat een dergelijke toestand van materie, het zogenaamde quark-gluon plasma (QGP) ook bestond in het vroege heelal, slechts enkele microseconden na de Big Bang. Uit alle meetbare grootheden die gevoelig zijn voor de QGP eigenschappen is gebleken dat de Foerier coëfficiënten v_n, die de anisotrope stroming karakteriseren, de meeste informatie verschaffen. In dit proefschrift worden de resultaten gepresenteerd van de recente anisotrope stroming metingen met de ALICE detector bij LHC energieën.

De fysica van anisotrope stroming is een zeer rijk onderzoeks gebied, zowel voor experimentatoren als voor theoretici. Dit proefschrift heeft als doel bij te dragen aan een beter begrip. Het is ook duidelijk dat er nog een lange weg te gaan is voordat we de anisotrope stroming volledig begrijpen. Met dit proefschrift hebben we geprobeerd om een stap voorwaarts te maken.

In een niet-centrale zware-ionenbotsing is het initiële transversale overlapgebied van de kernen niet symmetrisch. De ontstane drukgradient in het begin van de botsing is hierdoor verschillend in de x- en y-richting, hetgeen leidt tot een verschil in de transversale impulsverdelingen van de deeltjes in deze richtingen. Dit verschil van de deeltjesdistributies wordt anisotrope stroming genoemd en gekarakteriseerd door de coëfficiënten v_n. Deze coëfficiënten v_n worden gedefinieerd door een Fourier-reeks ontwikkeling van de transversale impulsverdelingen als functie van azimut. De metingen van deze coëfficiënten maakt het mogelijk om de toestandsvergelijking van het gecreëerde systeem te toetsen aan voorspellingen uit QCD.

Voor het bepalen van de v_n coëfficiënten wordt de grootste bijdrage in de systematische onzekerheid veroorzaakt door correlaties tussen de deeltjes die niet gegenereerd worden door de anisotrope stroming zelf, en door de verschillen in de anisotrope stroming in de individuele botsingen (die verder wel dezelfde karakteristieken hebben). In dit proefschrift is met behulp van een recent ontwikkelde analyse methode deze systematische onzekerheid bepaald.

De voor dit werk ontwikkelde analytische methode voor het anisotrope flow analyse, de zogenaamde 'Q-cumulants' is gebaseerd op het meten van de correlatie in azimut tussen twee en meer deeltjes, waarna het isoleren van de bijdrage van de echte meer deeltjes correlatie door middel van de zogenaamde cumulants wordt gedaan. Omdat correlaties niet gerelateerd aan het initiële transversale overlapgebied van de kernen voornamelijk uit slechts twee deeltjes correlaties bestaan zijn de meer-deeltjes cumulants (dat wil zeggen de echte multi-deeltjes correlaties), daar per definitie minder gevoelig voor. Tot voor dit proefschrift was er slechts een numerieke manier beschikbaar om dergelijke berekeningen te doen.

In dit proefschrift presenteren we ook onze resultaten van de anisotrope stroom van geladen deeltjes, gemeten in lood-lood botsingen bij een botsingsenergie van 2,76

TeV per nucleon paar. In november 2010, slechts 10 dagen na de eerste zware-ionen botsingen, heeft ALICE de eerste metingen van de elliptische stroming v_2 gepubliceerd[1]. Deze metingen laten zien dat de geproduceerde materie in zware-ion botsingen bij LHC energieën zich gedraagt als een bijna perfecte vloeistof. In dit proefschrift presenteren we de gepubliceerde resultaten met een meer gedetailleerde uitleg van de systematische onzekerheden, maar ook nieuwe en meer gedetailleerde elliptische flow metingen gemeten met een veel groter aantal botsingen.

Na de publicatie van de resultaten voor de elliptische stroming in [69] was ons volgende doel het meten van de hogere orde harmonische, v_3 (driehoekige stroming), v_4 en v_5. Deze analyse is ook recentelijk gepubliceerd in [70]. De meting laat zien dat de oneven harmonische, zoals v_3 en v_5, niet nul zijn. Omdat de oneven harmonische alleen niet nul zijn als de waarde fluctueert tussen de botsingen geeft de waarde van deze harmonische gedetailleerde informatie over het initiële transversale overlapgebied van de kernen.

Op dit moment is de analyse van anisotrope stroming bij LHC energieën is verre van voltooid. Aan het eind van 2011 was er de tweede periode van zware-ionen botsingen. Met de veel grotere hoeveelheid botsingen die toen gemeten zijn kunnen in de komende tijd hogere orde harmonischen, zoals v_4 of v_5 ook met multi-deeltjes cumulants gemeten worden. Een ander interessant onderwerp is de zoektocht naar aanwijzingen van anisotrope stroming in zeldzame proton-proton botsingen waar veel deeltjes worden geproduceerd en in de botsingen van protonen met zware-ionen welke aan het einde van 2012 voor het eerst zullen plaatsvinden.

[1] Op het moment van schrijven van dit proefschrift is deze publicatie nog steeds de meest geciteerde LHC fysica publicatie, met ongeveer 150 citaten in alleen al het eerste jaar.

Acknowledgments

Working at Nikhef as a PhD student, and for a short period as a postdoc, for the last five years proved to be a great and fruitful experience. During this period I made a (risky?) transition from theoretical to experimental physics. Although I came from theory, my supervisor Raimond Snellings hired me to work on a genuine experimental subject at Nikhef: I will always be indebted to him for this brave decision! With respect to this, I am also obliged to our group leader Thomas Peitzmann for approving that decision. Thanks to Raimond's guidance and patience, I eventually managed to reach the light. Although at some point he has surprisingly realized that the frame of mind of people in the part of the world I am originating from is strikingly different from the Dutch mentality, nevertheless he has managed to tolerate that—thanks to him for this in particular!

I would like to mention Rene Kamermans, who was my first promotor. I benefited a lot from our regular meetings that we were having during the first two years of my PhD. The discussions over these meetings were always enjoyable and I was extracting a great deal of useful things from them. Unfortunately his tragic death has terminated all that.

Special thanks go to Sergei Voloshin, who gave me the first and original idea from which eventually the Q-cumulants have emerged, and now form the bulk of the material presented in this thesis. Thanks to Paul for showing constant and close interest in this project and the encouragement I was constantly receiving from him in order to complete this project successfully. Thanks also to all other ALICE and STAR members who showed interest and helped. Thanks to Michiel for all useful discussions we had at Nikhef, and especially for reading in-depth my thesis (also all appendices!) and providing valuable feedback. At this point I want also to thank the other members of the reading committee, namely Frank, Thomas, Eric and Marcel, for approving the thesis.

Special thanks goes to Naomi, with whom I was sharing most of the work related duties during my PhD, both at Nikhef and CERN, as the subjects of our theses, and our PhD trajectories in general, were having a lot of things in common. Naomi, it was really a pleasure to have a colleague like you! Once Mikołaj joined our flow related efforts, suddenly the quality of the code in FLOW package became much better—special thanks to him as well for his programming expertise and willingness to share it any time any place.

I was lucky to always have great people around me as my officemates at Nikhef, starting from Joana and Despoina, than Mikołaj, Robbert, Nicolas, and finally Grazia, Mr. U and Redmer. *Anyhow,* I cannot stop here without mentioning Panos, who was together with Naomi my officemate at CERN. We were having regularly different/opposing opinions on a lot of subjects, *nevertheless* in majority of the cases we managed to find out at least some common sense. For the remaining cases in which we didn't, our discussions *most likely* need to be carried on forever.... *Last but not least:* Big thank to you for teaching me the secrets of doing analysis on Grid from scratch.

I would like to thank new colleagues at Nikhef, with whom unfortunately I won't be able to share more days: Alis, Mr. U and Carlos. Señorita, it's a pity that we didn't have enough time to reach the final conclusion on the "fundamental difference" issue.... Mr. U, thanks a lot for letting me know that you supported Croatia in the World Cup in 1998 (and that you even bought and wore Croatian national shirt in China that year)—that really made me feel proud! Señor Carlos, you are unfortunately still my only suspect behind the llama attack in St. Genis-Pouilly.

Besides my ALICE colleagues at Nikhef, I am also indebted a lot to Teus and Ed from the Nikhef' personnel department for their constant help with pretty much everything. Ed, I hope that during our lifetimes we will witness Ajax and Hajduk playing each other in some final.

I would like also to thank people from the part of our group based in Utrecht for creating constantly a friendly and motivating working atmosphere around: Adinda, Allessandro, Andre, Andrea, Astrid, Arie, Deepa, Geert-Jan, Kees, Marco (The Tolerant), Marek (Son of Poland), Marta, Martijn, Merijn, Misha, Piotr, Raoul, Redmer, Sandro, Sarah, Thomas and Ton.

Special thanks also to Tomislav Prokopec, my supervisor from the masters days in theoretical physics in Utrecht, who afterwards still remains in my life as a great friend.

Many thanks to Jens-Jørgen and the members of his group in Copenhagen where I am moving to work next, for hiring me as a postdoc there.

Thanks to Dave (my English housemate in Utrecht for the last couple of years) for bearing with me. I really hope that in the near future Leeds will again reach the top level, where they definitely belong.

At the end, most importantly, thanks to my family for their everlasting support.

Curriculum Vitae

- University education at *University of Zagreb*, Croatia: Graduate Engineer of Physics in 2004
  – Diploma thesis: *"On possible CPT violation in neutrino physics"*

- Master's Programme in Theoretical Physics at *Utrecht University*, The Netherlands: M.Sc. in Theoretical Physics in 2007
  – Master thesis: *"Quantum radiative corrections to slow-roll inflation"*

- 01.03.2007–01.10.2011: PhD in the ALICE group at *National institute for subatomic physics (Nikhef)* in Amsterdam, The Netherlands
  – PhD thesis: *"Anisotropic Flow Measurements in ALICE at the Large Hadron Collider"*

- 01.10.2011–31.12.2011: postdoc in ALICE group at *National institute for subatomic physics (Nikhef)* in Amsterdam, The Netherlands

- 01.02.2012: starting as a postdoc in ALICE group at *Niels Bohr Institute* in Copenhagen, Denmark